Characterisation of HBV and SARS-CoV-2 spike specific T cells and their association with viral control

Guihai Liu

Linacre College

University of Oxford

A Thesis Submitted for the Degree of

Doctor of Philography

Hilary Term 2023

Characterisation of HBV and SARS-CoV-2 spike specific T cells and their association with viral control

Guihai Liu, Linacre College, D.Phil Thesis, Hilary Term 2023

Abstract

T cell responses are crucial in viral clearance, but little is known of the role of cytotoxic $CD4^+$ T cells in the control of viral infection.

Chronic hepatitis B virus (HBV) infection is a global public health problem. In the first part of my study, HBx-specific T cell responses were investigated in patients with chronic HBV infection and their functional profiles were evaluated *in vitro*. Stronger HBx-specific T cell responses were associated with HBeAg clearance and lower HBsAg levels. $X_{146\text{-}154}$-specific $CD8^+$ T cells can produce effector cytokines and express CD107a when encountering HBV-infected $HepG2^{hNTCP}$ cells. Furthermore, they can kill HBV-infected cells and suppress HBV replication and antigen production. Among HBx-specific $CD4^+$ T cells, $X_{89\text{-}103}$-$CD4^+$ T cells showed the greatest cytotoxicity, while $X_{105\text{-}119}$-$CD4^+$ T cells did not exhibit any killing capacity. Interestingly, highly cytotoxic HBx-specific $CD4^+$ T cells displayed high functional avidity and degranulation, and can inhibit HBV replication *in vitro*. These data demonstrate the potent role of HBx-specific T cells in controlling HBV infection and highlight their potential for future interventions.

In March 2020, COVID-19 pandemic started in UK, my project expanded to study the role of T cell responses, in particular potential escape variants in circulating virus and cytotoxic $CD4^+$ T cells in SARS-CoV-2 infection. Robust SARS-CoV-2 specific memory T cell responses were observed in convalescent COVID-19 individuals. Three dominant spike $CD4^+$ T cell epitopes, one ORF3a and three nucleocapsid $CD8^+$ epitopes were identified in this study. We first showed that several mutations within nucleocapsid and ORF3a $CD8^+$ epitopes resulted in loss of T cell responses assessed by IFN-γ ELISpot assays and cytotoxic killing assays. This demonstrates the potential for T cell evasion and highlights the need for ongoing surveillance for variants capable of escaping T cell as well as humoral immunity.

We then characterised T cell responses to the three dominant spike $CD4^+$ T cell epitopes and evaluated their antiviral activity, including cytotoxicity and antiviral cytokine production. We found that $S_{866\text{-}880}$-specific $CD4^+$ T cells exhibited highest cytotoxicity and correlated with strongest antiviral efficacy, while $S_{166\text{-}180}$-specific $CD4^+$ T cells showed lowest cytotoxicity. Our single cell T cell receptor (TCR) analysis revealed diverse TCR usage including unexpected high level of public TCR usage among all three epitope specific T cells. Surprisingly, $CD4^+$ cytotoxic T lymphocytes (CTLs) were found to have signalling and cytotoxic pathways distinct from classical $CD8^+$ CTLs, with increased expression of chemokines and tissue homing receptors promoting migration. In addition, our longitudinal study showed that robust immune memory 6-9 months post-infection or vaccination provides $CD4^+$ T cells with potent antiviral activity.

In summary, our study in chronic HBV infection and SARS-CoV-2 infection revealed the unique features of $CD4^+$ CTLs that use distinct functional pathways to non-cytotoxic $CD4^+$ T cells and highlighted that induction of potent memory $CD4^+$ CTLs could be a potential approach for future vaccine designs by supporting early viral control.

Acknowledgements

First and foremost, I would like to thank my primary supervisor Prof. Tao Dong giving me the opportunity to study in Oxford. Tao has supervised every aspect of my projects with her wisdom, insight and enthusiasm, and provided a wide range of opportunities through my study. This thesis would not have been possible without her long-standing guidance and patience. I would also like to thank Prof. Yonghong Zhang for his valuable supports and guidance to the HBV project. I really appreciate my co-supervisor Dr Ushani Rajapaksa for helping me establish HBV infection system in the lab and giving me a lot of advice to HBV project. I would also like to greatly thank my co-supervisor Dr Yanchun Peng for supervising the SARS-CoV-2 project and providing numerous constructive advice, assistance, patience, and importantly passing on a wealth of knowledge about T cell culture techniques and assays. Thank you Peng for giving me so many supports in life and sharing so much delicious food with me.

All members of the Dong group and those of Zhang group deserve my huge gratitude for their help at various stages. Particularly, I would like to thank Xuan Yao, Suet Ling Felce, Zixi Yin, Elie Antoun, and all others working on the SARS-CoV-2 project. I am grateful to Megat Bin Abd Hamid and Rhys Woods for all their help in the lab. I would also like to thank Huanqin Sun, Guifang Qiao, Ling Qin, Chi Zhang, and all others working on the HBV project. I am grateful to all the participants for donating their samples and data for these analyses, and the

research teams involved in the consenting, recruitment, and sampling of these participants.

I would like to thank China Scholarship Council, NDM Scholarship of University of Oxford and my supervisor Tao for supporting my PhD study. I would also like to thank Delaney Dominey-Foy, Jane Taylor, and Elie Antoun for proofreading my thesis. Thank you all for your invaluable help. Thank Del for proofreading for me even during your holiday. I would like to thank my friends who have enriched my life in Oxford, especially Wenbo and Hong, and my friends who accompanied me for thesis writing in the library, especially Yuqi and Siyu, and my friend Jane for accompanying me up and down in life. Finally, I would like to thank my family, especially my mum, dad, sister, brother, and my niece and nephews for all their supports, encourage and patience during my D.Phil study. Thank you for always being there and giving me the endless supports.

Declarations

I declare that, unless otherwise stated, all work presented in this thesis is my own. Several aspects of the study relied upon collaboration where part of the work was conducted with or by others.

Study recruitment

Patients with chronic hepatitis B were recruited in the Bejing You'an Hospital in China. PBMCs were processed and stored by the Zhang group in You'an Hospital. COVID-19 patients were recruited from the John Radcliffe Hospital in Oxford, UK, between March 2020 and September 2021. COVID-19 clinical cohort establishment and clinical samples and data collection were performed by Julian C. Knight, Alexander J. Mentzer and Anastasia Fries. Samples from COVID-19 patients were processed and *ex vivo* ELISpot assays were conducted in collaboration with members of the Dong group, especially Yanchun Peng, Xuan Yao, Zixi Yin and Danning Dong.

Generation of HLA-DR-transduced HepG2^{hNTCP} cell line

The lentiviral construct was generated by Philip Hublitz and lentivirus production was performed by Ryan Beveridge. I conducted lentivirus infection of HepG2^{hNTCP} cells and generated HepG2^{hNTCP} cell line stably expressing HLA-DRA*01:01-DRB1*08:01.

Single-cell RNA sequencing

I did FACS staining for antigen-specific T cell sorting with help of Yanchun. Subsequent cell sorting was performed by Yanchun Peng, Craig Waugh, Sally-Ann Clark, Kevin Clark, and Paul Sopp. Sequencing libraries of smartseq2 scRNA-seq was prepared by Xuan Yao and 10x scRNA-seq was performed by Neil Ashley. Sequencing of smartseq2 and 10x scRNA-seq was performed by Timothy Rostron. ScRNA-seq data were analysed by Suet Ling Felce.

Mass spectrometry for proteome of $CD4^+$ killer and nonkiller clones

I identified spike-specific $CD4^+$ killer and nonkiller clones, set up experiments and prepared samples for mass spectrometry. Quality control of samples was run by Zhu Liang. Sample aliquoting and digestion, mass spectra acquisition and protein quantification were performed by Roman Fischer and Iolanda Vendrell. Data were analysed by Elie Antoun to identify differential proteins between killer and nonkiller clones.

SARS-CoV-2 infection

ACE2 lentiviral construct was generated by Philip Hublitz and lentivirus production was performed by Ryan Beveridge. ACE2-tranduced B cell lines were established by Zixi Yin. SARS-CoV-2 Victoria strain was propagated and titred by Peter A. C. Wing, while VOCs propagation and titration was performed by Xuan Yao and Zixi Yin. I carried out SARS-CoV-2 infection to evaluate antiviral efficacy of spike-specific T cells with buddy of Xuan Yao and Zixi Yin.

Viral mutations to escape SARS-CoV-2 specific T cells

Thushan I. de Silva and Tao Dong conceptualized the project of viral mutation part. Benjamin B. Lindsey, Nienyun Sharon Hsu, and Matthew D. Parker performed the viral sequence analyses. Immunodominant T cell responses were identified in collaboration with Yanchun Peng, Xuan Yao, Zixi Yin, and Danning Dong.

Associated Publications

Publications (Joint first author)

1. **Broad and strong memory $CD4^+$ and $CD8^+$ T cells induced by SARS-CoV-2 in UK convalescent individuals following COVID-19**

   Peng Y, Mentzer AJ, **Liu G**, Yao X, Yin Z, Dong D, Dejnirattisai W, et al.

   Nat Immunol. 2020 Nov;21(11):1336-1345. doi: 10.1038/s41590-020-0782-6.

2. **The impact of viral mutations on recognition by SARS-CoV-2 specific T cells**

   de Silva TI, **Liu G**, Lindsey BB, Dong D, Moore SC, Hsu NS, et al.

   iScience. 2021 Nov 19;24(11):103353. doi: 10.1016/j.isci.2021.103353.

3. **An immunodominant $NP_{105-113}$-B*07:02 cytotoxic T cell response controls viral replication and is associated with less severe COVID-19 disease**

   Peng Y, Felce SL, Dong D, Penkava F, Mentzer AJ, Yao X, **Liu G**, Yin Z, et al.

   Nat Immunol. 2022 Jan;23(1):50-61. doi: 10.1038/s41590-021-01084-z

Manuscript in preparation

Memory cytotoxic SARS-CoV-2 spike protein-specific $CD4^+$ T cells associate with viral control

Manuscript in preparation

Liu G, Felce SL, Yao X, Yin Z, Fries A, Mentzer AJ, et al.

Conference abstract

Memory HBx-specific T cells associate with viral control

Poster presentation in 2022 international HBV meeting

CONTENTS

Abbreviation

7-AAD	7-Aminoactinomycin D
ACE2	angiotensin-converting enzyme 2
ANOVA	analysis of variance
APC	allophycocyanin
APCs	antigen presenting cells
BCR	B cell receptor
cccDNA	covalently closed circular DNA
CCR	chemokine receptor
CD	cluster of differentiation
CDR	complementarity determining regions
CFSE	Carboxyfluorescein succinimidyl ester
CHB	chronic hepatitis B
CLIA	chemiluminecence immunoassay
CLIP	class II-associated invariant chain peptide
CMV	cytomegalovirus
COVID-19	Coronavirus infectious disease 2019
CTLA-4	cytotoxic T-lymphocyte associated protein-4
CTLs	cytotoxic T lymphocytes
DCs	dendritic cells
EBV	Epstein–Barr virus
ELISpot	IFN-γ enzyme-linked immunospot
ER	endoplasmic reticulum
FACS	fluorescence-activated cell sorting
FasL	Fas ligand
GM-CSF	granulocyte-machrophage colony-stimulation factor
HBeAg	hepatitis B e antigen

HBsAg	hepatitis B surface antigen
HBV	hepatitis B virus
HCC	hepatocellular carcinoma
Hcov	human coronavirus
HIV	human immunodeficiency virus
HLA	human leucocyte antigen
ICS	intracellular cytokine staining
IFN	interferon
IFNAR	type I interferon receptor
IFNGR	interferon gamma receptor
IL	interleukin
IL-2R	IL-2 receptor
ISG	IFN-stimulated gene (ISG)
ISGF3	IFN-stimulated gene factor 3
JAK1	Janus kinase 1
LAG-3	lymphocyte-activation gene-3
LAMP-1	lysosome-associated membrane protein-1
LDH	lactate dehydrogenase
Ii	invariant chain
MERS-CoV	Middle East respiratory syndrome coronavirus
MHC	major histocompatibility complex
MIP-1β	macrophage inflammatory protein-1β
NK	natural killer
NTCP	sodium taurocholate co-transporting polypeptide
NTD	N-terminal domain
ORF	open reading frame
PBMC	peripheral blood mononuclear cell
PD-1	programmed cell death protein-1

PegIFN-α	Pegylated interferon alpha
PegIFN-α	phycoerythrin
pgRNA	pregenomic RNA
PHA	polyhydroxyalkanoates
PPR	pattern-recognition receptor
qPCR	quantitative polymerase chain reaction
RANTES	regulated on activation, normal T cell expressed and secreted
RBD	receptor binding domain
rcDNA	relaxed circular DNA
RLRs	retinoic acid-inducible gene I-like receptors
SARS-CoV-2	Severe acute respiratory syndrome coronavirus 2
scRNA-seq	single cell RNA sequencing
Smc	Structural maintenance of chromosomes
STAT	signal transducer and activator of transcription
TAP	transporter associated with antigen processing
TCR	T cell receptors
Tfh	follicular helper T cells
TGF-β	transforming growth factor β
Th	helper T cells
Tim-3	T cell immunoglobulin and mucin-domain containing-3
TLRs	Toll-like receptors
TNFR	TNF receptor
TNF-α	tumour necrosis factor alpha
TRA	TCR α chain
TRAIL	tumor necrosis factor-related apoptosis-inducing ligand
TRB	TCR β chain
TYK2	tyrosine kinase 2
VOC	variants of concern

VOI	variants of interest
VUM	variants under monitoring
WHO	World Health Organization

List of Figures

Chapter 1

Chapter 2

Chapter 3

Appendices

List of tables

Chapter 3

Chapter 4

Chapter 5

Appendices

Chapter 1: Introduction

1.1 Host immune responses against virus infection

Host immune responses involve the innate immune system and the adaptive immune system, which act synergistically to protect the host from viral infection.

1.1.1 Innate immunity

The innate immune system is the first line of defence against viral infections. Innate immune cells recognise viral components such as genomic DNA, single-stranded RNA or double-stranded RNA produced in virus-infected cells via pattern-recognition receptors (PRRs)(Kawai & Akira, 2006; Takeuchi & Akira, 2009). Three types of PRRs are involved in virus recognition by innate immune system, including Toll-like receptors (TLRs), retinoic acid-inducible gene I (RIG-I)-like receptors (RLRs), and nucleotide oligomerization domain-like receptors. Of these receptors, TLRs and RLRs are crucial in the production of type I interferons (IFNs), such as multiple IFN-α molecules and IFN-β, and proinflammatory cytokines.

1.1.1.1 Type I IFNs

Type I IFNs are produced by various cell types, such as macrophages, fibroblasts, and plasmacytoid dendritic cells. The type I IFN receptor (IFNAR) consists of two subunits IFNAR1 and IFNAR2. Ligation of IFNAR activates Janus kinase 1 (JAK1) and tyrosine kinase 2 (TYK2), then phosphorylated signal transducer and activator of transcription 1 (STAT1) and STAT2 lead to the dimerisation, nuclear

translocation and forming of the IFN-stimulated gene factor 3 (ISGF3) complex. The binding of this complex to promoter regions of IFN-stimulated gene (ISG) induces expression of numerous ISGs in the cell, which restrict viral replication(Ivashkiv & Donlin, 2014). Antiviral effects of type I IFNs have been reported *in vitro* and in mice in various viral infections(McNab, Mayer-Barber, Sher, Wack, & O'Garra, 2015). IFN-α suppresses hepatitis B virus (HBV) replication and transcription *in vitro* and in transgenic mice(Belloni et al., 2012). IFN-α treatment reduces the levels of HBV DNA, covalently closed circular DNA (cccDNA) and pregenomic RNA (pgRNA) in HepG2 cells transfected with HBV genome. Similar results are observed in chimeric mice infected with HBV. Pegylated IFN-α (PegIFN-α) is an administered therapy in patients with HBV infection.

Type type I IFNs also stimulate the adaptive immune response and modulate $CD4^+$, $CD8^+$, B cell responses(McNab et al., 2015). IFN-α promotes $CD4^+$ T cells to differentiate into IFN-γ producing type 1 helper T cells (Th1)(Brinkmann, Geiger, Alkan, & Heusser, 1993), while extends proliferation and clonal expansion of antigen-specific $CD8^+$ T cells(Bon et al., 2006). In chronic HBV infection, PegIFN-α treatment does not restore HBV-specific $CD8^+$ T cell quantity and function. in contrast, PegIFN-α increases activation and proliferation of $CD56^{high}$ natural killer (NK) cells with upregulated expression of IFN-γ and tumour necrosis factor-related apoptosis-inducing ligand (TRAIL)(Micco et al., 2013).

1.1.1.2 Natural killer (NK) cells

NK cells are the main effector lymphocytes involved in the innate immune

response, which play an essential role in host immune defence against viral infections. NK cells constitutively express transcripts for some cytokines, such as IFN-γ, and contain preformed cytotoxic molecules including granzymes and perforin in their intracellular granules(Lanier, 2008). Thus, NK cells are ready armed with cytotoxic and cytokine-producing effector functions and are suited for early defence. NK cells do not express clonotypic antigen-specific receptors dependent on somatic gene recombination. However, activating and inhibitory receptors on cell surface allow them to distinguish target cells from normal cells to prevent random killing(Lanier, 2005). NK cells also express CD16, the activating Fc receptor for antibody (IgG), which enables NK cells to attack virus-infected cells coated with antibody specific to virus via antibody-dependent cell cytotoxicity(Lanier, 2008). NK cells elicit cytolytic activity through two essential mechanisms(Abel, Yang, Thakar, & Malarkannan, 2018). The first mechanism involves the activation of death receptors on the surface of target cells, including TRAIL receptor and Fas (CD95)(Abel et al., 2018). The activation of TRAIL receptor and Fas by their cognate ligands, TRAIL and FasL, present on NK cells, initiates pro-apoptotic signalling pathways and finally induces target cell death. The primary mechanism of cytotoxicity executed by NK cells is mediated via granules which contain granzymes and perforin(Abel et al., 2018). Granules are delivered to target cells through cell membrane fusion then release enzymes that lead to activation of the intrinsic apoptosis program within the target cells. These two killing mechanisms are also utilised by cytotoxic T cells.

1.1.2 Adaptive immune response

The adaptive immune response is the other sophisticated arm of the immune system involving T and B cells. B cells produce antibodies with a range of functions, such as neutralising antibodies that prevent or limit infection and reinfection, but can also act as antigen presenting cells (APCs). T cells are broadly segregated by surface expression of $CD4^+$ and $CD8^+$, each providing crucial components of protective immunity against viral infection.

1.1.2.1 Humoral immune response

The humoral immune response is mediated by antibodies. Antibodies are immunoglobulin proteins that are synthesised and secreted by differentiated B cells called plasma cells. To induce plasma cell differentiation and subsequent antibody production, pathogenic antigen binds to B cell receptor (BCR) on naïve B cells. Binding induces antigen internalisation and degradation into peptides that are presented by major histocompatibility complex (MHC) class II molecules on the B cell surface. The peptide-MHC class II complex presented by B cells activates armed $CD4^+$ follicular helper T cells (Tfhs). Signals from both the BCR binding to antigen and the activated Tfhs induce naïve B cells to proliferate and differentiate into plasma cells that produce specific antibodies(Koutsakos, Nguyen, & Kedzierska, 2019). Antibodies can inhibit viral attachment to host cells or interrupt viral entry process by binding to them, which is termed neutralisation. Neutralising antibodies are essential for vaccine-mediated protection against infectious disease. Antibodies also trigger the innate effector processes of

"*complement activation*" and "*opsonisation*" that contribute to viral clearance(Burton, 2002). Complement leads to direct virolysis through a cascade of innate effector protein cleavages. Opsonisation promotes phagocytosis and viral clearance through recognition of antibodies by Fc and complement receptors expressed on phagocytes.

1.1.2.2 T cell immune response

T cell responses play critical roles in controlling viral infections and have a range of functions such as antigen-dependent cell-mediated killing and assistant other immune cell immunogenic functions. In an antiviral immune response, T cells pass through three characteristic stages, including activation and expansion, followed by contraction and the formation of memory T cells (Fig. 1.1)(Kaech, Wherry, & Ahmed, 2002; Wherry & Ahmed, 2004). The activation and expansion phase is initiated in lymphoid tissues, where antigen stimulation induces naïve T cells to clonally expand and differentiate to gain effector functions. Effector T cells can kill virus-infected cells and secrete cytokines to inhibit viral replication. In the weeks following viral clearance (acute infection), the majority (>90%) of activated effector T cells die, which is often referred to as the contraction phase. The

surviving antigen-specific T cells eventually form a pool of long-lived memory T cells.

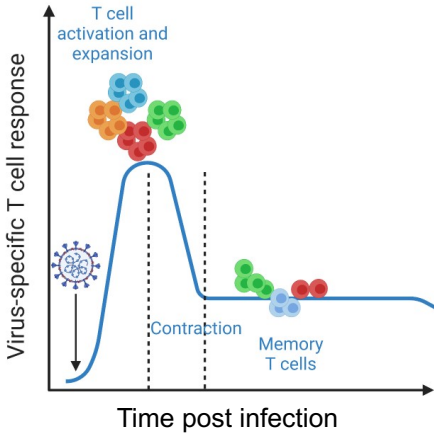

Fig. 1.1 The dynamics of an antiviral T cell response. The three phases of T cell response to viral infection include expansion, contraction, and memory. Figure is created with BioRender.com.

1.1.2.2.1 T cell recognition of viral infection via T cell receptor (TCR)

T cells with mature T cell receptors (TCRs) can recognise cognate antigens presented by MHC molecules on the surface of virus-infected cells. This specific activation acts as the primary mechanism in the effector T cell responses, helping to clear viral infection.

1.1.2.2.1.1 Antigen processing and presentation

1.1.2.2.1.1.1 Human leucocyte antigen (HLA)

MHC are found in all higher vertebrates and include two major types, MHC class I and MHC class II. The HLA is a highly polymorphic gene locus located on the short arm of chromosome 6 (6p21.31) that encodes MHC molecules in humans(Choo, 2007). Polymorphisms are driven by the selection of

advantageous alleles that mediate enhanced MHC antigen presentation, greater antigen recognition and thereby improved host immune responses(Doherty & Zinkernagel, 1975). To provide a higher level of protection against pathogen immune evasion, MHC is polygenic with numerous functional gene products. In humans, HLA comprises three regions, class I, II, and III. Of these, the class I region consists of the classical *HLA-A*, *-B*, and *-C* genes which encode α chains (heavy chains) of class I molecules, HLA-A, -B, and -C respectively. Whereas class II region encodes three pairs of α and β chains comprised of class II molecules, termed HLA-DR, -DP, and -DQ. The class III does not encode HLA molecules, but has genes for components, TNFs, and others(Choo, 2007).

HLA class I molecules are expressed on the surface of almost all cells, while class II molecules are expressed only on B cells, activated T cells, and professional APCs including monocytes, macrophages, and dendritic cells (DCs)(Choo, 2007). HLA class I molecules comprise glycosylated heavy chains and noncovalently bound extracellular β2-microrglobulin which is invariant. The heavy chain has three extracellular domains, α1, α2, and α3, of which α1 and α2 domains form the antigen peptide binding groove to accommodate 8- to 10-residue peptides. Class II molecules are heterodimers containing α and β chains, with extracellular domains α1 and β1 forming the antigen binding groove(Choo, 2007).

1.1.2.2.1.1.2 Antigen processing and presentation

MHC molecules were first described in a transplantation in order to explain graft rejection in patients with graft vs host disease(Hull, 1970). MHC was first

understood to present self-producing proteins onto the cell surface, known as the direct antigen presentation pathway. MHC was subsequently established as the major presenter of foreign proteins, especially by APCs(Benacerraf & McDevitt, 1972). APCs play a major role in the initial presentation of pathogenic antigen for the priming, activation and maintenance of T cell responses.

The antigen peptides recognised by T cells are known as epitopes. Epitopes of 8-10 amino acids are derived from proteins expressed within cells (e.g. virus-infected cells and cancer cells) and are presented on MHC class I molecules to $CD8^+$ T cells(Bertoletti & Ferrari, 2016; Rock & Goldberg, 1999). Intracellular proteins are degraded in the proteasome into peptides(Blum, Wearsch, & Cresswell, 2013; Vyas, Veen, & Ploegh, 2008). The peptides are delivered to the endoplasmic reticulum (ER) by the transporter associated with antigen processing (TAP) which is a heterodimeric protein composed of TAP1 and TAP2 subunits. In the ER, peptide is loaded onto nascent MHC class I molecules facilitated by members of the peptide-loading complex, such as tapasin, calreticulin and ERp57. Then peptide-loaded MHC class I molecules are transported via the Golgi complex and presented on the cell surface. In addition, $CD141^+$ DCs can cross-present exogenous antigens through MHC class I molecules to $CD8^+$ T cells(Haniffa et al., 2012).

The binding groove of MHC class II molecules is open and usually accommodates peptides of 13-25 residues(Chicz et al., 1992). Epitopes of 13-25 amino acids are derived from internalised pathogens and are presented to $CD4^+$ T cells by MHC

class II molecules on professional APCs (Roche & Furuta, 2015). APCs utilise several distinct pathways to capture foreign antigens, including macropinocytosis, phagocytosis, receptor-mediated endocytosis and autophagy. The internalised antigens are transported to the endosomal-lysosomal antigen-processing compartment where they are processed and loaded on nascent MHC class II molecules(Blum et al., 2013; Roche & Furuta, 2015; Vyas et al., 2008). Nascent MHC class II molecules bind to invariant chain (Ii) and are presented on cell surface. Ii-MHC class II complex on the cell surface is internalised by endocytosis enabled by recognition of the targeting motifs comprised of Ii. Ii-MHC class II complex is then delivered from the early endosome to the antigen-processing compartment, where Ii is proteolysed into class II-associated invariant chain peptide (CLIP). Only after CLIP removal from CLIP-MHC class II complex by the enzyme HLA-DM, peptides can bind onto MHC class II molecules. Peptide-MHC class II complex is directed to the cell surface via the tubulovesicular endosome fusion with the plasma membrane.

1.1.2.2.1.2 TCR

T cells recognise antigens depending on the interaction between TCRs and MHC molecules. TCRs are highly diverse heterodimers consisting of two glycosylated polymorphic polypeptides. TCR diversity is associated with the effective control of viral infection. The most common TCR in humans is the αβ TCR. This is composed of covalently linked α chain (TRA) and β chain (TRB) by a disulphide bond(Meuer et al., 1983; Rabbitts et al., 1985). A less common human TCR is γδ

TCR. Each TCR chain is composed of two extracellular domains known as the constant region, and the variable region. The variable region is important for antigen recognition and contains three hypervariable loops in its uppermost part, termed the complementarity determining regions (CDR1, CDR2 and CDR3). The CDR3 region has the direct contact with the peptide antigen, and therefore is essential for antigen recognition during the TCR interaction with peptide-MHC complex (Fig. 1.2).

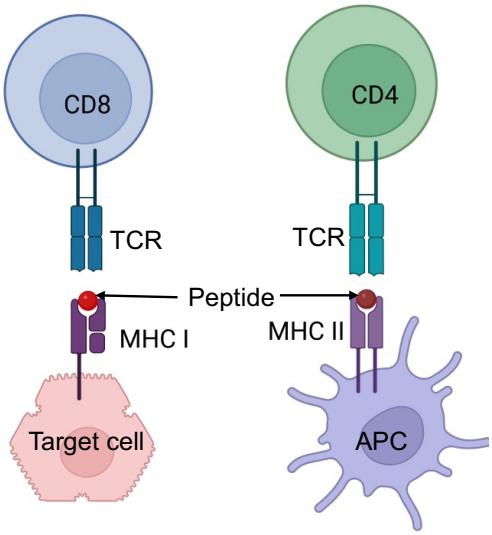

Fig. 1.2 Schematic representation of TCR structures and interaction of peptide. TCR recognises endogenous antigen presented by MHC class I on target cell ($CD8^+$ T cell) or exogenous antigen presented on MHC class II in APC ($CD4^+$ T cell). APC, antigen presenting cell; MHC, major histocompatibility complex; TCR, T cell receptor. Figure is created with BioRender.com.

TCRs are highly variable molecules due to somatic DNA rearrangements of the whole *TRA* and *TRB* gene loci during T cell development. This process involves selection of two (for *TRA*) or three (for *TRB*) gene segments: variable (V) and joining (J) segments, and an additional diversity (D) gene segment for TRB, to

form the final rearranged TCR DNA sequence. The V(D)J recombination is a site-specific recombination process directed by the lymphoid-specific recombinase that is encoded by recombination activating gene-1 and -2, and ubiquitously expressed DNA repair proteins(Bassing, Swat, & Alt, 2002). The process also involves the deletion and insertion of nucleotides at the V-D, D-J and V-J junctions. Most of the variation of each chain relies on CDR3 that is encoded by V(D)J. Additional variations in α and β pairing in individual T cells further increase the total number of possible TCR combinations. The diverse TCR repertoire is selected through positive and negative thymic selections to ensure only $CD4^+$ and $CD8^+$ T cells that recognise non-self-peptides presented on MHC are maintained in the body(Ernst, Surh, & Sprent, 1995; Kisielow, Teh, Blüthmann, & von Boehmer, 1988). It is estimated that the actual T cell repertoire present in an individual is around 10^{13} clonotypes(Laydon, Bangham, & Asquith, 2015). During disease (e.g. viral infection), T cells that recognise viral peptides presented on MHC are primed and activated. Activated T cells proliferate and differentiate into memory T cells which dominant the T cell pool during infection(Ferrari et al., 1990; Jung et al., 1991). The naïve T cell TCR repertoire is highly diverse, with a wide variety of clonotypes. This is in contrast to memory T cells, which contribute less than 1% of the total repertoire but account for one-third of T cell population in adults(Arstila et al., 1999).

During disease, each antigenic epitope may generate a variety of distinct yet cognate TCRs, named clonotypes. Hereby, each TCR responds to the same

antigenic epitope but with variation in their TRA/TRB sequence or αβ TCR pairing. Some TCRs have private specificity, and are only observed in one individual. In contrast, some TCRs specificity is public, which are shared between individuals and exhibit clonal dominance in various viral infections such as influenza A, Epstein–Barr virus (EBV), cytomegalovirus (CMV), HBV, and human immunodeficiency virus (HIV). Public TCRs are believed to be due to a process known as convergent recombination during V(D)J gene rearrangement(Miles, Douek, & Price, 2011; Venturi, Price, Douek, & Davenport, 2008). The first level of convergent recombination involves multiple recombination events, including different splicing of germline V, D and J segments and random nucleotide addition and depletion, to produce the same nucleotide sequences. The second level involves multiple nucleotide sequences encoding the same amino acid sequence. However, the biological effects of public TCRs remain elusive.

1.1.2.2.2 $CD8^+$ T cell response

$CD8^+$ T cells are one of the critical components of the adaptive immune system. Upon activation, $CD8^+$ T cells can proliferate rapidly and induce highly specific effector responses against viral infection. The primary function of $CD8^+$ T cells is cytotoxic activity via immune killing. It is well established that $CD8^+$ cytotoxic T lymphocytes (CTLs) elicit cytotoxicity through two major mechanisms mediated by granules, and Fas ligand (FasL) and TRAIL respectively, similar to NK cells. Additionally, $CD8^+$ T cells can secrete cytokines and chemokines, such as tumour necrosis factor alpha (TNF-α) and IFN-γ to control virus infections via noncytolytic

pathways(Guidotti & Chisari, 2001).

1.1.2.2.2.1 Proliferation

Upon stimulation, antigen-specific T cells become activated and clonally expand. Activated T cells upregulate proliferation-associated genes such as interleukin (IL)-2. IL-2 is an α helical protein produced by antigen-activated T cells, which binds to the IL-2 receptor (IL-2R) complex consisting of three subunits, IL-2R α (CD25), IL-2β (CD122) and a common gamma chain (γc (CD132)). While both CD122 and CD132 are also components of other interleukin receptor complexed (e.g. IL-15 and IL-4), CD25 binds specifically to IL-2(Giri et al., 1994; Russell et al., 1993). This specific binding helps to recruit CD122 and CD132 to form the IL-2 receptor complex that has increased affinity for IL-2, thereby significantly inducing efficient IL-2-dependent proliferation signalling(Stauber, Debler, Horton, Smith, & Wilson, 2006). The formation of IL-2R complex induces phosphorylation of JAK-3 which activates the downstream STAT-5 transcription factor pathway, that facilitates STAT-5 nuclear translocation and binding to IL-2 locus promoter, thereby inducing IL-2 transcription and subsequent protein synthesis(Friedmann, Migone, Russell, & Leonard, 1996). The resulting IL-2 production and secretion into the surrounding milieu feeds back and contributes to further CD25 ligation, therefore facilitating a IL-2-IL-2R positive feedback loop, especially in the inflammatory state(Busse et al., 2010).

1.1.2.2.2.2 Cytokine production

Upon simulation with pathogenic antigens, $CD8^+$ T cells can induce production of important cytokines, such as TNF-α, IL-2, and IFN-γ, and chemokines such as macrophage inflammatory protein (MIP)-1β and RANTES (regulated on activation, normal T cell expressed and secreted, CCL5) to help the immune response against virus infection. TNF-α is a pleiotropic cytokine that contributes to antitumour effect, cytotoxicity and the defence against viruses. Its antiviral effect was first described to vesicular stomatitis virus infection *in vitro*(Mestan et al., 1986). Antiviral function of TNF-α is discovered to be mediated through both TNF receptor 1 and 2 (TNFR1 and TNFR2) *in vivo*(Ruby, Bluethmann, & Peschon, 1997). TNF-α ligation to TNFR1 induces target cell death(Wajant, Pfizenmaier, & Scheurich, 2003). The cytoplasmic death-domain contained in TNFR1 can activate caspases in virus-infected cells, which is known to initiate the process of cell apoptosis. In addition to apoptotic cell death, TNF-α recruits innate immune cells such as monocytes, NK cells, and APCs, and initiates antigen-specific T cell and B cell responses to control viral infection(Sedger & McDermott, 2014).

IFN-γ is the only one member of type II interferon family. It was first discovered to interfere with virus replication in 1957(Ijzermans & Marquet, 1989). IFN-γ elicits biological effects by binding to the type II IFN receptor which consists of two subunits, IFN gamma receptor 1 and 2 (IFNGR1 and IFNGR2)(Platanias, 2005). Type II IFN receptor is expressed on almost all cell types. The ligation and dimerisation of IFNGR1 and IFNGR2 induces JAK-1 and JAK-2 phosphorylation

and activation that leads to phosphorylation and homodimerisation of STAT-1. Homodimers of STAT-1 translocate to the nucleus and bind IFN-γ-activated elements in the promoter of some ISGs and subsequent induce expression of some genes(Platanias, 2005). This pathway enables the formation of the immunoproteasome and the induction of TAP proteins for enhanced antigen presentation. Most importantly, IFN-γ induces target cells intrinsic antiviral defence when combined with TNF-α and other inflammatory cytokines. Furthermore, IFN-γ regulates TFNR expression levels on cell surface(Sedger & McDermott, 2014), thereby synergising with TNF-α to promote antiviral function(Wong & Goeddel, 1986).

1.1.2.2.2.3 Granule-mediated cytotoxicity

On the other hand, $CD8^+$ T cells exert antiviral activity via direct lysing virus-infected cells. The cytotoxicity of $CD8^+$ T cells is mediated through two major mechanisms, of which the essential killing mechanism is mediated by granules. Cytotoxic granules are released from T cells in response to TCR recognition of peptide-MHC complex displayed on target cells. Upon TCR engagement, cytolytic granules containing lysosomes are polarised towards the cell membrane by cytoskeletal machinery within T cells. Polarisation towards the membrane leads to degranulation of vesicles containing cytotoxic molecules such as perforin and granzymes into the immunological synapse(Barry & Bleackley, 2002; Voskoboinik, Smyth, & Trapani, 2006). Degranulation can be detected by the presence of lysosome-associated membrane protein-1 (LAMP-1), also known as CD107a, on

the membrane of T cells.

Perforin released into the immunological synapse forms transient pores in the plasma membrane of target cells, through which granzymes diffuse(Voskoboinik et al., 2006). Once entering the cytoplasm, granzyme B activates caspases to induce the cellular apoptotic cascade. Granule-mediated cytotoxicity is highly efficient, inducing target cell apoptosis within five minutes of T cell engagement(Stinchcombe, Bossi, Booth, & Griffiths, 2001).

1.1.2.2.2.4 FasL- and TRAIL-mediated cytotoxicity

T cell cytotoxicity is also mediated by FasL and TRAIL pathways. In perforin knock-out mice, perforin-deficient CTLs can induce residual killing *in vitro* by expressing FasL(Kägi et al., 1994). FasL engagement with the death receptor Fas on the target cell surface can induce programmed cell death. The expression of FasL on the T cell surface is regulated by two mechanisms. The first involves transporting FasL-containing vesicles to the cell membrane for cell surface expression. The second involves upregulated FasL transcription and translation as early as two hours post T cell activation(He, Gong, & Ostergaard, 2010). In contrast, TRAIL induces apoptosis of the target cell by interaction with death receptor-4 (DR4)(Pan et al., 1997).

1.1.2.2.3 $CD4^+$ T cells

$CD4^+$ T cells play pivotal roles in the adaptive immune response. They help B cells produce neutralising antibodies, regulate macrophage function, and induce

and maintain $CD8^+$ T cell responses by licensing DCs and promoting interaction between DCs and $CD8^+$ T cells(Laidlaw, Craft, & Kaech, 2016). Depending on the pattern of stimulatory signals during priming, naïve $CD4^+$ T cells differentiate into various helper T cell subsets characterised by cytokine production profiles, cell surface receptors and transcription factors. These subsets include Th1, Th2, Th9, Th17, Th22, induced regulatory T (iTreg) cells, and Tfh cells.

1.1.2.2.3.1 Helper T cells

In 1986, it was initially demonstrated that $CD4^+$ T cells are composed of distinctive populations with different functions(Mosmann, Cherwinski, Bond, Giedlin, & Coffman, 1986). $CD4^+$ T cell clones from mice were divided into two major populations termed Th1 and Th2 based on their cytokine production. IFN-γ is the signature cytokine of Th1 cells, which is often combined with IL-2 and TNF-α secretion. In contrast, Th2 cells fail to produce IFN-γ, and are defined by signature cytokines IL-4, IL-5 and IL-13. The principal cytokines produced by Th17 is IL-17a and IL-21. iTreg cells produce TGF-β, IL-10 and IL-35, and signature cytokines of Tfh cells are IL-6 and IL-21. Cytokine production is regulated by transcription factors and STAT proteins. T-bet is the major transcription factor for Th1 cell differentiation and induced IFN-γ production. Conversely GATA3 promotes Th2 cell differentiation and IL-4, IL-5 and IL-13 production. RORγt, Foxp3 and Bcl-6 are the master regulator of Th17, iTreg and Tfh cells respectively.(Zhu & Paul, 2008; Zhu, Yamane, & Paul, 2010)

1.1.2.2.3.2 $CD4^+$ cytotoxic T cells

In addition to helper subsets, $CD4^+$ T cells have also been described to possess cytotoxic activity. $CD4^+$ CTLs exert killing of target cells in an MHC class II-dependent fashion. Cytotoxicity of $CD4^+$ T cells was initially observed in T cell lines and clones(Feighery & Stastny, 1979; Maimone, Morrison, Braciale, & Braciale, 1986). This has raised doubts that $CD4^+$ T cell cytotoxicity was an *in vitro* artefact resulting from long-term *in vitro* culture. However, *ex vivo* studies in humans have since demonstrated $CD4^+$ T cell cytotoxic functions in viral infections, such as influenza, CMV, HIV and hepatitis virus(Aslan et al., 2006; Juno et al., 2017; Soghoian et al., 2012; Wilkinson et al., 2012). $CD4^+$ T cell cytotoxicity was further observed *in vivo* in mice infected with lymphocytic choriomeningitis virus (LCMV)(Hildemann et al., 2013). Moreover, due to current advances in the technology to investigate single-cell transcriptomics, infiltrating $CD4^+$ CTLs were explored in tumours and their capacity to kill tumour cells was validated *ex vivo*(Oh et al., 2020). $CD4^+$ T cell anti-tumour cytotoxicity is regulated by Treg cells.

$CD4^+$ CTLs elicit target cell killing through the same cytotoxicity pathways utilised by $CD8^+$ T cells, mediated by granules, FasL and TRAIL (Juno et al., 2017). When compared to $CD8^+$ CTLs, $CD4^+$ CTLs store less intracellular granzyme B and express lower levels of perforin. However, they showed equivalent antiviral efficacy(Lin et al., 2014).

The development of helper $CD4^+$ T cell subsets is regulated by environmental cytokines and transcription factors, however the mechanisms regulating $CD4^+$ CTLs differentiation remain largely unknown. Both naïve and differentiated $CD4^+$ T cells can acquire cytotoxicity. A number of factors have been implicated in $CD4^+$ T cells acquiring cytotoxic function, such as T-bet and Eomes. T-bet can induce granzyme B and perforin expression in $CD4^+$ T cells via binding to their gene promoters, which is regulated by Blimp-1(Hua et al., 2013). In addition to T-bet, Eomes has been implicated in controlling granzyme B expression in $CD4^+$ T cells(Qui et al., 2011). Eomes also induces IFN-γ expression and FasL upregulation, which may result in acquisition of cytotoxic function. Collectively, these studies provide a substantial insight into the development of $CD4^+$ CTLs, but the precise mechanisms of differentiation and function remain elusive.

1.2 HBV

1.2.1 Epidemiology

HBV infection is a serious public health problem worldwide. According to the World Health Organization (WHO) data, at least two billion people, which accounts to one-fourth of the world's population, have been infected with HBV. More than 250 million people are chronically infected with HBV globally, and that more than one million die of HBV-related end stage liver disease, liver cirrhosis or hepatocellular carcinoma (HCC) annually(Revill et al., 2019; Sarin et al., 2016; Yuen et al., 2018). HBV infection is spread through perinatal and horizontal transmission including exposure to infected blood and body fluids. Both viral and

host factors contribute to the outcome of HBV infection. The age at infection is the most critical host factor for the development of chronic infection which is defined as the persistence of hepatitis B surface antigen (HBsAg) for more than 6 months(Trépo, Chan, & Lok, 2014; Yuen et al., 2018). Perinatal infection results in chronic infection for 80-90% infants. Conversely, less than 5% of otherwise healthy adults infected by HBV by horizontal transmission results in chronic infection.

1.2.2 HBV virus and life cycle

HBV is a partially double-stranded DNA virus, a prototype virus of the Hepadnaviridae family. Hepatocytes are the sole site of productive HBV infection(Walter, Keist, Niederöst, Pult, & Blum, 1996). The 42nm infectious virion (Dane particle) is equipped with an envelope containing HBsAg that encloses an internal nucleocapsid particle of 27nm. The nucleocapsid particle shields a partially double-stranded, relaxed circular DNA (rcDNA) genome of 3.2 kilobase (kb). HBV genome is the smallest and most compact among DNA viruses, with four partially overlapping open reading frames (ORFs) for polymerase, core, x and surface proteins(Gish et al., 2015; Iannacone & Guidotti, 2022; Tong & Revill, 2016).

HBV entry into hepatocytes involves the interaction between a specific domain of the HBV large envelope protein, with the high-affinity receptor on the surface of the hepatocyte, which was identified as the sodium taurocholate co-transporting polypeptide (NTCP)(H. Yan et al., 2012). Upon entry, HBV rcDNA is released,

transported into the nucleus and converted into cccDNA(Seeger & Mason, 2015). cccDNA is the template for transcription of mRNAs and pgRNA using the host DNA-dependent RNA polymerase. pgRNA is selectively packaged inside core particles, followed by reverse transcription to rcDNA genome mediated by the viral polymerase within the nucleocapsid particle(Jones & Hu, 2013). Such nucleocapsids can either be enveloped for release as infectious virions or trafficked back to the nucleus for cccDNA amplification. Double-stranded linear DNA replicated from pgRNA can then serve as the template for host genome integration(Tong & Revill, 2016).

1.2.3 Natural history of chronic HBV infection

Chronic HBV infection is a dynamic process. The natural history can be divided into five major phases characterised by levels of HBV DNA and alanine aminotransferase, presence of hepatitis B e antigen (HBeAg) and HBsAg, as well as liver necroinflammation and fibrosis(Liver, 2017; Yuen et al., 2018). These five phases include HBeAg-positive chronic HBV infection, HBeAg-positive chronic hepatitis B (CHB), HBeAg-negative chronic HBV infection, HBeAg-negative CHB, and HBsAg-negative phase. These phases do not occur sequentially and do not occur in all individuals with chronic HBV infection, and do not always occur either. The previously used terms were immune tolerance, immune active and /or clearance, and immune control and/or residual phases respectively.

1.2.4 The role of T cell responses in HBV infection

HBV-specific T responses play critical roles in controlling and resolving viral infection. HBV-specific $CD8^+$ T cells can clear HBV-infected hepatocytes by cell-mediated cytolytic activity and control viral replication without cytolysis by secreting cytokines such as TNF-α and IFN-γ where are both found to suppress HBV DNA replication in HBV producing (the human hepatoma cell line 2.2.15) (Phillips et al., 2010) and HBV-infected hepatocytes (HepaRG and primary human hepatocytes)(Xia et al., 2016). Furthermore, TNF-α and IFN-γ impair HBV cccDNA stability and thereby leads to loss of HBV cccDNA in hepatocytes. TNF-α and IFN-γ also reduce HBeAg production by HBV-infected hepatocytes.

HBV-specific $CD4^+$ T cells can help B cells to secrete neutralising antibodies, and induce and maintain successful $CD8^+$ T cell responses. Moreover, they execute effector function such as producing antiviral cytokines like TNF-α, IFN-γ and IL-2. It is reported that higher frequencies of functional HBV-specific memory $CD4^+$ T cells are associated with HBsAg loss(Hoogeveen et al., 2022). Higher Frequencies of TNF-α, IFN-γ or IL-2 producing HBV-specific $CD4^+$ T cells, but not $CD8^+$ T cells, are observed in patients acquired functional cure from chronic HBV infection compared to HBsAg-positive patients. However, TNF-α/IFN-γ profile of HBV-specific (core and surface protein) $CD4^+$ T cells, assessed by ICS after *in vitro* expansion of specific T cells, is discovered to be associated with clinical outcomes in patients with chronic HBV infection(Wang et al., 2020). HBV-specific $CD4^+$ T cells predominantly produce TNF-α in chronic HBV infection, and have

been shown to correlate with liver damage. Whereas IFN-γ producing HBV-specific $CD4^+$ T cells are associated with the decrease of HBsAg and viral clearance(Wang et al., 2020). Of note, $CD4^+$ CTLs have been found in patients with HBV infection(Aslan et al., 2006; Penna et al., 1992). However, the antigen specificity and effect on HBV infection of these $CD4^+$ CTLs is unclear.

Quantitative defect and dysfunction of HBV-specific T cell responses contribute to viral persistence. When compared to acute infection, the frequency of HBV-specific $CD4^+$ and $CD8^+$ T cells in patients with chronic infection is lower(Bertoletti & Ferrari, 2016; Boni et al., 2007). Additionally, HBV-specific T cells in chronic infection are significantly exhausted with high expression levels of inhibitory receptors, including programmed cell death protein (PD)-1, cytotoxic T-lymphocyte associated protein (CTLA)-4, lymphocyte-activation gene (LAG)-3, T cell immunoglobulin and mucin-domain containing (Tim)-3, and CD244(2B4)(Raziorrouh et al., 2010; A. Schurich et al., 2011; Ye et al., 2015). Persistent exposure of T cells to HBV antigens and the tolerogenic environment in the liver are thought to be essential for inducing and maintaining T cell exhaustion and inactivation(Maini & Pallett, 2018). This is supported by T cell functional restoration in patients with suppressed HBV replication after long-term treatment of nucleos(t)ide analogues(Boni et al., 2012b).

1.3 Severe acute respiratory syndrome coronavirus 2 (SARS-CoV-2)

1.3.1 Epidemiology

Coronavirus infectious disease 2019 (COVID-19), a global pandemic beginning in 2020, is caused by SARAS-CoV-2 infection(Zhou et al., 2020; Zhu et al., 2020). SARS-CoV-2 can spread through airborne, virus-bearing aerosols and contact transmission(Lotfi, Hamblin, & Rezaei, 2020; Zhang, Li, Zhang, Wang, & Molina, 2020). The majority of COVID-19 infections are relatively mild with recovery typically within 2-3 weeks, while a relatively low number of patients develop severe illnesses. As of September 2022, more than 600 million cases have been confirmed worldwide, and over six million deaths(WHO, 2022b).

1.3.2 SARS-CoV-2

SARS-CoV-2 is an enveloped virus with positive-sense, single-stranded RNA genome. It belongs to the genus betacoronavirus(Lu et al., 2020), together with SARS-CoV (with 79% homology), human coronavirus (HCoV)-OC43, HCoV-HKU1 and Middle East respiratory syndrome coronavirus (MERS-CoV, with 50% homology). The SARS-CoV-2 genome is packaged with structural proteins, including spike, envelope, membrane, and nucleoprotein. Additionally, the viral genome expresses non-structural proteins that modulate viral replication and host immune responses, such as ORF1a, ORF1b, ORF3a, ORF6, ORF7a, and ORF8(Kim et al., 2020). HCoV-OC43 and HCoV-HKU1 cause seasonal common cold. Conversely, SARS-CoV, MERS-CoV, and SARS-CoV-2 are the three

coronaviruses that have emerged in the last two decades and cause serious disease in humans.

SARS-CoV-2 entry into the host cell relies on spike interaction with angiotensin-converting enzyme 2 (ACE2), which was originally identified as the obligate receptor for SARS-CoV(Li et al., 2003). The receptor binding domain (RBD) of spike mediates direct contact with ACE2. When compared to SARS-CoV, the mutations in the RBD of SARS-CoV-2 spike are associate with a higher binding affinity to ACE2(Yan et al., 2020). In addition to ACE2, transmembrane protease, serine 2 (TMPRSS2) facilitates viral fusion entry by activating SARS-CoV-2 spike protein, by cleaving the S2 subunit(Jackson, Farzan, Chen, & Choe, 2022).

Numerous variants of SARS-CoV-2 have emerged worldwide which may be largely attributed to the scale of the pandemic. The sheer volume of viral replication subsequently increased the opportunity for adaptive mutations to occur. Many of the mutations affect viral properties, such as transmissibility, virulence, and disease severity. Based on this, viral variants have been categorised as variants of concern (VOC), variants of interest (VOI), and variants under monitoring (VUM). As of September 2022, five VOCs have rapidly spread and become the dominant circulating variants. They are Alpha (B.1.1.7), Beta (B.1.351), Gamma (P.1), Delta (B.1.617.2) and Omicron (B.1.1.529)(WHO, 2022a). Mutations frequently occur within the RBD and N-terminal domain (NTD) of spike, which act to diminish the function of many neutralising antibodies, and thereby facilitate host cell entry. The spread of variants is associated with immune

evasion of neutralising antibodies that are induced by vaccination and prior natural infection(Cao et al., 2022; Planas et al., 2021; Zhou et al., 2021). To visualise the differences between spike from the five VOCs and the original SARS-CoV-2 Wuhan strain, the aligned amino acid sequences and mutations are shown in Appendix Fig. 1.1.

1.3.3 The role of T cell immune responses in SARS-CoV-2 infection

T cell responses are essential to control SARS-CoV-2 infection and underpin vaccine efficacy. Early robust induction of T cell responses is associated with clinical protection(Bergamaschi et al., 2021). Circulating effector $CD8^+$ T cells expand at earlier stages of infection, and to higher levels in asymptomatic patients and those with mild symptoms(Bergamaschi et al., 2021). This is notably observed within seven days and peaking in fourteen days post-symptom onset. When compared to people with asymptomatic and mild disease, the reduction of $CD8^+$ T cells with effector memory phenotype and those expressing granzyme K in PBMCs is observed in patients with severe disease, detected by flow cytometry(Notarbartolo et al., 2021). In addition, in acute SARS-CoV-2 infection, Th1 responses are associated with mild disease, and conversely patients with severe symptoms have a $CD4^+$ T cell response skewed toward Th2 profile(Notarbartolo et al., 2021). However, the specificity of these T cells in the above studies was not identified and antiviral activity was not evaluated.

SARS-CoV-2 specific T cell responses have been identified using overlapping peptide pools spanning the sequences of viral structural and non-structural

proteins. COVID-19 convalescent individuals recovering from severe disease show stronger and broader memory T cell responses against SARS-CoV-2 assessed by IFN-γ ELISpot assays(Peng et al., 2020). Conversely, the proportion of SARS-CoV-2 specific $CD8^+$ T cells that produce TNF-α, IFN-γ or IL-2 is higher in individuals with mild disease, when compared to severe illness. Memory SARS-CoV-2 specific $CD4^+$ T cells are Th1 biased and display polyfunctional profile with simultaneous expression of CD154, TNF-α, IFN-γ, and IL-2(Cohen et al., 2021). In addition, $CD4^+$ T cells mount a broader response targeting multiple SARS-CoV-2 proteins. Conversely, $CD8^+$ T cells preferentially recognise the nucleocapsid protein, and the frequency of spike-specific $CD8^+$ T cells is remarkably lower. Cytotoxic $CD4^+$ T cells are also demonstrated in blood(Meckiff et al., 2020) and the lungs in COVID-19 patients(Kaneko et al., 2021).

Most SARS-CoV-2 vaccines induce adaptive immune responses against the spike protein. Therefore, deep characterisation of spike-specific immune responses resulting from natural infection is essential. Spike-specific T cells are $CD4^+$ dominant and support B cells to generate neutralising antibodies(Moss, 2022). Neutralising antibody titre positively correlates with spike-specific circulating Tfh cells(Juno et al., 2020). But little is known about dominant spike-specific $CD4^+$ T cell responses and their direct antiviral efficacy.

1.4 Specific aims and objectives

The aims of this thesis are to:

- **Map and characterise HBx-specific T cells (Chapter 3)**

Chronic HBV infection remains a significant health burden worldwide. HBV-specific T cell responses play pivotal roles in controlling viral infection. However, it is challenging to characterise HBV-specific T cells due to the low frequency in chronic infection. Numerous studies have elucidated core-, surface- and polymerase-specific T cells, but characterisation and functional profile of T cells against x protein remains largely unknown. I aim to:

1. Investigate the association of HBx-specific T cell responses with outcome of chronic HBV infection.
2. Identify immunodominant $CD4^+$/$CD8^+$ HBx-specific T cell responses in chronic HBV infection.
3. Characterise HBx-specific $CD4^+$/$CD8^+$ T cells, including functional avidity, cytokine profile, killing capacity and proliferation.
4. Evaluate antiviral activity of HBx-specific $CD4^+$/$CD8^+$ T cells using HBV infection cell model, $HepG2^{hNTCP}$ cell line.
5. Investigate TCR usage of HBx-specific $CD4^+$/$CD8^+$ T cell.

- **Viral mutations to escape SARS-CoV-2 specific T cell responses (Chapter 4)**

Numerous variants of SARS-CoV-2 have emerged worldwide due to its continuous evolution. As of September 2022, five VOCs have spread rapidly and become dominant in their area of origin or circulating worldwide. It has been well

studied that these variants escape from neutralising antibodies induced by vaccines or prior natural infection, which results from mutations in the RBD and NTD of spike. However, the majority of SARS-CoV-2 spike-specific $CD4^+$ and $CD8^+$ T cell responses generated by vaccination or previous infection are preserved and able to cross-recognise variants(Keeton et al., 2022; Tarke et al., 2022). The impact of viral mutations within other proteins except spike on T cell responses remain unclear. Thus, I aim to:

1. Characterise memory SARS-CoV-2 specific T cell responses in individuals recovered from COVID-19.
2. Identify immunodominant SARS-CoV-2 specific $CD4^+$ and $CD8^+$ T cell responses.
3. Evaluate the impact of the mutations within dominant SARS-CoV-2 epitopes on T cell functions.
4. Sequence TCR repertoires of polyclonal T cell lines employed to assess T cell functions, and to explore whether the variant evasion is biased to specific TCR clonotype.

- **Characterise dominant SARS-CoV-2 spike-specific $CD4^+$ T cell responses (Chapter 5)**

Rapid induction of SARS-CoV-2 specific T cell responses is associated with a favourable clinical prognosis. Recent SARS-CoV-2 $CD4^+$ T cell studies have been focused on the regulatory and helper function of these $CD4^+$ T cells. However,

effector function and antiviral activity of SARS-CoV-2 specific $CD4^+$ T cells remains largely unknown. Combining specific single cell transcriptomic profiling with TCR sequencing analysis and *in vitro* T cell functional assays, I aim to:

1. Identify immunodominant spike-specific $CD4^+$ T cell responses in individuals that have recovered from COVID-19.
2. Characterise the effector function of spike-specific $CD4^+$ T cells, including antigen sensitivity, cytokine production and cytotoxicity.
3. Assess the antiviral efficacy of spike-specific $CD4^+$ T cells using SARS-CoV-2 infected ACE2-transduced B cell lines.
4. Investigate the association of spike-specific $CD4^+$ T cell antiviral activity with cytotoxicity and cytokine production, alongside antigen load on virus-infected target cells.
5. Evaluate TCR usage and public TCR clonotypes amongst dominant spike-specific $CD4^+$ T cells.
6. Identify cytolytic pathways employed by spike-specific $CD4^+$ CTLs.
7. Investigate TCR repertoire changes and the antiviral activity of dominant spike-specific $CD4^+$ T cells over time post infection.

Chapter 2: Materials and Methods

2.1 Study participants

2.1.1 Patients with chronic HBV infection

Patients with chronic HBV infection were recruited from the Bejing YouAn Hospital in China. Peripheral blood was collected, and peripheral blood mononuclear cells (PBMCs) were isolated and stored by collaborators in Beijing YouAn Hospital. Written informed consent was obtained from all patients. Ethical approval was given by the YouAn Hospital Research Ethics Committee in China and by the Oxford Tropical Research Ethics Committee in England (OxTREC Ref. 60-11).

Clinical definitions of patients with HBV infection were defined as described in ref(Sarin et al., 2016). All patients were HBsAg seropositive for six months or more and in HBeAg positive/negative CHB or HBeAg negative chronic HBV infection stage. Chronic HBV infection is characterised by the presence of serum HBsAg for more than six months with HBeAg positive or negative. HBeAg clearance was defined as the loss of HBeAg in a person who was previously HBeAg positive. All participants were tested negative for HIV and HCV.

2.1.2 COVID-19 patients

COVID-19 patients were recruited from the John Radcliffe Hospital in Oxford, UK, between March 2020 and September 2021 by identification of patients hospitalised during the SARS-CoV-2 pandemic and recruited into the Sepsis Immunomics study. Patients were sampled at least 28 days after symptom onset.

Written informed consent was obtained from all patients. Ethical approval was given by the South Central-Oxford C Research Ethics Committee in England (ref. 19/SC/0296).

All COVID-19 patients were confirmed to have tested positive for SARS-CoV-2 using PCR with reverse transcription from an upper respiratory tract (nose and throat) swab tested at an accredited laboratory. The degree of severity was identified as mild, severe or critical infection, according to recommendations from the World Health Organization. Patients were classified as having mild symptoms if they did not require oxygen (that is, their oxygen saturation was greater than 93% on ambient air) or if their symptoms were managed at home. A large proportion of our mild cases were admitted to hospital for public health reasons during the early phase of the pandemic even though they had no medical reason to be admitted to hospital. Severe infection was defined as one of the following conditions in a patient confirmed as having COVID-19: respiratory distress with a respiratory rate of >30 breaths per minute; blood oxygen saturation of <93%; or arterial oxygen partial pressure/FiO2<300 mmHg. Critical infection was defined as: respiratory failure requiring mechanical ventilation or shock; or other organ failures requiring admission to an intensive care unit. Since the severe classification could potentially include individuals spanning a wide spectrum of disease severity, ranging from patients receiving oxygen through a nasal cannula through to those receiving non-invasive ventilation, we also calculated the SaO_2/FiO_2 ratio at the height of patient illness as a quantitative marker of lung

damage. This was calculated by dividing the oxygen saturation (as determined using a bedside pulse oximeter) by the fraction of inspired oxygen (21% for ambient air; 24% for nasal cannulae; 28% for simple face masks; 28, 35, 40 or 60% for Venturi face masks; or precise measurements for non-invasive or invasive ventilation settings). Patients not requiring oxygen who had oxygen saturations (if measured) greater than 93% on ambient air or managed at home were classified as having mild disease. Viral swab Ct values were not available for all patients. In addition, we standardised all of our analyses to the day of symptom onset.

2.2 Preparation of PBMCs

Blood was collected into ethylenediaminetetraacetic acid (EDTA) tubes (patients with chronic HBV infection) or heparin tubes (COVID patients), then PBMCs were isolated from fresh blood using lymphoprep density gradient centrifugation. Plasma was collected and aliquoted after centrifugation at 1500rpm for 10min without brake. Then blood was diluted with the same volume of RPMI medium and layered on lymphoprep at a volume ratio 2:1 follwed by centrifuging at 2000rpm for 20min without brake. Subsequently, PBMCs were aspirated and washed twice with RPMI. After counting, PBMCs were used for ELISpot assay or cryopreserved for further research.

2.3 Synthetic peptides

2.3.1 HBV peptides

A total of 393 15-mer peptides overlapping by 11 amino acid residues and spanning the consensus sequence of HBV genotypes circulating in China, covering core, surface, x and polymerase proteins, were designed using the software PeptGen (http://www.hiv.lanl.gov/content/sequence/PEPTGEN/peptgen.html) and synthesised (purity >75%). The overlapping peptides were placed into one-dimensional pools with each peptide pool containing no more than 52 single peptides (Appendix Table 2.1). Peptide pools recognised by T cells were divided into small pools, and each small pool comprised 6-10 individual peptides.

Peptides of two identified HBV-specific $CD8^+$ epitopes were synthesised by Sigma with purity>90%.

2.3.2 SARS-CoV-2 overlapping peptides

A total of 423 15- to 18-mer peptides overlapping by ten amino acid residues and spanning the full proteome of SARS-CoV-2 Wuhan strain except ORF1 were designed as described as for the HBV peptides and synthesised (purity >75%; ProImmune). The overlapping peptides spanning SARS-CoV-2 were assigned to a two-dimensional matrix system in which each peptide was represented in two different peptide pools. Each peptide pool contained no more than 16 individual peptides. The first dimension of the peptide matrix system was designed so that

peptides from different source proteins were separated into different pools (Appendix Table 2.2).

2.4 Cell lines and T cell clones

2.4.1 Generation of EBV-transformed B lymphoblastoid cell lines

EBV-transformed B lymphoblastoid cell lines were established to work as APCs and as target cells for some killing assays. 5×10^5 PBMCs were resuspended in 200µl of supernatant from B95-8 cells and added to round-bottom 96-well plate, 100µl per well. Then incubated 5-6hrs at 37°C in 5% CO2. Following incubation, 100µl of R20 (RPMI 1640 medium with 20% FBS, 2 mM glutamine and 100 mg/ml of penicillin–streptomycin) was added to each well and cyclosporin A (CSA) added to a final concentration of 1µg/ml. Cells were fed with R20 every 3–6 days and lines were expanded when medium became yellow and cells were confluent.

2.4.2 Generation of ACE2-transduced B cell lines

ACE-2 transduced B cells were established as described previously(Peng et al., 2022). The cDNA for the human *ACE2* gene (ENSG00000130234) was cloned into a lentiviral vector backbone (Addgene plasmid ID 17488), then co-transfected with packaging plasmids pMD2.G and psPAX2 into HEK293-TLA using PEIpro (Polyplus) to produce lentivirus. EBV-transformed B cell lines were infected with ACE2-coding lentivirus followed by cell sorting via flow cytometry to enrich ACE2-expressing B cells. B cells with stable expression of ACE2 were maintained with 0.5 µg/ml of puromycin (Thermo Fisher Scientific). *Mycoplasma* testing was

carried out every 4 weeks with all cell lines using MycoAlert detection kit (Lonza).

2.4.3 Generation of HLA-B*54:01- or HLA-DRA*01:01-DRB1*08:01-transduced HepG2^{hNTCP} cell lines

The cDNA for *HLA-B*54:01* (HLA00367) was cloned into a lentiviral vector with IRES2- EGFP (Fig. 2.1A), then co-transfected with packaging plasmids pMD2.G and psPAX2 into HEK293-TLA using PEIpro (Polyplus) to produce lentivirus. Similarly, lentivirus co-expressing HLA-DRA*01:01(HLA00662) and DRB1*08:01(HLA00723) was constructed (Fig. 2.1B). HepG2^{hNTCP} cells were infected with HLA-B*54:01- or HLA- DRA*01:01-DRB1*08:01-coding lentivirus by spinoculation. After trypsinization of nearly confluent HepG2^{hNTCP} cells, cells were resuspended with lentivirus at 1 TU/cell to a concentration of 2×10^6 cells/ml. Then seeded 1ml cell resuspension in each well of a six-well plate and spun down at 500g for 2hrs, followed by incubation overnight at 37°C in 5% CO_2. Subsequently, inoculation medium was removed and fresh D10 (DMEM medium with 10% FBS, 2 mM glutamine and 100 mg/ml of penicillin–streptomycin) was added. HLA-B54:01 and HLA-DR expression on HepG2^{hNTCP} cells was detected by GFP or HLA-DR staining using flow cytometry at day 3, 4, and 5 post lentivirus infection. HepG2^{hNTCP} cells expressing corresponding HLA alleles were sorted and enriched. Finally, HepG2^{hNTCP} cells with stable expression of transduced HLA alleles were maintained with 10 µg/ml of puromycin (Thermo Fisher Scientific). Wild type HepG2^{hNTCP} cell line was kindly supplied by Prof. Dr. Stephan Urban.

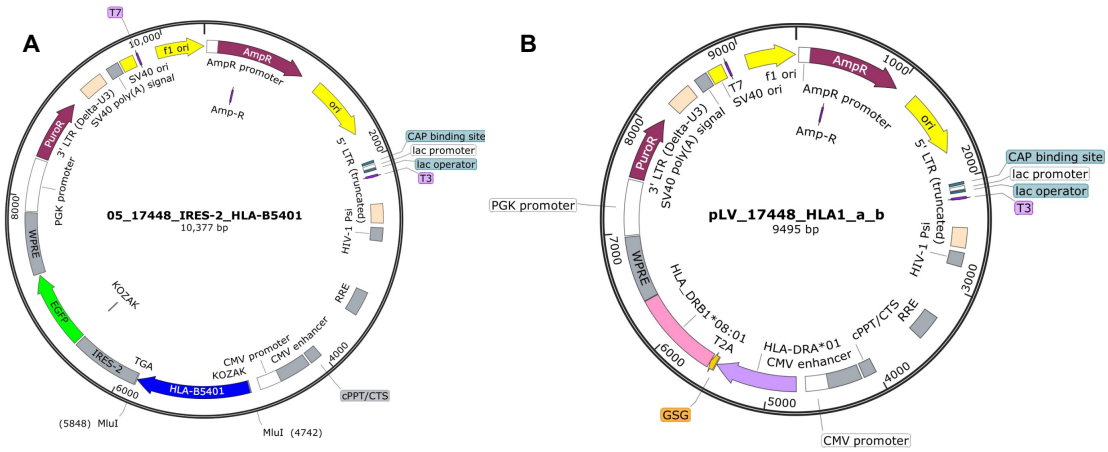

Fig. 2.1 Schematic structure of lentiviral constructs. Lentiviral construct of HLA-B*54:01 (A) and HLA-DRA1*01:01-DRB1*08:01 (B). Figure is created with SnapGene.

2.4.4 HepAD38 cell line

HepAD38 cell line inducibly produces HBV, which was kindly provided by Prof. Dr. Stephan Urban. HepAD38 cells were cultured in complete medium (DMEM/F-12 (Dulbecco's modified Eagle's/F-12 medium) with 10% FBS, 2 mM glutamine and 100 mg/ml of penicillin–streptomycin, non essential amino acids and 400µg/ml of geneticin) with or without tetracycline that inhibited HBV production. Cryopreserved HepAD38 cells were thawed into a T25 flask (Costar) in 5ml of complete media and the media was changed 24 hours later. Upon 80-90% confluency, the cells were washed once with PBS. Cells were subsequently trypsinized and washed once with complete media. Then resuspended cells with complete media and split into 2 T75 flasks. Cells were split twice a week.

2.4.5 Generation of T cell lines

To generate short-term antigen-specific T cell lines, 2 x 10^6 PBMCs were pulsed with 10 µM of peptides at 37°C for one hour, then washed once with R10 (RPMI

1640 medium with 10% FBS, 2 mM glutamine and 100 mg/ml of penicillin–streptomycin) and cultured in H10 (RPMI 1640 medium with 10% AB human serum, 2 mM glutamine and 100 mg/ml of penicillin–streptomycin) at 2-2.5 x 10^5 cells in 100µl per well of a round bottom 96-well plate (Costar). IL-2 was added to a final concentration of 200 IU/ml on day 3. Cells were fed with H10 with 200IU/ml every three days. At day 10-14, antigen specificity of short-term T cell lines was identified using IFN-γ ELISpot assay or ICS.

2.4.6 Establishment of T cell clones

2.4.6.1 HBV-specific T cell clones

TNF-α producing cells post stimulation with peptides were sorted from short-term T cell lines by fluorescence-activated cell sorting (FACS) using TNF-α secretion assay (Miltenyi). Subsequently, sorted cells were stimulated with irradiated allogeneic PBMCs, 1-2 cells with 2-2.5 x 10^5 irradiated PBMCs per well of a round bottom 96-well plate. Cultured in H10 containing polyhydroxyalkanoates (PHA) at a concentration of 50µg/ml. IL-2 was added to a final concentration of 200 IU/ml on day 3. Medium was refreshed every three days and the cells were split when the medium got yellow and cells were confluent. On day 12-14, T cell clones were confirmed for antigen specificity using ELISpot assay. Then, antigen-specific T cell clones were expanded with irradiated allogeneic PBMCs every 2-3 weeks.

2.4.6.2 SARS-CoV-2 specific T cell clones

SARS-CoV-2 S_{756}- and S_{866}-specific $CD4^+$ T cell clones were established by

FACS sorting tetramer$^+$ CD4$^+$ T cells, whereas other epitope-specific T cell clones were generated by sorting cytokine producing cells using TNF-α, IFN-γ and IL-2 secretion assays (Miltenyi). These tetramer$^+$ or cytokine producing cells were sorted from thawed PBMCs or short-term T cell lines at day 10-14 and clonally expanded as described above.

2.5 Pentamer/tetramer staining

SARS-CoV-2 epitope peptide-MHC class I Pentamers and peptide-MHC class II tetramers, except $S_{166\text{-}180}$-DPB1*04:01 tetramer, were supplied by ProImmune. $S_{166\text{-}180}$-DPB1*04:01 monomer and its negative control (PVS-DPB1*04:01) were obtained from from the National Institute of Health (NIH) Tetramer Core Facility (Atlanta, USA). Peptide-MHC class I monomers of HBV epitopes were constructed in the lab.

2.5.1 Tetramerisation of peptide-MHC molecule complex

$S_{166\text{-}180}$-DPB1*04:01 monomer and its negative control (PVS-DPB1804:01) were tetramerised using a conjugation kit of streptavidin labelled with allophycocyanin (APC) (Invitrogen). 25µl of streptavidin-APC was added to 100µg monomers followed by shaking at 4°C for 30 minutes protecting from light. This was repeated until 100µl of streptavidin-APC was added in total.

$Core_{26}$-A*02:10 and X_{146}-B*54:01 monomers were tetramerised using streptavidin and labelled with phycoerythrin (PE) (Sigma). Each vial contained 50µg of monomers. Similarly, 12.5, 12.5 and 25µl of streptavidin-PE was

successively added to monomers, with each individual addition followed by shaking.

2.5.2 Pentamer and tetramer staining

PBMCs, T cell cells or T cell clones were resuspended in R10 and labelled with peptide-MHC class I Pentamer or tetramer conjugated to PE. Following incubation at 37°C for 15 minutes, dead cells were first labelled with live/dead fixable Aqua dye (Invitrogen) and then with the surface markers and subsequent intracellular markers. Prior to adding peptide-MHC class II tetramer, T cell surface Fc receptors were blocked with Human TruStain FcX (Biolegend) to avoid non-specific binding. Moreover, tetramer incubation time was extended to 30 minutes.

2.6 Assays to evaluate antigen-specific T cell functions

2.6.1 IFN-γ enzyme-linked immunospot (ELISpot) assay

Ex vivo assays were carried out using either freshly isolated or cryopreserved PBMCs. Peptides were added to $2x10^5$ PBMCs at a final concentration of 2 μM for 16-18 hours. Plates were developed following manufacturer's instructions (Mabtech). For *in vitro* ELISpot assays, autologous and allogeneic EBV-transformed B cell lines were loaded with peptides, and subsequently cocultured with T cell clones or bulk cell lines at an effector:target (E:T) ratio of 1:50 for at least 6hrs. To quantify antigen-specific responses, mean spots of the control wells were subtracted from the sample wells, and the results expressed as spot forming units (SFU) per 10^6 PBMCs. Responses were considered positive if results were

at least 3x the mean of the quadruplicate negative control wells and >25 SFU/10^6 PBMCs. If negative control wells had >30 SFU/10^6 PBMCs or positive control wells (PHA stimulation) were negative, the results were excluded from further analysis.

2.6.2 Intracellular cytokine staining (ICS)

Short-term T cell lines were stimulated with peptides for six hours or T cell clones were cocultured with B cell lines loaded with peptides at 37°C for six hours with GolgiPlug and GolgiStop and stained with CD107a-PE (BD Bioscience). Cells were subsequently stained with Live/Dead Fixable Aqua dye (Invitrogen) followed by surface staining with CD4/CD8-PE-Cy7 (BD, Biosciences). Cells were permeabilised with Fixation/Permeabilisation solution (BD, Biosciences), then stained with IFN-γ-AF488 (BD Biosciences), TNF-α-APC (eBioscence) and IL-2-BV421 (BioLegend). Negative controls without peptide or without virus infection were set up for each sample. Samples were run on Attune NxT Flow Cytometer (software v.3.2.1) and analysed using FlowJo v.10 software (FlowJo LLC). Antibodies used for flow cytometry were shown in Table 2.1.

Table 2.1 Flow cytometry antibody information

Marker	Fluorophore	Supplier	Cat number	Clonotype	Lot number	Dilution
CD14	BV510	BioLegend	367124	63D3	B280762	1:50
CD16	BV510	BioLegend	302048	3G8	B289732	1:50
CD19	BV510	BioLegend	302242	HIB19	B281769	1:50
CD19	BV421	BioLegend	302234	HIB19	B342418	1:50
CD14	PE-CF594	BioLegend	367134	63D3	B268423	1:50
CD16	PE-CF594	BioLegend	302054	3G8	B274232	1:50
CD19	PE-CF594	BioLegend	302252	HIB19	B277039	1:50
CD3	BV785	BioLegend	317330	OKT3	B255880	1:33
CD4	FITC	BD Bioscience	347413	SK3/SK4	0349302	1:25
CD4	APC	BD Bioscience	345771	SK3	1111911	1:33
CD4	PE	BD Bioscience	345769	SK3	0335661	1:50
IFNγ	AF488	BD Bioscience	557718	B27	1299826	1:33
IFNγ	PE-Cy7	BD Bioscience	557643	B27	1046592	1:50
TNFα	APC	eBioscience	17-7349-82	Mab11	2330486	1:500
IL-2	BV421	BioLegend	500328	MQ1-17H12	B320878	1:33
CD107a	PE	BD Bioscience	555801	H4A3	0300011	1:20
ACE2	Primary	R&D	AF933	Polyclonal	HOK0620051	1:20
anti-goat	AF647	AbCam	ab150135		GR3324428-3	1:1000
CD3	FITC	BD Bioscience	340542	SK7	0106592	1:20
CD4	BV421	BioLegend	344632	SK3	B321520	1:50
CD8	BV421	BioLegend	344748	SK1	B331004	1:50
CD8	APC	BD Bioscience	340584	SK1	0162290	1:50
Perforin	FITC	Arigo Biolaboratories	ARG23363	B-D48	110915	1:14
granzyme B	APC/Fire750	BioLegend	372210	QA16A02	B344347	1:33
CD45RA	BV711	BioLegend	304138	HI100	B330318	1:33
CCR7	BV421	BD Bioscience	566743	2-L1-A	1123814	1:33
CD4	PerCP-cy5.5	BD Bioscience	560650	RPA-T4	0195614	1:33
CD8	BUV805	BD Bioscience	612889	SK1	0230991	1:33
CD3	BUV395	BD Bioscience	564001	SK7	1194980	1:100

2.6.3 Cytokine production assessment

To assess cytokine production, T cells were cocultured with B cell lines loaded with peptides at an E:T ratio of 2:1 for 48 hours at 37°C in 5% CO_2. Negative control wells without peptides were set up for each sample. 50ul of supernatant was then collected for cytokine measurement. Cytokines including IFN-γ, TNF-α, IL-2, IL-4, IL-6, IL-10, IL-13, RANTES and GM-CSF were quantified using the Bio-Plex Pro Human Cytokine Assay (Bio-Rad) following manufacturer's instruction. Standard wells containing all cytokines were set up for standard curve. Subsequently, samples were run on Bio-Plex 200 (Bio-Rad). Concentrations were analysed by the Bio-Plex Manager (Bio-Rad) using four-parameter logistic model.

2.6.4 CFSE-based cytotoxic T lymphocyte killing assay

EBV-transformed B lymphoblastoid cell lines were labelled with 0.5 μM carboxyfluoroscein succinimidyl ester (CFSE, ThermoFisher), then loaded with peptides at 37°C for one hour. To assess the MHC class II-dependence of the killing, B cells were treated with either 40ug/ml anti-HLA-DR antibody (BioLegend) or isotype control (BioLegend) at room temperature for one hour prior to being loaded with peptides. Subsequently, B cells were washed, counted and cocultured with T cells at desired E:T ratios at 37°C for six hours. Samples were then stained with 7-AAD (eBioscience) and CD19-BV421 (BioLegend). Cell death was assessed based on the presence of $CFSE^{+}CD19^{+}7\text{-}AAD^{-}$ (live) cells. Negative controls containing B cells without peptide pulsed and T cells were included for each sample. Samples were run on Attune NxT Flow Cytometer

(software v.3.2.1) and analysed using FlowJo v.10 software (FlowJo LLC).

2.6.5 CFSE-based proliferation assay

B cell lines were pulsed with titrated peptide (0.08μM, 0.4μM, 2μM, 5μM, 10μM) and then irradiated. T cells were stained with 0.5μM CFSE (ThermoFisher) before coculture with the irradiated B cells at 37°C for 72-96 hours. Cells were subsequently stained with 7-AAD (BioLegend) and CD4/CD8-BV421. Samples were then run on Attune NxT Flow Cytometer (software v.3.2.1) and analysed using FlowJo v.10 software (FlowJo LLC).

2.7 Sequencing of TCR repertoire

2.7.1 Deep sequencing of TCR repertoire of T cell clones

To sequence T cell clone TCR usage, total RNA was extracted from 5 x 10^5 cells of each clone using RNeasy Micro Kit (Qiagen), and 100-300ng of the RNA from each clone was used for the generation of full-length TCR repertoire libraries using SMARTer Human TCR a/b Profiling Kit/v2 (Takara) following the supplier's instruction. After purification, libraries of all clones were pooled and sequenced using MiSeq reagent Kit v.3 (600 cycles) on MiSeq (Illumina) with MiSeq Control Software v.2.6.2.1. Sequencing BCL files were converted to FASTQ files using bcl2fastq. TCRs were extracted using MiXCR and parsed into R as described earlier. TCRs were filtered to retain 1α1β or 2α1β for each clone.

2.7.2 TCR sequencing

RNA was extracted from T cell clones or bulk cell lines using the RNeasy Mini kit

(Qiagen), and cDNA was then synthesised employing SMARTer RACE cDNA amplification kit (Takara) following manufacturer's instructions. Subsequently, cDNA was amplified for TCR α and β chains using the PCR Advantage kit (Takara) with primers specific for *TRAC* (5'-GGAACTTTCTGGGCTGGGGAAGAAGGTGTCTTCTGG -3') and *TRBC* (5'-TGCTTCTGATGGCTCAAACACAGCGACCT-3'). PCR product was purified using the Monarch DNA Gel Extraction kit (New England BioLabs) and then cloned into TOPO TA and transformed into TOP10 competent cells (ThermoFisher) before being plated on lysogeny *broth (*LB) agar medium. Plasmid DNA was isolated and sent for sequencing.

2.8 Single cell RNA sequencing (scRNA-seq)

2.8.1 Cell sorting for scRNA-seq

2.8.1.1 $S_{166-180}$-specific $CD4^+$ T cells

$S_{166-180}$-specific $CD4^+$ T cells were sorted using cytokine secretion assay following the manufacturer's instructions (Miltenyi Biotec). Briefly, 1-3 x 10^6 cells were stimulated with $S_{166-180}$ peptide at a final concentration of 10 μM for five hours. Subsequently, cells were washed and incubated with TNF-α, IFN-γ, and IL-2 catching antibody for 45 mins, followed by staining with CD3-FITC, CD4-APC, CD14-PE-CF594, CD19-PE-CF594 and CD16-PE-CF594 (BD Biosciences), CD8-BV421 (BioLegend). Before sorting, cells were stained with Propidium Iodide (PI) (eBioscience) to exclude nonviable cells. After exclusion of nonviable/$CD14^+$/$CD19^+$/$CD16^+$cells, $CD3^+CD8^-CD4^+$TNF-α^+/IFN-γ^+/IL-2^+ cells

were sorted for scRNA-seq using a BD FACSAria Fusion sorter or BD FACS Aria III (BD Biosciences). Single cells were directly sorted into 96-well PCR plates (Thermo Fisher Scientific) and stored at −80°C for further SmartSeq2 analysis. Bulk cells were sorted into 1.5ml Eppendorf tubes (Eppendorf) for 10x scRNA-seq.

2.8.1.2 $S_{751-765}$- and $S_{866-880}$-specific $CD4^+$ T cells

$S_{751-765}$-and $S_{866-880}$-specific $CD4^+$ T cells were sorted with peptide-MHC-class II tetramers. In brief, 1-3 x 10^6 cells were stained with APC-conjugated HLA-DRB1*15:01 $S_{751-765}$ and $S_{866-880}$ tetramers (ProImmune) respectively. Live/dead fixable Aqua dye (Invitrogen) was used to exclude nonviable cells from the analysis. Cells were washed and stained with the following surface antibodies: CD3-FITC, CD4-PE (BD Biosciences), CD14-BV510, CD19-BV510, CD16-BV510 and CD8-BV421(BioLegend). After exclusion of nonviable/$CD14^+$/$CD19^+$/$CD16^+$cells, $CD3^+CD8^-CD4^+$tetramer$^+$ were sorted for scRNA-seq using the same sorter as above. Single cells sorted and stored at −80°C for further SmartSeq2 analysis, and bulk cells were sorted for 10x scRNA-seq as described previously.

2.8.2 SmartSeq2 scRNA-seq

ScRNA-seq with *ex vivo* sorted TNF-α^+/IFN-γ^+/IL-2^+ or tetramer$^+$ cells was performed using SmartSeq2 analysis. Reverse-transcription (RT) and PCR amplification were performed with the exception of using ISPCR primer with biotin

tagged at the 5′ end and increasing the number of cycles to 25. Sequencing libraries were prepared using the Nextera XT Library Preparation Kit (Illumina) and sequencing was performed on Illumina NextSeq sequencing platform with NextSeq Control Software v.4.

2.8.3 10x scRNA-seq

ScRNA-seq with TNF-α^+/IFN-γ^+/IL-2^+ or tetramer$^+$ cells sorted from short-term T cell lines was performed using Chromium Next GEM Single Cell V(D)J Reagent Kits (10x Genomics, PN-1000006) following manufacturer's instruction. Briefly, the cell suspension was loaded on 10X Chromium Controller (10x Genomics) to generate Gel Bead-in-Emulsions (GEMs). cDNA was amplified for the subsequent 5' gene expression (GEX) library (10x Genomics, PN-1000020), TCR library (10x Genomics, PN-1000005) and cell surface protein library construction (10x Genomics, PN-1000080). The 5' GEX libraries were sequenced on Illumina NovaSeq sequencing platform with NovaSeq Control Software v.1.7.5 (Illumina). The TCR libraries sequence were performed on Illumina MitSeq sequencing platform with MiSeq Control Software v.4 (Illumina).

2.9 In vitro live virus infection assays

2.9.1 HBV infection assays

2.9.1.1 HBV virus stocks

To generate HBV with high titre, supernatant of HepAD38 cells, which were cultivated in complete media without tetracycline, was collected followed by

clarifying at 3500rpm for 40min and filtering at 0.45μM. Subsequently the supernatant was concentrated using ultracentrifuge at 200,000g for two hours at 4°C through a 20% sucrose-density gradient. Following ultracentrifuging, all supernatant was removed without touching the virus pellet. The pellet was then resuspended with RPMI medium at approximately 100-fold concentration. Viruses were aliquoted then stored at -80°C. To detect the titre of concentrated HBV, DNA was extracted from 200μl virus using QIAamp DSP virus spin kit (Qiagen), followed by virus quantification using artus HBV RG PCR kit (Qiagen).

2.9.1.2 Live HBV infection

After trypsinization of nearly confluent cells, HepG2^{hNTCP} cells were resuspended in D10 to a concentration of 5×10^5/ml. 1×10^6 cell suspension was seeded in each well of six-well plate and cultured at 37°C in 5% CO_2. When cells reached 80-90% confluence, the medium was replaced with replication medium (DMEM medium with 10% FBS, 2 mM glutamine, 100 mg/ml of penicillin–streptomycin, and 2.5% DMSO). After three days, cells were inoculated with HBV (250μl virus, 50 μl 40% polyethylene glycol (PEG), 200 μl replication medium) for 24 hours at 37°C, after which cells were washed three times with PBS and cultured in replication medium at 37°C for seven days. Medium was replaced every 2-3 days.

2.9.1.3 T cell responses to live HBV infection

On day 7 post infection, medium of HepG2^{hNTCP} cells was discarded and cells were washed three times with PBS, followed by trypsinization. Cells were

resuspended in D10 and washed once. Then HepG2^{hNTCP} cells were cocultured with T cells at a desired E:T ratio for 6 hours with GolgiPlug, GolgiStop and CD107a (BD Bioscience). CD107a and cytokine TNF-α, IFN-γ, and IL-2 expression of T cells were assessed by ICS. Control wells of uninfected HepG2^{hNTCP} cells coculturing with T cells were included.

2.9.1.4 Lactate dehydrogenase (LDH)-based cytotoxicity assay

To evaluate the cytotoxicity of HBx-specific T cells to HBV-infected hepatocytes, HepG2^{hNTCP} cells were digested with trypsin, washed and counted on day 7 post-infection. Cells were resuspended in D10 to a concentration of 5×10^5 cells/ml and used to seed 200µl cell suspensions into each well of a 48-well plate. Cells were incubated at 37°C for 3-4 hours to let cells adhere to the bottom of the plate, then T cells in 200µl of H10 were added to each well at corresponding E:T ratios. Control wells containing HBV-infected HepG2^{hNTCP} cells only or cocultured with irrelevant T cells were included. After 72h, 50µl of supernatant was collected from each well. Levels of LDH released by dead cells was assessed using CytoTox 96 non-radioactive cytotoxicity assay (Promega), following manufacturer's instructions.

2.9.1.5 Live HBV suppression assay

On day 7 post infection, 5×10^4 HepG2^{hNTCP} cells in 100µl of D10 in each well of flat-bottom 96-well plate, were cocultured with 100µl of T cells in H10 at varying E:T ratios for 72 hours. Control wells containing HBV-infected HepG2^{hNTCP} cells

only or cocultured with irrelevant T cells were included. Supernatant was collected from each well and stored at -80°C for further detection of HBsAg and HBeAg. Cells were washed three times with PBS to remove T cells, then HepG2^{hNTCP} cells were lysed with RLT plus buffer (Qiagen) and stored at -80°C for further HBV DNA assessment.

2.9.1.5.1 HBsAg and HBeAg suppression

Secreted HBsAg and HBeAg levels in the supernatant were determined quantitatively by chemiluminescence immunoassay (CLIA) using commercial kits (Antobio) following manufacturer's instructions. 50µl of supernatant was collected and added to each well of the plate which had been precoated with antibodies cognate to HBsAg or HBeAg and incubated at 37°C for one hour protected from light. Following washing, 50µl of mixed substrates of A and B were added to each well and incubated at room temperature for at least 10min prior to plate reading. The plate was read with FLUOstar Omega reader at the luminescence detection mode. Concentrations were analysed using four-parameter logistic model. Suppression rate was calculated by the reduction of antigen concentrations when antigen-specific T cells were present.

2.9.1.5.2 Suppression of HBV DNA replication

Both DNA and RNA were extracted from HBV-infected HepG2^{hNTCP} cell lysis using AllPrep DNA/RNA Micro Kit (Qiagen). HBV DNA copies were quantified by real-time PCR using artus HBV RG PCR kit (Qiagen) following manufacturer's

instructions. 2μl of extracted DNA or standards were added into each well and the reaction volume was 10μl/well in 96-well plate. Triplicate wells were included for each sample and standard. Samples were run on 7500 Fast Real-Time PCR machine (Applied Biosystem). Suppression rate was calculated by the reduction of virus copies when antigen-specific T cells present.

2.9.2 Live SARS-CoV-2 infection

2.9.2.1 T cell responses to live SARS-CoV-2 infection

SARS-CoV-2 was propagated and titrated as previous described(Peng et al., 2022). The Omicron variant was provided by G. Screaton(Dejnirattisai et al., 2022). AEC2-transduced BCLs were infected with SARS-CoV-2 viruses at an MOI of 0.1 for two hours at 37°C, after which cells were washed and incubated at 37°C for 24 hours. Subsequently, cells were washed and cocultured with T cells at an E:T ratio of 1:1 for 6 hours with GolgiPlug, GolgStop and CD107a (BD Bioscience). Then CD107a expression and cytokine TNF-α, IFN-γ and IL-2 production of T cells were assessed by ICS.

2.9.2.2 Live SARS-CoV-2 virus suppression assay

B cell lines expressing ACE2 were infected with SARS-CoV-2 viruses at MOI 0.1 for two hours at 37°C. Cells were then washed and cocultured with T cells at an E:T ratio of 4:1 at 37°C. Control wells containing only virus-infected targets were included. After 48 hours of incubation, cells were washed with PBS and lysed with RLT buffer (Qiagen), followed by RNA extraction using RNeasy 96 Kit (Qiagen).

Viral copies were quantified using real-time qPCR, and the virus suppression rate was calculated by the reduction of viral copies when antigen-specific T cells were present.

2.10 Data analysis

2.10.1 ScRNA-seq data

2.10.1.1 SmartSeq2 scRNA-seq data processing

BCL files were converted to FASTQ format using bcl2fastq v2.20.0.422 (Illumina). FASTQ files were aligned to human genome hg19 using STAR v2.6.1d. Reads were counted using featureCounts (subread v2.0.0). The resulting counts matrix was analyzed in R v4.0.1 using Seurat v4.0.1.

2.10.1.2 10x scRNA-seq data processing

BCL files were converted to FASTQ files using cellranger mkfastq (Cellranger v.5.0.0). Counts matrices and sample demultiplexing was carried out using cellranger count (CellRanger) using with Feature Barcode options. For additional donor deconvolution, cellSNP v.0.3.2 was used to generate a list of SNPs from Cellranger output (BAM files), followed by Vireo v.0.5.6 to demultiplex sequencing data into individual patients from pooled sequenced libraries. The resulting counts matrix was analysed in R using Seurat.

2.10.1.3 ScRNA-seq analysis

Cells were filtered using the following criteria: minimum number of cells

expressing specific gene = 3, minimum number of genes expressed by cell = 200 and maximum number of genes expressed by cell = 4000. Cells were excluded if they expressed more than 5 – 10% mitochondrial genes. Patient-specific cells were integrated using Harmony v.1.0 to remove batch effects. The AddModuleScore function (Seurat) was used to look at the expression of specific gene sets (Supplementary Table 4). The average expression of a gene set was calculated, and the average expression levels of control gene sets were subtracted to generate a score for each cell relating to that particular gene set. Higher scores indicate that that specific signature is more highly expressed in a particular cell compared with the rest of the population. Cells with a module score ≥ 1 were defined as perforin-high; cells with a score ≤ 0.25 were defined as perforin-low. The FindMarkers function (Seurat) was used to evaluate differentially expressed genes (DEGs) between two conditions using MAST (Model-based Analysis of Single Cell Transcriptomics) statistical test, with different sequencing batches as latent variables. DEGs were visualized on volcano plots using EnhancedVolcano v1.6.0 and VlnPlot (Seurat).

2.10.1.4 SmartSeq2 and 10x TCR processing

TCR sequences were reconstructed from SmartSeq2 scRNA-seq FASTQ files using MiXCR v.3.0.13 to produce separate TRA and TRB output files for analysis. The output files were transferred into R using tcR v.2.3.2. TCR sequences were extracted from 10x VDJ sequencing using cellranger vdj (Cellranger). The resulting filtered_contig_annotations.csv file was analysed in R.

2.10.1.5 Single cell TCR repertoire analysis

TCRs were filtered to retain 1/2α or 1β; paired αβ cells consist of 1α1β or 2α1β. Clonotypes were defined as α (CDR3α amino acid + TRAV), β (CDRβ amino acid +TRBV) or paired αβ (CDR3α amino acid + TRAV + CDRβ amino acid +TRBV). Public clonotypes were defined as shared clonotypes between two or more patients. Circo plots were plotted using circlize v.0.4.12 showing paired TRAV-TRBV. Pie charts showing α clonotypes were plotted using ggplot2 v.3.3.2. Box plots comparing public/private clonotypes were plotted using ggplot2 and ggpubr v.0.4.0. Longitudinal TCRs were represented graphically using ggalluvial v.0.12.2.

2.10.2 Statistical analysis

EC_{50} calculations were performed with GraphPad Prism 9, all other statistics were analysed with IBM SPSS Statistics 27. Figures were made with GraphPad Prism 9. Chi-square was used to compare ratio difference between two groups. Data distribution normality was examined with Kolmogorov-Smirnov test. Mann-Whitney U test was employed to compare two groups, and Kruskal-Wallis one-way ANOVA was used to compare three groups. Correlation analysis was performed using Spearman's rank correlation coefficient. EC_{50} of T cell clones was calculated by using nonlinear regression with variable slope (four parameters) in a dose–response–stimulation model with GraphPad Prism. Statistical significance was set at $P<0.05$ and all tests were 2-tailed. For statistical analyses conducted using R, MAST test was used to find DEGs between two conditions, taking into account variation in batches and represented by volcano plots and

violin plots (adjusted *P* value shown). A Mann-Whitney nonparametric U-test was used for comparison between groups of public/private clonotypes (boxplots), the adjusted *P* value is shown (Benjamini-Hochberg). ns, not significant; *$P < 0.05$, **$P < 0.01$, ***$P < 0.001$, ****$P < 0.0001$.

Chapter 3: Characterisation of HBx-specific T cells

3.1 Introduction

HBV, a partially double-stranded hepatotropic DNA virus, causes acute and chronic hepatitis B in humans. The 3.2kb HBV genome is the smallest and most compact among DNA viruses, containing four overlapping open reading frames for polymerase, core, x and surface proteins(Gish et al., 2015; Tong & Revill, 2016). Both viral and host factors contribute to the outcome of HBV infection. The likelihood of HBV infection becoming chronic depends on the age when a person gets infected. HBV infection within the first five years of life most likely leads to chronic infection, which is defined as the persistence of HBsAg for six months or more(Trépo et al., 2014; Yuen et al., 2018). Patients with chronic HBV infection are at greater risk to develop liver cirrhosis and HCC(Sarin et al., 2016). More than 250 million people are chronically infected with HBV worldwide, resulting in more than one million deaths per year from HBV-related end stage liver disease, liver cirrhosis and hepatocellular carcinoma (HCC)(Revill et al., 2019; WHO, 2017). Thus, chronic HBV infection remains a significant public health burden worldwide.

Sustained HBsAg loss is a functional cure of CHB, since sterilising cure is not feasible due to the persistence of integrated HBV DNA and viral cccDNA(Lok, Zoulim, Dusheiko, & Ghany, 2017). Therefore, HBsAg clearance is the primary goal of treatment, indicating complete suppression of HBV replication and viral protein expression, alongside improved clinical outcomes. HBeAg loss is a

valuable therapy endpoint, representing a partial immune control of chronic infection (Liver, 2017). However, HBsAg loss is only rarely achieved even with long-term treatment. It is affected by HBeAg status, HBV DNA level and serum level of HBsAg (Kim et al., 2014; Yeo et al., 2019).

HBV-specific T cell responses are crucial to HBV clearance(Antonio Bertoletti & Ferrari, 2016; Adam J. Gehring & Protzer, 2019; Rivino et al., 2018; Wang et al., 2020). $CD8^+$ T cells can control and even eliminate HBV by lysing HBV-infected hepatocytes and secreting cytokines such as TNF-α and IFN-γ which control viral infection by noncytolytic mechanisms(Hoh et al., 2015; Xia et al., 2016). Whereas HBV-specific $CD4^+$ T cells can induce and maintain successful $CD8^+$ T cell responses, as well as execute effector function such as producing antiviral cytokines like TNF-α, IFN-γ, and IL-2. Of note, $CD4^+$ cytotoxic T lymphocytes (CTLs) are found in patients with HBV infection(Aslan et al., 2006; Penna et al., 1992). However, antigen specificity and function of these $CD4^+$ CTLs are unknown.

Dysfunction and impaired HBV-specific $CD4^+$ and $CD8^+$ T cells contribute to infection persistence(Bertoletti & Ferrari, 2016; Jung & Pape, 2002; Liang et al., 2015; Rehermann, 2013). Persistent exposure of T cells to HBV antigens is fundamental for maintaining T cell dysfunction. T cells can be stimulated not only by antigens presented by infected hepatocytes or APCs, but also by soluble HBsAg and HBeAg(Jin, Shih, & Berkower, 1988; van Montfoort et al., 2016). This is supported by functional restoration of T cells after HBsAg clearance(Boni et al.,

2012a; Zhu et al., 2016). Impaired HBV-specific T cell responses are also associated with the induction of immune checkpoints including PD-1, CTLA-4, 2B4, and Tim-3, which are highly expressed on HBV-specific T cells during chronic infection(Boni et al., 2007; Raziorrouh et al., 2010; Schurich et al., 2011). Therefore, characterisation of HBV-specific T cells poses a significant challenge due to T cell dysfunction and low T cell frequency in chronic infection.

Many reports of HBV-specific T cell responses have focused on T cells targeting core, polymerase and surface proteins(Hoogeveen et al., 2019; Schuch et al., 2019; Wang et al., 2020). However, T cell response against x protein (HBx) remains largely unknow. HBx is a small protein containing only 154 amino acids and expressed only on HBV-infected hepatocytes. It plays a major role in the development of HCC as well as HBV replication(Levrero & Zucman-Rossi, 2016). HBx promotes the viral gene expression by destroying structural maintenance of chromosomes (Smc) complex Smc5/6 that constitutively blocks extrachromosomal DNA transcription(Decorsière et al., 2016).

The aim of this project was to investigate the association of *ex vivo* HBx-specific T cell responses with clinical outcomes and characterise the *in vitro* functional profile, in particular, antiviral activity of HBx-specific T cells in patients with chronic HBV infection.

3.2 Results

3.2.1 HBx-specific T cell responses are associated with the outcome of chronic HBV infection

HBV core (HBc)-, surface (HBs)-, x (HBx)- and polymerase (HBp)-specific T cell responses in patients with chronic HBV infection were assessed by *ex vivo* IFN-γ ELISpot assays (*N*=74) with overlapping peptide pools spanning the consensus sequence of HBV genotypes (Appendix Table 2.1). Clinical and demographical information of these patients is shown in Appendix Table 3.1. First, we assessed HBV-specific T cell responses using *ex vivo* IFN-γ ELISpot assay. As shown in Fig. 3.1A and B, chronic HBV infection patients with HBeAg clearance displayed stronger HBx-specific T cell responses than those who were HBeAg positive (*N*=28 and *N*=46; *P*=0.023). Moreover, compared to HBeAg-positive patients, the proportion of responders to HBx was higher in HBeAg-negative patiens (*N*=28 and *N*=46; *P*=0.022). Whereas, no significant differences were observed regards HBc-, HBs- and HBp-specific T cell responses between HBeAg positive and negative patients (Fig. 3.1A, *P*=0.194, 0.734 and 0.829 respectively). Of note, the HBsAg level in patients showing HBx-specific T cell responses was significantly lower than that in those without HBx T cell responses (*N*=8 and 63; *P*=0.005; Fig. 3.1C). In summary, these data suggest that HBx-specific T cell responses might influence the clinical outcome of patients with chronic HBV infection and contribute to virus control.

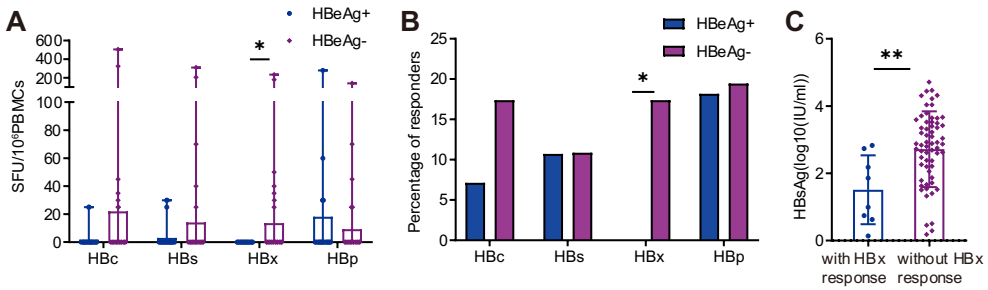

Fig. 3.1 HBV-specific T cell responses in chronic HBV infection. HBV-specific T cell responses targeting core, surface, x and polymerase proteins were assessed in patients with chronic HBV infection by ex vivo IFN-γ ELISpot assays. (A) Comparison of HBV-specific T cell responses between HBeAg positive (*N*=28) and HBeAg negative (*N*=46) patients. (B) Comparison of responder proportion between HBeAg positive (*N*=28) and HBeAg negative (*N*=46) patients. (C) Comparison of HBsAg levels between patients having (*N*=8) and not having HBx T cell response (*N*=63). Mann-Whitney U-test was used to compare distributions of two groups, ratio was compared using Chi-square test, and the two-tailed P value was calculated. * P<0.05, **P<0.01. SFU, spot-forming unit.

3.2.2 Identification of Immunodominant HBx-specific CD8⁺ and CD4⁺ T cell responses in patients with HBeAg loss

To explore the mechanisms of HBx-specific T cells associated with HBeAg-negative infection, immunodominant T cell responses were identified in seven patients who exhibited HBx-specific T cell responses.

3.2.2.1 Generating HBx-specific CD4⁺ and CD8⁺ bulk T cell lines and clones

Short-term T cell lines reactive to HBx were set up using PBMCs. TNF-α producing CD4⁺/CD8⁺ T cells post stimulation with the HBx peptide pool were sorted by FACS using TNF-α secretion assay, with no stimulation as negative control of each short-term T cell line for gating (Fig. 3.2). Subsequently, sorted cells were expanded *in vitro* as clones and bulk cell lines.

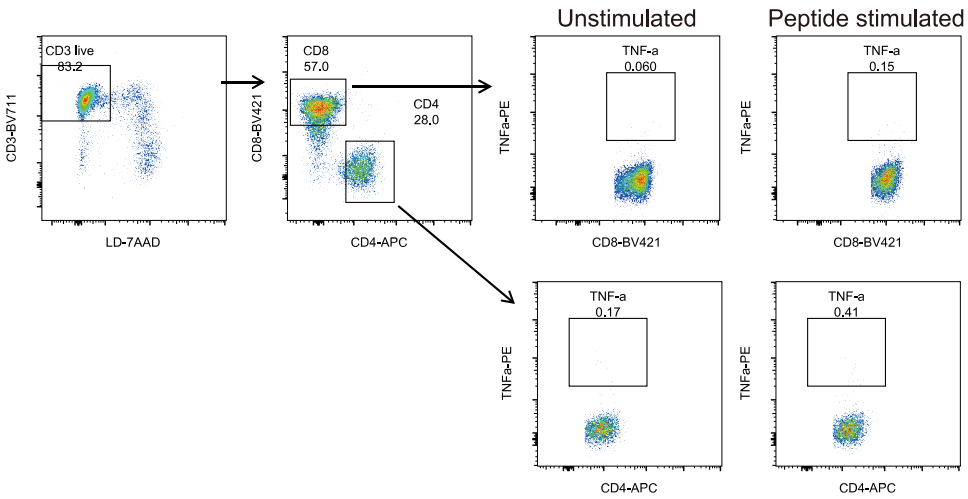

Fig. 3.2 Gating strategy of sorting TNF-α producing T cells. Short-term T cell lines were set up using PBMCs stimulated with peptide pools. TNF-α-producing T cells post stimulation were sorted by FACS from short-term T cell line to generate antigen-specific T cell bulk lines and clones. Negative control without peptide stimulation was included for each T cell line.

3.2.2.2 Identifying antigen specificity and HLA-restriction of HBx-specific CD4$^+$ T cells

The antigen specificity of CD4$^+$ T cell clones and bulk cell lines were identified by ELISpot assay using peptide-loaded autologous B cell lines (Fig. 3.3A). First, T cells were stimulated by autologous B cells loaded with small pools containing 6-10 overlapping peptides. Then, B cells were loaded with each single peptide in the small pool that can induce T cell response and cocultured with T cells for ELISpot. This result showed that T cell clones derived from patient S1 responded to peptide $X_{29\text{-}43}$(PVSGPLGTLPSPSPS) and peptide $X_{105\text{-}119}$(TTDLEAYFKDCLFKD), and T cell clones from patient S13 recognised peptide $X_{89\text{-}103}$(LPKVLHKRTLGLSAM). ELISpot results of identifying epitopes X_{29} and X_{105} and their HLA-restriction are not shown.

As the binding groove of MHC class II molecules is open and usually accommodates peptides of 13-25 residues to present to $CD4^+$ T cells(Chicz et al., 1992), the single peptide of 15 amino acid length that stimulated $CD4^+$ T cell response can be regarded as the epitope and was not further optimised.

To identify the restriction of $CD4^+$ T cell responses to HLA-DR, DQ or DP, T cells were treated with titrated levels of either anti-HLA-DR or -DQ antibodies (BioLegend) prior to peptide stimulation and ELISpot assays. X_{29}-specific T cell response was blocked by anti-DQ antibody, while X_{89}-specific T cell response was inhibited by anti-DR (Fig. 3.3B). In contrast, X_{105}-specific T cell response did not decrease with anti-DQ or -DR block. It demonstrates that X_{29}-, X_{89}- and X_{105}-specific T cell responses were restricted by HLA-DQ, -DR and -DP respectively. Then HLA-restriction of $CD4^+$ T cell epitopes were further determined by ELISpot assay using peptide-pulsed HLA-matched and -unmatched B cell lines (Fig. 3.3C). The ELISpot results indicate that X_{29}-specific T cells were restricted by HLA-DQB1*03:01, whereas the epitope of X_{89} and X_{105} was restricted by HLA-DRB1*08:01 and DPB1*05:01 respectively.

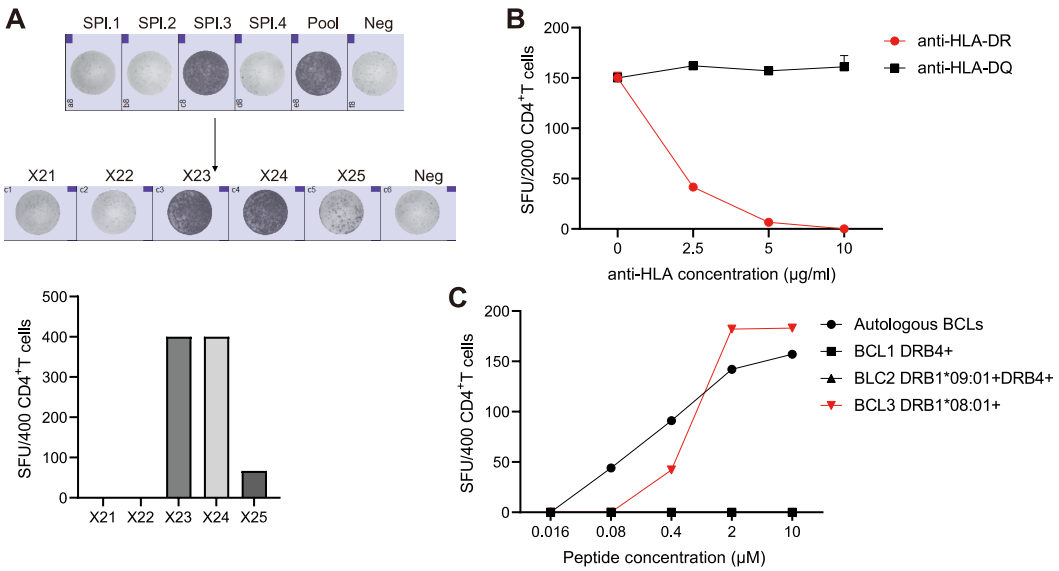

Fig. 3.3 HBx-specific CD4$^+$ T cell epitope X_{89} and HLA-restriction identification. Epitope X_{89} and HLA-restriction was identified by *in vitro* ELISpot assays using HBx-specific CD4$^+$ T cell bulk cell line. (A) Single peptide identification. Autologous B cells loaded with small pool3 induced HBx-specific CD4$^+$ T cell response. Single peptide X23 contained in the small pool3 stimulated the same level of T cell response. (B) HBx-specific CD4$^+$ T cells were treated with titrated concentrations of anti-HLA-DR or anti-HLA-DQ prior to peptide stimulation for ELISpot. HBx-specific CD4$^+$ T cell responses were inhibited by anti-HLA-DR, rather than anti-HLA-DQ. (C) To identify HLA-restriction, HBx-specific CD4$^+$ T cells were cocultured with HLA-matched and -unmatched B cell lines loaded with titrated peptide.

3.2.2.3 Identifying optimal epitope and HLA-restriction of HBx-specific CD8$^+$ T cells

Similarly, single peptides that recognised by CD8$^+$ T cell clones and bulk cell lines were identified by ELISpot assays using autologous B cell line loaded with small peptide pools and subsequently single peptides (Fig. 3.4A). HBx-specific CD8$^+$ T cells recognised the long peptide $X_{140\text{-}154}$(KLVCSPAPCNFFTSA).

Then to identify HLA-restriction of $CD8^+$ T cell response, T cells were cocultured with autologous B cell line, HLA typing of which was A*24:02-A*24:02-B*15:18-B*54:01-C*01:02-C*07:04, and allogeneic B cell lines with un- and matched HLA typing loaded with peptide. As shown in Fig. 3.4A, B cell lines carrying HLA-B*54:01-C*01:02 and A*24:02-B*54:01-C*01:02 respectively stimulated the equivalent T cell response as autologous B cell line, while B cell line carrying HLA-A*24:02, C*01:02 or B*15:18 did not induce T cell response. Thus, HBx-specific $CD8^+$ T cell response was restricted by HLA-B*54:01.

$CD8^+$ epitopes are usually of 8-10 residues in length. The optimal epitope within the long peptide (15aa) recognised by $CD8^+$ T cells was predicted using the Immune Epitope Database analysis resource (http://tools.iedb.org/mhci). The top six peptides with the strongest binding to B*54:01 were synthesised as shown in Table 3.1. Then, ELISpot was carried out using autologous B cells that were separately loaded with titrated predicted peptides, and the long peptide, then cocultured with $CD8^+$ T cells. The synthesised peptide of amino acids APCNFFTSA elicited the strongest T cell responses. Therefore, the optimal epitope recognised by $CD8^+$ T cells is $X_{146\text{-}154}$ (APCNFFTSA) (Fig. 3.4B). To further confirm this optimal CD8 epitope, peptide-HLA class I-tetramer X_{146}-B*54:01 was constructed in the lab. As observed from (Fig. 3.4C), X_{146}-specific $CD8^+$ T cells were positively stained with this tetramer.

So far, I have identified three $CD4^+$ T cell epitopes and one $CD8^+$ epitope of HBx. The amino acid sequences and HLA-restriction of these epitopes are shown in Table 3.2.

Table 3.1 Predicted $CD8^+$ T cell epitope contained in long peptide $X_{140-154}$

HLA allele	Position	Length	Amino acid sequence	Method	Percentile rank
B*54:01	141-154	14	LVCSPAPCNFFTSA	ann	0.26
B*54:01	143-154	12	CSPAPCNFFTSA	ann	0.41
B*54:01	146-154	9	APCNFFTSA	Consensus	0.5
B*54:01	142-154	13	VCSPAPCNFFTSA	ann	0.77
B*54:01	144-154	11	SPAPCNFFTSA	ann	0.78
B*54:01	144-152	9	SPAPCNFFT	Consensus	1.9

Consensus method includes ann, comblib_sidney2008, and smm

Table 3.2 Location, sequence, and HLA-restriction of identified HBx-specific $CD4^+$ and $CD8^+$ epitopes

Epitope	Position	Amino acid sequence	$CD4^+$/$CD8^+$ T cell epitope	HLA-restriction
X_{29}	29-43	PVSGPLGTLPSPSPS	$CD4^+$	DQB1*03:01
X_{89}	89-103	LPKVLHKRTLGLSAM	$CD4^+$	DRB1*08:01
X_{105}	105-119	TTDLEAYFKDCLFKD	$CD4^+$	DPB1*04:02
X_{146}	146-154	APCNFFTSA	$CD8^+$	B*54:01

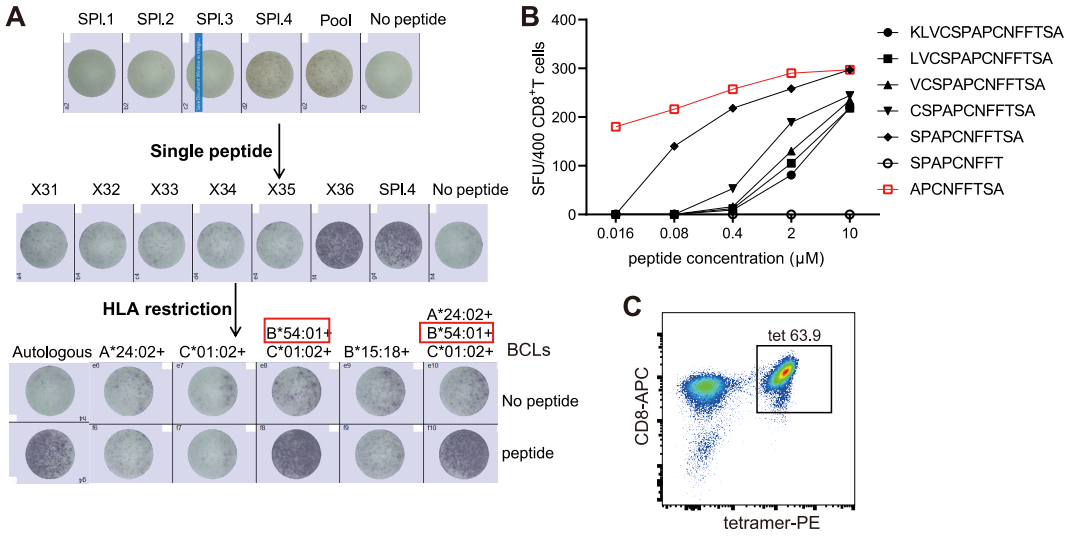

Fig. 3.4 HLA-restriction and optimal epitope identification of HBx-specific CD8$^+$ T cells. (A) Single peptide containing epitope was identified by *in vitro* ELISpot assays using HBx-specific CD8$^+$ T cell bulk line cocultured with autologous B cells loaded with peptide small pools and single peptides. HLA-restriction was identified using HLA-matched and -unmatched B cell lines loaded with single peptide. (B) Optimal epitope was confirmed by ELISpot assays coculturing T cells will autologous B cells loaded with titrated peptides. (C) Optimal epitope and HLA-restriction was verified by tetramer staining using HBx bulk T cell line.

3.2.3 Identification of HBc- and HBs-specific T cell epitopes

In order to compare functional profiles of HBx-specific T cells with T cells targeting other proteins, I also identified dominant HBc- and HBs-specific T cell responses. Similar to identification of HBx-specific T cells described above, TNF-α producing CD4$^+$/CD8$^+$ T cells were sorted post stimulation with peptide pools and the potential antigen-specific T cells were expanded *in vitro* to establish T cell clones and bulk cell lines.

3.2.3.1 Identifying $CD4^+$ and $CD8^+$ T cell epitopes of HBc and HLA-restriction

Antigen specificity and HLA-restriction of HBc-specific $CD4^+$ T cell clones were identified similarly to HBx-specific T cell clones (Fig. 3.5A). ELISpot results showed that small pool4 stimulated T cell response, in which the single peptide core38 ($C_{116\text{-}130}$(LEYLVSFGVWIRTPP)) induced the strongest T cell response. Thus, the epitope recognised by HBc-specific $CD4^+$ T cells was $C_{116\text{-}130}$.

To identify HLA-restriction of HBc-specific $CD4^+$ T cells, T cells were treated with titrated anti-HLA-DQ and anti-DR prior to peptide stimulation (Fig. 3.5B). The data showed that T cell responses were not blocked by anti-DQ or anti-DR antibody, which demonstrates that HBc-specific $CD4^+$ T cell response is restricted by HLA-DP. HLA typing of autologous B cell line is HLA-DPB1*05:01 and DPB1*135:01. Allogeneic B cell line bearing DPB1*05:01 but not DPB1*135:01 was loaded with peptide C_{116}, this stimulated the equivalent T cell responses as seen with the autologous B cell line (Fig. 3.5C). Hence, the HLA-restriction of C_{116}-specific $CD4^+$ T cells was HLA-DPB1*05:01.

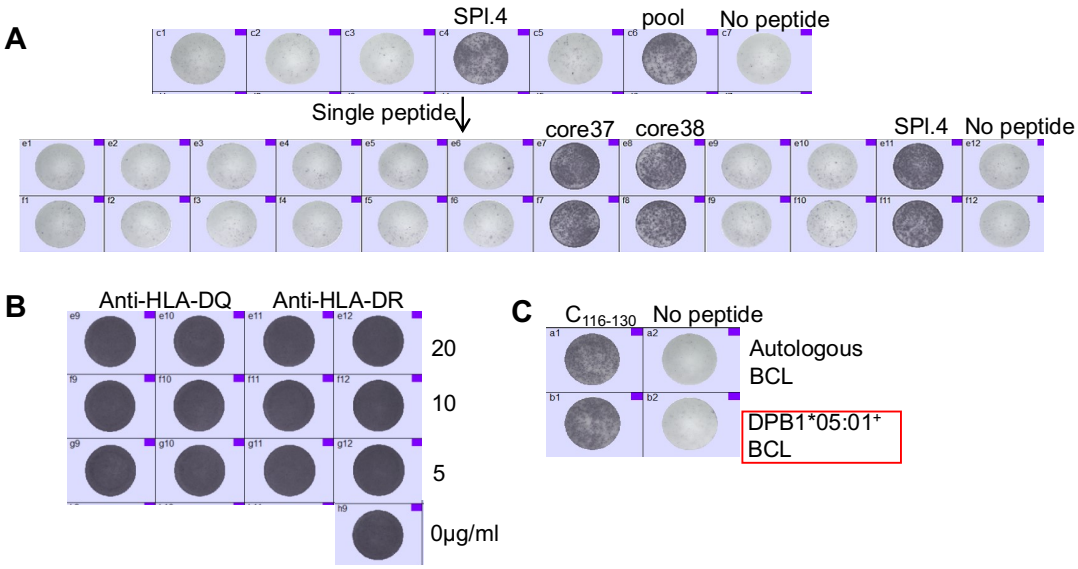

Fig. 3.5 HBc-specific CD4$^+$ T cell epitope and HLA-restriction identification. Epitopes and corresponding HLA-restriction of HBc-specific CD4$^+$ T cells were identified by ELISpot assays using HBc-specific T cell bulks. (A) CD4$^+$ T cell epitope C_{116} identification by in vitro ELISpot assays using autologous B cells loaded with small peptide pools and then single peptides respectively. (B) HLA-DR, -DQ and -DP restriction to HBc-specific CD4$^+$ T cell responses. (C) HLA-restriction of HBc-specific CD4$^+$ T cells was identified by ELISpot using autologous B cell line (DPB1*05:01$^+$DPB1*135:01$^+$) and allogenic B cell line (DPB1*05:01$^+$DPB1*135:01$^-$) loaded with C_{116} epitope peptide. BCL, B cell line.

Meanwhile, I observed strong IFN-γ response elicited by HBc-specific CD8$^+$ T cells to the small peptide pool containing single peptide core12 and to peptide core12 itself, indicating the potential epitope was contained within this peptide. The long peptide core12 contained a reported HLA-A*02:01 CD8$^+$ T cell epitope of $C_{18\text{-}27}$(FLPSDFFPSV)(M. K. Maini et al., 1999), and the patient from whom HBc-specific CD8$^+$ T cells derived is HLA-A*02:10 positive. This suggests that the epitope recognised by HBc-specific CD8$^+$ T cells is restricted by A*02:10. The optimal epitope restricted by HLA-A*02:10 was predicted using the Immune

Epitope Database analysis resource (http://tools.iedb.org/mhci). Among the top three predicted peptides (C_{18-26}(FLPSDFFPS), C_{19-27}(LPSDFFPSI) and C_{16-24}(LSFLPSDFF)), C_{18-26} induced greater T cell responses than the long peptide core12, whereas the other two peptides were not recognised by HBc-specific $CD8^+$ T cells (Fig. 3.6A). Collectively, the optimal $CD8^+$ T cell epitope was C_{18}-FLPSDFFPS.

To confirm HLA-restriction, T cell responses stimulated by B cell lines loaded with titrated peptides of the optimal epitope were assessed using ELISpot assay. HLA-A*02:10^+ B cell line induced notably stronger T cell response than A*02:01^+ B cell line (Fig. 3.6B). Thus, C_{18}-FLPSDFFPS-A*02:10 monomer was constructed in the lab and tetramer was conjugated to PE. The HLA-restriction and the optimal epitope of HBx-specific $CD8^+$ T cells were further confirmed by tetramer staining (Fig. 3.6C). C_{18}-specific $CD8^+$ T cells were positively stained with this tetramer.

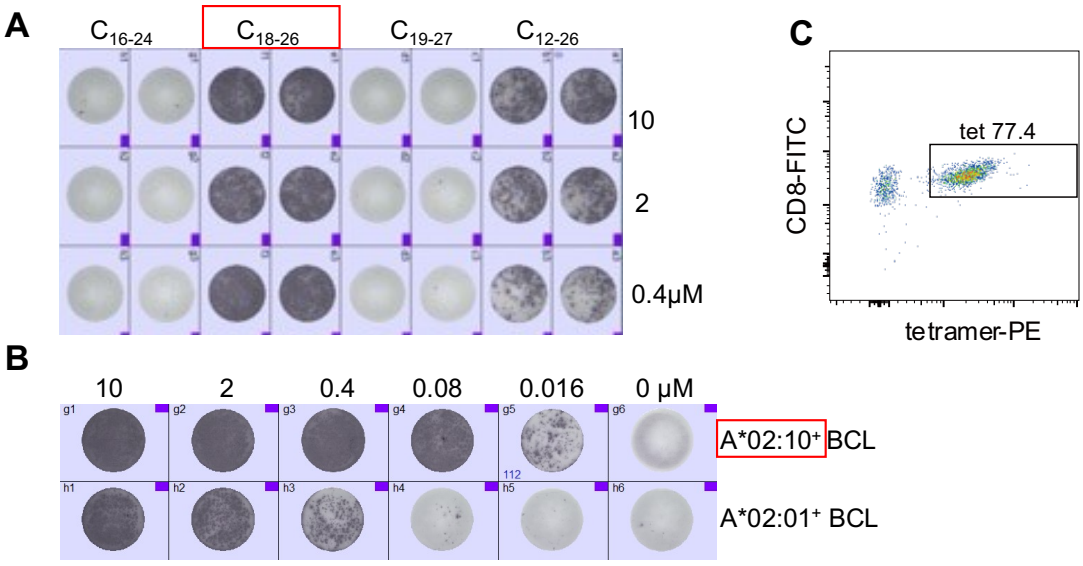

Fig. 3.6 HBc-specific $CD8^+$ T cell epitope and HLA-restriction identification. Epitopes and corresponding HLA-restriction of HBc-specific $CD8^+$ T cells were identified

by ELISpot assays using HBc-specific T cell bulk lines. (A) Optimal $CD8^+$ T cell epitope contained in the long peptide C_{12-26} was predicted and confirmed with ELISpot assay by coculturing HBc-specific $CD8^+$ T cells with autologous B cells loaded with titrated peptides. (B) HBc-specific $CD8^+$ T cell HLA-restriction was confirmed by ELISpot using autologous B cell line that was HLA-A*02:10 and allogenic B cell line carrying HLA-A*02:01 loaded with titrated epitope peptide. (C) Optimal HBc-specific $CD8^+$ T cell epitope and HLA-restriction was verified by peptide-MHC tetramer staining. BCL, B cell line.

3.2.3.2 Identify HBs $CD4^+$ T cell epitope and HLA-restriction

Short-term T cell lines specific to HBs were set up and TNF-α producing $CD4^+$ T cells were sorted using TNF-α secretion assay followed by subsequent expansion. Specificity of T cell clones and bulk lines against HBs was verified using ELISpot assay after the first round of feeder-expansion then by ICS for each successive round. As described above, the antigen specificity of $CD4^+$ T cell clones and bulk lines were identified by ELISpot assay (Fig. 3.7A). The ELISpot results demonstrated that HBs-specific $CD4^+$ T cells responded to the epitope S49 ($S_{182-196}$(FFLLTRILTIPQSLD)). The response was blocked by anti-HLA-DR but not anti-DQ, thus, this epitope S_{182} is presented by HLA-DR molecules to T cells (Fig. 3.7B). Furthermore, peptide loaded DRB1*12:01$^+$DRB3$^+$ B cell line induced the same level of T cell response as autologous B cell line, while neither $DRB3^+$ or DRB1*14:01$^+$DRB3$^+$ B cell line stimulated T cell responses (Fig. 3.7C). Therefore, S_{182}-specific $CD4^+$ T cell response is restricted to HLA-DRB1*12:01. This was further confirmed with ELISpot assay by coculturing HBs-specific $CD4^+$ T cells with autologous B cell line and allogenic DRB1*12:01$^+$ B cell line loaded with

titrated epitope peptide (Fig. 3.7D). Allogenic B cell line carrying DRBA*12:01 induced the equivalent T cell responses as seen to autologous B cell.

Collectively, I have identified one HBc-specific $CD8^+$, one HBc- and one HBs-specific $CD4^+$ epitopes as shown in Table 3.3. Of these, epitope C_{116} was previously identified, but its HLA-restriction was not defined(Penna et al., 1997).

Table 3.3 Location, sequence, and HLA-restriction of identified HBc- and HBs-specific T cell epitopes

Epitope	Protein	Position	Amino acid sequence	$CD4^+/CD8^+$ T cell response	HLA-restriction
C_{18}	core	18-26	FLPSDFFPS	$CD8^+$	A*02:10
C_{116}	core	116-130	LEYLVSFGVWIRTPP	$CD4^+$	DPB1*05:01
S_{182}	surface	182-196	FFLLTRILTIPQSLD	$CD4^+$	DRB1*12:01

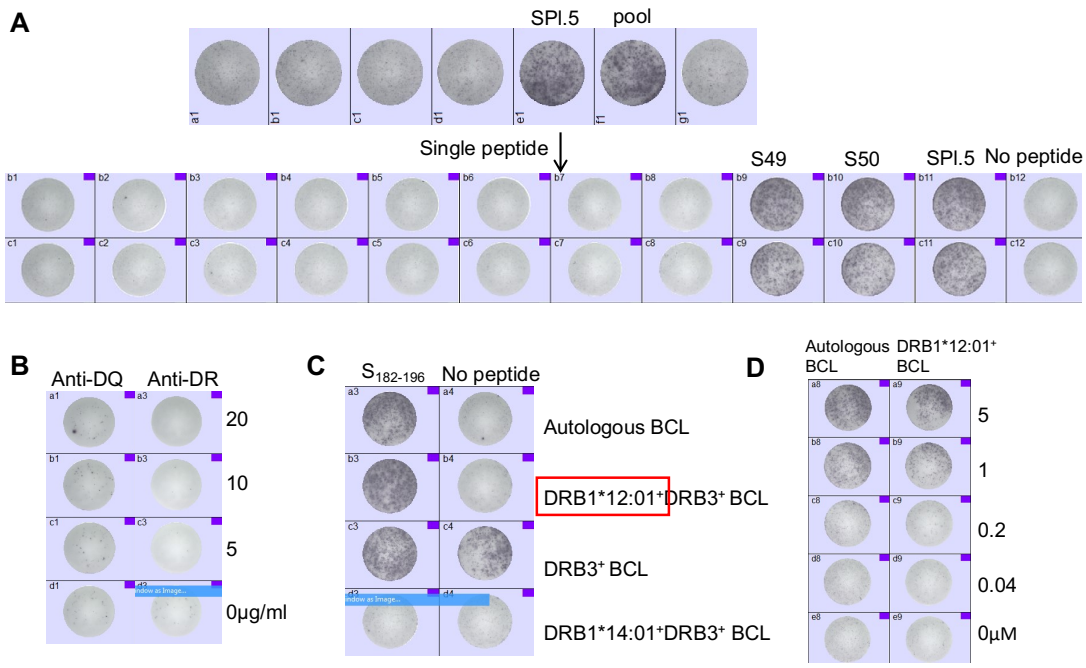

Fig. 3.7 Identifying HBs-specific $CD4^+$ T cell epitope and HLA-restriction. T cell epitope and HLA-restriction was identified by *in vitro* ELISpot assays using HBs-specific $CD4^+$ T cell bulk line. (A) HBc-specific $CD4^+$ T cell epitope identification by coculturing

HBs-specific $CD4^+$ T cells with autologous B cells loaded with small pools and subsequently single peptides. (B) HBs-specific $CD4^+$ T cells were blocked with anti-HLA-DR and -DQ prior to peptide stimulation for ELISpot. (C) To identify HLA-restriction, HBs-specific $CD4^+$ T cells were cocultured with HLA-matched and -unmatched B cell lines loaded with epitope peptide. (D) HBs-specific $CD4^+$ T cell HLA-restriction was confirmed by coculturing T cells with autologous B cells and allogenic B cells bearing DRB1*12:01 loaded with titrated epitope peptide. BCL, B cell line.

3.2.4 HBx_{146}-specific $CD8^+$ T cells exhibit high functional avidity and strong cytotoxicity

Twelve X_{146}-specific $CD8^+$ T cell clones and one bulk line were established from patient S19, and the antigen sensitivity of four of these T cell clones was assessed using ICS by coculturing T cells with autologous B cells loaded with titrated peptide. The gating strategy is shown in Fig. 3.8. X_{146}-specific $CD8^+$ T cells showed high functional avidity in terms of cytokine production including TNF-α, IFN-γ and IL-2, alongside with CD107a expression, with low EC_{50} (Fig. 3.9A).

Meanwhile, cytokine levels released by X_{146}-specific $CD8^+$ T cell clones into supernatant were measured by Luminex. Control wells were included for each clone, which contained only B cells or T cells coculturing with B cells without peptide pulse. When calculating cytokine secretion, the background of unstimulated T cells was subtracted from the respective experimental condition. Consistently, X_{146}-specific $CD8^+$ T cells stimulated by 0.4μM of peptide-pulsed B cells produced high levels of TNF-α and IFN-γ, with relatively lower levels of IL-2 and IL-5 (Fig. 3.9B). Interestingly, X_{146} $CD8^+$ T cells produced high levels of IL-10

at rest, and IL-10 expression decreased upon antigen stimulation (Fig. 3.9C). To confirm IL-10 was produced by T cells but not B cells, control wells containing only B cells were analysed. Only low levels of IL-10 ((18.02±3.861) pg/ml) were detected in these wells, which was subsequently subtracted to calculate IL-10 production by T cells.

Moreover, I assessed proliferation capacity of these X_{146}-specific $CD8^+$ T cell clones from patient S19, the proliferation dynamics of these T cell clones showed inter-patient variability, with 60% of CL5 and CL2, and 20% of CL15 and CL19 cells entering into G1 phase within four days of stimulation by autologous B cells loaded with 0.4μM of peptide (Fig. 3.9D). X_{146}-specific $CD8^+$ T cells were capable of killing HLA-B*54:01-transduced $HepG2^{hNTCP}$ cells loaded with peptide, even at the low E:T ratio of 1: 4 (Fig. 3.9E).

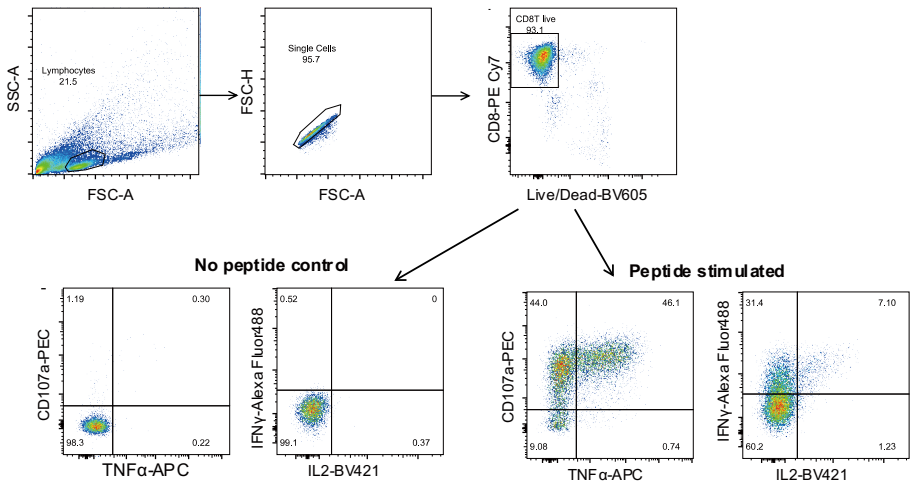

Fig. 3.8 The gating strategy for cytokine production and CD107a expression of HBV-specific T cells. X_{146}-specific $CD8^+$ T cell cytokine TNF-α, IFN-γ and IL-2 production, and CD107a expression were assessed by ICS when activated by peptide-loaded B cells, or HBV-infected $HepG2^{hNTCP}$ cells.

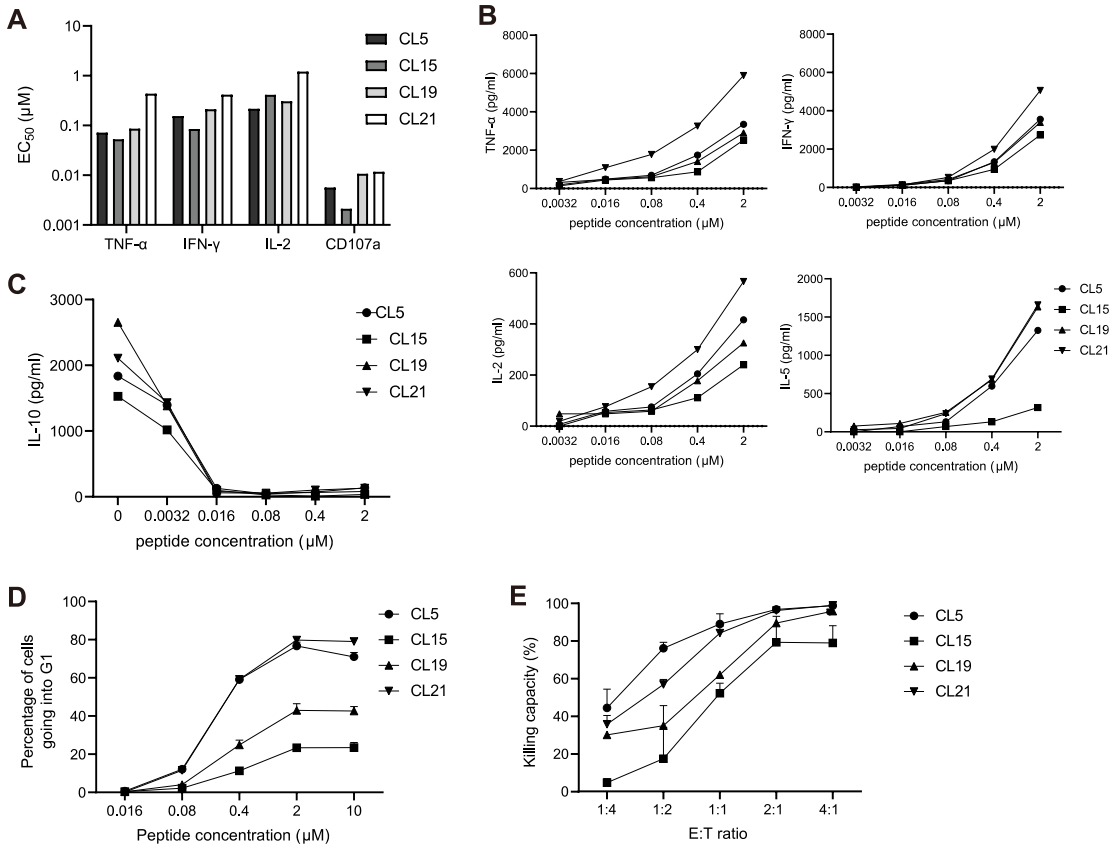

Fig. 3.9 Characterisation of X_{146}-specific $CD8^+$ T cells. Functional profiles of X_{146}-specfic $CD8^+$ T cells were evaluated *in vitro* using X_{146}-specific $CD8^+$ T cell clones. (A) X_{146}-specific $CD8^+$ T cell functional avidity (antigen sensitivity) upon stimulation was assessed by ICS. EC_{50} was calculated by cytokine TNF-α, IFN-γ and IL-2 production, and CD107a expression. (B) Cytokine (TNF-α, IFN-γ IL-2 and IL-5) levels secreted by X_{146}-specific $CD8^+$ T cells upon stimulation were measured by Luminex. (C) Cytokine IL-10 secreted by X_{146}-specific $CD8^+$ T cells at resting and upon stimulation. (D) X_{146}-specific $CD8^+$ T cell proliferative capacity when stimulated by autologous B cells loaded with titrated peptide. (E) X_{146}-specific $CD8^+$ T cell cytotoxicity to B*54:01-transduced $HepG2^{hNTCP}$ cells that were loaded with 0.4μM of peptide. T cells were cocultured with target cells at different E:T ratios for five hours, and killing capacity was assessed using CSFE-based cytotoxicity assay. ICS, intracellular cytokine staining.

3.2.5 Establishment of *in vitro* virus suppression system by coculturing HBx-specific T cells with HBV-infected $HepG2^{hNTCP}$ cells

Functional assays using B cell lines loaded with peptide are quite artificial, thus it

is very important to set up in vitro HBV infection system to evaluate antiviral activity of HBV-specific T cells.

3.2.5.1 Generation of HepG2^{hNTCP} cell line stably expressing HLA-B*54:01

HLA typing of wild type HepG2^{hNTCP} cell line is A*02:01-A*24:02-B*35:14-B*51:08-C*04:01-C*16:02. Hence, HepG2^{hNTCP} cells with stable expression of B*54:01 was established to act as targets for X_{146}-specific $CD8^+$ T cells. RNA was extracted from patient S19 B cell line bearing HLA-B*54:01, followed by cDNA synthesis. cDNA corresponding to B*54:01 was amplified using specific forward (5'-AGAGTAACGCGTATGCGGGTCACGGCACCCCGA-3') and reverse (5'-AGTTACGCGTTCAAGCTGTGAGAGACACATCAGAGCCCTGGGCACT-3') primers (Fig. 3.10A). Purified PCR product was cloned into TOPO TA vector and transformed into TOP10 competent cells. Transformed cells were plated onto LB agar and cultured at 37°C overnight. 48 colonies were picked and underwent PCR. Aliquots of each PCR product was run by gel electrophoresis and colonies containing plasmids with the optimal length in base pairs were cultured in LB (Fig. 3.10B). Optimal colonies were subsequently harvested for plasmid extraction and the plasmids were subsequently sequenced. The plasmid possessing the exact sequence (HLA00367) was digested with restriction enzyme MluI, followed by running through a gel and gel purification (Fig. 3.10C). cDNA of HLA-B*54:01 was subsequently cloned into a lentiviral vector which already contained EGFP, then transformed into DH5α competent cells and plated into agar. After colony culture and PCR (Fig. 3.10D), plasmid of lentiviral constructs was extracted and

sequenced to ensure B*54:01 cDNA was inserted correctly. Finally, the lentiviral construct was co-transfected with packaging plasmids pMD2.G and psPAX2 into HEK293-TLA using to produce lentivirus.

HepG2^{hNTCP} cells were transduced with the generated lentivirus. The expression of HLA-B*54:01 on HepG2^{hNTCP} cells was detected by flow cytometry from day 2 to day 10 post transduction (Fig. 3.10E). As there was no readily available B*54:01 specific antibody, surrogate B*54:01 expression was determined by GFP co-transduction and expression. The MFI of GFP and fraction of cells expressing GFP were highest on day 5. Hence, GFP expressing HepG2^{hNTCP} cells were sorted on day 5 post transduction, then cultured in medium containing puromycin. GFP expression was regularly checked, and only when ≥90% of cells were GFP positive where HepG2^{hNTCP} cells used for HBV-infection or peptide pulse (Fig. 3.10F). The ability of B*54:01 transduced HepG2^{hNTCP} cells to present X_{146} epitope was confirmed using ICS (Fig. 3.10G). X_{146}-specific $CD8^+$ T cells recognised peptide presented by HepG2^{hNTCP} cells and produced comparable levels of TNF-α as X_{146}-specific $CD8^+$ T cells stimulated by autologous B cells loaded with the same concentration of peptide.

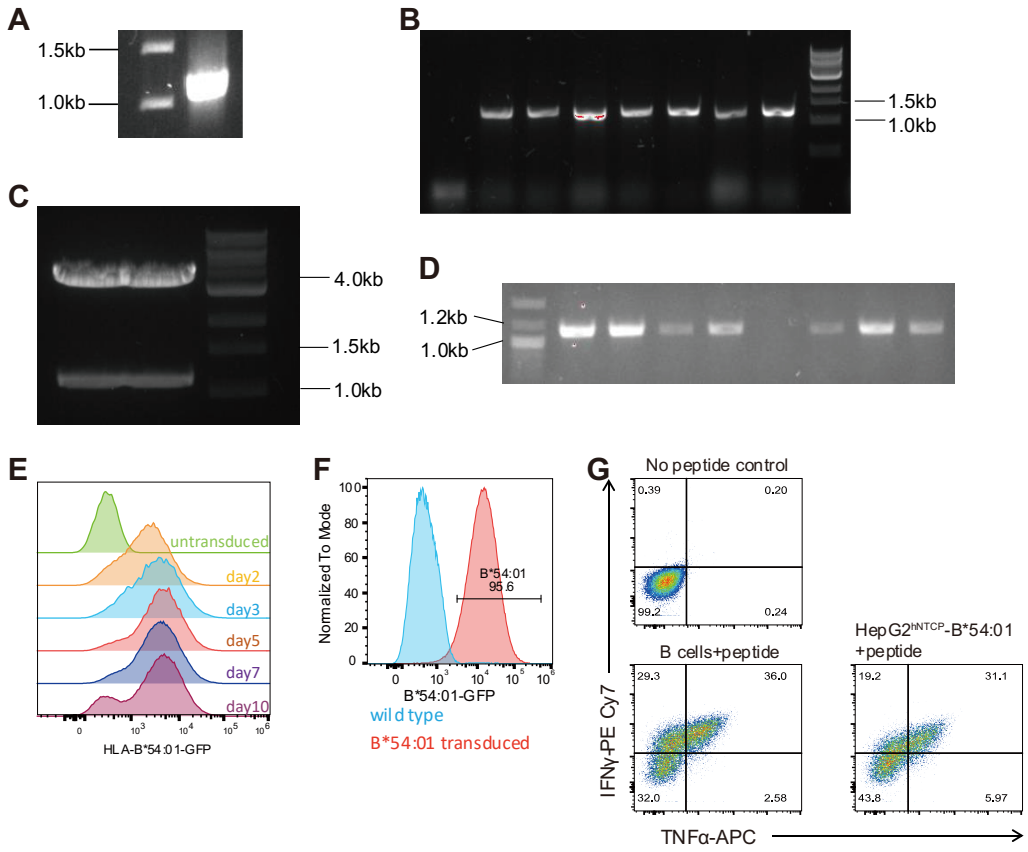

Fig. 3.10 Generation of HepG2^{hNTCP} cell line stably expressing HLA-B*54:01. HLA-B*54:01 was transduced into HepG2^{hNTCP} cells and expressed on the cell surface. (A) DNA gel running of amplified B*54:01 cDNA by PCR using specific primers. (B) DNA gel running of colony PCR products to check whether B*54:01 cDNA was cloned into TOPO TA vector. (C) Gel electrophoresis result of TOPO TA vector cloned with B*54:01 cDNA which was digested with restriction enzyme. (D) DNA gel electrophoresis result of colony PCR products with lentiviral construct as template. (E) GFP expression in HepG2^{hNTCP} cells at different time points post-transduction with B*54:01 lentivirus. (F) B*54:01 expression on the surface of HepG2^{hNTCP} cells. (G) The ability of HepG2^{hNTCP} cells, that stably expressed B*54:01, to present X_{146} epitope peptide to X_{146}-specific $CD8^+$ T cells.

3.2.5.2 Establish HepG2^{hNTCP} cell line with stable co-expression of HLA-DRA*01:01 and DRB1*08:01

Wild type HepG2^{hNTCP} cell line does not express HLA-DR. Thus, to investigate

antiviral activity of X_{89}-specific $CD4^+$ T cells, a $HepG2^{hNTCP}$ cell line co-expressing HLA-DRA*01:01 and DRB1*08:01 was generated. cDNA of DRA*01:01 and DRB1:08:01 was cloned into a lentiviral vector, with T2A sequence connected between the two cDNAs. This enabled DRA*01:01 and DRB1:08:01 co-expression on $HepG2^{hNTCP}$ cells after lentivirus transduction. HLA-DR expressing $HepG2^{hNTCP}$ cells were sorted on day 5 post lentivirus transduction (Fig. 3.11A). HLA-DR expression on $HepG2^{hNTCP}$ cells was measured by flow cytometry prior to HBV infection, and only when the frequency was $\geq$85%, $HepG2^{hNTCP}$ cells would be infected with HBV to evaluate antiviral efficacy of X_{89}-specific $CD4^+$ T cells (Fig. 3.11B). Antigen presentation capacity of HLA-DR transduced $HepG2^{hNTCP}$ cells was confirmed using ICS by coculturing X_{89}-specific $CD4^+$ T cells with half of the number of B cells or DR-transduced $HepG2^{hNTCP}$ cells loaded with titrated peptides. The data showed that X_{89}-specific $CD4^+$ T cell responses induced by DR-transduced $HepG2^{hNTCP}$ cells were lower than those stimulated by B cells (Fig. 3.11C). This indicates the ability of DR-transduced $HepG2^{hNTCP}$ cells to present $CD4^+$ T cell epitope antigens was lower in comparison of B cells. Even though $\geq$85% of $HepG2^{hNTCP}$ cells were HLA-DR positive, the amount of HLA-DR molecules expressed on each $HepG2^{hNTCP}$ cell surface might be lower than that on each B cell.

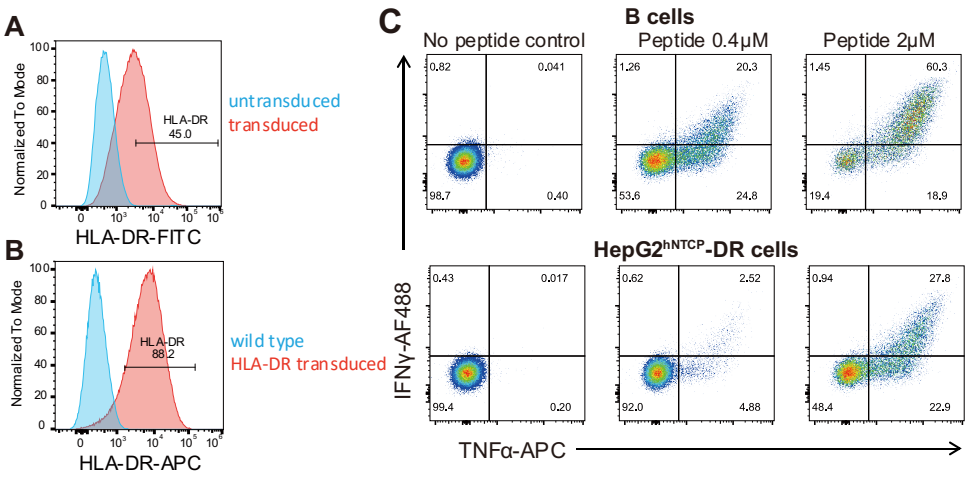

Fig. 3.11 Establishment of HepG2^{hNTCP} cell line with steady co-expression of HLA-DRA*01:01 and DRB1*08:01. HepG2^{hNTCP} cells were transduced with lentivirus cloned with both DRA*01:01 and DRB1*08:01 cDNAs. (A) HLA-DR expression on HepG2^{hNTCP} cells on day 5 post-transduction assessed by flow cytometry. (B) HLA-DR expression levels on HepG2^{hNTCP} cells were checked prior to HBV infection. (C) The comparison of peptide presentation capacity between HLA-DR-expressing HepG2^{hNTCP} cells and B cells.

3.2.5.3 *In vitro* HBV infection and coculturing with T cells

HepAD38 cell line inducibly produces HBV with stable transfection of cDNA of HBV pgRNA(Ladner et al., 1997). Hence, HepAD38 cells were cultured in medium without tetracycline and supernatant was collected when cells got approximately 90% confluent, followed by clarifying at 3500rpm for 40min and filtering at 0.45μM. Subsequently, the supernatant was concentrated, and virus titre was quantified by real-time PCR. The titre of virus stock was 7.4×10^{9}IU/ml (equal to 4.15×10^{10}copies/ml) with standard curve and application plot shown in Fig. 3.12A.

HepG2^{hNTCP} cells were infected at approximately multiplicities of HBV genome equivalents of 5000 and incubated for 24 hours following three days of

transformation with DMSO (Fig. 3.12B). On day 7 post-infection, the infection rate was detected by flow cytometry. HepG2^{hNTCP} cells were washed three times with PBS, then stained with Live/Dead Fixable Violet dye (Invitrogen). After subsequent permeabilization, cells were stained with anti-core antibody (DAKO, the antibody has been discontinued) followed by the staining of secondary antibody (anti-rabbit-AF488). The result showed that approximately 6% of HepG2^{hNTCP} cells expressed HBV core protein (Fig. 3.12C). Meanwhile, HepG2hNTCP cells were cocultured with HBV-specific T cells to evaluate their antiviral activity.

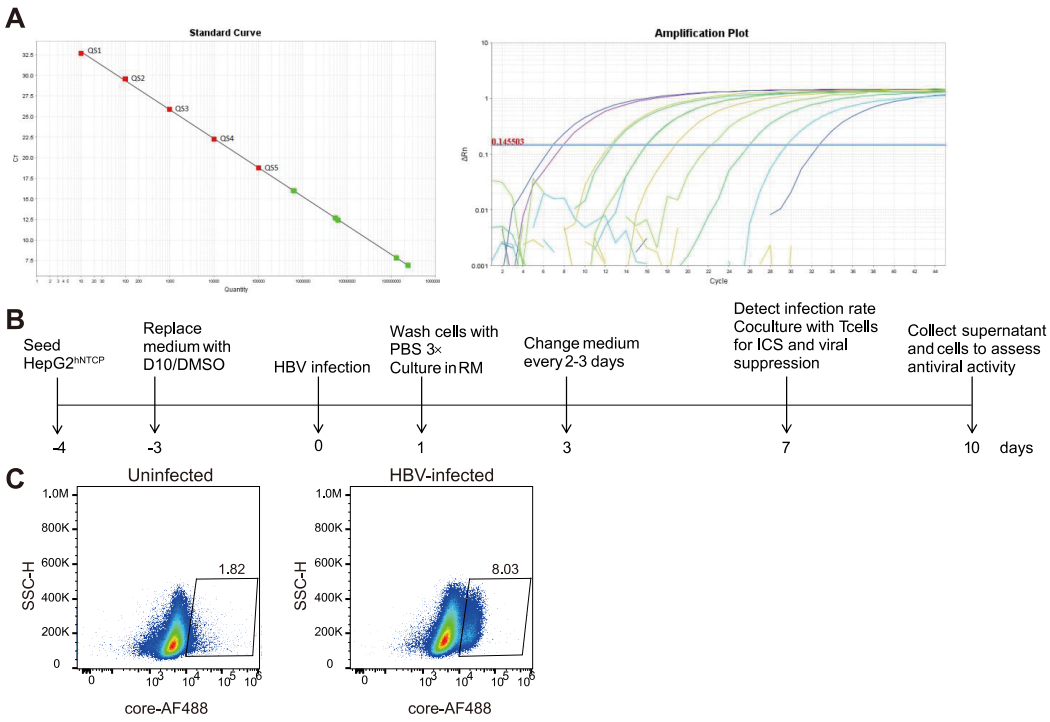

Fig. 3.12 *In vitro* HBV infection system. (A) Standard curve and amplification plot of real-time PCR measuring HBV viral stock titre. (B) Workflow of HBV infection, ICS, and viral suppression. (C) HBV infection rate assessed by flow cytometry staining with core antibody.

3.2.6 X_{146}-specific $CD8^+$ T cells display strong antiviral efficacy

HLA-B*54:01-HepG2^{hNTCP} cells were infected with HBV, then cocultured with X_{146}-specific $CD8^+$ T cells at an E:T ratio of 1:1 for 6 hours. X_{146} $CD8^+$ T cells can recognise HBV-infected cells assessed by ICS and produce cytokines and express CD107a after activation. A high proportion of T cells from four clones were activated when encountering HBV-infected cells, with 36-48% T cells expressing CD107a (degranulation marker) (Fig. 3.13A and B). Moreover, among T cells producing cytokines, the majority expressed both TNF-α and IFN-γ, while minimal cells produced IL-2 (Fig. 3.13C).

X_{146}-specific $CD8^+$ T cells showed strong cytotoxicity targeting HBV-infected HepG2^{hNTCP} cells. When cocultured with HBV-infected B*54:01-HepG2^{hNTCP} cells at an E:T ratio of 1:1, both CL5 and CL21 killed approximately 80% of HepG2^{hNTCP} cells (Fig. 3.13D), which was assessed by LDH-based cytotoxicity assay. Whereas the repression of HBeAg secretion was relatively lower with 25.45-36.54% of HBeAg suppressed by X_{146}-specific $CD8^+$ T cell clones when cocultured at an E:T ratio of 1:4 in comparison with irrelevant T cells (Fig. 3.13E). Conversely, remarkable suppression of HBV replication was observed in HepG2^{hNTCP} cells, and a dramatic reduction of HBsAg levels was seen in the supernatant within 72 hours after coculture at E:T ratios of 1:4 and 1:1 (Fig. 3.13F-G). Over 80% of HBV DNA was repressed in HepG2^{hNTCP} cells at an E:T ratio of 1:4 (Fig. 3.13F). Consistently, 78.88-92.19% of HBsAg was suppressed by X_{146}-specific $CD8^+$ T cell clones when cocultured at an E:T ratio of 1:4 in comparison with irrelevant T

cells (Fig. 3.13G). The suppression of HBsAg was more significant at an E:T ratio of 1:1 with a ~95% decrease in levels secreted (Fig. 3.13G).

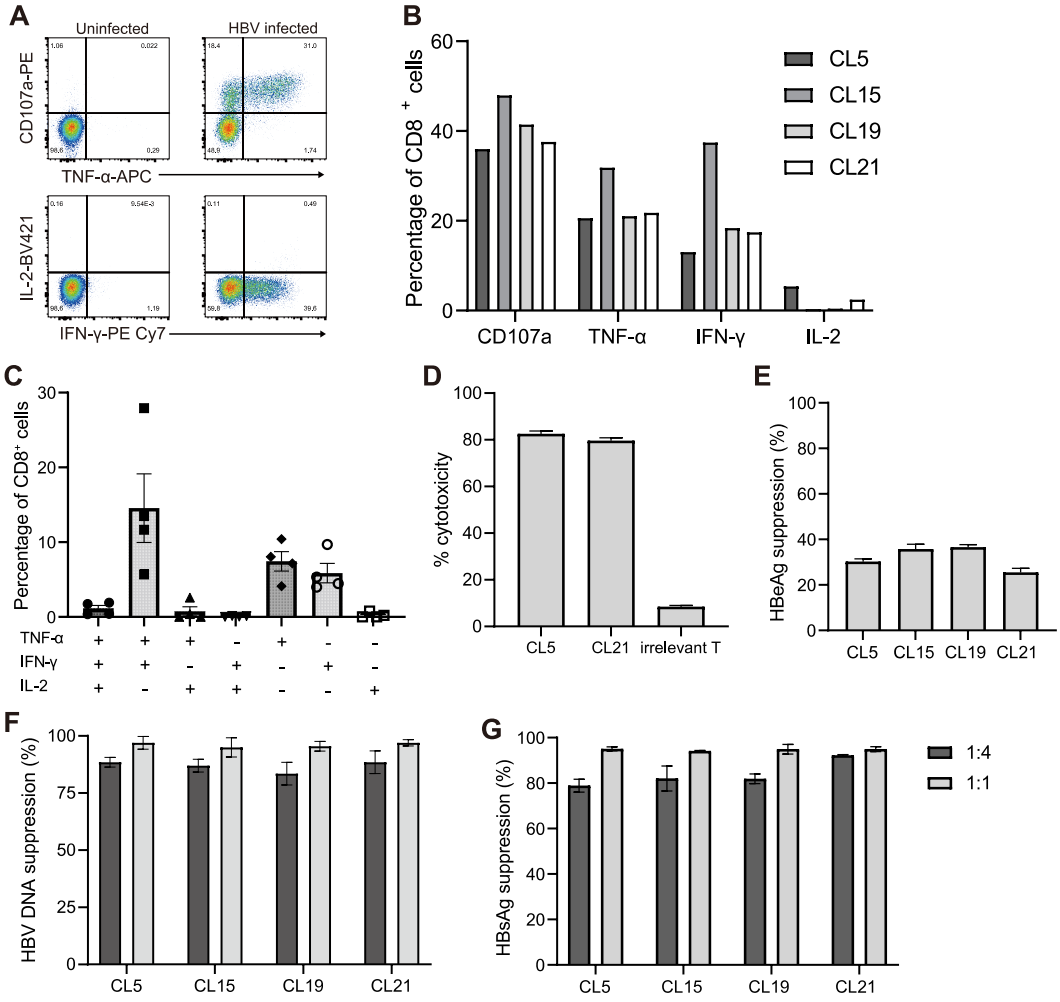

Fig. 3.13 X_{146}-specific $CD8^+$ T cell antiviral activity. Antiviral effector function of X_{146}-specific $CD8^+$ T cells was evaluated by *in vitro* HBV infection using T cell clones and bulk. (A) Representative ICS flow cytometry plots measuring TNF-α, IFN-γ, IL-2, and CD107a expression in $CD8^+$ T cells cocultured with HBV-infected $HepG2^{hNTCP}$ cells. (B) Frequency of $CD8^+$ T cells expressing TNF-α, IFN-γ, IL-2, or CD107a when encountered HBV-infected $HepG2^{hNTCP}$ cells. (C) Percentage of polyfunctional $CD8^+$ T cells expressing one to three cytokines assessed by ICS coculturing with HBV-infected $HepG2^{hNTCP}$ cells. (D) X_{146}-specific $CD8^+$ T cell cytotoxicity to HBV-infected $HepG2^{hNTCP}$ cells at an E:T ratio of 1:1. (E) Repression of HBeAg production at an E:T ratio of 1:1. Suppression of intracellular HBV DNA in HBV-infected $HepG2^{hNTCP}$ cells (F) and secreted HBsAg in the

supernatant (G) at E:T ratios of 1:4 and 1:1.

3.2.7 HBx-specific CD4$^+$ T cells show effector function

I also characterised HBx-specific CD4$^+$ T cell responses that were identified in this study by using, X_{29}-, X_{89}- and X_{105}-specific T cell clones generated from patient S1 and S13. I found that all clones expressed cytokines including TNF-α, IFN-γ and IL-2 upon antigen stimulation (Fig. 3.14A). Antigen sensitivity of these CD4$^+$ T cell clones was measured by ICS. X_{29}-specific T cell clones displayed the highest antigen sensitivity, with the lowest EC_{50} calculated from TNF-α, IFN-γ and IL-2 production (*P*=1.0167E-9, 0.015 and 0.012 respectively; Fig. 3.14A). Consistently, X_{29}-specific T cells released the highest levels of TNF-α and IL-2 into the supernatant when activated by peptide-loaded B cells, which were measured by Luminex (*P*=0.065 and 0.028; Fig. 3.13B), while X_{89} CD4$^+$ T cells produced the highest level of IFN-γ (*P*=0.000305; Fig. 3.14B). In contrast, X_{105} CD4$^+$ T cell clones did not produce IFN-γ or IL-2, but instead secreted the highest level of IL-10 (*P*=0.014; Fig. 3.14C). X_{29}-, X_{89}- and X_{105}-speciifc CD4$^+$ T cells did not show any significant differences in the production of IL-4, IL-5 and IL-13 (*P*=0.151, 0.074 and 0.155 respectively; Fig. 3.14D).

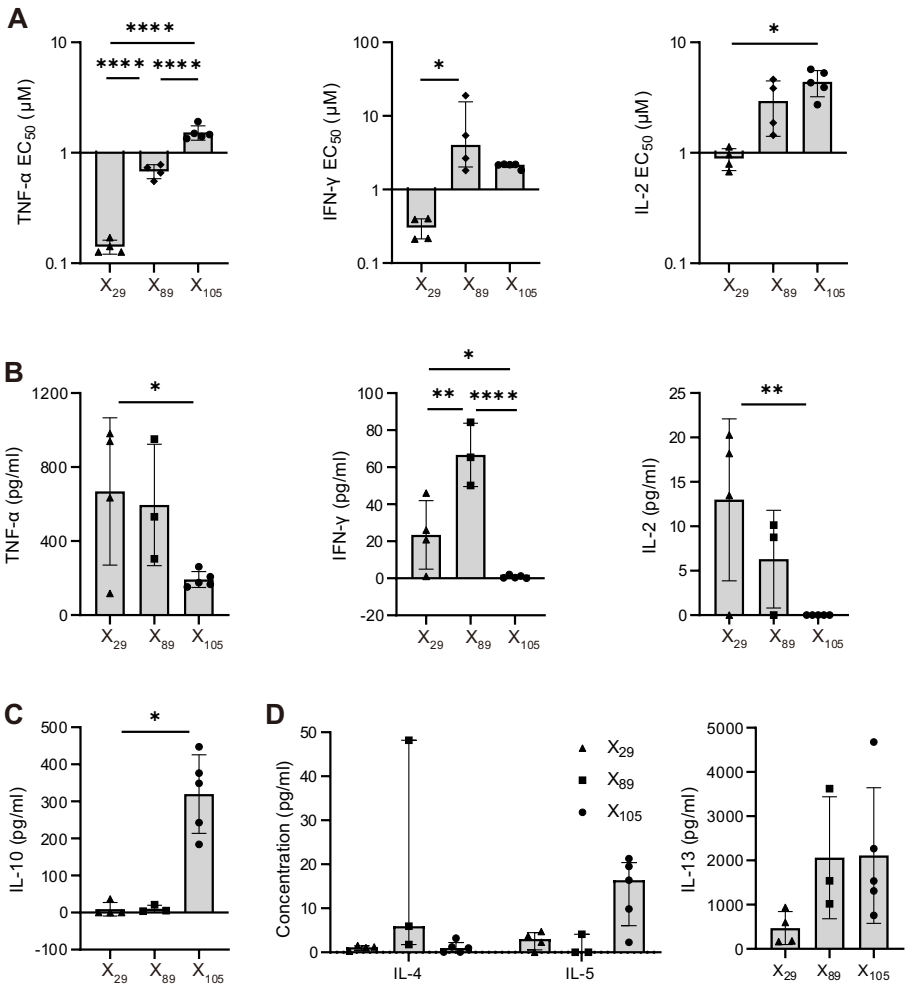

Fig. 3.14 Comparison of HBx-specific CD4⁺ T cell effector function. Functional avidity and cytokine production was assessed in vitro using $CD4^+$ T cell clones targeting the three x epitopes. (A) Comparison of antigen sensitivity. EC_{50} was calculated by cytokine production (TNF-α, IFN-γ, and IL-2) upon stimulation assessed by ICS using autologous B cells loaded with titrated peptide. (B) Comparison of cytokine TNF-α, IFN-γ, and IL-2 secretion in the supernatant measured by Luminex. Comparison of cytokine IL-10 (C) and IL-4, IL-5, IL-13 (D) production upon stimulation. Kruskal-Wallis one-way ANOVA was used to compare IFN-γ EC_{50}, IL-2 EC_{50}, IL-10 level, and IL-5 level, and one-way ANOVA for the other comparison among three groups. The two-tailed *P* value was calculated. **P*<0.05, ***P*<0.01, ****P*<0.001, *****P*<0.0001.

Taken together, X_{29}- and X_{89}-specific $CD4^+$ T cells display profiles of Th1 cells, whereas X_{105}-specific $CD4^+$ T cells are more Th2-like cells. Compared to C_{116}- and S_{182}-specific $CD4^+$ T clones, HBx $CD4^+$T cells displayed comparable antigen-

sensitivity as C_{116} T cells, while X_{29}-spepcifc T cells showed much higher functional avidity than S_{182} T cells (*P*=0.009; Fig. 3.15A). According to cytokine profiles (Fig. 3.15B), C_{116}-specific $CD4^+$ T cells showed both Th1 and Th2 profiles with production of both Th1 cytokines (IFN-γ and IL-2) and Th2 cytokines (IL-5 and IL-13). In contrast, S_{182}-specific $CD4^+$ T cells were more Th2-like with production of IL-13.

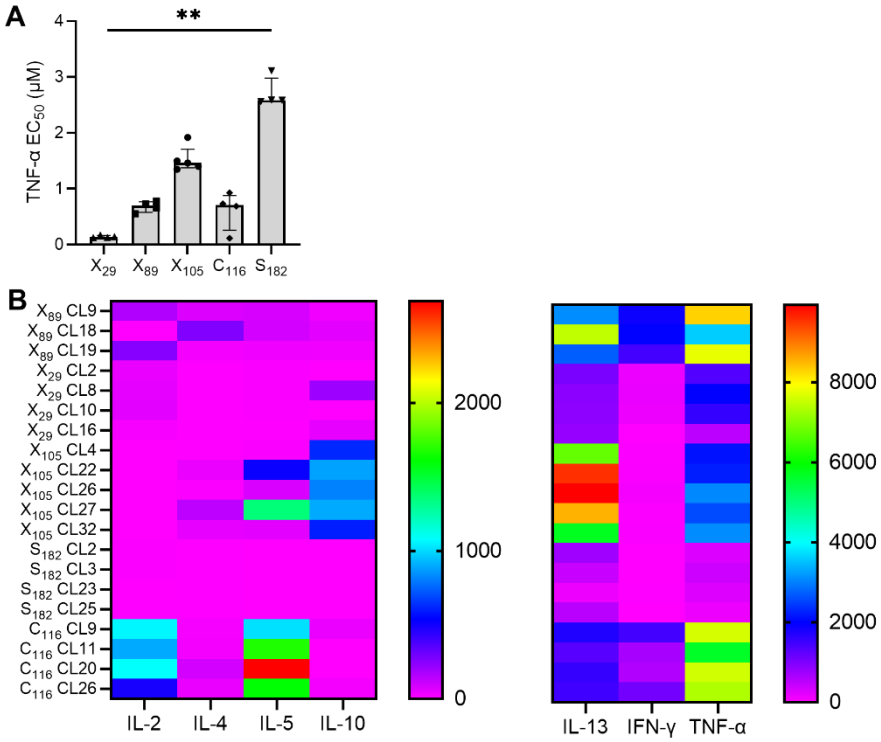

Fig. 3.15 Comparison of effector function amongst HBx, HBc and HBs-specifc $CD4^+$ T cells. Effector function of $CD4^+$ T cell clones reactive to each of HBx, HBc, and HBs epitopes was assessed *in vitro* using autologous B cells loaded with epitope peptide. (A) Comparison of EC_{50} of TNF-α production upon stimulated by titrated peptide loaded B cells. (B) Profile of cytokines secreted upon stimulation. Cytokine levels in the supernatant were assessed by Luminex. Kruskal-Wallis one-way ANOVA was used to compare TNF-α EC_{50} among five groups. The two-tailed *P* value was calculated. ***P*<0.01.

Interestingly, in addition to producing cytokines, X_{29}- and X_{89}-specific $CD4^+$ T cell

clones were capable of killing target cells by more than 10% (Fig. 3.16A). X_{89}-specific CD4$^+$ T cells displayed the strongest killing, whereas X_{105} T cell clones did not show killing potential (*P*=0.00007; Fig. 3.16A). Although X_{29}- and X_{89}-specific CD4$^+$ T cells exhibited weaker cytotoxicity when compared to X_{146}-specific CD8$^+$ T cells (P=0.000002; Fig. 3.16B), our data still highlight the existence of HBV-specific CD4$^+$ CTLs following HBV infection.

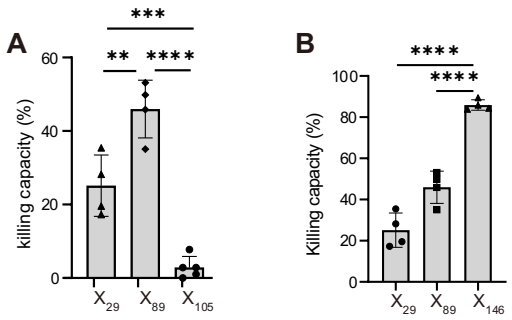

Fig. 3.16 Killing capacity of HBx-specific CD4$^+$ T cells. Killing capacity of T cell clones were assessed by CFSE-based cytotoxicity assays using peptide-loaded autologous B cells as targets. Comparison of killing capacity among CD4$^+$ T cells specific to the three x epitopes (A) and between HBx-specific CD4$^+$ T cells and CD8$^+$ T cells (B). One-way ANOVA was exployed to compare killing capacity among three groups and the two-tailed P value was calculated. ***P*<0.01, ****P*<0.001, *****P*<0.0001.

3.2.8 Cytotoxicity of HBx-specific CD4$^+$ T cells is associated with degranulation and antigen sensitivity

To explore the mechanisms underlying cytotoxicity of these HBx-specific CD4$^+$ T cells, I first analysed killing capacity and degranulation, and observed a positive association between killing ability and degranulation activity, which was measured by CD107a expression upon antigen stimulation, including the frequency of T cells expressing CD107a and CD107a expression intensity (*N*=13; *R*=0.740,

P=0.004; *R*=0.654, *P*=0.015; Fig. 3.17A). Moreover, a negative correlation between cytotoxicity and EC_{50} of TNF-α was noted (*R*=-0.692, *P*=0.009, Fig. 3.17B). These data demonstrate that cytotoxicity of HBx-specific $CD4^+$ T cells is associated with antigen-sensitivity and degranulation.

Activated $CD8^+$ CTLs carry out their cytotoxic activity primarily by releasing cytotoxic granules consisting of perforin and granzymes, which subsequently induce apoptosis of target cells. To determine the pathway mediating the killing of target cells by HBx-specific $CD4^+$ CTLs, X_{29}- and X_{89}-specific $CD4^+$ T cell clones were treated with concanamycin A (CMA), an inhibitor of perforin(Kataoka et al., 1996), prior to adding to target cells loaded with peptide. The cytolytic activity mediated by HBx-specific $CD4^+$ T cell clones was partially blocked by CMA, resulting in decreased killing capacity (Fig. 3.17C). Moreover, a comparable reduction in the levels of cytotoxicity were induced by CMA blocking, even when target cells were loaded with increasing concentrations of peptide (0.4, 2, and 10μM) (Fig. 3.17D and E). This demonstrates that cytotoxicity blocked by CMA is independent of peptide concentration. In contrast, the killing of target cells by C_{116}-specific $CD4^+$ T cells cannot be blocked by CMA (Fig. 3.17F). In summary, our data suggest that granule-based pathway contributes to the cytolytic activity of HBx-specific $CD4^+$ T cells, while cytotoxicity of C_{116}-specific $CD4^+$ T cells is not mediated by granules.

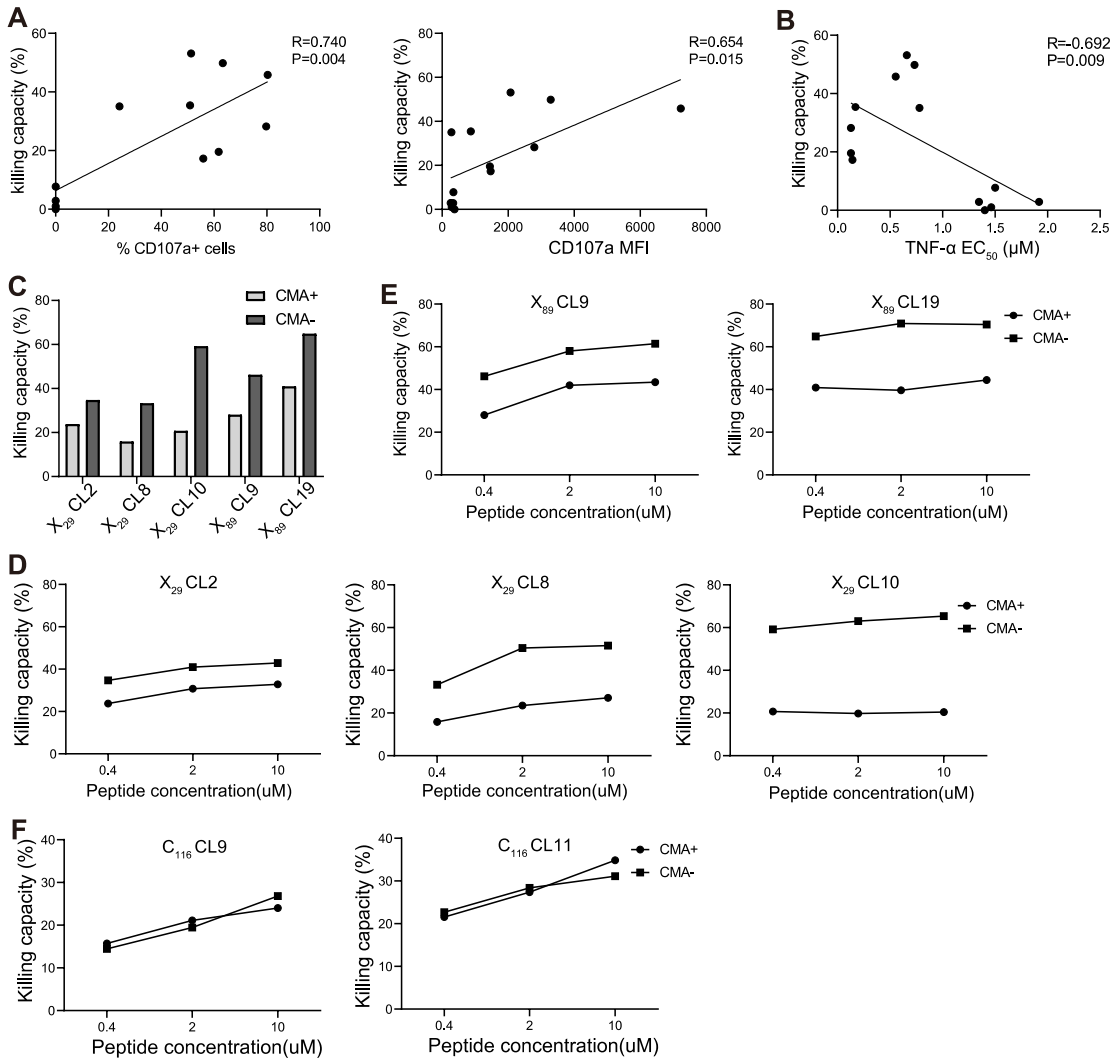

Fig. 3.17 Association of HBx-specific CD4⁺ T cell cytotoxicity with degranulation and antigen sensitivity. Correlation of HBx-specific CD4⁺ T cell cytotoxicity with CD107a expression on T cells (A) and EC_{50} of TNF-α production (B) upon stimulation. (C) Killing capacity of X_{29}- and X_{89}-specific CD4⁺ T cell clones with and without CMA treatment, when cocultured with autologous B cells loaded with 0.4μM peptide. Inhibition of CMA blocking on T cell killing exerted by (D)X_{29}-, (D) X_{89}-, and (E) C_{116}-specific CD4⁺ T cell clones, when cocultured with autologous B cells loaded with different peptide concentrations. MFI, median fluorescent intensity. Correlation analysis was performed using Spearman's rank correlation coefficient.

3.2.9 HBx-specific CD4⁺ T cells display antiviral activity

To assess the antiviral activity of X_{89}-specific CD4⁺ T cells, HepG2^{hNTCP} cell line

stably co-expressing HLA-DRA*01:01 and HLA-DRB1*08:01 was established, which originally did not express HLA-DR (Fig. 3.11A). HLA-DR-transduced HepG2^{hNTCP} cells were infected with HBV and after seven days, cocultured with X_{89}-specific CD4$^+$ T cells at an E:T ratio of 1:2 for 6 hours. T cell responses were subsequently assessed by ICS. X_{89}-specific CD4$^+$ T cells can recognise HBV-infected cells, but the response was low with 2.5% cells expressing TNF-α (Fig. 3.18A).

To evaluate the factors that mediated the low response of X_{89}-specific CD4$^+$ T cells to HBV-infected HepG2^{hNTCP} cells, the antigen load of X_{89} epitope presented by HBV-infected cells was assessed. X_{89}-specific CD4$^+$ T cell line was cocultured with target cells at an E:T ratio of 1:2, either infected with HBV or loaded with titrated peptides, then assessed T cell responses by ICS (Fig. 3.18B and C). The antigen load in HBV-infected cells was determined to be equivalent to the peptide concentration that induced the same level of response as virus-infected cells. It was estimated that 0.039μM of the epitope X_{89} antigen was presented on HBV-infected HepG2^{hNTCP} cells. Meanwhile, the antigen load of CD8$^+$ T cell epitope X_{146} in HBV-infected HepG2^{hNTCP} cells was also evaluated, and approximately 0.26μM of the epitope antigen was presented on HBV-infected cells (Fig. 3.18D and E). This is notably higher than that was observed with X_{89} epitope. It seems that the low response of X_{89}-specific CD4$^+$ T cells when encountering HBV-infected HepG2^{hNTCP} cells is caused by low antigen load in virus-infected cells.

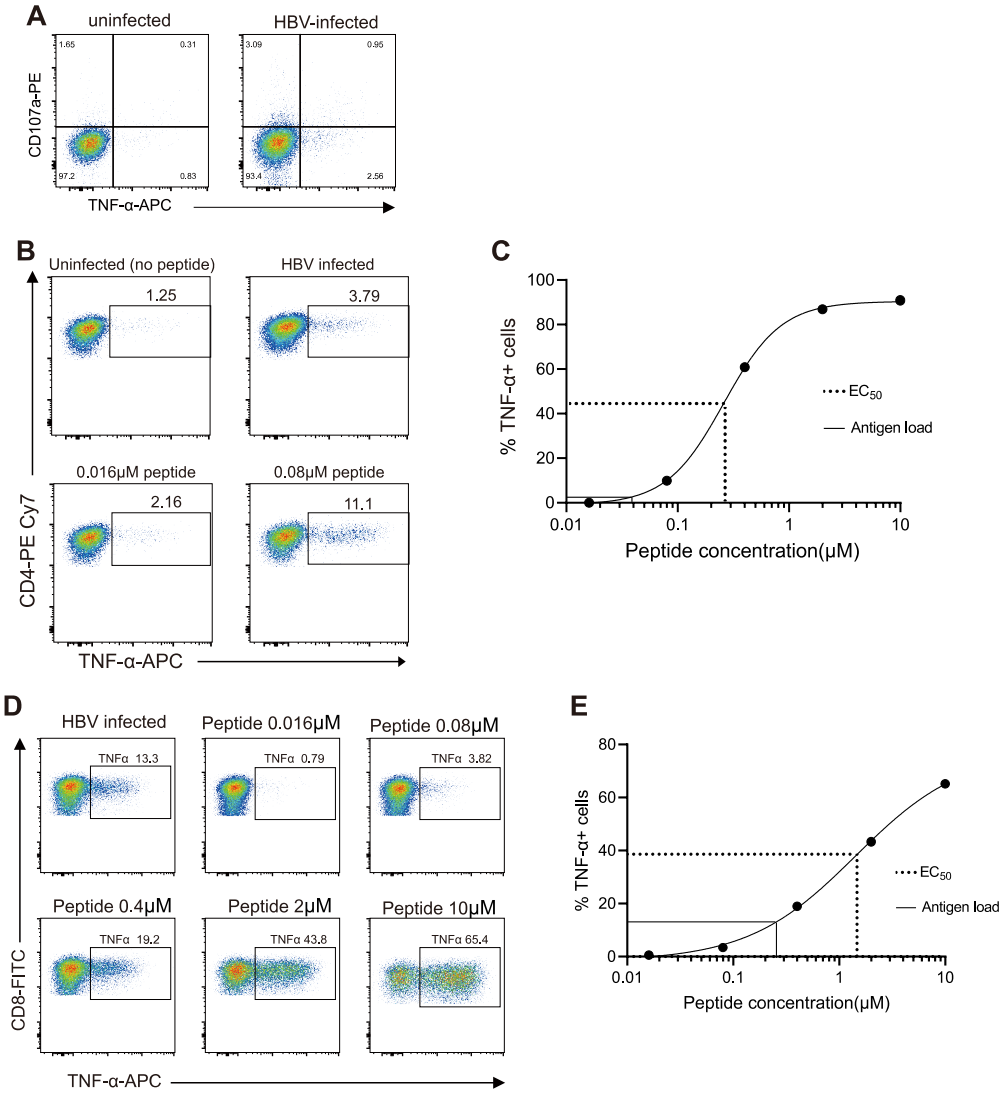

Fig. 3.18 X_{89} and X_{146} epitope antigen load on HBV-infected HepG2hNTCP cells. (A) TNF-α and CD107a expression by X_{89}-specific $CD4^+$ T cells when encountered HBV-infected $HepG2^{hNTCP}$ cells. Representative flow cytometry plots measuring TNF-α expression by X_{89}-specific $CD4^+$ T cells (B) and X_{146}-specific $CD8^+$ T cells (D) after incubation with $HepG2^{hNTCP}$ cells infected by HBV or loaded with titrated peptide. (C) Estimated antigen load of X_{89} epitope (C) and X_{14} epitope (E) on HBV-infected cells and EC_{50} of T cell response. Dashed line represents the estimated epitope antigen load on virus-infected cells whereas solid line shows the EC_{50} of T cell response.

Contrary to their low level of cytokine producing cells, X_{89}-specifc $CD4^+$ T cells elicited good cytotoxic activity targeting HBV-infected $HepG2^{hNTCP}$ cells (Fig. 3.19A). CL9 and CL19 killed 15.11% and 24.96% of virus-infected cells

respectively at an E:T ratio of 2:1 within 72hrs. More importantly, X_{89}-specific $CD4^+$ T cells were also capable of suppressing HBV replication and viral antigen production (Fig. 3.19B-D). CL9, CL19, and bulk line efficiently inhibited HBV replication, with more than 50% and 65% reduction of intracellular HBV DNA at the E:T ratio of 1:1 and 2:1 respectively (Fig. 3.19B). They also suppressed more than 20% of HBeAg production at E:T ratios of both 1:1 and 2:1 (Fig. 3.19D). The repression of HBsAg secretion is weaker: HBsAg levels only reduced by 13.06%, 8.21% and 21.55% respectively at an E:T ratio of 2:1, with lower levels of HBsAg reduction observed at E:T ratio of 1:1 (Fig. 3.19C). As expected, when compared to X_{146}-specific $CD8^+$ T cells (Fig. 3.13F and G), X_{89}-specific $CD4^+$ T cells exhibited a much lower suppression of HBV replication and HBsAg production.

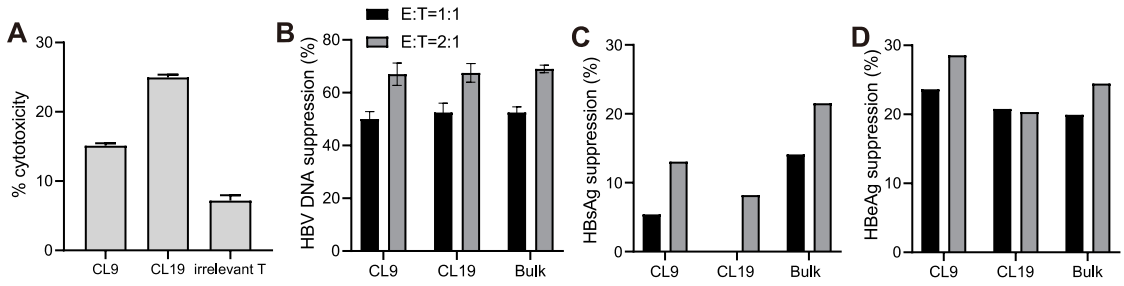

Fig. 3.19 X_{89}-specific $CD4^+$ T cell antiviral function. HBx-specific $CD4^+$ T cell antiviral efficacy was evaluated *in vitro* using T cell bulk and clones. (A) T cell cytolytic activity to HBV-infected HepG2hNTCP cells at an E:T ratio of 2:1. T cell suppression to intracellular HBV DNA (B), secreted HBsAg (C) and HBeAg (D).

3.2.10 TCR usage of HBx-specific T cells

To evaluate whether diverse functional phenotypes of HBx-specific $CD4^+$ and $CD8^+$ T cells which were observed above was due to different TCR usage of the cells, TCR of four clones targeting each epitope were sequenced. cDNA was

synthesised from each clone's RNA using SMARTer RACE cDNA amplification kit (Takara). Then, *TRAV* and *TRBV* was amplified with primers specific for *TRAC* and *TRBC* respectively (Fig. 3.20A). Purified PCR product was cloned into TOTPO TA vector and transformed into TOP10 competent cells, followed by plating into LB agar plates. Subsequently, colony PCR was carried out before plasmid extraction (Fig. 3.20B). Colonies transformed with *TRAV*- or *TRBV*-inserted plasmids were cultured in LB medium and then plasmid was extract using miniPrep (Qiagen) for Sanger sequencing. TCRs of HBx-specific T cell clones are analysed and shown in Table 3.4. X_{29}-specific $CD4^+$ T cell clones shared the TCR with identical amino acid sequences of CDR3 of both α and β chains, while X_{89} reactive T cell clones shared identical β chain with CL27 and CL33 bearing one α chain of TRAV17 and CL9 and CL19 bearing two α chains of TRAV16 and TRAV17, but the CDR3 amino acid sequences of TRAV17 of the four clones were identical. X_{146}-specific $CD8^+$ T cell clones also shared the same α and β chains of TCR with identical amino acid sequence of CDR3.

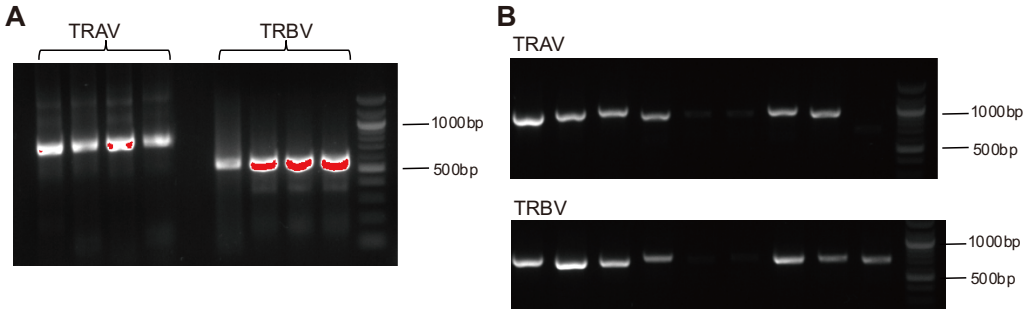

Fig. 3.20 TCR sequencing of HBx-specific T cell clones. (A) Amplification of TRAV and TRBV cDNA from T cell clone. (B) Colony PCR of TOP10 competent cells

transformed with TRAV or TRBV cloned TOPO TA plasmid.

Table 3.4 TCR usage of HBx-specific T cell clones

Epitope	clone	CDR3 α	TRAV	CDR3 β	TRBV
X_{29}	CL2	CAVAGGGATNKLIF	TRAV21	CASSLEPNEKLFF	TRBV4-2
	CL8	CAVAGGGATNKLIF	TRAV21	CASSLEPNEKLFF	TRBV4-2
	CL10	CAVAGGGATNKLIF	TRAV21	CASSLEPNEKLFF	TRBV4-2
	CL16	CAVAGGGATNKLIF	TRAV21	CASSLEPNEKLFF	TRBV4-2
X_{89}	CL9	CALPATGANSKLTF /CATTNDYKLSF	TRAV16/17	CASSRWRPEEETQYF	TRBV5-1*01
	CL19	CALPATGANSKLTF /CATTNDYKLSF	TRAV16/17	CASSRWRPEEETQYF	TRBV5-1*01
	CL27	CATTNDYKLSF	TRAV17	CASSRWRPEEETQYF	TRBV5-1*01
	CL33	CATTNDYKLSF	TRAV17	CASSRWRPEEETQYF	TRBV5-1*01
X_{146}	CL5	CAPGAYNTDKLIF	TRAV12-2	CASRVGLGGAYEQYF	TRBV12-4
	CL15	CAPGAYNTDKLIF	TRAV12-2	CASRVGLGGAYEQYF	TRBV12-4
	CL19	CAPGAYNTDKLIF	TRAV12-2	CASRVGLGGAYEQYF	TRBV12-4
	CL21	CAPGAYNTDKLIF	TRAV12-2	CASRVGLGGAYEQYF	TRBV12-4

3.3 Discussion

HBV-specific T cell responses play a pivotal role in controlling virus replication and viral eradication. Quantitative and qualitive defects of HBV-specific T cells contribute to infection persistence. In this project, *ex vivo* T cells responses targeting core, surface, polymerase, and x proteins in patients with chronic HBV infection were assessed. The frequency of patients having HBx-specific T cell responses was low in chronic HBV infection, with 17.39% (8/46) in the HBeAg clearance group and 0% (0/28) in the HBeAg-positive group. An association between HBx-specific T cell responses and HBeAg loss, as well as lower HBsAg level in the blood was observed in CHB patients. In a CHB cohort, lower serum HBsAg level was discovered to be an important predictor for HBsAg loss(Chen et al., 2014). The above data indicate that HBx-specific T cells might contribute to

HBV infection control.

Within this study of HBx-specific T cell responses, one $CD8^+$ and three $CD4^+$ T cell epitopes of x protein were identified from patients with CHB. Broader HBx-specific $CD4^+$ T cell responses were also observed in acute HBV infection(Hoogeveen et al., 2022), and very few HBx CD8 epitopes were identified. This could be due to relative small size of x protein that consists of 154 amino acids, and may lack epitopes that can be properly presented and processed to common HLA types. This may explain why X_{146}-specific $CD8^+$ T cell responses are restricted by the rare HLA allele HLA-B*54:01, that has a frequency of 3% among population(Zou, Shen, Qiang, Zhu, & Li, 2021). In contrast, $CD4^+$ T cell responses targeting X_{29}, X_{89} and X_{105} are restricted by HLA-DQB1*03:01, DRB1*08:01 and DPB1:04:02 respectively. DQB1*03:01 is the most frequent HLA-DQB1 allele in the Chinese population with a frequency of 20%(Zou et al., 2021). With broader HLA-restriction and more prevalent HLA allele, HBx-specific $CD4^+$ T cell responses are more likely to be predominant in the population than $CD8^+$ T cell responses.

X_{146}-specific $CD8^+$ T cell responses were further characterised, which displayed high functional avidity with low EC_{50} in terms of TNF-α, IFN-γ and IL-2 production and CD107a expression, strong cytotoxic activity and proliferating capacity. X_{146}-specific $CD8^+$ T cells also executed strong responses including TNF-α and IFN-γ cytokine production and CD107a expression when encountering HBV-infected $HepG2^{hNTCP}$ cells. Most importantly, X_{146} $CD8^+$ T cells are able to kill 80% HBV-

infected HepG2^{hNTCP} cells within 72hrs at an E:T ratio of 1:1 and elicited remarkable antiviral activity, including suppression of HBV replication in HepG2^{hNTCP} cells and antigen production in the supernatant. The degree of antiviral efficacy resulting from antiviral cytokines or direct killing of virus-infected cells by the T cells is an area of future research. Collectively, our data demonstrated that X_{146}-specific CD8+ T cells can efficiently control HBV infection. Although X_{146}-specific CD8$^+$ T cells displayed strong function and executed efficient antiviral activity *in vitro*, the *ex vivo* characteristics of these T cells need to be unveiled. Future research may include using X_{146}-B*54:01-tetramer to explore the differentiation phenotype and cytotoxic molecule expression of X_{146}-specific T cells by flow cytometry.

Among the three CD4$^+$ T cell epitopes of x protein identified in this study, X_{29}-specific T cells displayed highest antigen sensitivity with the lowest EC_{50} calculated by TNF-α, IFN-γ and IL-2 production. Classified by cytokine profile, X_{29}- and X_{89}-specific CD4$^+$ T cells were more Th1-like, while X_{105} CD4$^+$ T cells were Th2-like. Of note, both X_{29}- and X_{89}-specific CD4$^+$ T cells elicited killing capacity, although it was not as high as the cytotoxicity mediated by X_{146} CD8$^+$ T cells. Killing capacity of HBx-specific CD4$^+$ T cells was positively correlated with CD107a expression, which indicates that cytolytic activity of HBx-specific CD4$^+$ T cells is mediated by granule-based pathway. This is further confirmed by reduced killing capacity with CMA treatment. However, CMA only partially inhibited cytotoxicity of HBx-specific CD4$^+$ T cells, which indicates that other pathways

contribute to cytolytic activity. To resolve the doubt that cytotoxicity of HBx-specific $CD4^+$ T cells is induced by long-term cultivation, cytotoxic marker expression, such as perforin, granzyme B and FasL, on HBx-specific $CD4^+$ T cells will be assessed *ex vivo*.

Next, antiviral efficacy of X_{89}-specific $CD4^+$ T cells was investigated in vitro, using HBV infected $HepG2^{hNTCP}$ cells stably co-expressing HLA-DRA*01:01 and DRB1:08:01. X_{89}-specific $CD4^+$ T cells can kill HBV-infected $HepG2^{hNTCP}$ cells, but showed lower responses when encountering HBV-infected $HepG2^{hNTCP}$ cells in comparison to X_{146}-specific $CD8^+$ T cells, which may be attributed to low antigen load on HBV-infected cells. Our antigen-load assessment showed that approximately 0.039μM of X_{89} epitope antigen was presented on HBV-infected $HepG2^{hNTCP}$ cells, which is equivalent to 1/6.66 of the EC_{50} (0.2598μM) of the T cells, while 0.26 μM of X_{146} epitope antigen was presented on virus infected cells. Importantly, X_{89}-specific $CD4^+$ T cells suppressed HBV replication as well as HBsAg and HBeAg production. Of these, the suppression level of HBeAg was higher than HBsAg. In contrast, X_{146}-specific $CD8^+$ T cells elicited a greater suppression to HBsAg than HBeAg, which may suggest that the decrease in HBsAg levels resulted from HBV-infected cells cytotoxicity and clearance, whereas HBeAg suppression is caused by noncytolytic antiviral cytokines. In sum, both $CD4^+$ and $CD8^+$ HBx-specific T cells contribute to HBV infection control and viral clearance, but through different mechanisms.

The four X_{146}-specific $CD8^+$ T cell clones bearing the same TCR displayed

different functionality. CL21 produced higher levels of TNF-α, IFN-γ and IL-2 assessed by Luminex compared to the other clones, and higher proliferation ability than CL15 and CL19. In contrast, CL15 secreted the lowest levels of cytokines with stimulation of 0.4 and 2μM peptides, including TNF-α, IFN-γ, IL-2 and IL-5. CL15 exhibited weaker proliferation and killing capacity too than other clones. It suggests that X_{146}-specific $CD8^+$ T cell functions are regulated by more than TCR usage only. It has been well addressed that immune checkpoint inhibitors affect T cell functions(Abd Hamid et al., 2019). Expression of checkpoint inhibitors on X_{146}-specific $CD8^+$ T cell clones will be assessed and their impact on T cell function will be evaluated.

In chronic HBV infection, HBV-specific T cells are exhausted and impaired(Park et al., 2016; Raziorrouh et al., 2010; A. Schurich et al., 2011; Ye et al., 2015). Thus, adoptive transfer of engineered HBV-specific T cells can be a promising option to treat CHB. T cells grafted with HBV-specific TCRs were multifunctional of cytokine production and cytotoxicity, and were also able to eradicate HBV infection both *in vitro* and in mice, and eradicated HCC tumor in mice(Gehring et al., 2011; Wisskirchen et al., 2019). The HBx-specific TCRs identified could be considered to potential immunotherapy. For example, T cells transduced with TCRs of X_{89}- and X_{146}-specific T cells may efficiently kill HBx expressing cancer cells in HCC patients, and may display strong cytotoxicity towards HBV-infected cells and thereby control HBV infection in patients with CHB.

Chapter 4: Viral mutations to escape from SARS-CoV-2 specific T cell responses

4.1 Introduction

COVID-19, a global pandemic that began in 2020, is caused by SARS-CoV-2(Zhou et al., 2020; Zhu et al., 2020). As of September 2022, more than 600 million cases have been confirmed worldwide, with over six million deaths(WHO, 2022b). The wide range of the pandemic can be attributed to the huge levels of virus replication, which increases the risk of adaptive mutations. A great number of variants of SARS-CoV-2 have emerged worldwide, with mutations in the SARS-CoV-2 genome resulting from continuous viral evolution. These variants have been classified as VUMs, VOIs, and VOCs depending on their viral properties. Of these, VOCs evade adaptive immune responses induced by vaccination and previous natural infection, which is associated with the rapid spread of VOCs. Numerous studies have focused on humoral immunity and mutations in the RBD of the spike protein which is the target for many neutralising antibodies. Evasion from antibody neutralisation is reported in Beta (B.1.351), where mutations in RBD of spike results in tighter ACE2 binding and reduced neutralisation by monoclonal antibodies and sera generated in response to vaccination or previous SARS-CoV-2 infection(Zhou et al., 2021). Mutations in the RBD and NTD of the spike protein impairing the effectiveness of neutralising antibodies have also been observed in the Delta and Omicron variants(Cao et al., 2022; Planas et al., 2021).

Some viruses, such as HIV and influenza, are able to mutate to evade T cell responses. Evasion from antigen-specific $CD8^+$ T cells is reported in HIV-1, where rapid intra-host viral evolution renders T cell responses ineffective within weeks of acute infection(Goonetilleke et al., 2009). Several variants with mutations in $CD8^+$ T cell epitopes capable of evading T cell surveillance are described in influenza A (H3N2)(Voeten et al., 2000). Long-term adaptation of influenza A (H3N2) with improved ability to escape T cell recognition has been demonstrated with the loss of more than one $CD8^+$ CTL epitope every three years since its emergence (Woolthuis, van Dorp, Keşmir, de Boer, & van Boven, 2016). However, T cells specific to conserved proteins are protective against respiratory viral infections such as influenza, in particular, the broad heterosubtypic immunity(Hayward et al., 2015).

In terms of SARS-CoV-2, T cell responses play critical roles in controlling infection and underpinning vaccine efficacy. Early induction of T cell responses is correlated with clinical protection, in contrast, patients with severe illness exhibit reduced circulating effector $CD8^+$ T cells(Bergamaschi et al., 2021; Notarbartolo et al., 2021). In contrast to humoral immunity, the majority of the memory $CD4^+$ and $CD8^+$ T cell responses against the spike protein induced by vaccination or natural infection are preserved and able to cross-recognise SARS-CoV-2 variants. It has been reported that various vaccine platforms, including mRNA-1273, BNT162b2, Ad26.COV2.S, and NVX-CoV2373, induce broad T cell responses with a median of 11 $CD4^+$ and 10 $CD8^+$ T cell epitopes targeting spike(Tarke et

al., 2022). An average of 90% of spike-specific $CD4^+$ T cell recognition of variants is preserved, while $CD8^+$ T cell responses induced by vaccination retain 95% of overall recognition assessed by activation-induced marker assays(Tarke et al., 2022). Although the magnitude of $CD4^+$ and $CD8^+$ T cell responses to Omicron spike are lower than the response to spike with wild-type sequences in vaccinated and convalescent individuals, more than 70% of spike-specific $CD4^+$ and $CD8^+$ T cell responses are maintained against Omicron(Keeton et al., 2022). The above studies have focused on mutations in spike, but little is known about the potential for SARS-CoV-2 mutations in other proteins to impact T cell recognition.

In this chapter, we first evaluated the overall and immunodominant memory T cell responses against SARS-CoV-2 in individuals who had recovered from COVID-19 by *ex vivo* ELISpot using overlapping peptides spanning the full proteome of SARS-CoV-2 except ORF1. We then identified dominant $CD4^+$ and $CD8^+$ T cell epitopes by ELISpot. The optimal epitopes and HLA-restriction of these dominant $CD4^+$ and $CD8^+$ T cell responses were defined by ELISpot assays and further verified by T cell staining with peptide-MHC tetramers/Pentamer. Finally, we identified viral mutations accumulated in these dominant T cell epitopes through the datasets from CoV-GLUE and evaluated their impact on T cell functions, including functional avidity and killing capacity.

4.2 Results

4.2.1 Memory T cell responses against SARS-CoV-2 in convalescent COVID-19 individuals

PBMCs were collected from 42 individuals recovering from COVID-19, including 28 mild and 14 severe cases. Patients were sampled at least 28 days after onset of symptoms. SARS-CoV-2 specific T cell responses were assessed using *ex vivo* IFN-γ ELISpot assays with a panel of 423 overlapping peptides spanning the viral proteins except ORF1. All overlapping peptides were placed into a two-dimensional peptide matrix. Of these peptides, a total of 61 pools were tested with 29 in the first-dimension pools and each pool containing 3-16 single peptides as shown in Appendix Table 2.2. SARS-CoV-2 specific T cell responses were assessed using the 29 pools in the first dimension. To evaluate T cell responses targeting individual protein in each participant, T cell responses (SFU/10^6PBMCs) reactive to all overlapping peptide pools covering the corresponding protein were combined to demonstrate the magnitude of T cell responses, and the number of reactive pools represented the breath of T cell responses. The majority of the participants (24/28 mild cases and 14/14 severe cases) exhibited SARS-CoV-2 memory T cell responses to at least one of the peptide pools. The overall magnitude and breath of T cell responses against each SARS-CoV-2 protein in all participants are shown in Fig. 4.1 A and B. The magnitude and breath of the memory T cell responses varied among individuals. Epitopes recognised by T cells were distributed across a wide variety of virus proteins. In summary, strong

and broad memory T cell responses were induced following recovery from SARS-CoV-2 infection. These results were published in ref.(Peng et al., 2020).

4.2.2 Identification of immunodominant SARS-CoV-2 specific T cell responses

4.2.2.1 Identifying immunodominant peptides containing T cell epitopes

The peptides containing potential epitopes were identified from the analysis of ELISpot results with the two-dimensional peptide matrix and then confirmed by ELISpot assay using single peptides in 34 subjects (Fig. 4.2A). For example, Pool3 and Pool18 induced comparable T cell responses, with both pools having peptide S34. This indicates T cells recognised single peptide of S34, which was subsequently confirmed by ELISpot stimulated with S34 alone. S34 was recognised by 21 out of 40 participants, while S151 triggered T cell responses in 12 out of 37 donors. Two dominant peptides of nucleocapsid protein were also identified, with NP1 and NP51 recognised by three out of 34 participants respectively. ORF3a-28 was recognised by four out of 34 participants. Information of these dominant peptides is shown in Table 4.1. These dominant T cell responses were further confirmed using cultured short-term T cell lines.

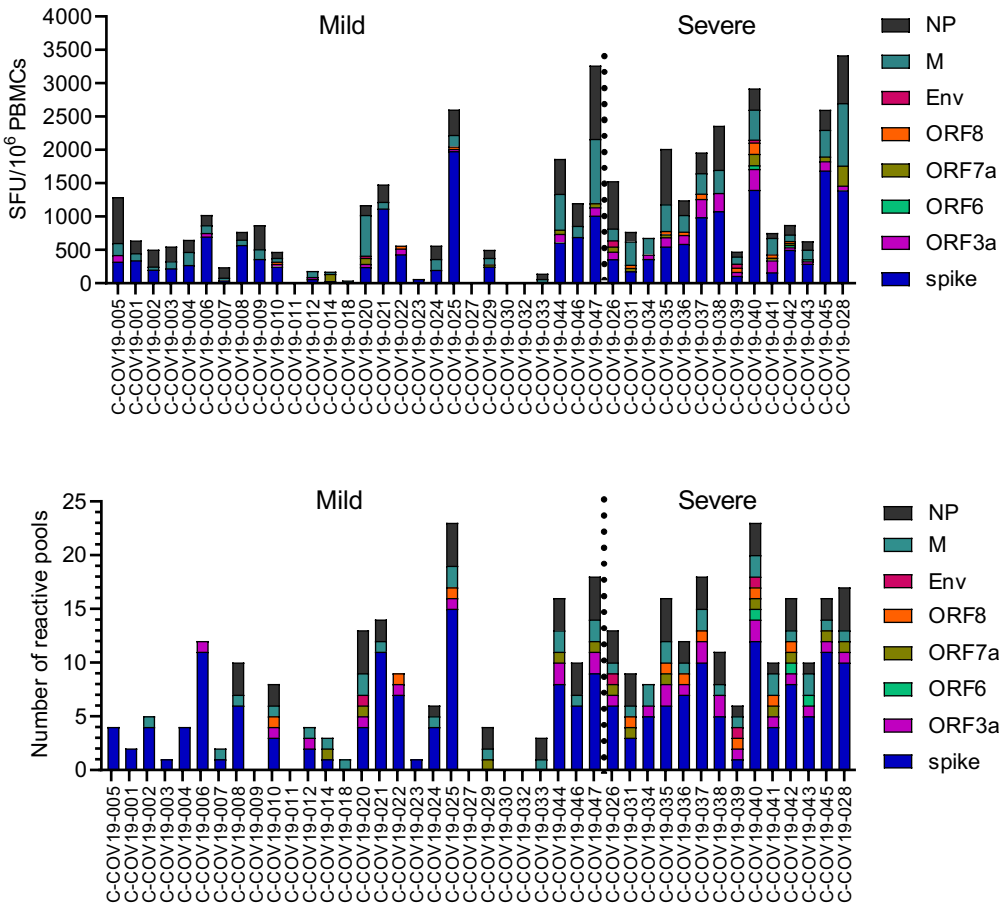

Fig. 4.1 Memory T cell responses specific to SARS-CoV-2 virus proteins in 42 convalescent patients infected with SARS-CoV-2. Of the 42 patients studied, 28 had mild symptoms while 14 showed severe symptoms. PBMCs were isolated and IFN-γ production was detected by ELISpot after incubation with SARS-CoV-2 peptides. (A) Magnitude of IFN-γ T cell responses for each individual. Each bar shows the total T cell responses of each individual specific to all of the SARS-CoV-2 protein peptides tested. Each colored segment represents the source protein corresponding to peptide pools eliciting IFN-γ T cell responses. (B) Breadth of T cell responses for each individual. The breadth of T cell responses was calculated by the number of peptide pools in the first-dimension (*N*=29) cells that responded to spot-forming units. The experiments were repeated in 35 participants where sample availability permitted. Env, envelope protein. SFU, spot forming unit.

Table 4.1 Immunodominant peptides containing T cell epitopes

Peptide	Protein	Position	Amino acid sequence	$CD4^+/CD8^+$ T cell response
ORF3a-28	ORF3a	206-225	YFTSDYYQLYSTQLSTDTGV	CD8
NP1	Nucleocapsid	1-17	MSDNGPQNQRNAPRITF	CD8
NP51	Nucleocapsid	352-369	LLNKHIDAYKTFPPTEPK	CD8
S34	Spike	166-180	CTFEYVSQPFLMDLE	CD4
S151	Spike	751-765	NLLLQYGSFCTQLNR	CD4

4.2.2.2 Generating polyclonal T cell lines and clones targeting immunodominant peptides

Short-term T cell lines targeting each identified immunodominant peptide were set up and T cells responses after stimulation with individual peptides were assessed by ICS at day12. NP1, NP51 and ORF3a-28 induced strong $CD8^+$ T cell responses, producing TNF-α and IFN-γ (Fig. 4.2B); whereas $CD4^+$ T cells elicited strong responses against dominant spike peptides S34 and S151 (Fig. 4.2C). TNF-α/IFN-γ/IL-2 producing T cells were sorted from short-term T cell lines after stimulation with their corresponding dominant peptides using cytokine catch assays, then expanded *in vitro* using feeder cells to generate antigen-specific polyclonal T cell lines and clones (Table 4.2).

Table 4.2 Polyclonal T cell line list

Antigenic peptide of T cell lines	Donor ID
ORF3a-28	C-COV19-059
	C-COV19-037
	C-COV19-005
	C-COV19-036
NP1	C-COV19-047
NP51	C-COV19-035 (A*11:01)
	C-COV19-036 (A*03:01)
S34	C-COV19-035
S151	C-COV19-038

4.2.2.3 Defining optimal epitopes and their HLA-restrictions

The optimal epitopes within the long peptides (NP1, NP51 and ORF3a-28) recognised by $CD8^+$ T cells, and the HLA-restriction matched to the donor's HLA typing were predicted using the Immune Epitope Database analysis resource (http://tools.iedb.org/mhci). As described in Chapter3, the optimal epitope amino acid sequences and HLA-restrictions were confirmed employing ELISpot assays by coculturing T cells of antigen-specific T cell lines with HLA-matched and -unmatched B cell lines loaded with peptides (Fig. 4.2D). ELISpot results demonstrated that NP1- and ORF3a-28-specific $CD8^+$ T cell responses were restricted by HLA-B*27:05 and A*01:01 respectively, while NP51-specific $CD8^+$ T cells were restricted by both A*03:01 and A*11:01. Immunodominant spike-specific $CD4^+$ T cell epitopes S34 and S151 were restricted by HLA-DPB1*04:01 and DRB1*15:01 respectively (Data are shown in Chapter 5). Peptide-MHC class I Pentamers of the identified optimal $CD8^+$ T cell epitopes were synthesised (ProImmune). The three $CD8^+$ T cell epitopes and HLA-restrictions were further

verified by Pentamer staining of T cells using flow cytometry (Fig. 4.2E). In summary, $CD8^+$ T cell epitopes $ORF3a_{207-215}$(FTSDYYQLY)-A*01:01, NP_{9-17}(QRNAPRITF)-B*27:05 and $NP_{361-369}$(KTFPPTEPK)-A*03:01/A*11:01 were identified. $NP_{322-331}$(MEVTPSGTWL), one defined SARS-CoV epitope(Ahmed, Quadeer, & McKay, 2020) with the identical amino acid sequence to SARS-CoV-2 was also identified in one out of 34 participants. Its HLA-restriction by B*40:01was confirmed by Pentamer staining (Fig. 4.2E). NP_{322}-B*40:01 $Pentamer^+$ cells were sorted by FACS from PBMCs and expanded *in vitro* to establish an NP_{322}-specific polyclonal T cell line and clones for further analysis. The four identified $CD8^+$ T cell epitopes are shown in Table 4.3. Epitope NP_9 and NP_{322} have previously been reported in ref.(Nelde et al., 2021), while NP_{326} and $ORF3a_{207}$ have been described in refs.(Ferretti et al., 2020; Kared et al., 2021).

The above data have been published in ref.(Peng et al., 2020).

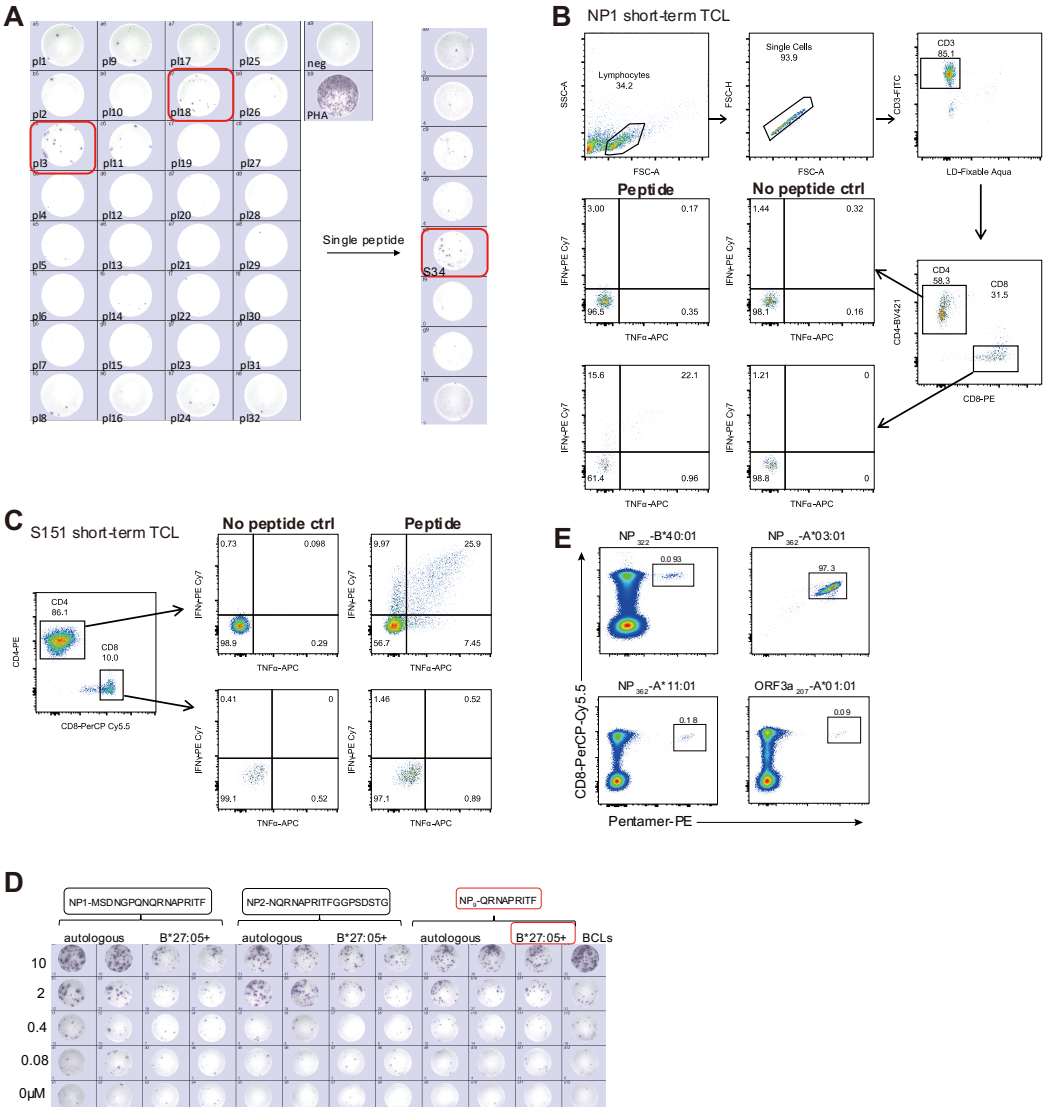

Fig. 4.2 Identification of immunodominant SARS-CoV-2 specific T cell responses in convalescent individuals. (A) Identification of single peptide containing potential T cell epitopes by ELISpot assays using a two-dimensional peptide matrix. T cell responses of short-term T cell line reactive to peptide NP1 (B) and S151 (C) upon stimulation with corresponding peptide. (D) Optimal epitope contained in NP1 and its HLA-restriction identification by ELISpot assays using HLA-matched and-unmatched B cell lines. (E) Pentamer staining of identified optimal CD8+ T cell epitopes using PBMCs or T cell bulk. BCL, B cell line.

4.2.3 Impact of viral mutations within immunodominant SARS-CoV-2 T cell epitopes on T cell recognition

To explore the potential for SARS-CoV-2 evading T cell responses, we carried out a proof-of-concept study, focusing on identifying common amino acid mutations within immunodominant T cell epitopes and evaluating the impact of any mutations on T cell function. 12 amino acid mutations were identified within the four $CD8^+$ T cell epitopes and two $CD4^+$ epitopes by searching the datasets downloaded from CoV-GLUE (http://cov-glue.cvr.gla.ac.uk/#/home) on July 30, 2021 (Table 4.3). 19 peptides including variant peptides and peptides with wild-type sequences were synthesised.

The functional avidity of SARS-CoV-2 specific $CD4^+$ and $CD8^+$ polyclonal T cell lines targeting these six immunodominant epitopes was assessed using IFN-γ ELISpot assays by coculturing T cells with B cell lines loaded with titrated wild type and variant peptides (Fig. 4.3A-F). Several mutations in $CD8^+$ T cell epitopes resulted in the complete escape from T cell response, including Q213K in $ORF3a_{207}$; P13S, P13T and P13L in NP_9; and T362I and P365S in NP_{361} (Fig. 4.3A, B and D respectively). In contrast, the T366I mutation in NP_{361} did not impair T cell responses, inducing a higher response and antigen sensitivity compared to wild-type peptide, with lower EC_{50} as calculated by IFN-γ ELISpot results (EC_{50} wild type: 231.3nM; T366I: 69.78nM; Fig 4.3D). Mutations Q9H in NP_9 and M177I in S_{166} impacted T cell responses at low concentrations of less than 0.4μM, with relatively higher EC_{50} (Fig. 4.3B and E respectively). Whereas mutations of T325I

in NP_{322}, L176F in S_{166} and R765L in S_{751} caused significant loss of T cell responses, with lower avidity observed to the variants in comparison with the wild-type peptides (Fig. 4.3C, E and F respectively).

Table 4.3 Dominant T cell epitopes and variants

Epitope	Position	Amino acid sequence	HLA-restriction	Variant	Frequency (%)	Countries	Global lineages
$ORF3a_{207}$	207-215	FTSDYYQLY	A*01:01	Q213K	0.059	56	95
NP_9	Sep-17	QRNAPRITF	B*27:05	Q9H	0.289	74	176
				P13L	0.978	97	194
				P13S	0.21	83	132
				P13T	0.102	45	81
NP_{322}	322-331	MEVTPSGTWL	B*40:01	T325I	0.069	52	109
NP_{361}	361-369	KTFPPTEPK	A*03:01/ A*11:01	T362I	0.293	85	165
				T366I	0.237	74	154
				P365S	0.794	73	142
S_{166}	166-180	CTFEYVSQPFLMDLE	DPB1*04:01	L176F	0.26	68	158
				M177I	0.083	60	92
S_{751}	751-765	NLLLQYGSFCTQLNR	DRB1*15:01	R765L	0.017	31	64
				R765H	0		

Frequency indicates % of sequences where variant is seen within the SARS-CoV-2 mutation dataset downloaded from CoV-GLUE (http://cov-glue.cvr.gla.ac.uk/#/home) on July 30, 2021. Global Lineages refers to Pango lineage assignment.

The impact of variants in $CD8^+$ T cell epitopes on killing capacity of CTLs was further investigated by CFSE-based cytotoxic assays using peptide loaded autologous B cell line. Consistent with the functional avidity assessed by ELISpot assays, Q213K in $ORF3a_{207}$, P13S, P13T and P13L in NP_9, and T362I and P365S in NP_{361} also resulted in the loss of killing capacity mediated by their respective $CD8^+$ T cell lines (Fig. 4.3G-I). T cell lines elicited less than 10% cytotoxicity when stimulated by these variants, even at a high E:T ratio of 4:1. While partial impairment of killing capacity was observed by variant T325I in NP_{322} (Fig. 4.3J).

Taken together, mutations Q213K in ORF3a$_{207}$, P13S, P13T and P13L in NP$_9$, and T362I and P365S in NP$_{361}$ led to complete loss of T cell recognition.

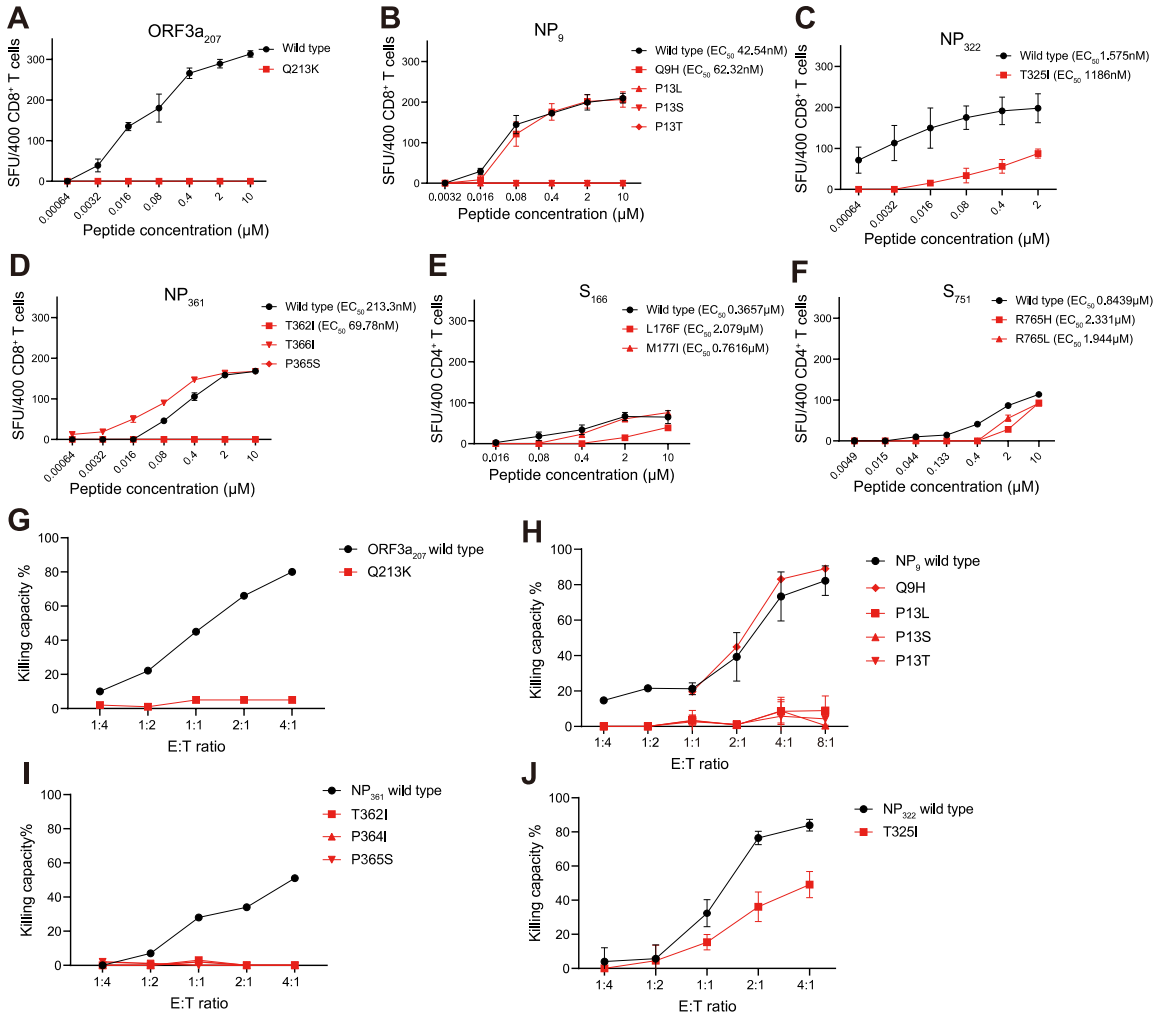

Fig. 4.3 Functional impact of mutation in dominant SARS-CoV-2 epitopes. (A-F) Recognition of wild-type (black) and mutant peptides by epitope-specific polyclonal T cell lines assessed by IFN-γ ELISpot assays. (G-J) Capacity of CD8+ T lines to kill autologous B cells loaded with wild-type (black) or mutant (red) peptides at different E:T ratios. SFU, spot forming unit.

4.2.4 The escape of variants from T cell responses is not TCR-biased

Variant evasion from T cell responses can be mediated by interrupting several mechanisms, including antigen processing, binding of MHC to peptide and TCR

recognition of peptide-MHC complex. To evaluate binding of MHC to variant peptide of epitope NP_{322} with mutation of T325I, competitive ELISpot assays were carried out. Briefly, autologous B cells were loaded with 0.04μM of wild-type peptide prior to being loaded with titrated mutant peptide, then cocultured with T cell line for 6hrs. T cell responses were subsequently assessed by ELISpot assay. T cell responses decreased when B cells loaded with wild-type peptide were exposed to increasing concentrations of mutant peptide (Fig. 4.4A), which indicated that the mutant peptide was able to compete with the wild-type peptide to bind to the MHC molecules. Thus, the binding of MHC to mutant peptide was not impaired and escape from T cells may be due to loss of TCR recognition.

To explore whether the loss of T cell recognition to variants was due to the absence of specific TCRs in the *in vitro* cultured polyclonal T cell lines, *ex vivo* T cell responses to wild-type and variant peptides of epitope NP_9 and NP_{361} were assessed by IFN-γ ELIPOT assays using PBMCs. The loss of T cell responses to variant peptides was confirmed in two HLA-A*03:01 and two B*27:05 convalescent COVID-19 donors (Fig. 4.4B), which is consistent with the observations from T cell lines against NP_{361} and NP_9. Therefore, the data generated using T cell lines are representative of circulating T cell responses to these epitopes. Furthermore, TCR usage of NP_9-, NP_{322}- and $ORF3a_{207}$-specific polyclonal $CD8^+$ T cell lines was sequenced as described in Chapter 3 of HBV-specific T cell clone TCR sequencing. 13-17 colonies were picked from each T cell line for sequencing. As shown in Table 4.4, a broad range of TCR clonotypes

were observed in ORF3a$_{207}$-specific CD8$^+$ T cell lines from the four donors, indicating that the Q213K variant escaped several TCRs (Fig. 4.4C). Similar findings were seen in the TCR repertoires of NP$_{322}$- and NP$_9$-specific T cell lines (Table 4.4).

Table 4.4 TCR β chain usage of polyclonal T cell lines

T cell line	Donor ID	CDR3	TRBV	TRBJ
NP$_{322}$	C-COV19-021	CASSLGPFGSGGDEQFF	TRBV7-8	TRBJ2-1
		CASSLDSAYEQYF	TRBV5-6	TRBJ2-7
		CASSAGVGANVLTF	TRBV27	TRBJ2-6
NP$_9$	C-COV19-047	CASSSTGIAAYGYTF	TRBV7-9	TRBJ1-2
		CASWGENTEAFF	TRBV7-6	TRBJ1-1
		CASSPSTSYEQYF	TRBV9	TRBJ2-7
		CASSSTGTESYEQYF	TRBV7-9	TRBJ2-7
ORF3a$_{207}$	C-COV19-059	CASSLIGQGGYTF	TRBV13	TRBJ1-2
		CASSQDLYNEQFF	TRBV16	TRBJ2-1
		CASSDPTSGELFF	TRBV2	TRBJ2-2
		CSVTRTHPRCYTF	TRBV20-1	TRBJ1-2
		CSARDPYRQASYNEQFF	TRBV20-1	TRBJ2-1
		CASSLGQEGANVLTF	TRBV6-5	TRBJ2-6
ORF3a$_{207}$	C-COV19-037	CAISQYRDNNEQFF	TRBV10-3	TRBJ2-1
		CASSLAGDLGTEAFF	TRBV5-1	TRBJ1-1
		CASSAWTGVGETQYF	TRBV5-1	TRBJ2-5
		CASSDSRTGR	TRBV6-4	TRBJ2-3
		CASREDQNTGELFF	TRBV6-6	TRBJ2-2
ORF3a$_{207}$	C-COV19-005	CASSVGGGSGETQYF	TRBV25-1	TRBJ2-5
		CASSLGGDSQEDQYF	TRBV7-3	TRBJ2-5
ORF3a$_{207}$	C-COV19-036	CASSPWTGIGQPQHF	TRBV5-1	TRBJ1-5
		CASSLGGSSTDTQYF	TRBV7-3	TRBJ2-3

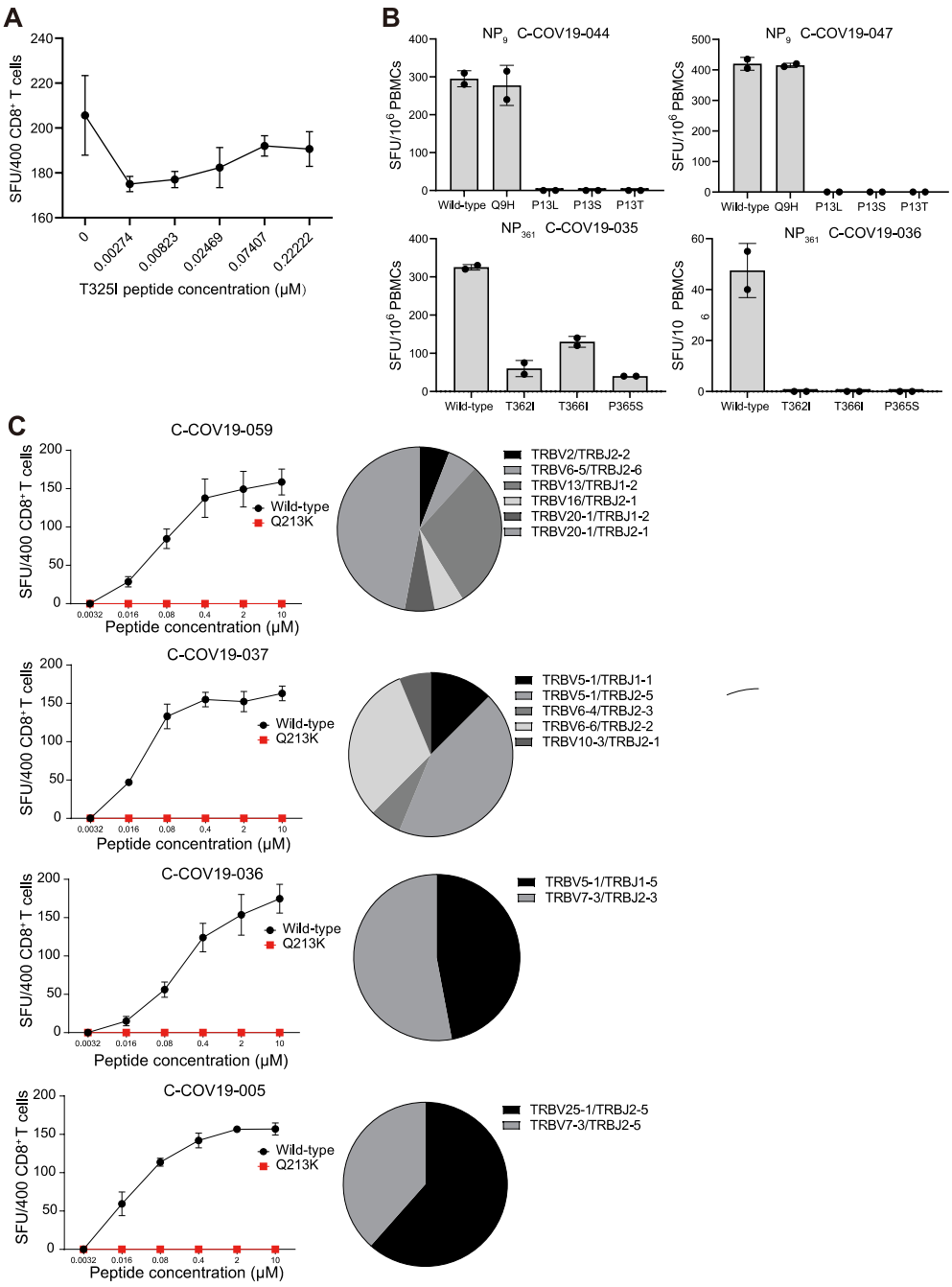

Fig. 4.4 The mechanisms mediating loss of T cell response to dominant SARS-CoV-2 T cell epitope variants. (A) Competitive binding to MHC-molecules of NP_{322} mutant peptide with wild-type peptide. (B) *Ex vivo* IFN-γ producing T cell responses induced by wild-type and mutant peptides of epitope NP_9 and NP_{361} assessed by ELISpot assays using PBMCs. (C) TCR repertoire of polyclonal $CD8^+$ T cell lines specific to epitope $ORF3a_{207}$ generated from four donors. The Q213K variant (red) showed complete loss of T cell recognition compared to wild-type peptide (black) in each donor with diverse TCR clonotypes in each T cell line.

4.3 Discussion

In this study, we demonstrate the presence of robust memory SARS-CoV-2 specific T cell responses in the blood of donors recovered from COVID-19. The majority of individuals (24/28 mild and 14/14 severe cases) exhibited T cell responses to at least one peptide. Immunodominant T cell responses specific to five peptides (S34, S151, NP1, NP51 and ORF3a-28) were identified using two-dimensional matrix peptide pools and confirmed by ELISpot using single peptide. Peptides S34 and S151 induced strong $CD4^+$ T cell responses, whereas NP1, NP51 and ORF3a-28 stimulated $CD8^+$ T cell responses, which were distinguished by ICS using short-term T cell lines. Epitope specificity and HLA-restrictions of these dominant T cell responses were further identified and verified by peptide-MHC tetramer staining for $CD4^+$ T cell epitopes and pentamer staining for $CD8^+$ epitopes. Two spike-specific $CD4^+$ T cell epitopes (S_{166}-DPB1*04:01 and S_{751}-DRB1*15:01), one ORF3a $CD8^+$ ($ORF3a_{207}$-A*01:01) and three nucleocapsid $CD8^+$ epitopes (NP_9-B*27:05, NP_{322}-B*40:01 and NP_{361}-A*03:01/A*11:01) were defined.

In order to evaluate the impact of viral variants on T cell functions, 12 amino acid mutations in the six T cell epitopes were identified (Table 4.3). Many variants were at relatively low frequency; however, they were prevalent amongst a wide range of countries and occurred in numerous viral lineages. Of these, Q213K in $ORF3a_{207}$, P13S, P13T and P13L in NP_9, and T362I and P365S in NP_{361} led to the complete loss of T cell responses, while T366I in NP_{361} did not impair T cell

responses. In fact, the mutation of T366I in NP_{361} resulted in higher T cell response and functional avidity compared to the wild-type peptide. Mutations T325I in NP_{322}, L176F in S_{166} and R765L in S_{751} caused partial loss of T cell responses, with lower antigen sensitivity observed to the variants compared with the wild-type peptides. A consistent effect on the cytotoxicity of CTLs was observed to mutations in the $CD8^+$ T cell epitopes. Q213K in $ORF3a_{207}$, P13S, P13T and P13L in NP_9, and T362I and P365S in NP_{361} resulted in the loss of killing elicited by the corresponding antigen-specific $CD8^+$ T cell lines. In summary, several mutations in $CD8^+$ T cell epitopes, including Q213K in $ORF3a_{207}$, P13S, P13T and P13L in NP_9, and T362I and P365S in NP_{361}, evaded T cell responses.

The mechanisms of variant evasion from T cell responses include antigen processing, binding of MHC to peptide and TCR recognition of the peptide-MHC complex. The competitive ELISpot results demonstrate that the binding of MHC to variant T325I in NP_{322} was not impaired. Thus, the loss of NP_{322}-specific T cell responses might be attributed to TCR recognition of peptide. The escape from *ex vivo* T cell responses was observed to variants of epitopes NP_9 and $ORF3a_{207}$. Furthermore, polyclonal T cell lines had diverse TCR repertoire, indicating that the variants escaped from diverse TCRs. Thus, loss of TCR recognition was likely not due to specific TCR.

As T cell responses targeting SARS-CoV-2 induced by both vaccination and natural infection are broad(Bertoletti, Bert, Qui, and Tan, 2021), combined with polymorphisms in the HLA genes, the selective escape of one particular T cell

epitope is restricted to a relatively small proportion of the population. Therefore, the polyclonal T cell responses of one individual are unlikely to significantly reduce due to mutations present in any circulating variant, consistent with observations in refs.(Keeton et al., 2022; Tarke et al., 2022). However, responses to T cell epitopes we have investigated are dominant in HLA-matched individuals across many cohorts, and A*03:01, A*11:01, A*01:01, and DPB1*04:01, DRB1*15:01 are common HLA alleles worldwide, the loss of T cell responses to these dominant epitopes may be significant. As population immunity against SARS-CoV-2, induced by vaccination and natural infection, increases rapidly(WHO, 2022b), the frequency of the variants described in this study should be monitored globally alongside mutations within all immunodominant T cell epitopes.

In this study, we only evaluated the capacity of MHC binding to mutant peptide T325I in NP_{322}. The binding of MHC to the other variants needs further investigation. Another limitation of this study is that T cell assays using peptide-loaded B cells cannot be utilised to investigate the impact of mutations within epitopes on antigen processing. In order to fully investigate the mechanisms of these escape mutations, a system delivering naturally processed antigens on the target cells is needed. Vaccinia virus expressing viral antigens of interest is one of them and has been widely used to study antigen processing and presentation in our lab and by other researchers(Lee et al., 2008; Levitskaya et al., 1995). Vaccinia virus expressing wild-type or variant sequences of the whole protein,

such as spike, ORF3a and nucleocapsid, will be generated and then used for infecting B cells or monocytes. The processing and presentation of wild-type and variant epitopes will be evaluated by assessing T cell responses following the coculturing with vaccinia virus-infected target cells.

Chapter 5: Memory cytotoxic SARS-CoV-2 spike-specific CD4$^+$ T cells associate with viral control

5.1 Introduction

Understanding the immune phenotype of SARS-CoV-2-specific T cells that are protective or pathogenic is pivotal to define therapeutic and prophylactic strategies to manage the COVID-19 pandemic(Bertoletti et al., 2021). Early T cell responses against diverse SARS-CoV-2 proteins associate with clinical protection(Bergamaschi et al., 2021; Notarbartolo et al., 2021; Peng et al., 2022; Tan et al., 2021). In contrast, patients with severe disease have reduced frequencies of circulating T cells and increased activation markers(Arunachalam et al., 2020; Hadjadj et al., 2020; Kuri-Cervantes et al., 2020; Laing et al., 2020; Mann et al., 2020; Mathew et al., 2020; Su et al., 2020). Compared to severe disease, circulating cytotoxic CD8$^+$ T cells, which are defined by HLA-DR and CD38 expression, increase earlier in mild patients and peak up to two weeks after symptom onset(Bergamaschi et al., 2021). These T cells are characterised by upregulated expression of NKG2D, IL-7 receptor and CD8. Circulating SARS-CoV-2-specific T cells are observed to peak within 15days after symptom onset(Tan et al., 2021). Higher frequencies of SARS-CoV-2 specific T cells, which were assessed by IFN-γ secreting ELISpot assays, are induced in mild patients and the earlier appearance of SARS-CoV-2 specific T cells are correlated with shorter duration of infection. Our previous study finds that $NP_{105-133}$-specific CD8$^+$ T cells are associated with less severe COVID-19 disease, and these T cells can

efficiently suppress virus replication control SARS-CoV-2 infection *in vitro*(Peng et al., 2022). There is an urgent need to for in-depth functional characterisation of virus-specific T cells during natural infection and following vaccination.

In addition to their "helper" role, mainly through interaction with antigen presenting cells and soluble mediators, the direct effector and antiviral function of virus-specific $CD4^+$ T cells have been studied in several human virus infection settings, such as influenza, CMV, and EBV(Juno et al., 2017). $CD4^+$ cytotoxic T cell responses were recently recognised to play an important role in the immune response to viral infections. However, most mechanistic studies investigating cytotoxic $CD4^+$ T cells were conducted in murine models; therefore, it is unclear if insights gained from such studies are relevant to human CTL responses(Juno et al., 2017). Recent SARS-CoV-2 $CD4^+$ T cell studies have been focused on the regulatory and helper function of these cells, such as Tfh cells and their role in assisting antibody production(Boppana et al., 2021; Lakshmanappa et al., 2021). An imbalance of regulatory and cytotoxic SARS-CoV-2-reactive $CD4^+$ T cells is found in hospitalised COVID-19 patients early in the disease(Meckiff et al., 2020). In the study, $CD154^+CD69^+CD4^+$ T cells post stimulation by overlapping peptides covering spike and membrane proteins were sorted and employed for single cell RNA sequencing. Higher proportions of cytotoxic SARS-CoV-2-reactive Tfh cells are found in hospitalised patients, and a significant negative correlation is observed between the proportion of $CD4^+$ CTLs and Treg. However, the roles of SARS-CoV-2 specific $CD4^+$ CTLs, whether they are protective or pathogenic, are

unknown. Cytotoxic $CD4^+$ T cells were also found to be significantly expanded in COVID-19 lung infiltrates and increased with disease severity(Kaneko et al., 2021). However, the specificity, effector function and antiviral activity of SARS-CoV-2 specific $CD4^+$ memory T cells were not known.

Current advances in technologies that combine population specific single cell transcriptomic profiling with TCR sequencing analysis and *in vitro* T cell functional assays have enabled us to study the quality of T cell responses and their ability to control virus replication(Peng et al., 2022). Multiple immunodominant SARS-CoV-2 spike-specific T cell epitopes have been identified and are frequently detected in individuals who have recovered from SARS-CoV-2 infection and following vaccination(Low et al., 2021; Painter et al., 2021; Peng et al., 2020).

In this study, we focus on three most dominant spike-specific $CD4^+$ T cell epitopes identified in a cohort of individuals who had recovered from SARS-CoV-2(Peng et al., 2020). We explore correlations with the quality of these spike-specific T cell responses and study their TCR repertoires, public TCR usage and their association with antiviral activity. We examine the potential mechanisms of antiviral activity in a specific cytotoxic subset of $CD4^+$ T cells using single cell transcriptome analyses of expanded T cell clones bearing the same TCRs as identified in single cell analysis, and proteomic profile analyses between T cell killer and non-killer clones.

5.2 Results

5.2.1 Identification of three immunodominant spike-specific CD4$^+$ T cell responses with effector function in individuals recovering from COVID-19

Three dominant SARS-CoV-2 spike protein (S) CD4$^+$ T cell epitopes: $S_{166\text{-}180}$ (CTFEYVSQPFLMDLE)(Mudd et al., 2021; Peng et al., 2020), $S_{751\text{-}765}$ (NLLLQYGSFCTQLNR)(Peng et al., 2020; Wragg et al., 2022) and $S_{866\text{-}880}$ (TDEMIAQYTSALLAG)(Peng et al., 2020) were identified in this and other studies. A minimal of 6/41 individuals responded to these peptides, regardless of their HLA type, in our study cohort(Peng et al., 2020).

5.2.1.1 Identification and HLA-restrictions of three immunodominant spike-specific CD4$^+$ T cell responses

As described in Chapter 4, immunodominant S_{166}-, S_{751}-, and S_{866}-specific T cell epitopes were identified in convalescent COVID-19 individuals by IFN-γ ELISpot assays using two-dimensional peptide matrix and confirmed by ELISpot of corresponding individual peptide.

The HLA-restriction of the epitope S_{166} was identified by IFN-γ ELISpot using antigen-specific T cell lines coculturing with HLA-matched and -unmatched B cell lines loaded with titrated peptides (Fig. 5.1A). All B cell lines carrying HLA-DPB1*04:01, which were loaded with peptide of epitope S_{166}, induced T cell responses of S_{166}-specific CD4$^+$ T cells, in contrast to B cell line that was DPB1*04:01 negative not stimulating T cell response. This indicated that S_{166}-

specific CD4$^+$ T cell responses were restricted by HLA-DPB1*04:01, which was further defined by S_{166}-DPB1*04:01 tetramer staining of spike-specific bulk CD4$^+$ T cell line (Fig. 5.1B). S_{166}-specific T cells are restricted by HLA-DPB1*04:01 and are also detected in vaccinated healthy donors(Mudd et al., 2021). Participants exhibiting S_{751}-, and S_{866}-specific T responses mostly carry HLA-DRB1*15:01, thus the two epitopes may be presented by DRB1*15:01. This was verified by peptide-MHC class II tetramer staining using PBMCs (Fig. 5.1C).

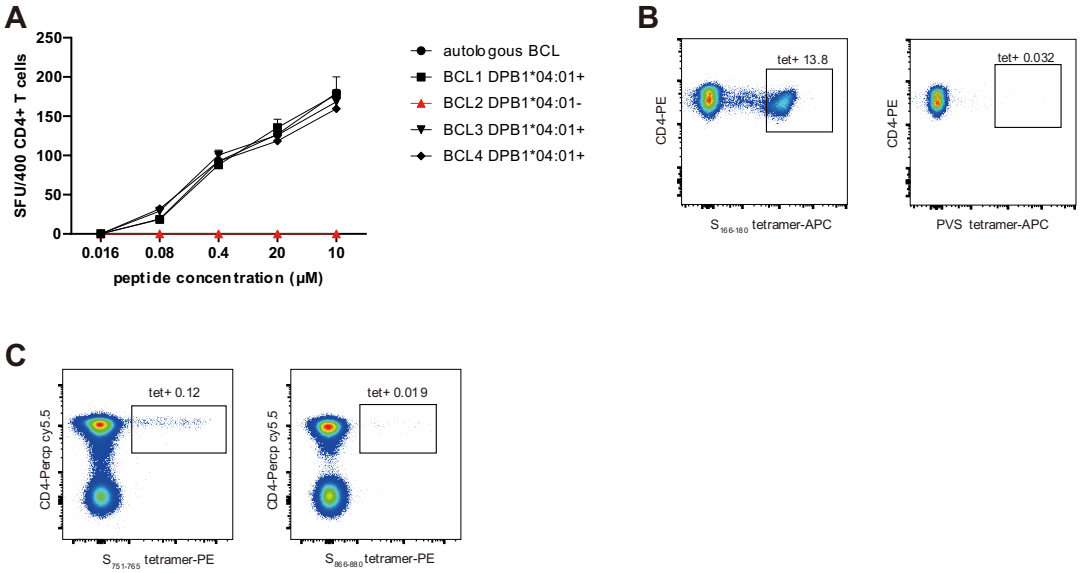

Fig. 5.1 HLA-restriction of the three dominant spike epitopes. (A) HLA-restriction of S_{166} was identified by coculturing S_{166}-specific bulk T cells with HLA-matched and -unmatched B cell lines loaded with titrated peptide. T cell response was assessed by IFN-γ ELISpot assay. (B) HLA-restriction of S_{166} was confirmed by peptide-DPB1*04:01 tetramer staining of bulk spike-specific CD4$^+$ T cell lines, with PVSKMRMATPLLMQA-DPB1*04:01 tetramer as negative control. (C) S_{751} and S_{866} HLA-restriction was confirmed by peptide-DRB1*15:01 tetramer staining of PBMCs from convalescent patients.

5.2.1.2 Immunodominance of three spike-specific CD4$^+$ T cell responses

Our cohort includes 45 individuals that had recovered from COVID-19, comprising 26 mild cases and 19 severe cases (including six critical cases) based on oxygen requirements during the acute illness (Appendix Table 5.1). There were no significant differences between mild and severe groups, in terms of gender proportion, age, and days post symptom onset when sampling (Fig. 5.2). As shown in Appendix Table 5.1, among all participants, 41 were HLA-DPB1 typed, and 26 (26/41, 63.41%) were HLA-DPB1*04:01 positive (13 mild and 13 severe cases); 45 were HLA-DR typed, and 17 (17/45, 37.78%) carried HLA-DRB1*15:01 (7 mild and 10 severe cases) (Fig. 5.3A).

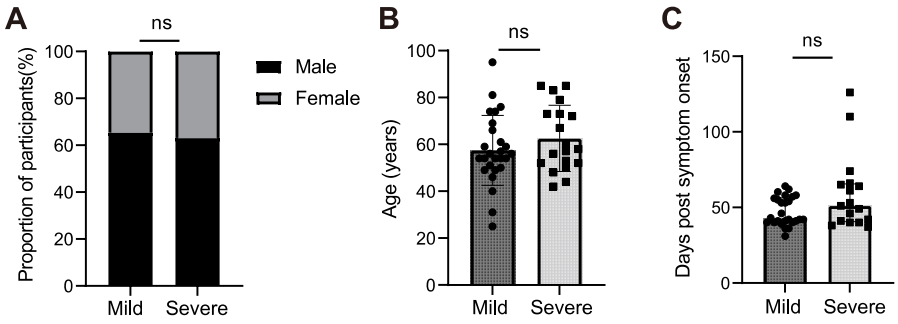

Fig. 5.2 Participant characteristics. (A) Comparison of gender distribution between mild (M/F=17/9) and severe (M/F=12/7) groups, *P*=0.878. (B) Comparison of age (*P*=0.251) and (C) days post symptom onset (*P*=0.163) when sampling between patient groups with mild and severe symptoms. Chi-square test (A), independent-sample *t* test (B) and Mann-Whitney *U* test (C) was used for analysis. The two-tailed *P* value was calculated. Data are shown in means ± standard deviation (SD) in B, and medians with interquartile ranges (IQRs) in C. M, male; F, female; ns, not significant.

The *ex vivo* IFN-γ ELISpot assays were carried out with convalescent samples collected 1-3 months post-infection from 25 HLA-DPB1*04:01 positive and 14

HLA-DRB1*15:01 positive cases. These ELISpot results revealed that 68% (17/25) of DPB1*04:01 individuals responded to S_{166} while 85.71% (12/14) and 71.43% (10/14) of DRB1*15:01 positive patients showed responses to S_{751} and S_{866} respectively (Fig. 5.3B). This further confirmed the immunodominance of these three epitopes. Among S_{166} responders, a high proportion of individuals (64.7%, 11/17) had recovered from severe disease (Fig. 5.3C) and with significantly stronger responses compared to individuals who had recovered from mild symptoms (P = 0.031; Fig. 5.3D). Although these data do not provide statistical evidence for an association of S_{751}- and S_{866}-specific T cell responses with disease severity, a higher proportion (60%, 6/10) of S_{866} responders was observed in participants who had recovered from mild disease compared to severe illnesses (Fig. 5.3C and D).

5.2.1.3 Effector function of immunodominant spike-specific $CD4^+$ T cells

5.2.1.3.1 Generation of $CD4^+$ T cell clones and polyclonal T cell lines targeting dominant spike epitopes

In order to further characterise these three dominant T cell responses, I generated 50 S_{166}-specific T cell clones, 54 S_{751}-specific T cell clones and 49 S_{866}-specific T cell clones from convalescent samples and evaluated their functionality. Briefly, to establish S_{166}-specific polyclonal T cell lines and clones, cytokine (TNFα-/IFN-γ/IL-2)-producing cells post stimulation with peptide of S_{166} epitope were sorted from short-term T cell lines and expanded clonally and bulk *in vitro*. Whereas S_{751}- and S_{866}-specific T cells were sorted by FACS with peptide-DRB1*15:01 tetramer

staining. Purity of T cell clones was checked with tetramer staining after each round of expansion, and functional assays were carried out only when purity was higher than 95% (Fig. 5.4A-C).

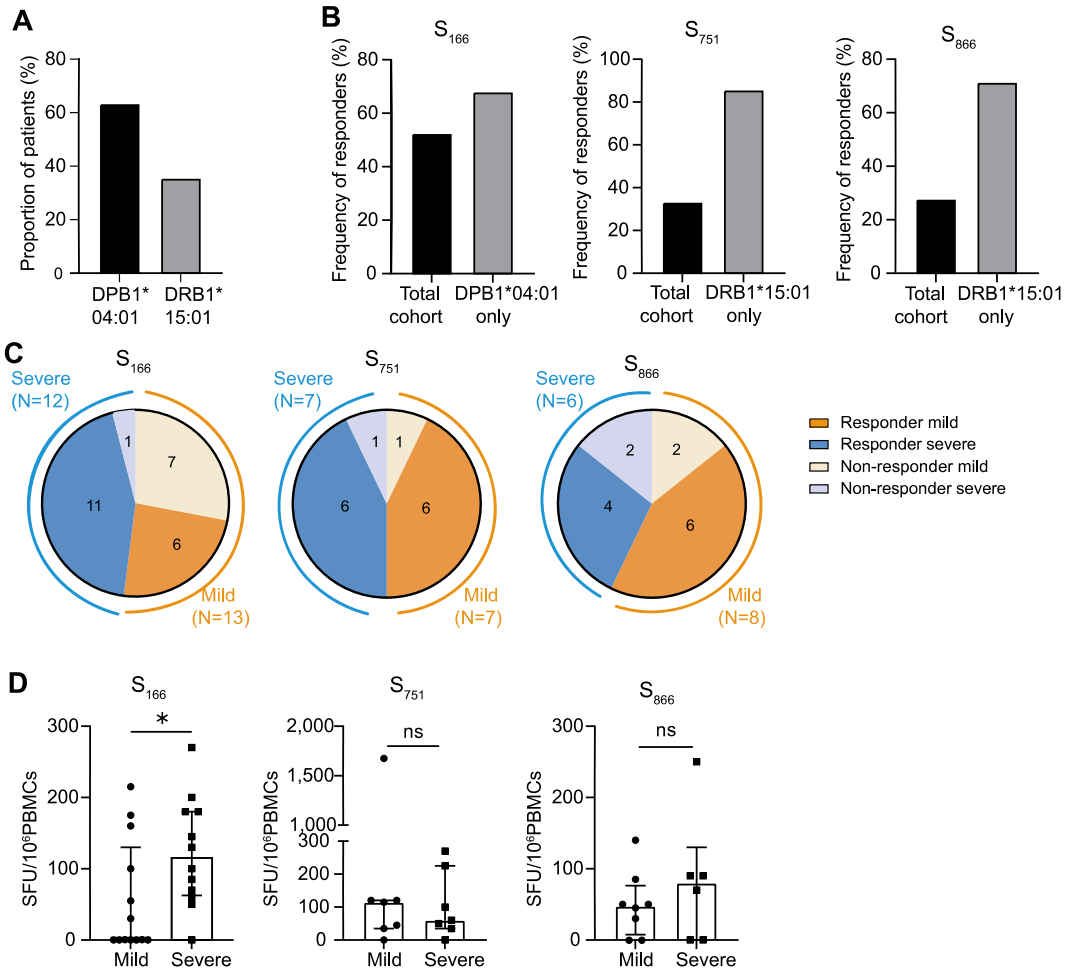

Fig. 5.3 Frequency and magnitude of response to S_{166}-DPB1*04:01, S_{751}-DRB1*15:01 and S_{866}-DRB1*15:01 epitopes in COVID-19 patients. (A) Proportion of patients with HLA-DPB1*04:01 (*N*=26/41) and DRB1*15:01 (*N*=17/45) in overall cohort. (B) Frequency of convalescent COVID-19 patients with T cells responding to S_{166} (*N*=21/40), S751-DRB1*15:01 (*N*=12/37) or S_{866}-DRB1*15:01 (*N*=10/36) peptide stimulation. (C) Proportion of DPB1*04:01 and DRB1*15:01 positive patients responding to S_{166}, S_{751} and S_{866} (*N*=17, 12, 10 respectively), and non-responders (*N*=8, 2, 4 respectively) with mild or severe COVID-19 disease. (D) Comparison of the magnitude of responses to S_{166}, S_{751}, and S_{866} epitopes between mild and severe DPB1*04:01 (*N*=13, *N*=12, *P*=0.031) or DRB1*15:01 positive responders (S_{751}: *N*=7, *N*=7, P=0.878; S_{866}: *N*=

8, *N*=6, *P*=0.470). Data are presented as medians with IQRs in D. The Mann-Whitney *U* test was used to compare distributions of two groups and the two-tailed *P* value was calculated. ns, not significant; **P*<0.05; SFU, spot-forming units.

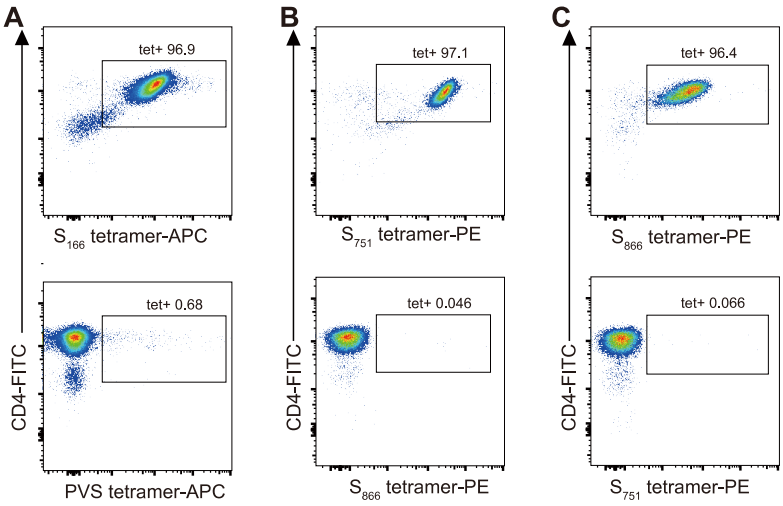

Fig. 5.4 Purity check of T cell clones and bulk lines by peptide-MHC class II tetramers after each round of expansion. Representative flow cytometry plots of (A) S_{166}-specific T cell clone, (B) S_{751}-specific T cell clone, and (C) S_{866}-specific T cell clone with corresponding tetramers (top panel) and negative tetramers (bottom panel).

5.2.1.3.2 Cytokine production of immunodominant spike-specific CD4⁺ T cells

To assess functional avidity of T cell clones, T cells were cocultured with B cells loaded with titrated peptides. Then cytokine expression was measured by ICS. All clones expressed cytokines including TNF-α, IFN-γ and IL-2 upon antigen activation (Fig. 5.5A). S_{866}-specific T cell clones displayed the highest antigen sensitivity, with the lowest EC_{50} calculated from TNF-α, IFN-γ, and IL-2 production. Consistently, when stimulated by B cells loaded with 2μM corresponding peptides, S_{866}-specific T cell clones secreted the highest levels of TNF-α, IFN-γ and IL-2 (Fig. 5.5B). The cytokine levels in the supernatant were measured by Luminex

after coculturing T cells with peptide-loaded B cells for 48 hours, with subtracting background levels of control wells containing T cells and B cells without peptides.

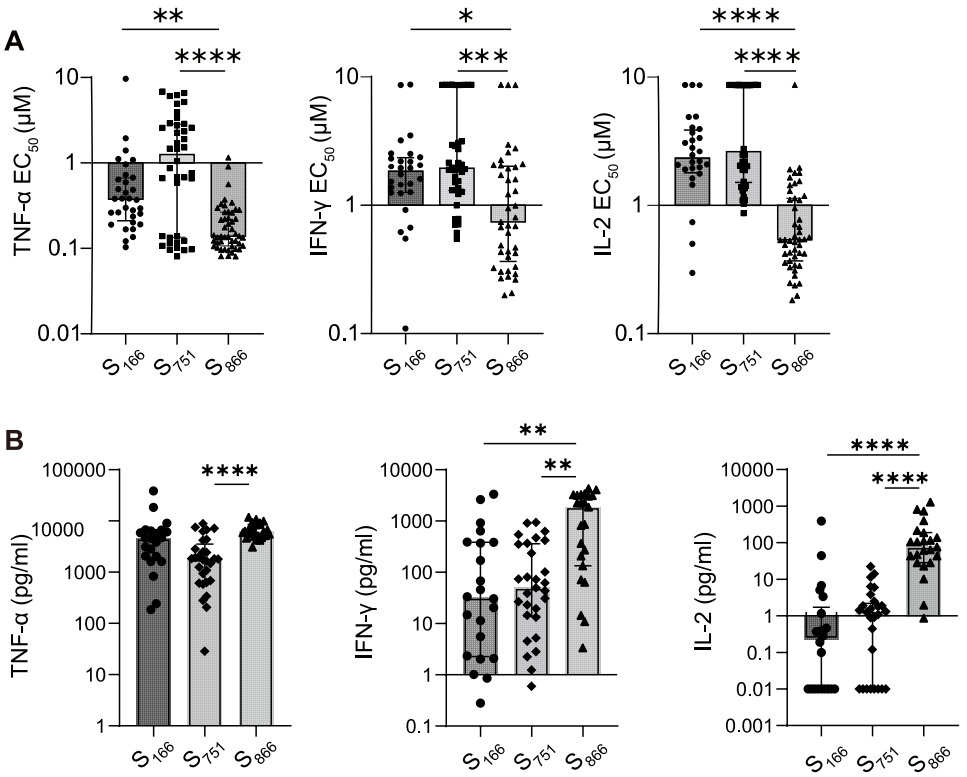

Fig. 5.5 Effector function of CD4$^+$ T cells targeting the three dominant spike epitopes. Comparison of EC_{50} of cytokine production (TNF-α, IFN-γ, and IL-2) (A) and cytokine levels secreted in the supernatant (B) upon stimulation with each of the three spike epitope peptides. (A) Cytokine production was assessed by ICS. *P* values were as follows: TNF-α: *P*=0.820 for S_{166} vs S_{751}; *P*=0.001 for S_{166} vs S_{866}; *P*=8.1803E-7 for S_{751} vs S_{866}; IFN-γ: *P*=0.334 for S_{166} vs S_{751}; *P*=0.038 for S_{166} vs S_{866}; *P*=0.00015 for S_{751} vs S_{866}; IL-2: *P*=1.000 for S_{166} vs S_{751}; *P*=3.6747E-8 for S_{166} vs S_{866}; *P*=3.1708E-13 for S_{751} vs S_{866}. (B) Cytokine levels in the supernatant were measured by Luminex. *P* values were as follows: TNF-α: *P*=0.063 for S_{166} vs S_{751}; *P*=0.066 for S_{166} vs S_{866}; *P*=0.00005 for S_{751} vs S_{866}; IFN-γ: *P*=1.000 for S_{166} vs S_{751}; *P*=0.001 for S_{166} vs S_{866}; *P*=0.0001 for S_{751} vs S_{866}; IL-2: *P*=1.000 for S_{166} vs S_{751}; *P*=3.6747E-8 for S_{166} vs S_{866}; *P*=3.1708E-13 for S_{751} vs S_{866}. Data are presented as medians with IQRs in A and B. Kruskal-Wallis one-way ANOVA was used to compare distributions among three groups, and the two-tailed *P* value was calculated. **P*<0.05, ***P*<0.01, ****P*<0.001, *****P*<0.0001.

5.2.1.3.3 Cytotoxicity of immunodominant spike-specific $CD4^+$ T cells

Interestingly, in addition to cytokine expression, a substantial proportion of T cell clones (4 from S_{166}, 8 from S_{751} and 22 from S_{866}) were observed to be capable of killing target cells by more than 10%, with the highest level of killing being 60% for S_{866} (Fig. 5.6A). The killing capacity of spike-specific $CD4^+$ T cell clones was assessed with CFSE-based cytotoxicity assays by coculturing T cells with B cells loaded with peptide at an E:T ratio of 4:1. Control wells containing T cells and B cells without peptide stimulation were included for each clone as negative control, when calculating killing capacity, background of negative control was subtracted to exclude nonspecific killing mediated by T cells. Killing of target cells by can be blocked by anti-HLA-DR antibody (Fig. 5.6B). With treatment of anti-HLA-DR antibody to target cells, killing capacity of S_{866}-specific T cell clones dramatically decreased to less than 10%. This indicates cytotoxicity of S_{866}-specific T cells is restricted to MHC class II molecules. These data highlight the existence of SARS-CoV-2-specific $CD4^+$ CTLs following SARS-CoV-2 infection. $CD4^+$ killer cells were defined as clones with killing capacity of > 10%. Among these spike-specific T cell clones, S_{866}-specific T cells showed the strongest cytotoxic and killing capacity ($P < 0.001$; Fig. 5.6A) and proportion of killer clones (61%; $P < 0.001$; Fig. 5.6C), whereas S_{166} T cells showed the least cytotoxic killing potential. Moreover, S_{866}-specific T cell clones showed comparable killing ability to SARS-CoV-2-specific $CD8^+$ T cell clones with similar killing EC_{50} (P=0.997; Fig. 5.6D).

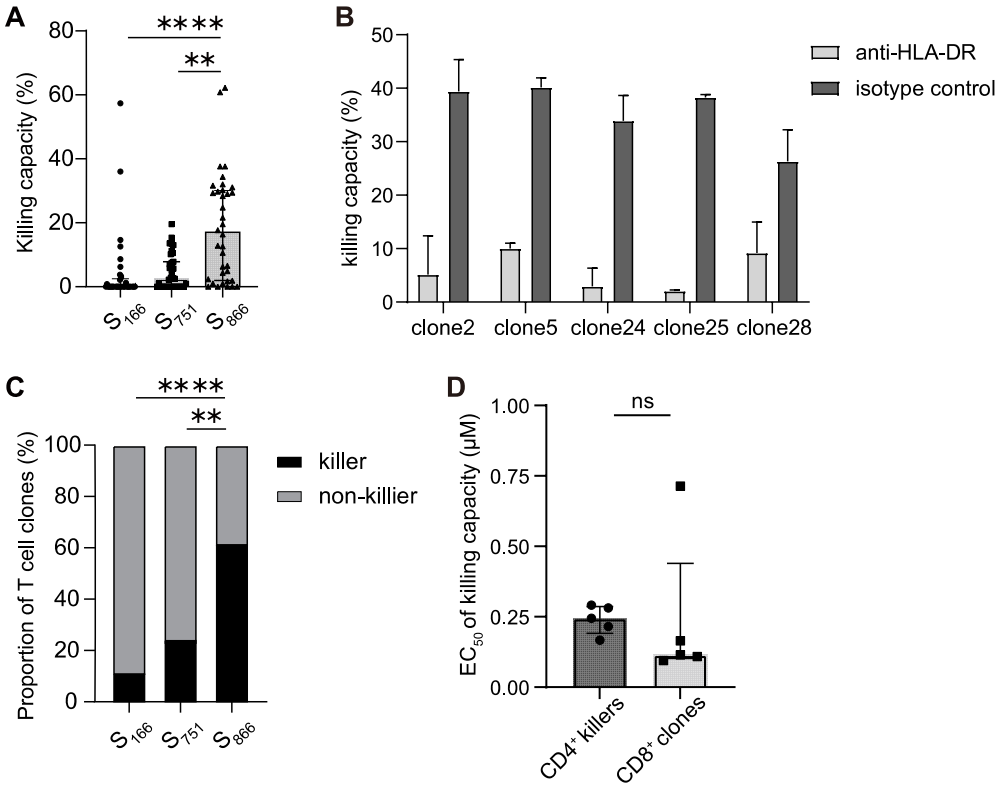

Fig. 5.6 Spike-specific CD4$^+$ T cell cytotoxic function. T cell killing capacity was assessed by CFSE-based cytotoxicity assays using T cell clones. (A) Comparison of killing capacity (%) across each epitope-specific CD4$^+$ T cells. P=0.251 for S_{166} vs S_{751}; P=3.8563E-7 for S_{166} vs S_{866}; P=0.001 for S_{751} vs S_{866}. (B) Prior to peptide loading, target cells were incubated with anti-HLA-DR antibody or isotype control. Blocking of MHC class II on target cells demolished T cell killing. (C) Proportion of CD4$^+$ T cell clones that can be divided as "killer" (black) or "non-killer" (grey) CD4$^+$ T cells. P=0.170 for $S_{166\text{-}180}$ vs $S_{751\text{-}765}$; P=0.00007 for $S_{166\text{-}180}$ vs $S_{866\text{-}880}$; P=0.001 for $S_{751\text{-}765}$ vs $S_{866\text{-}880}$. (D) Comparison of killing EC_{50} between S_{866}-specific T cell clones (N=5) and NP_{105}-B*07:02-specific T cell clones (N=5). Data are presented as medians with IQRs in A, and as means ± SD in B and D. Kruskal-Wallis one-way ANOVA was used for comparison of killing capacity was performed by (A), while Chi-square test for ratio comparison(C), and the independent-sample t test for killing EC_{50} comparison (D). The two-tailed P value was calculated. ns, not significant, **P<0.01, ***P<0.001. *****P<0.0001

5.2.2 Antiviral efficacy of immunodominant spike-specific $CD4^+$ T cells

To assess antiviral activity of SARS-CoV-2 specific T cells, *in vitro* SARS-CoV-2 virus infection system was established in our lab. To optimise SARS-CoV-2 infection, ACE2 expressing B cells were infected with Victoria stain at an MOI of 0.001, 0.01 and 0.1 respectively for two hours, then washed three times with PBS and cultured at 37°C. Virus copies in B cells were then quantified by real-time qPCR after six and 24hrs of infection. Only B cell line transduced with ACE2 can be infected with SARS-CoV-2 (Fig. 5.7A). The virus titre was highest at the MOI of 0.1 and infection for 24hrs compared. Thus, ACE2-expressing B cells were infected with SARS-CoV-2 at an MOI of 0.1 then cocultured with S_{166}-specific $CD4^+$ T cell clone after 24hrs infection, at E:T ratios of 1:1 and 1:2. Subsequent cytokine production and CD107a expression by T cells were assessed by ICS. As shown in Fig. 5.7B, when coculturing with SARS-CoV-2-infected B cells at E:T ratios of 1:1 and 1:2, comparable T cell responses were stimulated. Therefore, the E:T ratio of 1:1 was used for ICS to assess cytokine and CD107a expression by T cells.

Taking advantage of *in vitro* SARS-CoV-2 virus infection system, the antiviral activity of these spike-specific $CD4^+$ T cells was assessed. As shown in Fig. 5.7C, ACE2, the cell receptor of SARS-CoV-2, was transduced into EBV-transformed B cell lines. B cells expressing ACE2 were sorted and subjected to *in vitro* expansion with puromycin selection. B cells ectopically expressing ACE2 were infected with SARS-CoV-2 at an MOI of 0.1 then cocultured with spike-specific

$CD4^+$ T cells. T cell recognition of virus-infected cells was examined by ICS with coculturing at an E:T ratio of 1:1 for six hours, and the suppression of SARS-CoV-2 replication by T cells was assessed by quantifying the number of viral copies in the infected cells after 48 hours of coculturing an a E:T ratio of 4:1. The frequency of ACE2 expressing B cells was detected prior to SARS-CoV-2 infection by flow cytometry with primary antibody of human ACE2 and subsequent secondary antibody (anti-goat) staining (Fig. 5.7D). Virus-infected ACE2-expressing B cells were defined as target cells. The data showed that $CD4^+$ T cells targeting these three dominant spike epitopes can recognise virus-infected cells and produce cytokines after activation (Fig. 5.7E). S_{866}-specific T cells executed the highest proportion of TNF-α (P<0.001), IFN-γ (P<0.001), and IL-2 (P<0.001) producing $CD4^+$ T cells after encountering virus-infected B cell lines (Fig. 5.7F). More importantly, $CD4^+$ T cell clones targeting each of the three epitopes exhibited, to various extents, direct effector function against the virus, capable of suppressing virus replication (Fig. 5.7G). In particular, T cells targeting S_{866} showed significantly better antiviral efficacy compared to T cells targeting epitope S_{751} restricted by the same HLA-DRB1*15:01 (P=0.002).

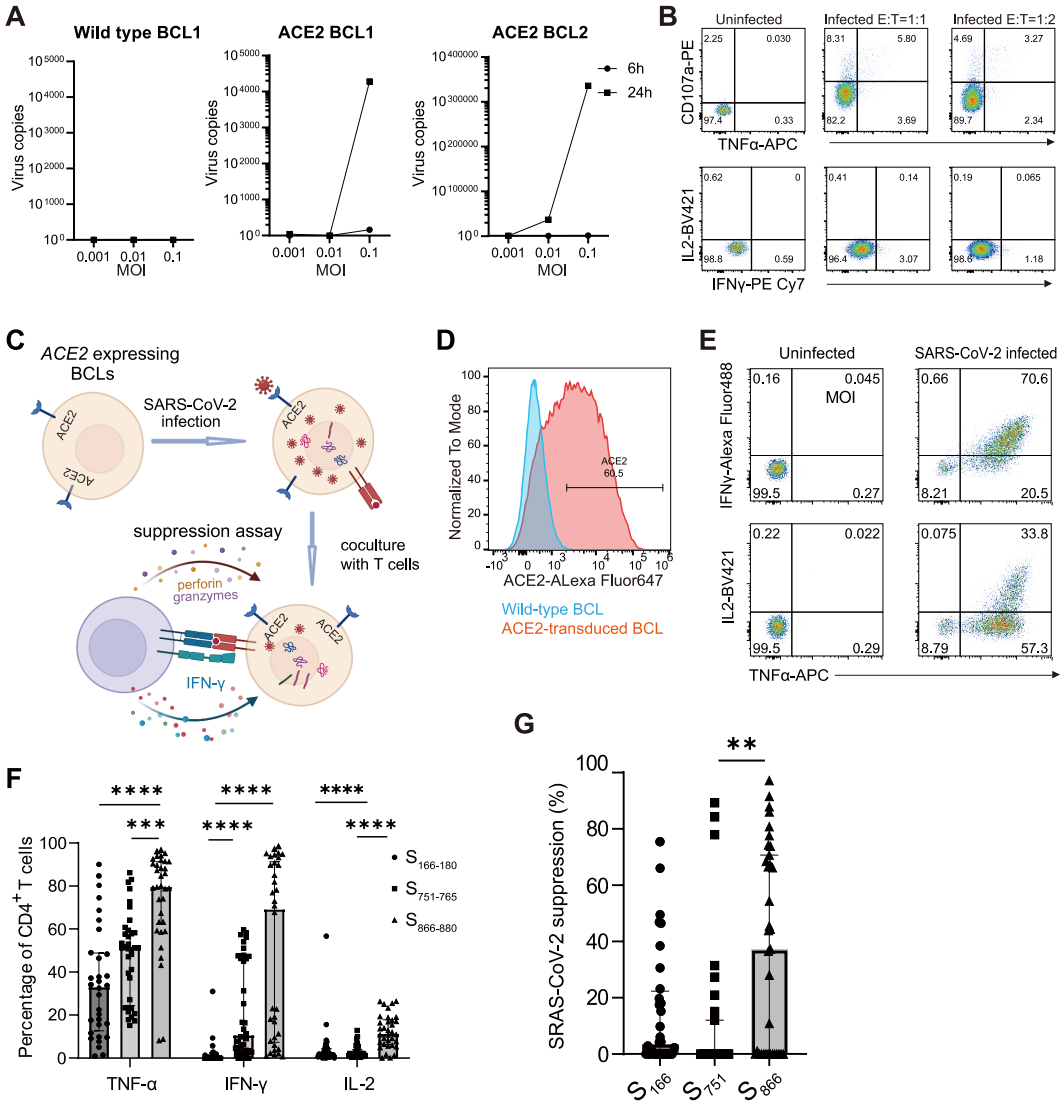

Fig. 5.7 Spike-specific CD4⁺ T cell antiviral effector function. (A) SARS-CoV-2 viral copies in B cells at different time points and MOIs. (B) T cell cytokine production and CD107a expression in response to SARS-CoV-2 infected B cells at E:T ratio of 1:1 and 1:2. (C) Schematic diagram detailing workflow of viral suppression and intracellular cytokine assays. (D) Representative flow cytometry histogram detecting ACE2 expression on B cells. (E) Representative ICS flow cytometry plots measuring TNF-α, IFN-γ, and IL-2 expression in CD4⁺ T cells incubated with SARS-CoV-2 infected B cell lines. (F) ICS data summarised for each epitope as percentage of CD4⁺ T cells expressing each cytokine. TNF-α: P=0.178 for S_{166} vs S_{751}; P=1.8419E-8 for S_{166} vs S_{866}; P=0.000141 for S_{751} vs S_{866}; IFN-γ: P=0.000003 for S_{166} vs S_{751}; P=6.5208E-12 for S_{166} vs S_{866}; P=0.071 for S_{751} vs S_{866}; IL-2: P=1.000 for S_{166} vs S_{751}; P=0.000002 for S_{166} vs S_{866}; P=0.000001 for S_{751} vs S_{866}. (G) Comparison of SARS-CoV-2 viral suppression

across spike-specific $CD4^+$ T cells. P=0.305 for S_{166} vs S_{751}; P=0.241 for S_{166} vs S_{866}; P=0.002 for S_{751} vs S_{866}. Data are presented as medians with IQRs (F and G). Kruskal-Wallis one-way ANOVA was used for analysis and the two-tailed P value was calculated. **P<0.01, ***P<0.001, ****P<0.0001. ICS, intracellular cytokine staining; BCLs, B cell lines.

5.2.3 Spike-specific $CD4^+$ T cell antiviral activity is associated with cytotoxic activity, cytokine production and antigen load

The highest effector function and antiviral efficacy were seen for S_{866}-specific $CD4^+$ T cells, suggesting significant effector function of cytotoxic $CD4^+$ T cell acting on virus infected cells and controlling virus replication. To explore whether this strong antiviral activity was a result of high effector function or exposure to high antigen loads, we examined single cell gene expression from tetramer-sorted short-term cultured T cell lines. As shown in Fig. 5.8A, live $CD4^+$tetramer$^+$ T cells with negative CD8 expression were sorted for 10X Chromium assays. First, we compared single cell gene expression profiles of T cells targeting S_{751} (N=1629) and S_{866} cells (N=2233) (Fig. 5.8B). We observed significant upregulation of genes encoding effector molecules, such as cytotoxic molecules *KLRK1* (P=1.37 x 10^{-44}), *GZMB* (P=6.13 x 10^{-4}) and *GZMK* (P=5.13 x 10^{-10}), and cytokines *CCL3* (P=2.79 x 10^{-6}), *CCL4* (P=4.4 x 10^{-8}), *TNF* (P=9.08 x 10^{-12}) in S_{866}-specific T cells compared to S_{751}-specific T cells (Fig. 5.8C). This further confirms the cytotoxic potential of S_{866}-specific T cells.

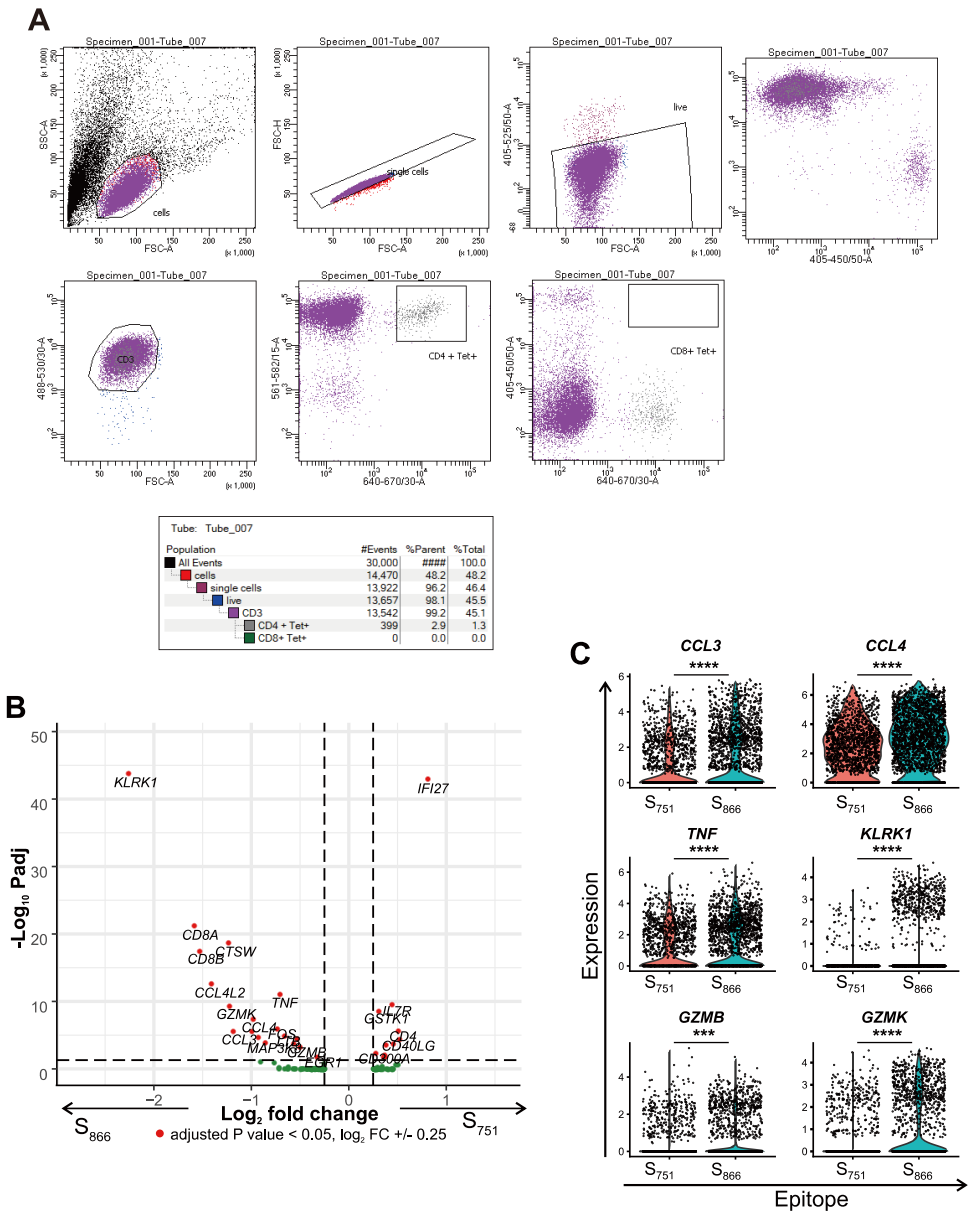

Fig. 5.8 Comparison of gene expression profiles between S_{751}- and S_{866}-specific CD4$^+$ T cells. (A) Gating strategy of sorting tetramer$^+$CD4$^+$ cells for SmartSeq2 and 10X single cell RNA-seq. Dump-BV510, CD3-FITC, CD4-PE, CD8-BV421, tetramer-APC. (B) Differentially expressed genes between S_{751}- (*N*=1629) and S_{866}-specific (*N*=2233) single cells from five patients. Single-cell data were generated by 10X Chromium. (C) Violin plots showing gene expression for *CCL3* (*P*=2.79E-6), *CCL4* (*P*=4.4E-8), *TNF* (*P*=9.08E-12), *KLRK1* (*P*=1.37E-44), *GZMK* (*P*=5.13E-10), and *GZMB* (*P*=6.13E-4). Single-cell data were generated by 10X Chromium. MAST statistical test was used with sequencing batches as latent variable (B). Adjusted *P* values are shown (C).

To estimate the antigen load of each epitope on virus-infected cells, I cocultured T cells of epitope-specific polyclonal T cell lines with the same number of target cells either infected with SARS-CoV-2 or loaded with variable amounts of peptide, then assessed T cell responses by ICS (Fig. 5.9A). The antigen load in virus-infected cells was equivalent to the peptide concentration that elicited a similar level of response to virus-infected cells. Surprisingly, much lower concentrations (equivalent to 0.06μM) of S_{866} peptide were presented on virus-infected cells, when compared to S_{166} (about 0.11μM) and S_{751} (equivalent to 2.57μM) (Fig. 5.9B). These data suggest that the higher antiviral activity of S_{866}-specific T cells is likely to result from strong cytotoxicity and high antigen sensitivity even when antigen load on the surface of infected cells was relatively low.

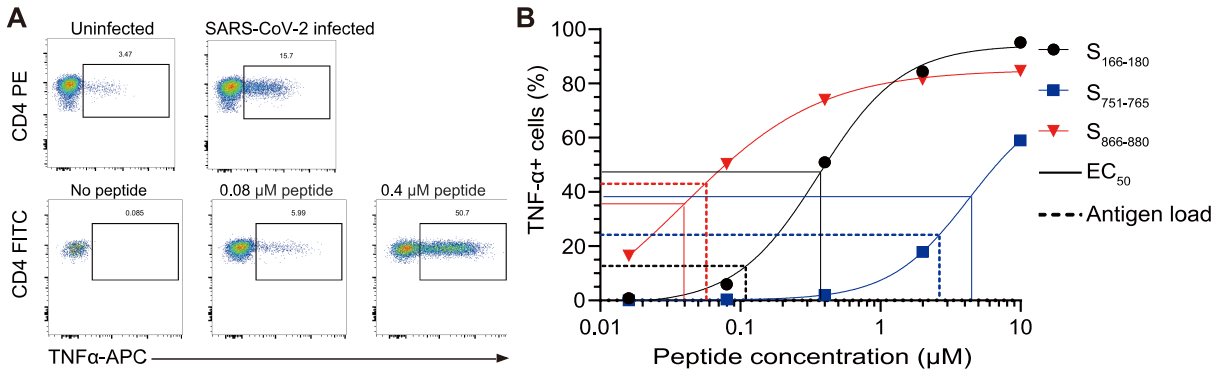

Fig. 5.9 Antigen load of each spike epitope on SARS-CoV-2 infected cells. (A) Representative flow cytometry plots measuring TNF-α expression after incubation with SARS-CoV-2 infected cells or peptide-loaded target cells. (B) Estimated antigen load of each epitope on virus-infected cells and EC_{50} of T cell response. S_{166} is shown as black circles, S_{751} in blue squares and S_{866} in red triangles. Dashed lines represent the estimated antigen-load of each corresponding epitope on virus-infected cells whereas solid lines show the EC_{50} of each T cell response.

5.2.4 Diverse TCR usage and public TCR clonotypes are commonly observed among immunodominant spike T cells

In this study, we applied SmartSeq2 and 10X to analyse TCR and gene expression of each spike epitope-specific T cells when cells being sorted from *ex vivo* PBMCs and short-term cultured T cell lines, respectively.

5.2.4.1 Diverse TCR usage

Single cell TCR sequences generated by SmartSeq2 with *ex vivo* stimulated and cytokine sorted S_{166} (*N*=152 cells from 5 patients, Fig. 5.10A), tetramer-sorted S_{751} (*N*=77 cells from four patients) and tetramer-sorted S_{866} (*N*=100 cells from four patients) -specific T cells from 1-3 months convalescent patients were analysed to assess TCR diversity. As shown in Fig. 5.10B, TCR repertoires of spike-specific $CD4^+$ T cells targeting the three dominant epitopes were highly diverse. Interestingly, each epitope displays a different dominant αV gene usage, with TRAV35, TRAV12-1 and TRAV26-1 being dominant for S_{166}-, S_{751}-, and S_{866}-specific T cells respectively, where each dominant αV gene pairs with multiple different βV genes (Fig 5.10B). This highlighted the importance of the α chain in these spike epitope TCRs; hence we decided to focus on the αV chain when investigating TCR clonotypes further.

5.2.4.2 Public TCR clonotypes

Single cells from epitope-specific T cells sampled at different timepoints (S_{166} *ex vivo* acute, *ex vivo* 1-3 months, short-term culture 9 months convalescence from

total 5 patients; S_{751} and S_{866} *ex vivo* acute, *ex vivo* 1-3 months, short-term culture 6 months and 9 months convalescence from total 6 patients) were analysed together to identify public clonotypes (CDR3 amino acid and V gene usage), which are unique clonotypes shared among more than one unrelated patient. We found that public α clonotypes (CDR3α and TRAV) were shared by many patients (Table 5.1) whereas β clonotypes (CDR3β and TRBV) were shared by a smaller number of patients (Table 5.2). For example, the maximum number of patients with one particular α clonotype (CAGTGNNRKLIW, TRAV 25) from S_{866}-specific T cells could be 6/6 whereas the highest number of patients sharing any β clonotype from the same epitope was 3/6 (Table 5.2). Of note, public TCR clonotypes with both α and β shared by one than one patient were also observed (Table 5.3). Examination of paired αβ public clonotypes revealed that the β public clonotypes were more diverse than α public clonotypes, with no clear dominant Vβ gene usage for any epitope. By focusing on α clonotypes, we reasoned that we would be better able to study the dominant α V genes for each epitope, which should also capture the diversity of β clonotypes.

Table 5.1 Public TCR α clonotypes for each spike epitope

Epitope	CDR3α	TRAV	No. of patients
S_{166}	CA**ALNY**GGSQGNLIF	TRAV35	5/5
	CAG**LLFK**AAGNKLTF	TRAV35	5/5
	CAG**LN**SGGSNYKLTF	TRAV35	3/5
	CAASGARGAQKLVF	TRAV29/DV5	2/5
S_{751}	CAASI**A**GSARQLTF	TRAV13-1	3/6
	CVVN**AR**SSNTGKLIF	TRAV12-1	5/6
	CVVN**I**GSSASKIIF	TRAV12-1	5/6
	CVVN**KRS**SSASKIIF	TRAV12-1	3/6
	CVVN**R**G**GYQ**K**V**TF	TRAV12-1	3/6
	CAASISGGYNKLIF	TRAV13-1	2/6
	CATGGSNYKLTF	TRAV17	3/6
	CAVGRYGGSQGNLIF	TRAV2	3/6
	CVVNKYSSNTGKLIF	TRAV12-1	2/6
	CVVNPKTSYDKVIF	TRAV12-1	2/6
	CVVNRGYSTLTF	TRAV12-1	2/6
	CVVPTGGGNKLTF	TRAV12-1	2/6
S_{866}	CAG**T**GNNRKLIW	TRAV25	6/6
	C**AV**AGNNRKLIW	TRAV25	3/6
	CIVR**A**ANQAGTALIF	TRAV26-1	3/6
	CIVRV**E**YNFNKFYF	TRAV26-1	4/6
	CV**AS**GGSNYKLTF	TRAV12-1	3/6
	CAFMKPVTQGAQKLVF	TRAV38-1	2/6
	CILRAPLSFGNEKLTF	TRAV26-2	2/6
	CIVRGLNAGNMLTF	TRAV26-1	2/6
	CIVRVGGSWGKLQF	TRAV26-1	2/6
	CIVRVLFGNEKLTF	TRAV26-1	2/6
	CIVRVLGGGYNKLIF	TRAV26-1	2/6
	CVVNPNARLMF	TRAV12-1	4/6
	CVVNRGSNYQLIW	TRAV12-1	2/6
	CVVNRGSSYKLIF	TRAV12-1	3/6
	CVVSGGSNYKLTF	TRAV12-1	3/6

Table 5.2 Public TCR β clonotypes for each spike epitope

Epitope	CDR3β	TRBV	No. of patients
S_{166}	CASSFRGDGYTF	TRBV5-1	2/5
	CASSPRDRVNTGELFF	TRBV9	2/5
	CASSQGVGYTF	TRBV4-1	2/5
	CASSYRGAYGYTF	TRBV6-2	2/5
	CASSYSGGQPQHF	TRBV6-5	2/5
	CAWRGGIGYTF	TRBV30	2/5
S_{751}	CASSEGAGSQPQHF	TRBV6-1	4/5
	CASSSSGGGSYEQYF	TRBV6-5	2/5
	CASSTPNRGNNQPQHF	TRBV19	2/5
	CASTEGASNQPQHF	TRBV6-1	2/5
S_{866}	CASSPLANEQFF	TRBV11-2	3/6
	CASSPTYEQYF	TRBV11-2	3/6
	CASSFGGSYGYTF	TRBV12-3	3/6
	CASSFGGNYGYTF	TRBV12-4	2/6
	CASSQVAAEQFF	TRBV3-1	3/6
	CASSLGPNSGNTIYF	TRBV5-1	2/6
	CASSLLTGSTDTQYF	TRBV5-1	2/6
	CASSLSGLDGYTF	TRBV5-1	2/6
	CASSLVSEKLFF	TRBV11-2	2/6
	CASSQVGAGTDTQYF	TRBV4-3	2/6

Table 5.3 Public TCR αβ clonotypes for each spike epitope

Epitope	CDR3α	TRAV	CDR3β	TRBV	No. of patients
S_{166}	CAGMNYGGSQGNLIF	TRAV35	CASSQGVGYTF	TRBV4-1	2/5
	CAGMNYGGSQGNLIF	TRAV35	CASSYRGAYGYTF	TRBV6-2	2/5
	CAGMNYGGSQGNLIF	TRAV35	CAWRGGIGYTF	TRBV30	2/5
	CAGQLYGGSQGNLIF	TRAV35	CASSFRGDGYTF	TRBV5-1	2/5
	CAGQLYGGSQGNLIF	TRAV35	CASSYSGGQPQHF	TRBV6-5	2/5
S_{751}	CVVNKGSSASKIIF	TRAV12-1	CASSEGASNQPQHF	TRBV6-1	4/6
S_{866}	CAGTGNNRKLIW	TRAV25	CASSFGAYGYTF	TRBV12-4	2/6
	CAGTGNNRKLIW	TRAV25	CASSFGGNYGYTF	TRBV12-3	2/6
	CAMNGGANSKLTF	TRAV12-3	CASSLGPNSGNTIYF	TRBV5-1	2/6
	CAVAGNNRKLIW	TRAV25	CASSQVGAGTDTQYF	TRBV4-3	2/6
	CIVRAANQAGTALIF	TRAV26-1	CASSQVAGEQYF	TRBV3-1	3/6
	CIVRVEYNFNKFYF	TRAV26-1	CASSPLANEQFF	TRBV11-2	3/6
	CIVRVSYNFNKFYF	TRAV26-1	CASSLVSEKLFF	TRBV11-2	2/6
	CVVNRGSSYKLIF	TRAV12-1	CASSQTYEQYF	TRBV11-2	3/6

Next, we sought to compare the proportion of public and private clonotypes from each epitope. S_{166}-specific T cells have higher proportions of TCRs matching public clonotypes compared to the other two epitopes (*N*=21 S_{166} public α clonotypes, *N*=16 S_{751} public, *N*=19 S_{866} public; Fig. 5.10C). We also investigated if there were any differences between public and private clonotype expansion for each epitope at different timepoints (acute, 1-3 months and 6-9 months convalescence) and found that T cells with public clonotypes were present at higher frequencies compared to cells with private clonotypes, with the exception of S_{866} at 6-9 months convalescence (acute: S_{166} *P*=1.7 x 10^{-6}, S_{751} *P*=0.04, S_{866} *P*=0.0098*;* 1-3 months: S_{166} *P*=1.4 x 10^{-15}, S_{751} *P*=6.3 x 10^{-8}, S_{866} *P*=3.8 x 10^{-6}; 6-9 months: S_{166} *P*=3.1 x 10^{-9}, S_{751} *P*=0.026, S_{866} *P*=0.15; Fig. 5.10D).

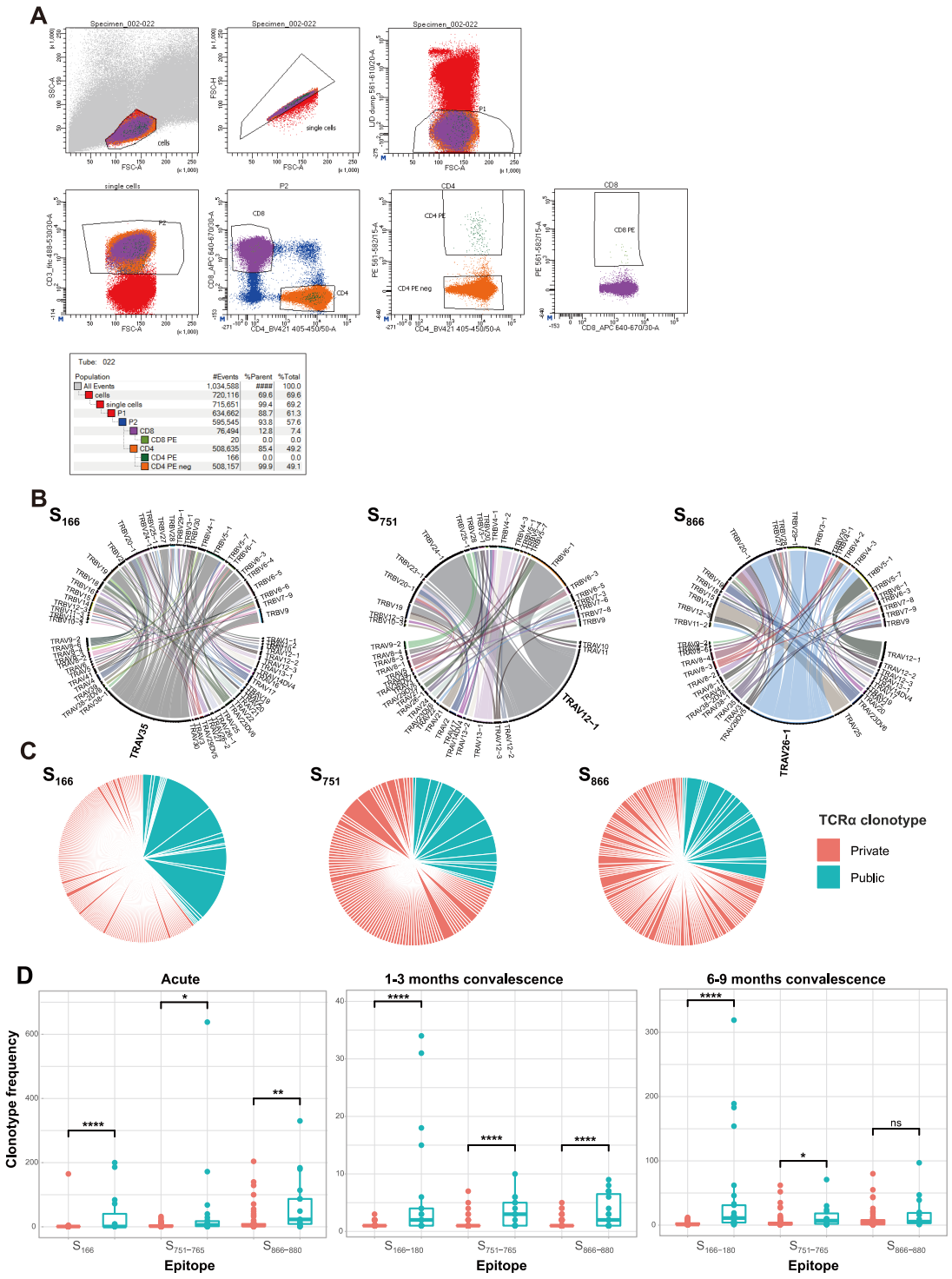

Fig. 5.10 TCR repertoire of S_{166}, S_{751}-, and S_{866}-specific $CD4^+$ T cells from COVID-19 patients. (A) Gating strategy of sorting TNF-α^+/IFN-γ^+/$IL2^+CD4^+$ cells for SmartSeq2 and 10X single cell RNA-seq. Dump-PE CF594, CD3-FITC, CD4-BV421, CD8-APC, TNF-α/IFN-γ/IL-2-PE. (B) Circos plots for each epitope depicting V αβ gene usage at 1 month convalescence (Smartseq2, *N*=5 patients and 152 S_{166} cells, *N*=4 patients and 77 S_{751} cells, *N*=4 patients and 100 S_{866} cells). (C) Pie charts depicting Vα clonotypes from 1

month convalescence for each epitope (Smartseq2, *N*=216 S_{166} clonotypes, *N*=117 S_{751} clonotypes, *N*=151 S_{866} clonotypes) with public (blue) and private (red) clonotypes highlighted. (D) Comparison between frequencies of public and private clonotypes for each epitope from T cells sampled from patients at different timepoints (*N*=3 patients and 335 acute clonotypes, *N*=4-5 patients and 484 1-3 months clonotypes and *N*=3 patients and 286 6/9 months clonotypes from convalescent disease). For boxplots, the lower and upper hinges represent the 25-75th percentiles, the central line represents the median, and the whiskers extend to the maximum and minimum values that are no greater than 1.5x the IQR. The MAST statistical test was used with sequencing batch as latent variable. Adjusted *P* values are shown. ns, not significant; **P*<0.05, ***P*<0.01, *****P*<0.001, *****P*<0.0001.

5.2.4.3 Functional differences between T cells with public and private TCRs

To further investigate differences between T cells with public and those with private TCRs, we looked at single cell gene expression between these two groups. *Ex vivo* stimulated and cytokine sorted S_{166}-specific single cells with public TCRs (*n* =128 cells) had higher expression of activation markers [*IFNG* (*P* =2.92 x 10^{-5}), *FASLG* (*P* = 9 x 10^{-8}), *CD40LG* (*P* = 4.86 x 10^{-16}), *BTLA* (*P* = 1.48 x 10^{-3}), *PDCD1* (*P* = 1.61 x 10^{-3})], Th1 activators [*ID2* (*P* = 1.07 x 10^{-5})] and Th2 suppressors [*NR4A2* (*P* = 1.94 x 10^{-14}) and *IRF4* (*P* = 1.18 x 10^{-6}), Fig. 5.11A] compared with T cells with private TCRs (*N*=285 cells). This may indicate that high expansion of T cells with public clonotypes might drive a Th1 response in convalescent COVID-19 patients. Conversely, tetramer-sorted S_{866}-specific T cells from short-term culture with private TCRs (*N*=1325 cells) display higher expression of cytotoxic genes [*KLRK1* (*P*=5.65 x 10^{-8}), *GZMA* (*P*=1.22 x 10^{-3}), *GZMK* (*P*=2.95 x 10^{-5}), *NKG7* (*P*=3.92 x 10^{-4}), *CCL5* (*P*=1.19 x 10^{-8}), Fig. 5.11B]

compared with T cells with public TCRs (*N*=194 cells). Similar results were observed with S_{751}-specific T cells with higher expression of cytotoxic gene *GZMM* in T cells with private TCRs (Fig. 5.11C). In summary, these results highlight the potential different functional activities between epitope-specific T cells.

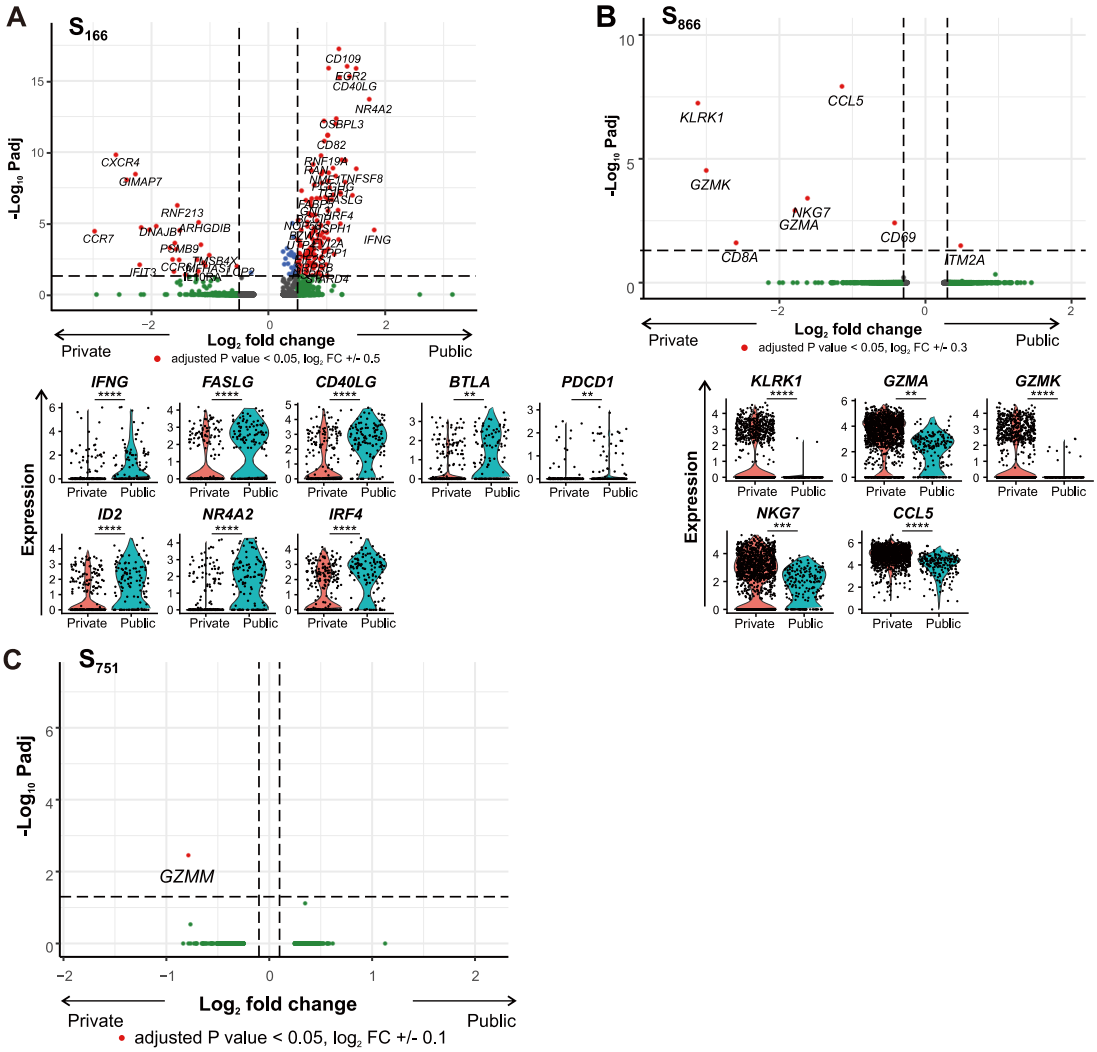

Fig. 5.11 Gene expression differences between T cells with private and public TCRs. (A) Differentially expressed genes from S_{166} single cells from 1 month convalescence (Smartseq2) between T cells with public (*N*=128) or private (*N*=285) clonotypes. Violin plots showing gene expression for *IFNG, FASLG, CD40LG, BTLA*, *PDCD1*, *ID2*, *NR4A2,* and *IRF4.* (B) Differentially expressed genes from S_{866} single cells from 6-9 months convalescence (10X Chromium) between T cells with public (*N*=194) or

private (*N*=1325) clonotypes. Violin plots showing gene expression for *KLRK1*, *GZMA*, *GZMK*, *NKG7,* and *CCL5.* (C) Differentially expressed genes from S_{751} single cells from 6 and 9 months convalescence (10X Chromium) between T cells with public (*N*=159) or private (*N*=767) clonotypes. The MAST statistical test was used with sequencing batch as latent variable. Adjusted *P* values are shown. ***P*< 0.01, *****P*< 0.001, *****P*<0.0001.

5.2.5 Cytotoxicity and function of spike-specific CD4$^+$ T cells are regulated by more than TCR usage alone

To explore whether the effector function of spike-specific CD4$^+$ T cells was due to their broad TCR usage, I compared antigen sensitivity and killing capacity of T cell clones bearing the same TCR. Firstly, TCRs of spike-specific CD4$^+$ T cell clones were sequenced and the sequencing results showed that these T cell clones possessed a wide variety of TCRs (Table 5.4 and Appendix Table 5.2). Consistent with TCRs analysed with scRNA-seq data, a wide variety of TCRs were observed in CD4$^+$ T cell clones specific to each epitope, with some clones sharing paired αβ of TCR clonotypes. S_{866}-specific CD4$^+$ T cell clones with the same TCRs had very different antigen sensitivities, reflected in a wide range of EC_{50} values for IFN-γ, TNF-α and IL-2 production (Fig. 5.12A). These T cell clones also displayed different cytokine profiles (including TNF-α, IFN-γ, IL-2, IL-4, IL-5, IL-6, IL-10, IL-13, RANTES, and GM-CSF) upon antigen stimulation, when cytokines in the supernatant were quantified by Luminex assay (Fig. 5.12B). Moreover, S_{866}-specific T cell clones with shared TCRs had distinct killing capacities (Fig. 5.12C), for example, clone 2 had 40% killing capacity while clone 3 showed minimal killing despite sharing the same TCR (TRAV12-1/TRBV5-1).

This suggested that the cytolytic activity of these spike-specific $CD4^+$ T cells was due to factors beyond TCR usage. This observation was further confirmed by variable expression levels of cytotoxic molecule genes, such as *PRF1*, *GZMA*, and *GZMB*, in tetramer-sorted S_{866} single cells from four patients (10X, *N*=399 cells) with the same TCR usage (Fig. 5.12D).

Table 5.4 T cell receptors of S866-specific T cell clones

Clone ID	CDR3α	TRAV	TRAJ	CDR3β	TRBV	TRBJ
clone1	CVVNPNARLMF	TRAV12-1	TRAJ31	CASSPLKGAIDTQYF	TRBV5-1	TRBJ2-3
clone2						
clone3						
clone4						
clone5						
clone6						
clone7						
clone8						
clone9						
clone10						
clone11						
clone12						
clone13	CVVNRGSNYQLIW	TRAV12-1	TRAJ33	CASSGRPDVYTQYF	TRBV7-2	TRBJ2-3
clone14						
clone17						
clone15	CIVSAQGGSEKLVF	TRAV26-1	TRAJ57	CASSLVYNTGELFF	TRBV11-2	TRBJ2-2
clone16	CAGAGNNRKLIW	TRAV25	TRAJ38	CASSLVSAGTDTQYF	TRBV11-2	TRBJ2-3
clone18	CIVRVTGSWGKLQF	TRAV26-1	TRAJ24	CSARQGVGEAFF	TRBV20-1	TRBJ1-1
clone19						
clone20	CKQYNFNKFYF/CAVNAYGGSQGNLIF	TRAV29DV5/TRAV8-1	TRAJ21/TRAJ42	CASSPGLQIQETQYF	TRBV5-5	TRBJ2-5
clone23						
clone21	CAVSAPGTASKLTF	TRAV8-4	TRAJ44	CASSVIAFGEQFF	TRBV6-1	TRBJ2-1
clone22	CAAAGNNRKLIW	TRAV25	TRAJ38	CASSGLAGGLYYYEQYF	TRBV21-1	TRBJ2-7
clone24	CAVSASFPRWDFNKFYF	TRAV8-6	TRAJ21	CASSLGRPGGAPNTEAFF	TRBV5-1	TRBJ1-1
clone25	CAVQAGRGTGNQFYF	TRAV20	TRAJ49	CASSSLGQANSPLHF	TRBV6-6	TRBJ1-6
clone37	CAVQAGRGTGNQFYF	TRAV20	TRAJ49	CASSSLGQANSPLHF	TRBV6-6	TRBJ1-6
clone38	CAVQAGRGTGNQFYF	TRAV20	TRAJ49	CASSSLGQANSPLHF	TRBV6-6	TRBJ1-6
clone26	CIVRVRTGANSKLTF	TRAV26-1	TRAJ56	CASSLSYAGLLTDTQYF	TRBV11-2	TRBJ2-3
clone27	CAASPPGDTGFQKLVF/CVVNLLRQGGKLIF	TRAV23DV6/TRAV12-1	TRAJ8/TRAJ23	CASSRDSLDTQYF	TRBV5-1	TRBJ2-3
clone28	CIAWRYGGSQGNLIF	TRAV26-1	TRAJ42	CATSPGSYEQYF	TRBV10-2	TRBJ2-7
clone29	CAASAMGQGAQKLVF/CAASARGGSNYKLTF	TRAV29DV5	TRAJ54/TRAJ53	CSASPLATQYF	TRBV20-1	TRBJ2-5
clone39						
clone30	CAVQAGRGTGNQFYF	TRAV20	TRAJ49	CASSFKGMPGELFF	TRBV7-9	TRBJ2-2
clone31	CIVRVLGGGYNKLIF	TRAV26-1	TRAJ4	CSALAGVSTDTQYF	TRBV29-1	TRBJ2-3
clone32	CIVRGLNAGNMLTF	TRAV26-1	TRAJ39	CASSPLGQGNSPLHF	TRBV6-6	TRBJ1-6
clone35						
clone33	CAGTGNNRKLIW	TRAV25	TRAJ38	CASSFGGSYGYTF	TRBV12-4	TRBJ1-2
clone36						
clone40						
clone34	CIVRVSYNFNKFYF	TRAV26-1	TRAJ21	CASSLLGETGDGYTF	TRBV11-2	TRBJ1-2
clone41						

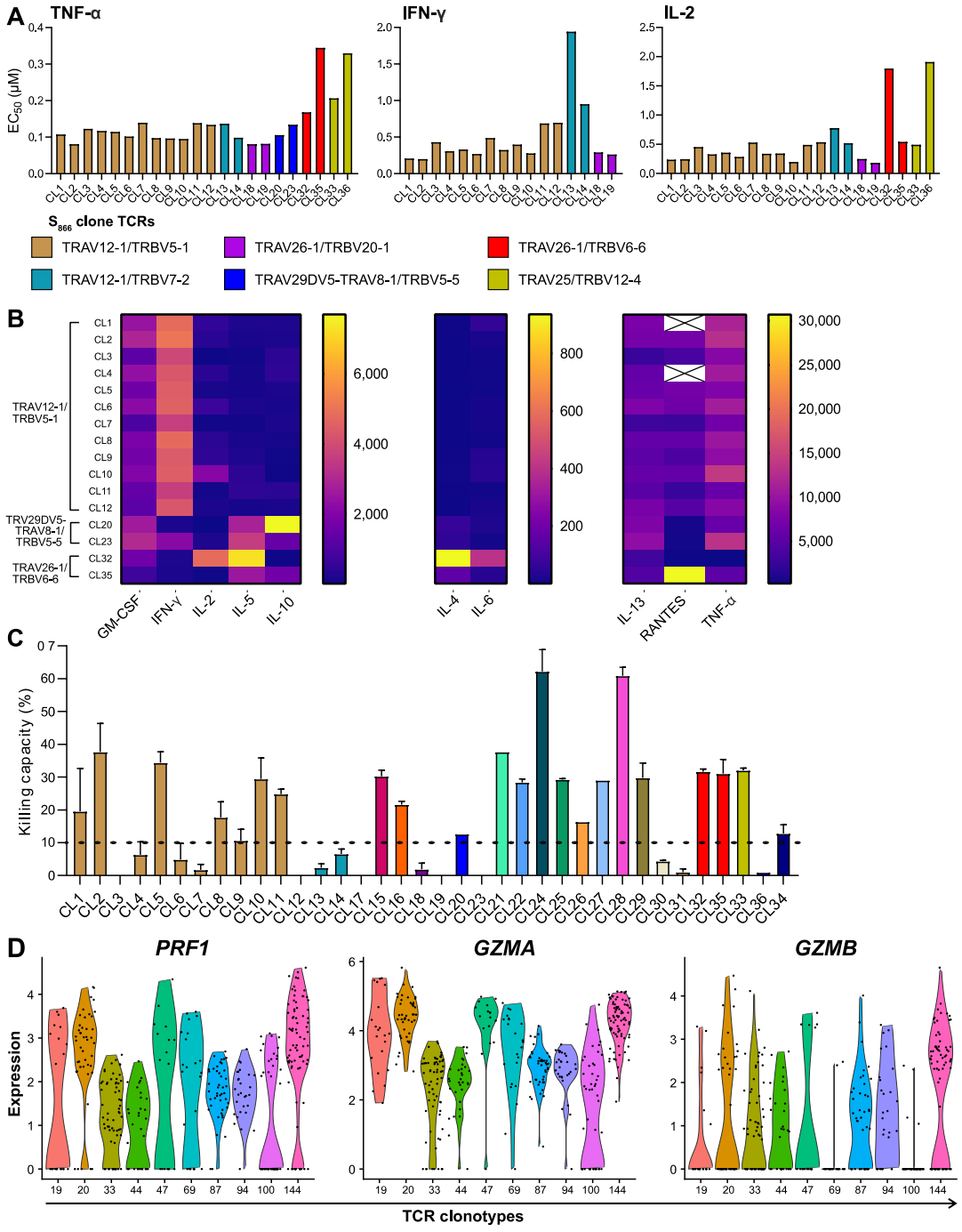

Fig. 5.12 S_{866}-specific $CD4^+$ T cell functionality relies on factors other than TCR usage. (A) EC_{50} of IFN-γ, IL-2 and TNF-α production by T cell clones with identical TCRs. (C) Cytokine profiles secreted by T cell clones with the same TCRs upon stimulation. Cytokine levels in the supernatant were assessed by Luminex. (C) Killing capacity of T cell clones with the same TCRs. Bar colours match figure legend from (A), other colours not shown in legend depict other TCRs. Data are presented as means ± SD. (D) Expression of cytotoxic molecules *PRF1*, *GZMA,* and *GZMB* on single cells with same TCRs.

5.2.6 Antiviral activity of spike-specific CD4$^+$ T cells strongly correlates with their killing capacity and IL-2 production

As previously highlighted, a number of spike-specific CD4$^+$ T cell clones were capable of suppressing SARS-CoV-2 replication (Fig. 5.7G). Whether this antiviral effector function was mediated via direct killing of virus-infected cells or by the expression of soluble inhibitory factors was further examined. Firstly, our data demonstrated that the antiviral activity of the CD4$^+$ T cell clones strongly correlated to the proportion of T cells producing IL-2 upon stimulation with virus-infected cells (R=0.226, P=0.030, Fig. 5.13A), but did not correlate with the proportion of cells producing TNF-α or IFN-γ (R=0.126, P=0.229; R=0.137, P=0.192; Fig. 5.13 B). Secondly, a significant association between

the killing capacity of spike-specific T cell clones and their potential to control virus replication was found (R=0.390, P<0.001; Fig. 5.13C). Indeed, we observed that killer clones (more than 10% killing capacity) could suppress virus replication more efficiently than non-killers (less than 10% of killing) (P=0.010, Fig. 5.13D), suggesting the importance of direct killing of virus-infected cells in viral control by CD4$^+$ CTLs. Strikingly, some non-killer clones were capable of inhibiting viral replication as efficiently as killers (Fig. 5.13D), indicating the potential contribution of soluble factors to viral control. Subsequently we compared cytokine and chemokine production of these viral suppressing non-killer CD4$^+$ T cell clones with other non-killers (Fig. 5.13E). We noticed that non-killer CD4$^+$ T cells capable of suppressing virus replication (suppressor clone) produced significantly higher

concentrations of IL-2 (P=0.040) and IFN-γ (P=0.040) than non-killer CD4$^+$ T cells incapable of viral suppression (non-suppressor clone), highlighting a role for IL-2 and possibly IFN-γ in CD4$^+$ T cell control of SARS-CoV-2 infection.

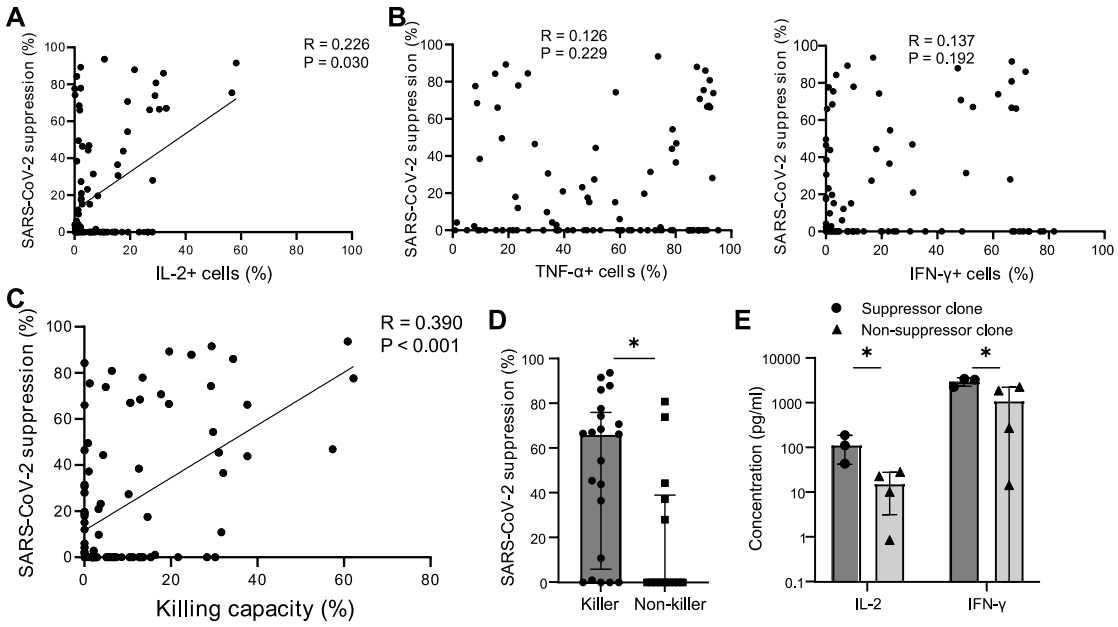

Fig. 5.13 Viral suppression by spike-specific CD4$^+$ T cells is correlated with IL-2 production and killing. Correlation of virus suppression with proportion of cells producing IL-2 (A), TNF-α and IFN-γ (B) (N=93). (C) Correlation of virus suppression with cell killing capacity of T cells (N=98). (D) Comparison of virus suppression between S_{866}-specific CD4$^+$ killer cells (N=21) and non-killer cells (N=14), P=0.010. (E) Comparison of cytokine production of CD4$^+$ non-killer cells with virus suppression (suppressor clone, N=3) and without virus suppression (non-suppressor clone, N=4). Data are presented as medians with IQRs in D and means ± SD in E. Correlation analysis was performed using Spearman's rank correlation coefficient. The Mann-Whitney U-test and independent-samples t test was used for analysis and the two-tailed P value was calculated. *P<0.05.

5.2.7 Spike-specific CD4$^+$ CTLs utilise distinct cytolytic pathways with increased migration potential

5.2.7.1 Spike-specific CD4$^+$ CTLs elicit cytotoxicity via perforin-mediated pathway

Activated CD8$^+$ CTLs carry out their killing function primarily by releasing cytotoxic granules containing perforin and granzymes, which subsequently induce apoptosis of target cells. Indeed, a positive correlation was observed between killing ability and degranulation activity, as measured by CD107a expression on S_{751}- and S_{866}-sepcific CD4$^+$ T cell clones, upon antigen stimulation (R=0.413, P=0.001; Fig. 5.14A). This suggests that high expression of CD107a can act as a potential marker for CD4$^+$ CTLs. To further determine whether the killing of target cells by spike-specific CD4$^+$ CTLs was mediated through the perforin-dependent pathway, S_{866}-specific CD4$^+$ T cell clones were treated with concanamycin A (CMA), an inhibitor of perforin, prior to adding to target cells loaded with peptide or infected with SARS-CoV-2. Killing capacity of T cell clones was assessed by CFSE-based CTL assays coculturing with B cells loaded with peptide, and suppression of SARS-CoV-2 was evaluated by coculturing with virus-infected ACE2 expressing B cells for 48hrs at an E:T ratio of 4:1. The cytolytic activity mediated by CD4$^+$ T cell clones was completely blocked by CMA, resulting in decreased (<10%) or ablated killing capacity (Fig. 5.14B), and reduced or no viral suppression (Fig. 5.14C). These data indicate that spike-specific CD4$^+$ CTLs elicited cytotoxicity through perforin-mediated pathway and

direct killing of target cells contributed to controlling SARS-CoV-2 infection. We also observed high frequency of S_{866}-specific $CD4^+$ T cells expressing both perforin (47.6% and 30.4%) and granzyme B (23.8% and 26.1%), when staining the PBMCs isolated from two patients with acute COVID-19 (Fig. 5.14D). This further confirmed constitutive existence of spike-specific $CD4^+$ CTLs and our observations on T cell clones were not due to the *in vitro* expansion.

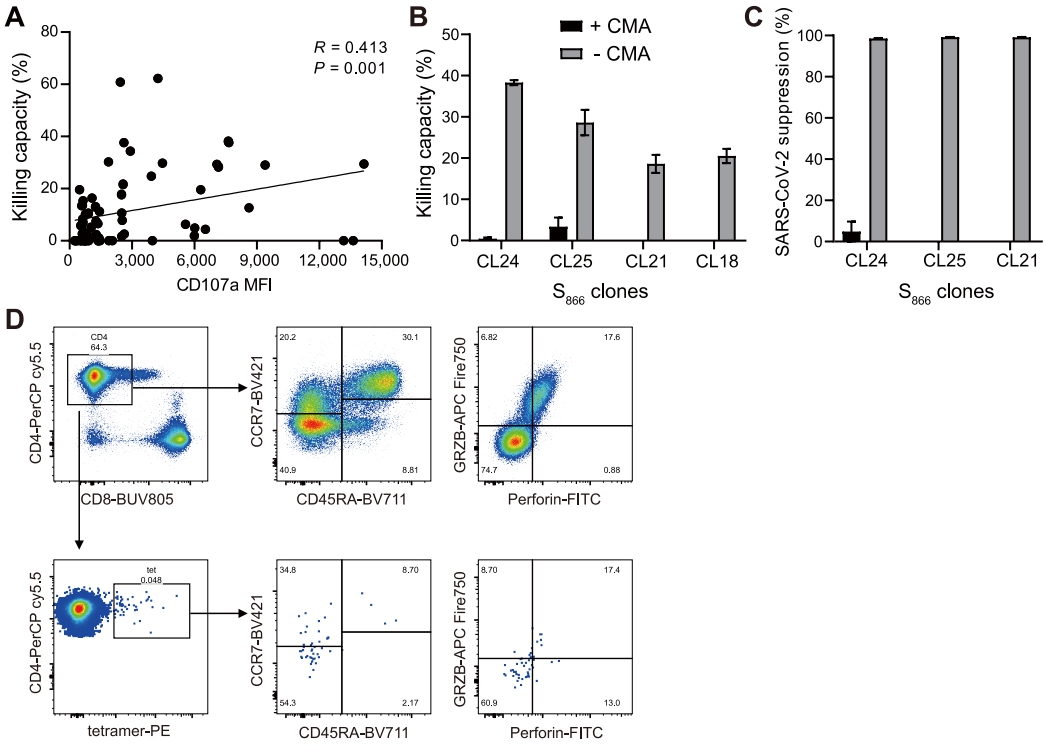

Fig. 5.14 Cytotoxicity of spike-specific $CD4^+$T cells is partially mediated through granules. (A) Association between T cell killing and CD107a expression (*N*=72). (B) T cell killing and (C) virus suppression by S_{866} T cell clones with and without CMA treatment. (D) Memory phenotype and cytotoxic status of S_{866}-specific T cells. PBMCs from acute infection were stained with S_{866}-DRB1*15:01 tetramer and markers of T cell memory and cytotoxicity. Representative flow cytometry plots of gating for different cell subsets. Correlation analysis was performed using Spearman's rank correlation coefficient. MFI, median fluorescent intensity.

5.2.7.2 Activated spike-specific CD4$^+$ CTLs display increased migration potential

To identify other factors involved with this perforin-mediated effective viral control, we analysed single-cell data generated by 10X Chromium, and grouped tetramer-sorted S_{866}-specific single cells from short-term cultured T cell lines into perforin-high (*N*=693 cells) and perforin-low (*N*=724 cells) subsets according to their perforin module scores (Table 5.5) and compared their gene expression profiles (Fig. 5.15A). Perforin-high T cells not only upregulated cytotoxic associated genes such as *GZMA* (*P*=4.43 x 10^{-144}), *NKG7* (*P*=1.03 x 10^{-139}), *GZMK* (*P*=4.34 x 10^{-39}), *KLRD1 (P*=2.01 x 10^{-2}) and *CTSW (P*=6.54 x 10^{-35}) but also genes associated with migration for example: chemokines such as *CCL3 (P*=8.48 x 10^{-16}), *CCL4 (P*=2.26 x 10^{-59}), *CCL5 (P*=9.29 x 10^{-82}), chemokine receptors *CCR3* (*P*=4.6 x 10^{-3}) and *IL2RG* (*P*=3.17 x 10^{-24}), tissue homing receptors *ITGB1* (*P*=1.19 x 10^{-8}), *ITGA4* (P=1.26 x 10^{-3}), *ITGAL* (*P*=3.78 x 10^{-4}) and inhibitory receptors such as *TIGIT* (*P*=2.82 x 10^{-4}) and *KLRG1* (*P*=1.94 x 10^{-2}) (Fig. 5.15B). This suggests there is increased migration potential of activated cytotoxic CD4$^+$ T cells to infected tissue site.

Table 5.5 Perforin gene module. Perforin and interacting genes taken from STRING (https://string-db.org/)

Gene symbol	Gene name
PRF1	Perforin
SRGN	Serglycin
GZMB	Granzyme B
NKG7	Natural killer cell granule protein 7
GZMH	Granzyme H
GNLY	Granulysin
GZMA	Granzyme A
CD8A	CD8
FASLG	Fas ligand
CD4	CD4
KLRK1	NKG2D

5.2.7.3 Spike-specific CD4$^+$ CTLs utilise distinct cytotoxic pathways from SARS-CoV-2 specific CD8$^+$ CTLs

To understand whether these spike-specific CD4$^+$ CTLs utilise similar cytolytic pathways as CD8$^+$ CTLs, we compared single cell gene expression, in particular the expression of effector molecules, between perforin-high CD4$^+$ cytotoxic T cells (tetramer-sorted S_{866} specific, *N*=693, 10X Chromium) and CD8$^+$ cytotoxic T cells (Pentamer-sorted $NP_{105-113}$-HLA-B*07:02-specific, *N*=1041, 10X Chromium) from short-term cultured lines(Peng et al., 2022) (Fig. 5.15C). We found that CD8$^+$ CTLs expressed significantly higher levels of granzyme B and H (*GZMB*, average $\log_2$ fold change =-2.68, P=2.24 x 10^{-25}; *GZMH,* average $\log_2$ fold change =-0.57, P=2.09 x 10^{-5}), classic cytolytic molecules secreted by CD8$^+$ T cells and induce apoptosis in target cells (Fig. 5.15D). Compared to CD8$^+$ CTLs, CD4$^+$ CTLs displayed upregulated expression of other cytolytic molecules such as *GZMM* (P=1.91 x 10^{-10}), *GZMK* (P=1.78 x 10^{-10}), *NKG7* (P=9.51 x 10^{-12}), *KLRK1* (P=8.3

x10^{-6}) and *CTSW* (*P*=2.86 x 10^{-11}), suggesting the involvement of different cytolytic machineries in CD4^{+} CTL killing.

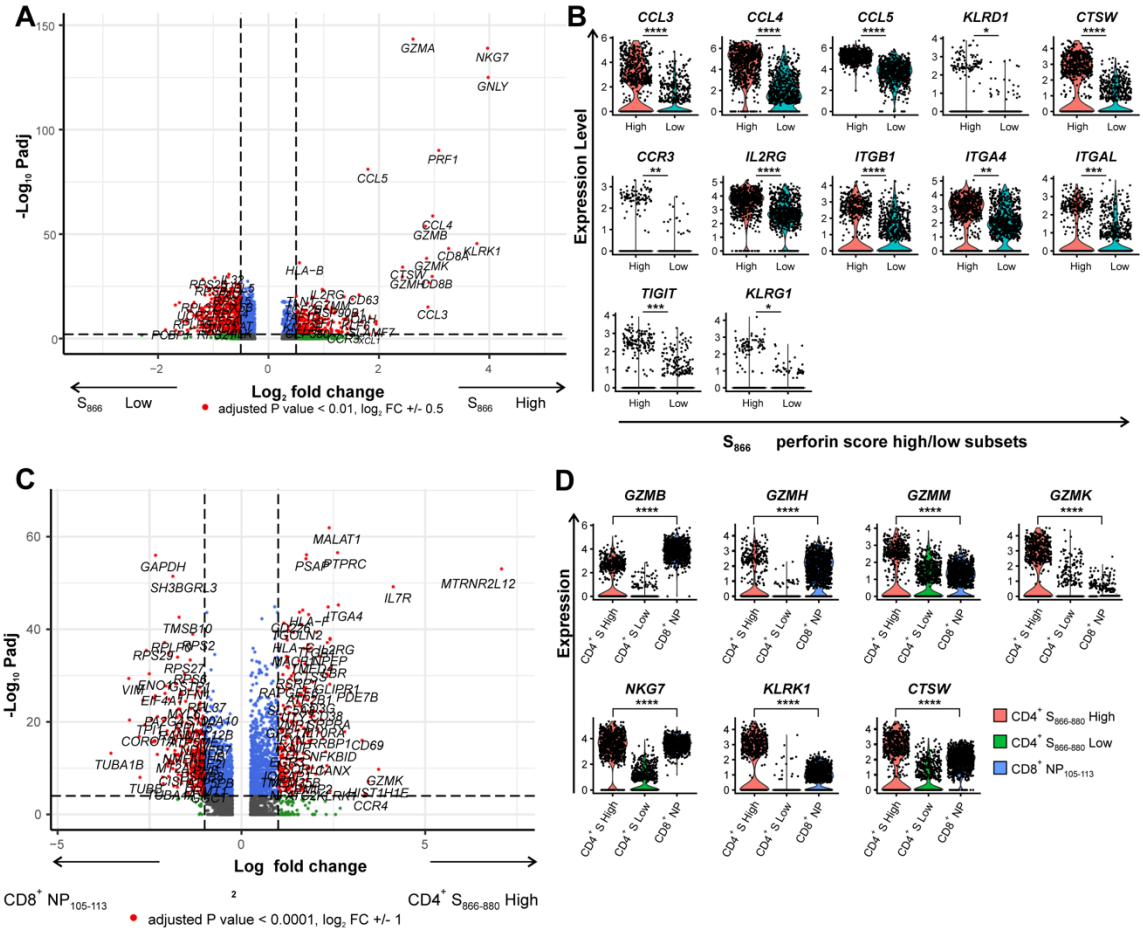

Fig. 5.15 Mechanisms mediating spike-specific CD4^{+} T cell cytotoxicity. (A) Comparison of gene expression between S$_{866}$-specific CD4^{+} single T cells (*N*=5 patients, 10X Chromium) with high perforin score (*N*=693) and low perforin score (*N*=724). (B) Differentially expressed genes between T cells with high and low perforin score (10X Chromium). (C) Comparison of gene expression between S$_{866}$-specific CD4^{+} T cells with high perforin score (*N*=5 patients and 693 cells from 10X Chromium) and tetramer-sorted B*07:02/NP$_{105}$-specific CD8^{+} CTLs (*N*=3 patient and 1041 cells from 10X Chromium). (D) Differentially expressed genes between CD4^{+} T cells with high perforin score (*N*=5 patients, 693 cells from 10X Chromium), CD4^{+} T cells with low perforin score (*N*=5 patients, 724 cells from 10X Chromium) and CD8^{+} CTLs (*N*=3 patients, 1041 cells from 10X Chromium). The MAST statistical test was used for analysis with sequencing

batch as latent variable and the two-tailed *P* value was calculated, adjusted *P* values are shown. **P*<0.05, ***P*<0.01, ****P*<0.001, *****P*<0.0001.

5.2.8 Mitochondrial function might regulate cytotoxicity of spike-specific CD4$^+$ T cells

To further explore cytotoxic machineries in CD4$^+$ CTL killing, proteomic profiles of S_{866}-specific CD4$^+$ T cell killer clones (clone5, clone24 and clone28) and non-killers (clone3 and clone36) were analysed by mass spectrometry, with clone3 and clone5 sharing paired αβ of TCR. T cell clones were stimulated with staphylococcal enterotoxin B (SEB) superantigen, with control wells containing T cells without stimulation for each clone. After stimulation, T cells were lysed using NP40 buffer, then supernatant only containing cytosolic fraction was collected and run for mass spectrometry. Approximately 7,000 proteins were quantified in each sample. First, we compared proteomic profiles between clone3 and clone5, which shared the same TCR. We found that 616 proteins were differentially expressed with 317 proteins upregulated in clone5 when unstimulated (Fig. 5.16A), while 1,006 proteins were differentially expressed with 493 proteins upregulated in clone5 when stimulated (Fig. 5.16B). Then we looked at protein expression between CD4$^+$ killer (clone5, clone24 and clone28) and non-killer (clone3 and clone36) group. We observed 362 differentially expressed proteins when T cells were not stimulated, of which 224 proteins were upregulated in killers (Fig. 5.16C). Whereas 443 proteins were differentially expressed between the two groups with 257 proteins upregulated in CD4$^+$ killers (Fig. 5.16D).

To further identify proteins associated with $CD4^+$ T cell cytotoxicity which are not TCR-dependent, we compared upregulated proteins between clone5 vs clone3 and killers vs non-killers, and found that 74 proteins were shared when unstimulated (Fig. 5.17A). 11 out of 15 biological processes enriched by the 74 proteins are correlated with mitochondrial activity and function (Fig. 5.17B). Whereas 134 proteins were upregulated in both clone5 compared to clone3 and killers in comparison with non-killers in stimulation condition (Fig. 5.17C). We found that 16 out of the top20 pathways enriched by the 134 upregulated proteins are associated with mitochondria (Fig. 5.17D). This enrichment was analysed using Gene Ontology. These data suggest that mitochondria activities and functions may contribute to the cytotoxicity of $CD4^+$ T cells.

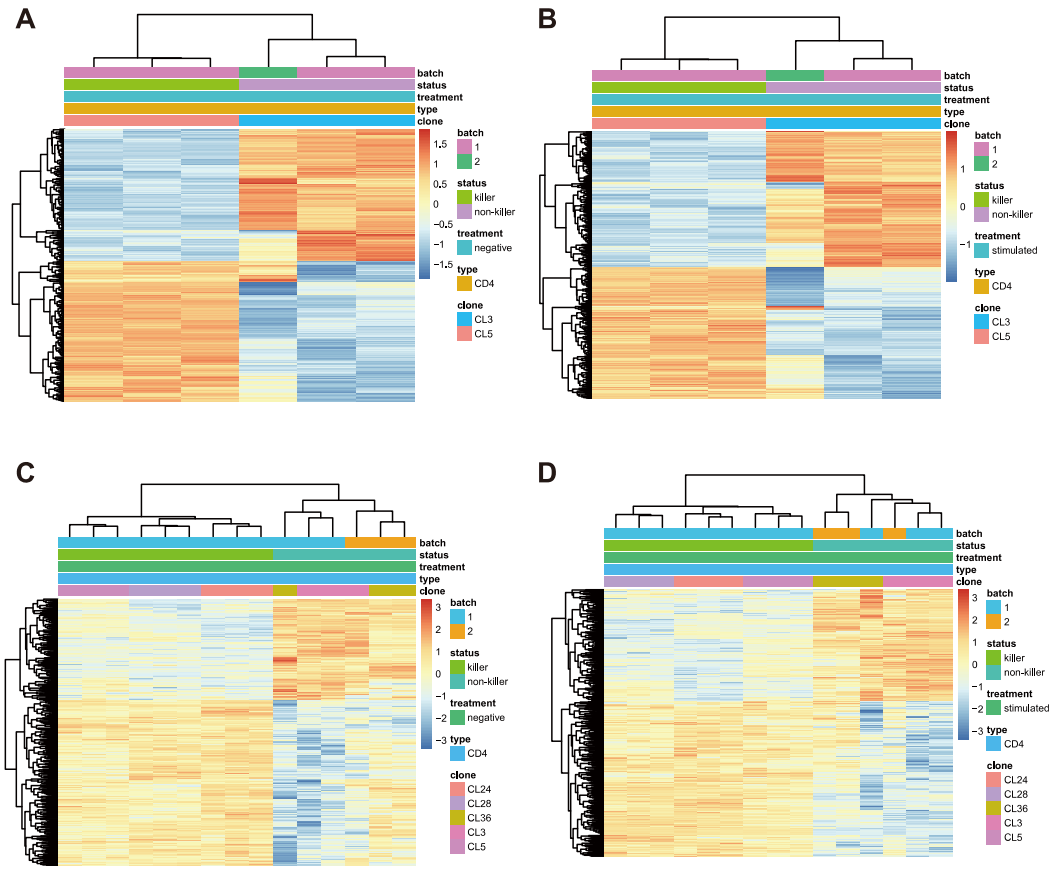

Fig. 5.16 Proteomic profiles between S_{866}-specific $CD4^+$ T cell killer and non-killer clones. Heatmap with cluster analysis with normalised values for sequenced proteins from S_{866}-specific $CD4^+$ T cell clone3 (non-killer) and clone5 (killer) that shared TCR clonotype, without stimulation (A) and with stimulation (B). Comparison of proteomic profiles between non-killers (clone3 and clone36) and killers (clone5, clone24 and clone28) without stimulation (C) and with stimulation (D). Linear model analysis was used for comparison with sequencing batch as latent variable and the two-tailed *P* value was calculated.

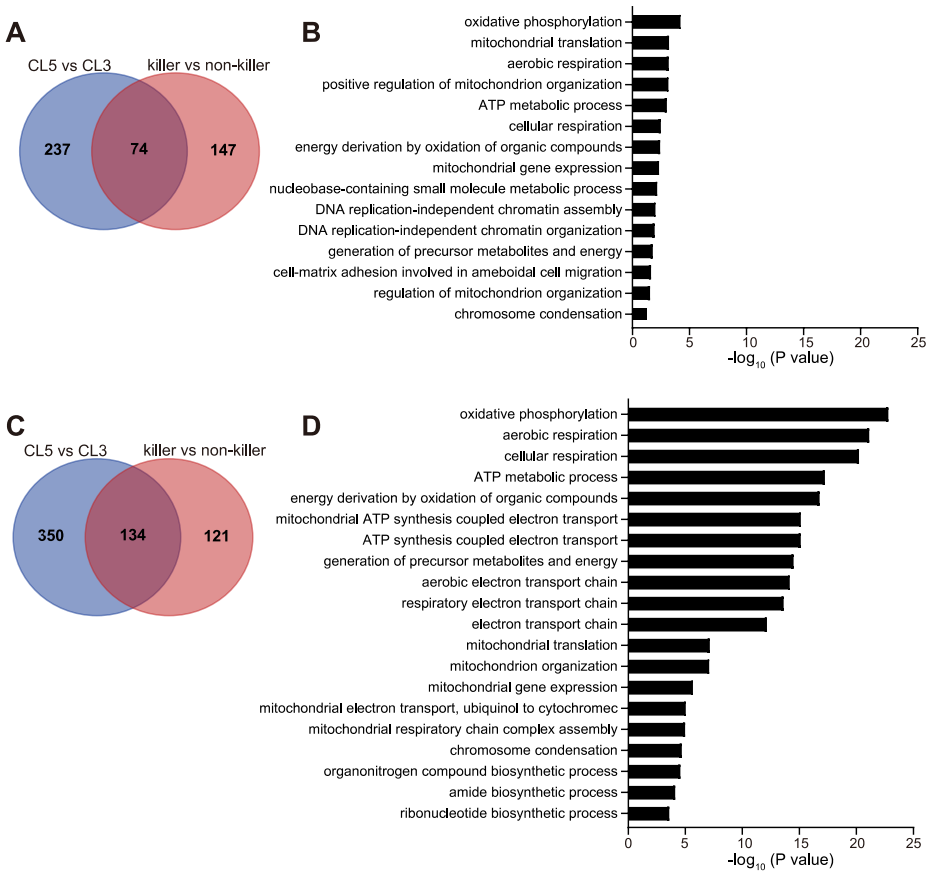

Fig. 5.17 Enriched pathways in S_{866}-specific $CD4^+$ Killer clones. Venn diagram analysis of upregulated proteins in clone5 and killer clones without stimulation (A) and upon stimulation (C). (B) Enriched pathways by upregulated proteins shared between clone5 and killer clones without stimulation. (D) Top 20 enriched pathways by proteins upregulated in both clone5 and killer clones with stimulation. Pathway enrichment was analysed using Gene Oncology database and ranked by adjusted *P* values.

5.2.9 Dominant spike-specific $CD4^+$ T cells are maintained nine months after infection with diverse TCR repertoire and preserved antiviral activity

To examine whether memory T cells established following natural infection could provide sufficient protection against secondary viral infection, we collected PBMCs from the same patients 6-9 months after infection. *Ex vivo* T cell responses against the three dominant spike epitopes (S_{166}, S_{751} and S_{866}) were assessed by IFN-γ ELISpot assays. Although T cell responses to these three

spike epitopes significantly declined 6-9 months after infection (Fig. 5.18A), we were able to sort, sequence, and expand these spike-specific $CD4^+$ T cells after *in vitro* antigen stimulation. Epitope-specific $CD4^+$ T cells were sorted from short-term T cell lines for 10X Chromium to analyse TCR usage and gene expression of spike-specific single cells. We discovered that the diversity of the TCR repertoire of these $CD4^+$ T cells were maintained 6-9 months after infection (Fig. 5.18B).

Next, polyclonal T cell lines targeting each spike epitope were established *in vitro*. The antiviral efficacy of these polyclonal T cell lines was assessed using our *in vitro* SARS-CoV-2 infection assays. ACE2 expressing B cells were infected with wild type or VOCs of SARS-CoV-2 at an MOI of 0.1, then cocultured with T cells at an E:T ratio of 1:1 for six hours to measure cytokine expression of T cells by ICS, or at an E:T ratio of 4:1 for 48 hours to assess virus suppression. The bulk lines targeting all three epitopes elicited strong responses against B cell lines infected with wild type SARS-CoV-2 (Victoria strain) and variants of concerns (VOCs; Delta and Omicron). Gating strategy of ICS data is shown in Fig. 5.19A. A great proportion of T cells expressed TNF-α with a relatively low frequency of T cells producing IFN-γ and IL-2, when the $CD4^+$ T cell lines encountered virus-infected target cells (Fig. 5.19B and C). Furthermore, these polyclonal $CD4^+$ T cell lines showed significant cytotoxic potential with upregulated CD107a expression (Fig. 5.19D). S_{866}-specific $CD4^+$ T cells had a greater proportion of IL-2 producing T cells and higher levels of CD107a expression compared to the

other two epitope-specific T cells, which were two factors associated with antiviral efficacy. In addition, these antigen-specific $CD4^+$ T cell lines are capable of suppressing wild type SARS-CoV-2 replication and showed strong inhibition against VOCs (Fig. 5.19E). Consistent with IL-2 and CD107a expression, S_{866}-specific $CD4^+$ T cell elicited stronger suppression to Victoria strain and VOCs. The last second amino acid of epitope S_{751}, which was asparagine was mutant to lysine (N767K) in Omicron, but this mutation did not impact S_{751}-specific T cell responses, including cytokine production and CD107a expression (Fig. 5.19C and D). Compared to Victoria strain, Omicron-infected target cells induced comparable proportions of T cells producing TNF-α, IFN-γ or IL-2 and levels of CD107a expression. In addition, this mutation did not impair virus suppression mediated by S_{751}-specific $CD4^+$ T cells (Fig. 5.19E). In summary, our data highlight the protective role of these dominant spike-specific $CD4^+$ T cells in secondary infection against different SARS-CoV-2 variants.

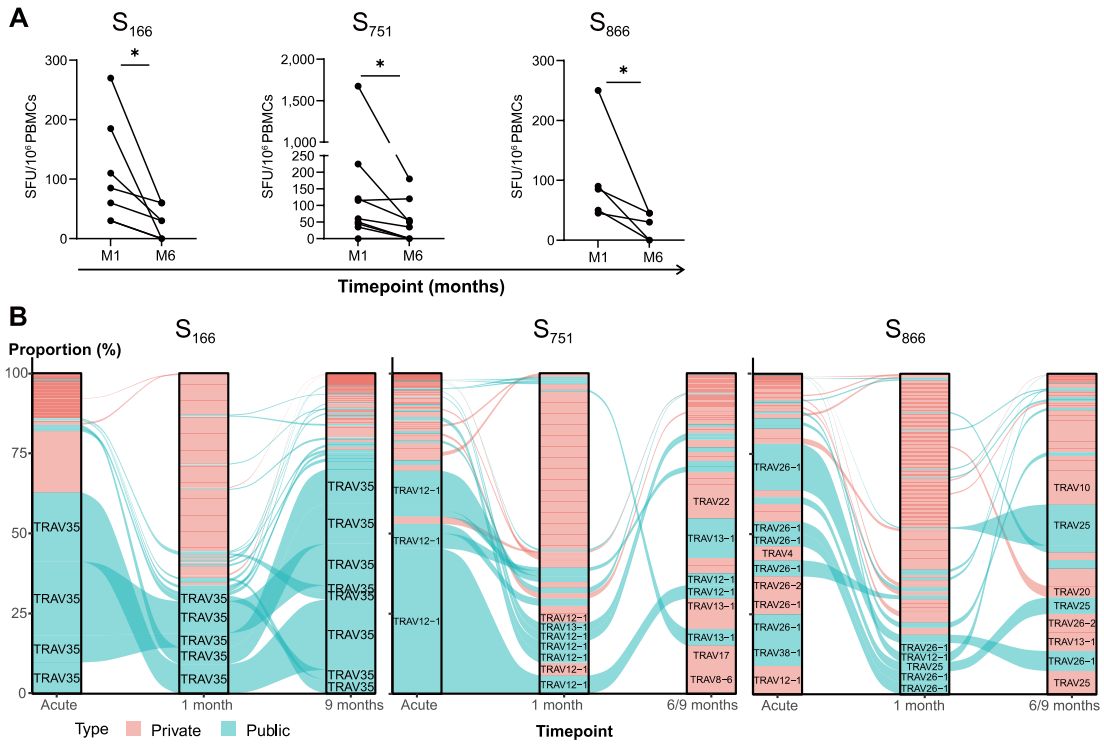

Fig. 5.18 Characterisation of S_{166}-, S_{751}- and S_{866}-specific $CD4^+$ T cell response at 6-9 months convalescence. (A) Comparison of S_{166}-, S_{751}- and S_{866}-specific $CD4^+$ T cell response between one and six months of convalescence. S_{166}: *N*=7, *P*=0.017; S_{751}: *N*=9, *P*=0.017; S_{866}: *N*=5, *P*=0.043. (B) TCR repertoires of S_{166}-, S_{751}- and S_{866}-specific $CD4^+$ T cells at acute infection, one month and 6-9 months convalescence. TCR clonotypes coloured pink and blue are private TCRs and public TCRs, respectively. For clarity only TRAV gene usage is shown rather than full α clonotype (CDR3α amino acid sequence + TRAV).

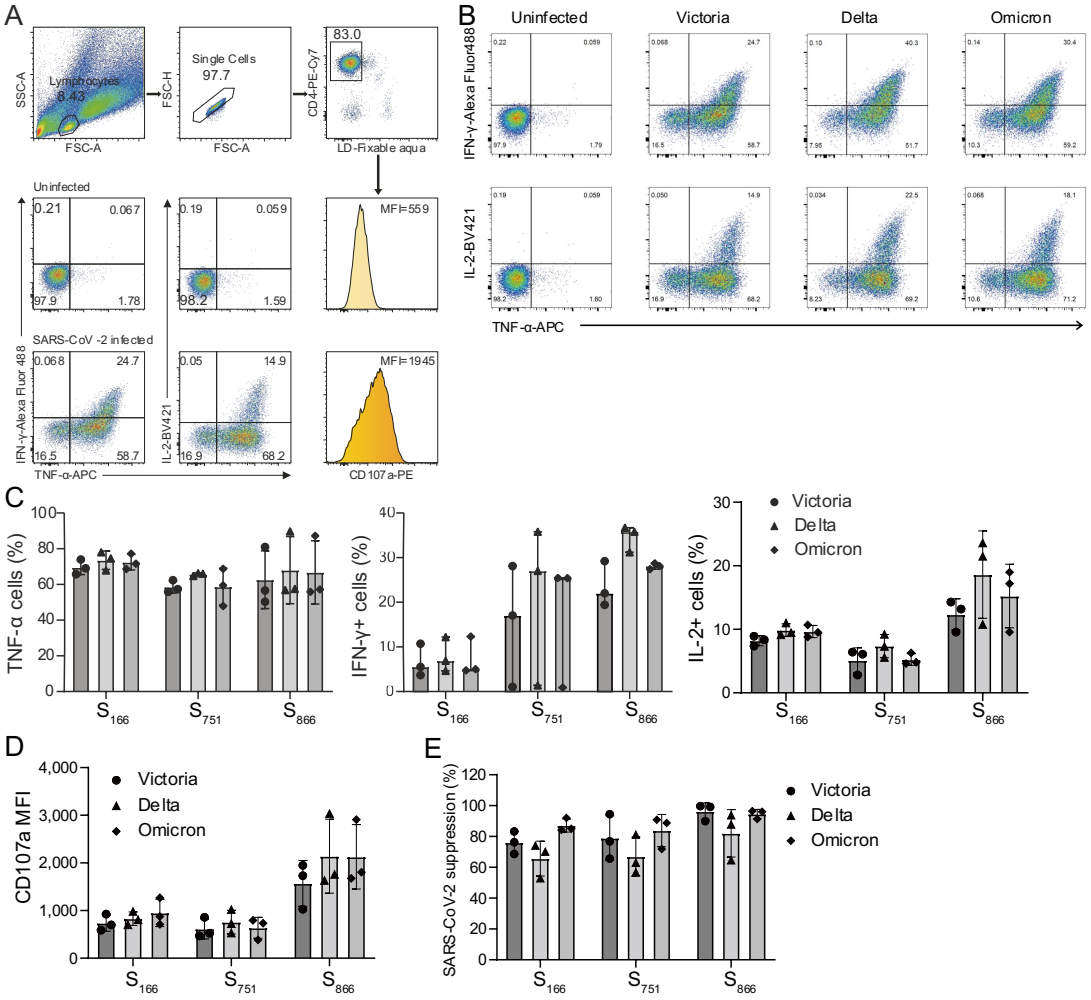

Fig. 5.19 Antiviral function of S_{166}-, S_{751}-, and S_{866}-specific $CD4^+$ T cell response at 6-9 months convalescence. (A) The gating strategy of identifying TNF-α, IFN-γ, and IL-2 producing cells, and expression intensity of CD107a. (B) Representative ICS flow cytometry plots measuring TNF-α, IFN-γ, and IL-2 expression in S_{866}-specific T cell line from C-COV19-064 at six months incubated with B cells infected with SARS-CoV-2 Victoria, Delta or Omicron variants (uninfected B cells shown as negative control). (C) TNF-α^+, IFN-γ^+, and IL-2^+ cell frequency and (D) CD107a expression in S_{166}-, S_{751}- and S_{866}-specific $CD4^+$ T cell bulk lines at 6-9 months when cocultured with B cells infected with SARS-CoV-2 Victoria, Delta or Omicron variants. Data represent one of two independent experiments with similar results. (E) Inhibition of SARS-CoV-2 replication by S_{166}-, S_{751}-, and S_{866}-specific $CD4^+$ T cell bulk lines at 6-9 months. Single representative experiment shown as means±SD. MFI, median fluorescent intensity.

Wilcoxon matched-pair signed-rank was used to compare T cell responses between month1 and month6. *P<0.05.

5.3 Discussion

In this study, we focus on the three most immunodominant spike-specific $CD4^+$ T cell responses identified in our cohort restricted by common HLA class II alleles (S_{166}-DPB1*04:01, S_{751}-DRB1*15:01 and S_{866}-DRB1*15:01), which are dominant in individuals with corresponding HLA typing. Significant differences are observed between these responses in functional avidity/antigen sensitivity, cytotoxic capacity, cytokine profile and their effector function in response to virus-infected cells and suppression of virus replication. S_{866}-specific $CD4^+$ T cells display the highest functional avidity and greatest killing capacity, and also show the strongest responses to SARS-CoV-2 infected cells and direct control of virus replication. The higher effector function of S_{866}-specific T cells is further confirmed by single cell data. Compared to S_{751}-specific $CD4^+$ T cells, S_{866}-specific T cells exhibit higher expression levels of effector genes (*CCL4*, *CCL4* and *TNF*) and cytotoxic genes (*KLTK1*, *GZMB* and *GAMK*). Interestingly, the estimated antigen load in SARS-CoV-2 infected cells assessed by antigen sensitivity assays and *in vitro* virus infection assays reveals significant differences among these three epitopes. Despite over ten times less estimated S_{866} epitope peptide loaded on the MHC class II molecules of infected cells than S_{751}, S_{866}-specific T cells display much higher antiviral activity for both cytokine production and direct viral control than S_{751}-specific T cells. The fact that S_{866}-specific $CD4^+$ T cell responses display

significantly higher overall antigen sensitivity than S_{751} T cells may compensate the lower antigen load on the surface of SARS-CoV-2 infected cells. These results indicate that the efficient antiviral efficacy elicited by S_{866}-specific $CD4^+$ T cells is likely to contribute to strong cytotoxicity and high functional avidity.

Highly diverse TCR repertoires and public TCRs are observed in the immunodominant spike-specific $CD4^+$ T cells. S_{166}-specific $CD4^+$ T cell responses feature dominant public TCR usage, in particular TRAV35, which is biased to Th1 cell subset(Han et al., 2019) (i.e. high *ID2* expression) and suppressed Th2 transcriptomic profiles(Zheng et al., 2009) (i.e. high Th2 suppressor *IRF4* and *NR4A2* expression). In contrast, S_{866}-specific CD4+ T cell with private TCRs have higher expression of cytotoxic genes (*KLRK1*, *GZMA*, *GZMK* and *NKG7*) and migration marker (*CCL5*). TCR repertoire analysis surprisingly reveals that over 30% of TCRs are public in all three epitope specific responses at all time points studied, including public clonotypes with shared αV and βV sequences. There are also different dominant TRAV usages across these three epitope specific T cells, with S_{166} dominated by TRAV35, S_{751} by TRAV12-1 and S_{866} by TRAV25, TRAV26-1 and TRAV12-1 clonotypes.

We also find that spike-specific cytotoxic $CD4^+$ T cells may use different signalling and cytotoxic molecules compared to classical $CD8^+$ T cells; $CD4^+$ CTLs express *GZMK* and *GZMM* significantly higher whereas $CD8^+$ CTLs express much higher *GZMB* and *GZMH*. In addition, NK activation receptor NKG2D (*KLRK1*) and

NKG7, known to be important for cytotoxic degranulation(Malarkannan, 2020), are highly expressed on $CD4^+$ CTLs but not classical $CD8^+$ CTLs.

Surprisingly, we find that the functionality of these $CD4^+$ T cells, in particular cytotoxicity, appears to involve mechanisms beyond TCR usage alone. S_{866}-specific $CD4^+$ T cell clones sharing the same TCR exhibit a broad range of killing capacity, which correlate with their ability to control virus replication in SARS-CoV-2 infected cells. However, T cells that do not exhibit killing activity can still suppress virus replication and produce high levels of IL-2 and IFN-γ. In addition, we observe an overall significant association between the proports of IL-2 producing T cells and the antiviral efficacy of all three epitope responses, suggesting direct antiviral effector function of $CD4^+$ spike-specific T cells independent of cytotoxicity.

Finally, even the immune memory T cell responses targeting the three dominant spike epitopes decreased significantly at month 6-9 compared to month 1-3 post infection, the diversity of TCR repertoire is maintained. Furthermore, spike-specific $CD4^+$ T cells from month 6-9 are still capable of producing cytokines and expressing CD107a when encountered original SARS-CoV-2 and VOCs infected target cells. These $CD4^+$ T cells demonstrate potent antiviral efficacy to the original SARS-CoV-2, Delta and Omicron variants, suggesting memory responses to spike protein, induced by vaccine or natural infection, may contribute to protection against secondary infections to all VOCs, including

Omicron, by direct killing of virus-infected cells and/or antiviral cytokine and chemokine production.

In summary, this study provides evidence of cytotoxic $CD4^+$ T cells in SARS-CoV-2 virus infection and new insights on the potential mechanisms related to this important group of $CD4^+$ cells at a single cell level. Induction of potent $CD4^+$ cytotoxic cells by vaccination could be an attractive approach for novel vaccine designs to support early viral control.

Chapter 6: Overall Discussion and Future Directions

The adaptive immune system includes the humoral and T cell immune responses. T cells are an essential component of cellular immunity, playing a pivotal role in host defences against viral infection. During primary viral infection, naïve B cells are triggered by a multitude of signals such as viral antigen binding to BCR to proliferate and differentiate into plasma cells(Koutsakos et al., 2019). Plasma cells produce a range of antigen-specific antibodies, of which, neutralising antibodies can bind virus and thereby inhibit virus attaching or entering host cells. Antibodies also induce effector function, such as virolysis, ADCC, and phagocytosis, to abolish viral infection(Burton, 2002).

The combined humoral and cellular immune responses are essential for optimal control of viral infection. When first encountering viral antigen in lymphoid tissues, naïve T cells are primed and activated by TCR recognition of viral peptide-MHC complex, subsequently T cells clonally expand(Kaech et al., 2002; Wherry & Ahmed, 2004). The frequency of antigen-specific T cells has been shown to expand 1000-fold in mice during the primary infection(Kaech et al., 2002). Alongside the rapid and dramatic proliferation, T cells also differentiate to acquire antiviral effector function(Wherry & Ahmed, 2004). Compared to naïve T cells, effector cells have increased expression of chemokine receptors, such as CCR5 and CCR2, and decreased expression of lymph node homing receptors, such as CCR7 and CD62L. This enables them to migrate to infection tissues. Effector $CD8^+$ T cells constitutively express cytotoxic molecules, such as perforin and

granzymes, and antiviral cytokines IFN-γ and TNF-α(Kaech et al., 2002). Thus, upon antigen stimulation, effector $CD8^+$ T cells can specifically and rapidly direct virus-infected cells and secrete antiviral cytokines to control and ameliorate viral infection. Naïve $CD4^+$ T cells can differentiate into a range of helper subsets, such as Th1 cells producing cytokines IFN-γ, TNF-α and IL-2, or Th2 cells secreting IL4, IL-5 and IL13(Kaech et al., 2002). Alongside helping B cell responses and enhancing $CD8^+$ T cell responses, effector $CD4^+$ T cells also exert antiviral activity by producing antiviral cytokines. In the 2-3 weeks following viral clearance, the majority of effector T cells die. Only 5-10% effector cells survive, gradually acquiring memory properties and eventually go into a pool of long-lived memory T cells(Wherry & Ahmed, 2004). These memory T cells exhibit homeostatic self-renewal via antigen-independent proliferation for long-term maintenance.

Acute infection is defined by viral clearance. In contrast, it is referred to as chronic infection where virus persists, such as HIV, hepatitis C virus, and HBV infection in humans. Viruses utilise multiple strategies to prevent elimination and establish chronic infection, including continuous productive replication, cellular latency and reactivation, alongside viral DNA integration into host genome(Virgin, Wherry, & Ahmed, 2009). On the other hand, dysfunctional virus-specific T cell responses in the host contribute to persistent viral infection. In acute infection, virus-specific memory T cells can more rapidly respond to antigen stimulation during secondary infections; expand and develop multiple effector functions quicker than primary infection when re-encountering viral antigen(Kaech et al., 2002). However, during

chronic infection, the proliferative potential of virus-specific memory T cells in response to antigen is remarkably reduced. Moreover, virus-specific $CD8^+$ T cells in chronic infection are exhausted with loss of effector functions(Virgin et al., 2009; Wherry, 2011; Wherry & Ahmed, 2004). The loss of effector functions is hierarchical with some functions exhausted early, such as IL-2 production, TNF-α production, and cell-mediated cytotoxicity, whereas others persisting longer such as IFN-γ production. Eventually, virus-specific $CD8^+$ T cells are deficient in near all effector functions and may even be physically depleted. Highly exhausted HBV-specific $CD4^+$ and $CD8^+$ T cells have been observed in patients with chronic HBV infection(Raziorrouh et al., 2010; A. Schurich et al., 2011; Ye et al., 2015). HBV-specific T cell dysfunction is driven by both prolonged exposure to antigen and negative regulatory pathways(Maini & Pallett, 2018). Due to ubiquitous and persistent HBV virions, subviral particles, and soluble viral antigens including HBeAg and HBsAg, the TCRs on HBV-specific T cells are perpetually triggered. This eventually leads to T cell exhaustion. HBV-specific T cells express high levels of inhibitory receptors, such as PD-1, CTLA4, Tim-3, and 2B4, which coregulate T cell exhaustion. Additionally, immunoregulatory cytokines IL-10 and transforming growth factor β (TGF-β) produced by a range of cell types in the liver also influence T cell exhaustion.

Many studies investigating primary acute infections involve animal models as there is a generalised lack of human primary infection models. This was revolutionised with the emergence of SARS-CoV-2 infection, which has become

the perfect model to study the evolution of antigen-specific T cell responses during primary infection and subsequent repeat antigen exposures during vaccination or re-infection. This study explored our COVID-19 cohort. This is composed of longitudinal samples that were collected during acute infection, and during convalescence at 1-3 months and 6-9 months post infection. Participants in our cohort received 2-3 doses of COVID-19 vaccines after recovering from SARS-CoV-2 infection. PBMC samples were collected after each vaccination dose. In this study, we identified immunodominant SARS-CoV-2 specific memory T cell responses in patients with 1-3 months of convalescence, whilst also characterising the three most dominant spike-specific $CD4^+$ T cell responses (S_{166}, S_{751} and S_{866}) that exhibited cytokine production, antiviral activity, and a diverse TCR repertoire. Of these, S_{166}- and S_{751}-specific T cell responses have also been observed in vaccinated individuals(Mudd et al., 2021; Wragg et al., 2022). To explore the SARS-CoV-2 specific memory T cell pool after repeat antigen stimulation, future research will include investigation of immunodominant spike-specific T cell responses post each vaccination compared to those induced by primary SARS-CoV-2 infection. This aims to evaluate the changes in immunodominance in the memory T cell pool, including dominant T cell epitopes and T cell response magnitudes. Secondly, the frequency of the three dominant spike-specific T cells in PBMCs after each dose vaccine will be assessed by peptide-MHC tetramer staining. Thirdly, T cell phenotype and function of the three dominant spike-specific T cell responses post each vaccination will be evaluated by investigating gene expression profiles using scRNA-seq. Lastly, the TCR

repertoires of spike-specific T cells after vaccination will be evaluated by analysing paired scTCR-seq data. By comparing the frequency, phenotype, function, and TCR repertoire of the three dominant spike-specific T cell responses between primary infection convalescence, first vaccination dose, and second vaccination dose, the evolution of antigen-specific memory T cells acute infection with repeat antigen exposure will be explored.

Chronic HBV infection in humans is a good model to study memory T cell evolution with persistent antigen exposure. Dominant HBx-specific T cell responses were identified in this study. HBx-specific T cells may give better insights to the effect of persistent antigen stimulation on antigen-specific memory T cells when compared to HBc- and HBs-specific T cells. As HBV core and surface proteins are contained not only in HBV virions and subviral particles, but are also soluble antigens, it is too complex to quantify antigen levels of core and surface proteins. Conversely, x protein is only expressed on HBV-infected cells and transformed hepatocytes, and not contained within HBV virions(Levrero & Zucman-Rossi, 2016). Future research will investigate a cohort of patients with chronic HBV infection in Beijing You'an Hospital; participants are followed up every 3-6 months. Immunodominant HBx-specific T cell responses identified in this study will be studied in a time-course study in this prospective cohort. As HBV-specific T cells are significantly exhausted in chronic HBV infection, HBx-specific T cell frequency will be assessed in PBMCs by tetramer staining rather than ELISpot and ICS assays. T cell phenotype, effector function, and TCR repertoire

will also be analysed using scRNA-seq by tetramer-sorting HBx-specific T cells. This aims to identify how antigen-specific memory T cells evolve overtime in chronic HBV infection with persistent exposure to antigen; comparisons will be drawn to acute infection to identify therapeutically relevant pathways of immune dysfunction. The limitation of the two infection models in humans is that antigen levels to which T cells are exposed cannot be measured, thus we cannot evaluate the effect of antigen levels on memory T cell evolution.

HBV infection induces HCC development and x protein, viral regulatory protein, has been shown to play a critical role in hepatocyte transformation(Levrero & Zucman-Rossi, 2016). HBx-specific T cell responses investigated in this study correlate with HBeAg clearance and lower HBsAg levels. This may result from HBV infection control by HBx-specific T cells, which is supported by *in vitro* observations of antiviral efficacy induced by HBx-specific T cells. Tumour resident memory HBV-specific $CD8^+$ T cells (core, surface and polymerase-specific $CD8^+$ T cells) have been shown to correlate with improved prognosis in HBV-associated HCC patients(Cheng et al., 2021). However, the influence of HBx-specific T cells on HCC development is unclear. Further research will investigate HBx-specific T cell responses in a HBV-associated HCC cohort established in Beijing YouAn Hospital that have longitudinal samples prior-to and post HCC development. HBx-specific T cell responses will be characterised by phenotype, function and TCR repertoire and their effect on HCC development will be analysed.

The cytotoxic function of $CD4^+$ T cells was first observed in cultured T cell lines

and clones, then displayed *ex vivo* in various viral infections and subsequently *in vivo* in mice(Aslan et al., 2006; Hildemann et al., 2013; Juno et al., 2017; Soghoian et al., 2012; Wilkinson et al., 2012). Virus-specific $CD4^+$ CTLs were also discovered in both SARS-CoV-2 infection and chronic HBV infection in this study, that exerted antiviral activity when encountering virus-infected target cells. S_{866}-specific $CD4^+$ T cells elicited cytolytic activity via the perforin-mediated pathway, whilst also constitutively expressing perforin and granzyme B *ex vivo*. Thus, the cytotoxic effector function of S_{866}-specific $CD4^+$ T cells was not induced by long-term culture. HBx-specific $CD4^+$ T cell cytotoxicity is associated with functional avidity and degranulation during chronic infection. Conversely, no correlations were observed between cytotoxicity and functional avidity in spike-specific $CD4^+$ T cells during acute infection. This suggests that cytotoxic activity of $CD4^+$ T cells is differentially regulated in acute and chronic infections.

Effector $CD8^+$ T cells constitutively express perforin and granzyme B, which are degranulated upon antigen activation to elicit rapid killing of target cells. Serial cytotoxicity of $CD8^+$ CTLs requires translation of cytolytic molecules in mitochondria(Lisci et al., 2021). Whereas S_{866}-specific $CD4^+$ T cells bearing the same TCR display distinct cytotoxic activity and various levels of perforin expression. To further explore the mechanisms mediating $CD4^+$ T cell cytotoxicity, the proteomic profiles of $CD4^+$ killer and non-killer clones have been analysed and hundreds of proteins are identified to be upregulated in killer clones. These upregulated proteins are largely involved in mitochondrial activity and function,

which further implicates the mitochondria in affecting perforin and granzyme expression in $CD4^+$ T cells. Mitochondrial function will be further studied in $CD4^+$ killer and non-killer clones.

Appendices

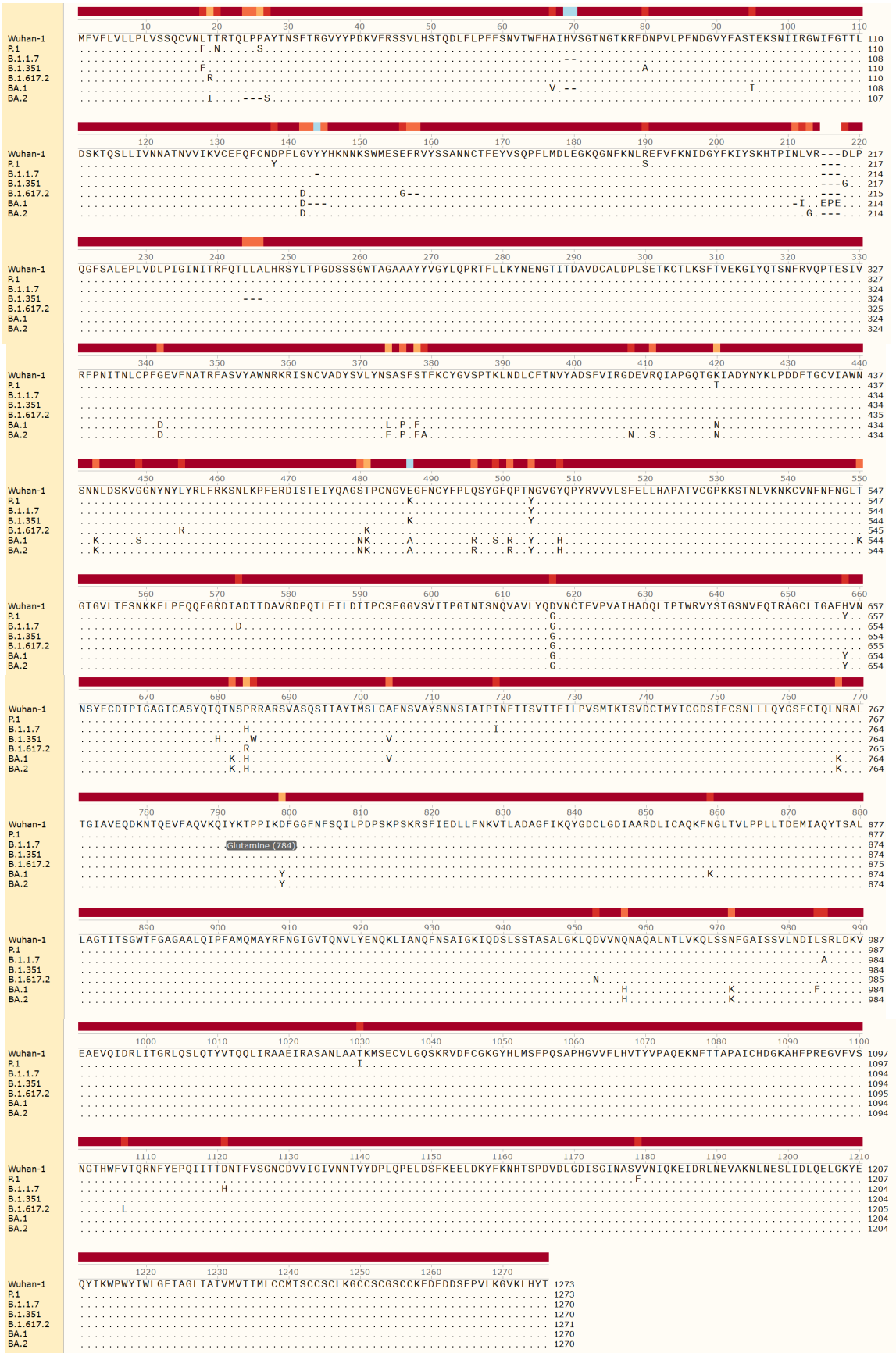

Appendix Fig. 1.1 Amino acid conversion of spike between VOCs and origin Wuhan strain. Spike sequenced were aligned using MUSCLE by software SnapGene. Dot represents identical amino acid and dash for amino acid depletion. P.1: Gamma, B.1.1.7: Alpha, B.1.351: Beta, B.1.617.2: Delta, BA.1 and BA.2: Omicron.

Appendix Table 2.1 HBV overlapping peptide pool

Core pool	SPl1	core1	core2	core3	core4	core5	core6	core7	core8	core9	core10	
	SPl2	core11	core12	core13	core14	core15	core16	core17	core18	core19	core20	
	SPl3	core21	core22	core23	core24	core25	core26	core27	core28	core29	core30	
	SPl4	core31	core32	core33	core34	core35	core36	core37	core38	core39	core40	
	SPl5	core41	core42	core43	core44	core45	core46	core47	core48	core49	core50	core51
Surface pool1	SPl1	S1	S2	S3	S4	S5	S6	S7	S8	S9	S10	
	SPl2	S11	S12	S13	S14	S15	S16	S17	S18	S19	S20	
	SPl3	S21	S22	S23	S24	S25	S26	S27	S28	S29	S30	
	SPl4	S31	S32	S33	S34	S35	S36	S37	S38	S39	S40	
	SPl5	S41	S42	S43	S44	S45	S46	S47	S48	S49	S50	
Surface pool2: S51-S98.												
X pool	SPl1	X1	X2	X3	X4	X5	X6	X7	X8	X9	X10	
	SPl2	X11	X12	X13	X14	X15	X16	X17	X18	X19	X20	
	SPl3	X21	X22	X23	X24	X25	X26	X27	X28	X29	X30	
	SPl4	X31	X32	X33	X34	X35	X36					
Polymerase pool1: P1-P52, pool2: P53-P104; pool3: P105-156; pool4: P157-208												

Appendix Table 2.2 Two-dimensional matrix peptide pool of SARS-CoV-2

		Pool17	Pool18	Pool19	Pool20	Pool21	Pool22	Pool23	Pool24	Pool25	Pool26	Pool27	Pool28	Pool29	Pool30	Pool31	Pool32
Spike	Pool1	S1	S2	S3	S4	S5	S6	S7	S8	S9	S10	S11	S12	S13	S14	S15	S16
	Pool2	S17	S18	S19	S20	S21	S22	S23	S24	S25	S26	S27	S28	S29	S30	S31	S32
	Pool3	S33	S34	S35	S36	S37	S38	S39	S40	S41	S42	S43	S44	S45	S46	S47	S48
	Pool4	S49	S50	S51	S52	S53	S54	S55	S56	S57	S58	S59	S60	S61	S62	S63	S64
	Pool5	S65	S66	S67	S68	S69	S70	S71	S72	S73	S74	S75	S76	S77	S78	S79	S80
	Pool6	S81	S82	S83	S84	S85	S86	S87	S88	S89	S90	S91	S92	S93	S94	S95	S96
	Pool7	S97	S98	S99	S100	S101	S102	S103	S104	S105	S106	S107	S108	S109	S110	S111	S112
	Pool8	S113	S114	S115	S116	S117	S118	S119	S120	S121	S122	S123	S124	S125	S126	S127	S128
	Pool9	S129	S130	S131	S132	S133	S134	S135	S136	S137	S138	S139	S140	S141	S142	S143	S144
	Pool10	S145	S146	S147	S148	S149	S150	S151	S152	S153	S154	S155	S156	S157	S158	S159	S160
	Pool11	S161	S162	S163	S164	S165	S166	S167	S168	S169	S170	S171	S172	S173	S174	S175	S176
	Pool12	S177	S178	S179	S180	S181	S182	S183	S184	S185	S186	S187	S188	S189	S190	S191	S192
	Pool13	S193	S194	S195	S196	S197	S198	S199	S200	S201	S202	S203	S204	S205	S206	S207	S208
	Pool14	S209	S210	S211	S212	S213	S214	S215	S216	S217	S218	S219	S220	S221	S222	S223	S224
	Pool15	S225	S226	S227	S228	S229	S230	S231	S232	S233	S234	S235	S236	S237	S238	S239	S240
	Pool16	S241	S242	S243	S244	S245	S246	S247	S248	S249	S250	S251	S252	S253			

Others		Pool-O-14	Pool-O-15	Pool-O-16	Pool-O-17	Pool-O-18	Pool-O-19	Pool-O-20	Pool-O-21	Pool-O-22	Pool-O-23	Pool-O-24	Pool-O-25	Pool-O-26	Pool-O-27	Pool-O-28	Pool-O-29
ORF3a	Pool-O-1	ORF3a-1	ORF3a-2	ORF3a-3	ORF3a-4	ORF3a-5	ORF3a-6	ORF3a-7	ORF3a-8	ORF3a-9	ORF3a-10	ORF3a-11	ORF3a-12	ORF3a-13	ORF3a-14	ORF3a-15	ORF3a-16
	Pool-O-2	ORF3a-17	ORF3a-18	ORF3a-19	ORF3a-20	ORF3a-21	ORF3a-22	ORF3a-23	ORF3a-24	ORF3a-25	ORF3a-26	ORF3a-27	ORF3a-28	ORF3a-29	ORF3a-30	ORF3a-31	ORF3a-32
	Pool-O-3	ORF3a-33	ORF3a-34	ORF3a-35													
ORF6	Pool-O-4	ORF6-1	ORF6-2	ORF6-3	ORF6-4	ORF6-5	ORF6-6	ORF6-7									
ORF7a	Pool-O-5	ORF7a-1	ORF7a-2	ORF7a-3	ORF7a-4	ORF7a-5	ORF7a-6	ORF7a-7	ORF7a-8	ORF7a-9	ORF7a-10	ORF7a-11	ORF7a-12	ORF7a-13	ORF7a-14	ORF7a-15	
ORF8	Pool-O-6	ORF8-1	ORF8-2	ORF8-3	ORF8-4	ORF8-5	ORF8-6	ORF8-7	ORF8-8	ORF8-9	ORF8-10	ORF8-11	ORF8-12	ORF8-13	ORF8-14	ORF8-15	ORF8-16
Env	Pool-O-7	Env-1	Env-2	Env-3	Env-4	Env-5	Env-6	Env-7	Env-8	Env-9							
M	Pool-O-8	M1	M2	M3	M4	M5	M6	M7	M8	M9	M10	M11	M12	M13	M14	M15	M16
	Pool-O-9	M17	M18	M19	M20	M21	M22	M23	M24	M25	M26	M27	M28				
NP	Pool-O-10	NP1	NP2	NP3	NP4	NP5	NP6	NP7	NP8	NP9	NP10	NP11	NP12	NP13	NP14	NP15	NP16
	Pool-O-11	NP17	NP18	NP19	NP20	NP21	NP22	NP23	NP24	NP25	NP26	NP27	NP28	NP29	NP30	NP31	NP32
	Pool-O-12	NP33	NP34	NP35	NP36	NP37	NP38	NP39	NP40	NP41	NP42	NP43	NP44	NP45	NP46	NP47	NP48
	Pool-O-13	NP49	NP50	NP51	NP52	NP53	NP54	NP55	NP56	NP57	NP58						

Appendix Table 3.1 Clinical and demographic information of patients with chronic HBV infection

Patient ID	Gender	Age (years)	HBsAg	HBsAg (IU/ml)	HBsAb	HBeAg	HBeAb	HBcAb
S1	F	43	+	677.3	-	-	+	+
S2	M	45	+	488.7	-	-	+	+
S3	M	60	+	42.23	-	-	+	+
S4	M	46	+	687.2	-	-	-	+
S5	F	52	+	150.9	-	-	+	+
S6	M	36	+	20790	-	+	-	+
S7	F	29	+	29011	-	+	-	+
S8	F	33	+	3329	-	-	+	+
S9	F	31	+	5142	-	+	-	+
S10	M	29	+	1350	-	+	-	+
S11	F	39	+	27628	-	+	-	+
S12	F	47	+	531.4	-	-	+	+
S13	M	41	+	4.22	+	-	-	+
S14	F	27	+	834.3	-	+	-	+
S14	M	50	+	294.4	-	-	+	+
S15	M	27	+	566.6	-	+	-	+
S16	F	27	+	16547	-	+	-	+
S17	F	23	+	394.9	-	+	-	+
S18	F	35	+	NA	-	-	+	+
S19	M	44	+	51.9	-	-	-	+
S20	F	23	+	21.09	-	-	+	+
S22	M	45	+	545.1	-	-	-	+
S23	M	39	+	2062	-	+	-	+
S24	F	58	+	4345	-	+	-	+
S25	M	44	+	5.55	-	-	+	+
S26	M	52	+	114.1	-	+	-	+
S27	F	31	+	411.9	-	+	-	+
S28	M	33	+	4686	-	+	-	+
S29	F	29	+	762.5	-	+	-	+
S30	F	34	+	1579	-	-	+	+
S31	F	36	+	2246	-	-	-	+
S32	M	46	+	420.3	-	-	+	+
S33	F	32	+	1.53	+	-	+	+
S34	F	61	+	3930	-	+	-	+
S35	M	24	+	10805	-	+	-	+
S36	F	36	+	2616	-	+	+	+
S37	M	48	+	158.1	-	-	+	+
S38	M	45	+	242.1	-	-	+	+
S39	M	49	+	237.5	-	-	+	+
S40	M	37	+	9.8	-	-	-	+
S41	M	60	+	629.3	-	-	+	+

S42	M	46	+	737.8	-	+	-	+
S43	M	48	+	2267	-	+	-	+
S44	M	28	+	1095	-	-	-	+
S45	M	23	+	61.22	-	-	+	+
S46	F	37	+	31.99	-	-	+	+
S47	M	26	+	3073	-	+	-	+
S48	M	43	+	33.09	-	-	+	+
S49	F	59	+	4400	-	-	+	+
S50	M	30	+	52000	-	+	-	+
S51	F	63	+	182.7	-	-	+	+
S52	F	41	+	1673	-	-	+	+
S53	M	51	+	845.2	-	+	-	+
S54	M	47	+	25.18	-	-	+	+
S55	M	25	+	162.37	-	+	+	+
S56	F	44	+	1.96	-	-	+	+
S57	F	37	+	34.52	-	-	+	+
S58	F	28	+	20312	+	+	-	+
S59	M	29	+	2513	-	+	+	+
S60	F	30	+	764	-	-	+	+
S61	M	45	+	1.37	-	-	+	+
S62	F	33	+	72.59	-	-	+	+
S63	M	46	+	0.304	-	-	+	+
S64	F	53	+	46.47	-	-	+	+
S65	M	48	+	457	-	-	+	+
S66	M	59	+	740.9	-	+	+	+
S67	F	32	+	10820	+	+	-	+
S68	F	35	+	NA	-	-	+	+
S69	F	38	+	6180	-	-	+	+
S70	M	39	+	2.88	-	-	+	+
S71	F	56	+	3.19	-	-	+	+
S72	F	29	+	74.4	-	-	+	+
S73	F	48	+	1248	-	-	+	+
S74	F	32	+	3353	-	-	+	+

M, male; F, female; HBsAb, hepatitis B surface antibody; HBeAb, hepatitis B e antibody; HBcAb, hepatitis B core antibody; NA, not detected.

Appendix Table 5.1 Clinical characteristics of SARS-CoV-2 cohort

Participant ID	Gender	Age	Severity	Oxygen[1]	SaO2/FiO2[2]	Days post symptom onset			Vaccination before sampling	HLA-typing			
						Acute	Visit1	Visit2		DRB1-1	DRB1-2	DPB1	DPB2
C-COV19-001	M	59	mild	94	4.48	-	60	-	No	04:01	08:01	02:01:02	04:01:01
C-COV19-002	M	54	mild	94	4.48	-	56	236	No	07:01	15:01	04:01:01	13:01:01
C-COV19-003	F	46	mild	94	4.48	-	55	-	No	01:01	01:01	03:01:01	04:02:01
C-COV19-004	F	50	mild	94	4.48	-	54	235	No	13:02	15:01	04:02:01	04:02:01
C-COV19-005	M	56	asymptomatic	94	4.48	-	58	-	No	01:01	07:01	04:02:01	06:01:01
C-COV19-006	M	54	mild	94	4.48	-	58	231	No	03:01	15:01	-	-
C-COV19-007	M	54	mild	94	4.48	-	62	-	No	11:02	15:01	04:01:01	16:01:01
C-COV19-008	M	54	mild	94	4.48	-	53	-	No	04:01	13:02	03:01:01	13:01:01
C-COV19-009	F	54	mild	94	4.48	-	57	-	No	04:01	04:01	04:01:01	04:01:01
C-COV19-010	M	51	mild	94	4.48	-	40	-	No	04:01	11:04	02:01:02	04:02:01
C-COV19-011	F	81	mild	94	4.48	-	41	-	No	03:01	07:01	02:01:02	09:01:01
C-COV19-012	M	49	mild	94	4.48	-	41	-	No	01:01	13:02	03:01:01	04:01:01
C-COV19-013	F	49	mild	94	4.48	-	42	-	No	03:01	03:01	04:02:01	09:01:01
C-COV19-014	M	74	mild	94	4.48	-	41	-	No	01:01	07:01	02:01:02	02:01:02
C-COV19-018	M	59	mild	94	4.48	-	36	-	No	04:01	07:01	04:01:01	17:01:01
C-COV19-020	M	57	mild	94	4.48	-	31	-	No	01:01	12:01	04:02:01	23:01:01
C-COV19-021	M	61	mild	94	4.48	-	42	-	No	04:01	04:01	04:01:01	04:01:01
C-COV19-022	M	66	mild	94	4.48	-	39	-	No	03:01	03:01	04:01:01	04:01:01
C-COV19-024	M	40	mild	94	4.48	-	40	-	No	03:01	07:01	04:01:01	09:01:01
C-COV19-035	M	50	severe	94	3.92	-	53	-	No	07:01	14:04	04:01:01	13:01:01
C-COV19-036	F	57	severe	94	3.92	-	41	176	No	15:01	15:01	04:01:01	04:01:01
C-COV19-038	F	44	severe	94	3.92	-	40	-	No	08:01	15:01	03:01:01	04:01:01
C-COV19-042	M	85	severe	94	3.92	-	49	-	No	11:02	15:01	04:01:01	13:01:01
C-COV19-051	F	83	severe	88	3.67	-	64	-	No	03:01	03:01	03:01:01	04:01:01
C-COV19-062	F	56	mild	94	4.48	-	53	230	No	04:03	07:01	02:01:02	10:01:01
C-COV19-032	F	95	mild	95	4.52	-	43	-	No	04:01	07:01	04:01:01	06:01:01
C-COV19-030	M	25	mild	97	1.08	-	46	-	No	01:01	01:01	04:02:01	04:02:01
C-COV19-045	F	72	severe	94	3.36	-	46	254	No	04:01	15:01	04:01:01	04:01:01
C-COV19-039	M	79	severe	96	2.4	-	40	-	No	03:01	04:03	03:01:01	04:01:01
C-COV19-034	M	73	severe	92	3.83	-	38	249	No	03:01	15:01	02:01:01	04:01:01
C-COV19-054	F	56	critical	92	1.02	-	74	-	No	01:01	03:01	02:01:02	04:02:01
C-COV19-046	M	76	mild	94	4.48	-	42	252	No	04:01	15:01	04:01:01	04:01:01
C-COV19-048	F	31	mild	94	4.48	-	40	-	No	07:01	13:01	04:01:01	19:01:01
C-COV19-055	M	52	critical	89	1.78	-	65	-	No	01:01	03:01	01:01:01	04:02:01
C-COV19-050	M	85	severe	90	1.5	-	51	-	No	12:01	15:01	04:02:01	165:01:00
C-COV19-056	M	48	severe	90	1.13	-	61	-	No	01:01	04:01	04:01:01	04:01:01
C-COV19-047	M	69	mild	96	4.57	7	36	223	No	08:01	15:01	04:01:01	04:01:01
C-COV19-060	M	52	critical	97	1.21	-	66	-	No	04:05	15:03	-	-
C-COV19-059	M	73	severe	91	4.33	-	37	-	No	01:01	07:01	04:01:01	17:01
C-COV19-064	F	74	mild	92	4.38	6	64	223	No	07:01	15:01	02:01:02	11:01:01

C-COV19-061	M	60	severe	89	4.24	6	42	172	No	01:01	15:01	03:01:01	04:01:01
UKCOV180	M	67	critical	91	1.14	-	-	302	Yes(V2: 220d post dose1 and 146d post dose2)	15:01	15:01	-	-
UKCOV203	F	58	critical	92	0.92	20	126	279	Yes(V1: 54d post dose1; V2: 119d post dose2)	03:01	15:01	04:01:01	-
UKCOV212	F	42	severe	94	3.92	-	-	222	Yes(V2: 187d post dose1 and 64d post dose2)	07:01	15:01	-	-
UKCOV245	M	53	critical	75	0.75	29	110	269	Yes(V1: 29d post dose1; V2: 108d post dose2)	01:01	03:01	04:01:01	-

1. For mild patients recruited at home, 94% on air (FiO2 21%) was used as an estimate, all other patients were measured.
2. Oxygen denotes measured oxygen saturation at point of maximal level of oxygen support.

Appendix Table 5.2 T cell receptors of S166- and S751-spike-specific T cell clones

Clone ID	Epitope	CDR3_alpha	TRAV	TRAJ	CDR3_beta	TRBV	TRBJ
clone1	$S_{166-180}$	CAVQNYGGSQGNLIF	TRAV35	TRAJ42	CASSLRGQNTGELFF	TRBV5-1	TRBJ2-2
clone2	$S_{166-180}$						
clone3	$S_{166-180}$						
clone4	$S_{166-180}$						
clone5	$S_{166-180}$						
clone6	$S_{166-180}$						
clone7	$S_{166-180}$	CAGQNYGGSQGNLIF	TRAV35	TRAJ42	CATARRDRVNTGELFF	TRBV27	TRBJ2-2
clone8	$S_{166-180}$	CAGQLSGGSQGNLIF	TRAV35	TRAJ42	CASSRRQASLEAFF	TRBV7-2	TRBJ1-1
clone9	$S_{166-180}$						
clone10	$S_{166-180}$						
clone11	$S_{166-180}$						
clone12	$S_{166-180}$						
clone13	$S_{166-180}$	CAGLNYGGSQGNLIF	TRAV35	TRAJ42	CASSPRGAGVSYEQYF	TRBV5-1	TRBJ2-7
clone14	$S_{166-180}$	CAAAGGSYIPTF	TRAV12-2	TRAJ6	CSADSGGATDTQYF	TRBV20-1	TRBJ2-3
clone15	$S_{166-180}$	CAPQNYGGSQGNLIF	TRAV35	TRAJ42	CASSPRWPASVGGYTF	TRBV19	TRBJ1-2
clone16	$S_{166-180}$	CAALNYGGSQGNLIF/CAAAGGSYIPTF	TRAV35/TRAV12-2	TRAJ42/TRAJ6	CSADSGGATDTQYF	TRBV20-1	TRBJ2-3
clone17	$S_{166-180}$	CAYRSVNTGNQFYF	TRAV38-2DV8	TRAJ49	CASSLWQGVSYEQYF	TRBV5-1	TRBJ2-7
clone18	$S_{166-180}$	CAALNYGGSQGNLIF	TRAV35	TRAJ42	CASSPGIGYTF	TRBV4-1	TRBJ1-2
clone19	$S_{166-180}$	CAGMNYGGSQGNLIF	TRAV35	TRAJ42	CASSYRAGAGYTF	TRBV6-6	TRBJ1-2
clone20	$S_{166-180}$	CIVRVPGNQGGKLIF	TRAV26-1	TRAJ23	CSATIRGHEAFF	TRBV20-1	TRBJ1-1
clone21	$S_{166-180}$	CAGMNYGGSQGNLIF	TRAV35	TRAJ42	CASSRLGALGYTF	TRBV11-1	TRBJ1-2
clone22	$S_{166-180}$	CAASIRGNQGGKLIF	TRAV23DV6	TRAJ23	CASGQDLEQFF	TRBV7-9	TRBJ2-1
clone23	$S_{166-180}$	CAYMNYGGSQGNLIF	TRAV35	TRAJ42	CASRDSLSQYF	TRBV6-1	TRBJ2-3
clone24	$S_{166-180}$	CIVSPHTGTASKLTF	TRAV26-1	TRAJ44	CASSLRQGSLYGYTF	TRBV28	TRBJ1-2
clone25	$S_{166-180}$	CAGQLYGGSQGNLIF	TRAV35	TRAJ42	CASSAKGRAGETQYF	TRBV18	TRBJ2-5
clone26	$S_{166-180}$						
clone27	$S_{166-180}$	CAGMNYGGSQGNLIF	TRAV35	TRAJ42	CASSYATGISPSTGELFF	TRBV6-5	TRBJ2-2
clone28	$S_{166-180}$						
clone29	$S_{166-180}$						
clone30	$S_{166-180}$						
clone31	$S_{166-180}$						
clone32	$S_{166-180}$						
clone33	$S_{166-180}$	CAGRNYGGSQGNLIF	TRAV35	TRAJ42	CASSPERGGFGYTF	TRBV6-5	TRBJ1-2
clone34	$S_{166-180}$	CAGLNYGGSQGNLIF	TRAV35	TRAJ42	CASSVRERVNTGELFF	TRBV9	TRBJ2-2
clone35	$S_{166-180}$	CAGLNYGGSQGNLIF	TRAV35	TRAJ42	CASIDRPGSTRGYTF	TRBV6-1	TRBJ1-2
clone36	$S_{166-180}$	CAVMNYGGSQGNLIF	TRAV35	TRAJ42	CASSYSGRTGGFGIQYF	TRBV6-3	TRBJ2-4
clone37	$S_{166-180}$	CAALNYGGSQGNLIF	TRAV35	TRAJ42	CASSAGRGEGYTF	TRBV5-1	TRBJ1-2
clone38	$S_{166-180}$	CAPPIGNNRLAF	TRAV17	TRAJ7	CASSFRQGSRGYTF	TRBV6-1	TRBJ1-2
clone39	$S_{166-180}$	CAALNYGGSQGNLIF	TRAV35	TRAJ42	CARRDRDPNYGYTF	TRBV7-2	TRBJ1-2
clone40	$S_{166-180}$	CAGQLYGGSQGNLIF	TRAV35	TRAJ42	CASSFRGTNTGELFF	TRBV5-1	TRBJ2-2
clone41	$S_{166-180}$	CAASNYGGSQGNLIF	TRAV35	TRAJ42	CASSAGHLLYGYTF	TRBV6-1	TRBJ1-2

clone42	$S_{166-180}$	CAGQLYGGSQGNLIF	TRAV35	TRAJ42	CASSRRGSINTGELFF	TRBV27	TRBJ2-2
clone43	$S_{166-180}$	CAYRSIGSNTGKLIF	TRAV38-2DV8	TRAJ37	CASSLWTGSSYEQYF	TRBV5-1	TRBJ2-7
clone44	$S_{166-180}$	CAGQLYGGSQGNLIF	TRAV35	TRAJ42	CASNPRGVGTGELFF	TRBV6-5	TRBJ2-2
clone45	$S_{166-180}$	CLVGYNFNKFYF	TRAV4	TRAJ21	CASSPRGSNTGELFF	TRBV9	TRBJ2-2
clone46	$S_{166-180}$	CAGLLYGGSQGNLIF	TRAV35	TRAJ42	CASSRGGLEAFF	TRBV27	TRBJ1-1
clone47	$S_{166-180}$	CASMNYGGSQGNLIF	TRAV35	TRAJ42	CASSDSGGLGYTF	TRBV6-4	TRBJ1-2
clone48	$S_{166-180}$	CAGQLYGGSQGNLIF	TRAV35	TRAJ42	CASSAKGRAGETQYF	TRBV18	TRBJ2-5
clone49	$S_{166-180}$	CAGQLFKAAGNKLTF	TRAV35	TRAJ17	CASSPRMGQTQYF	TRBV7-3	TRBJ2-5
clone50	$S_{166-180}$	CAGQLFGGTASKLTF	TRAV35	TRAJ44	CASSLRQGSLYGYTF	TRBV28	TRBJ1-2

clone1	$S_{751-765}$	CAASIGGSARQLTF	TRAV13-1	TRAJ22	CASSQERVQGYEQYF	TRBV4-3	TRBJ2-7
clone2	$S_{751-765}$	CVVNIGSSASKIIF	TRAV12-1	TRAJ3	CASTEGSSNQPQHF	TRBV6-1	TRBJ1-5
clone3	$S_{751-765}$	CVVNKGSSASKIIF	TRAV12-1	TRAJ3	CASSEGAGSQPQHF	TRBV6-1	TRBJ1-5
clone4	$S_{751-765}$						
clone5	$S_{751-765}$						
clone6	$S_{751-765}$						
clone7	$S_{751-765}$						
clone8	$S_{751-765}$						
clone9	$S_{751-765}$						
clone10	$S_{751-765}$	CVVNKRSSNTGKLIF/CAVEVGYYGQNFVF	TRAV12-1/TRAV36DV7	TRAJ37/TRAJ26	CASSYISGQANYGYTF	TRBV12-3	TRBJ1-2
clone11	$S_{751-765}$	CVVNMRSSNTGKLIF	TRAV12-1	TRAJ37	CATSAVNRGDYNEQFF	TRBV24-1	TRBJ2-1
clone12	$S_{751-765}$						
clone13	$S_{751-765}$						
clone14	$S_{751-765}$						
clone15	$S_{751-765}$	CVVNRGYSTLTF	TRAV12-1	TRAJ11	CASSQSQVDTQYF	TRBV23-1	TRBJ2-3
clone16	$S_{751-765}$	CAASRAGTASKLTF	TRAV13-1	TRAJ44	CASSLSGFVVDTQYF	TRBV7-2	TRBJ2-3
clone17	$S_{751-765}$						
clone18	$S_{751-765}$						
clone19	$S_{751-765}$	CAASRYGNNRLAF	TRAV13-1	TRAJ7	CSASDRVNTGELFF	TRBV20-1	TRBJ2-2
clone20	$S_{751-765}$						
clone21	$S_{751-765}$						
clone22	$S_{751-765}$	CAELMNYGGSQGNLIF	TRAV25	TRAJ42	CATSDITGGDNQPQHF	TRBV24-1	TRBJ1-5
clone23	$S_{751-765}$	CAESSGGYQKVTF	TRAV13-2	TRAJ13	CASSRDSSNQPQHF	TRBV4-2	TRBJ1-5
clone24	$S_{751-765}$						
clone25	$S_{751-765}$						
clone26	$S_{751-765}$						
clone27	$S_{751-765}$						
clone28	$S_{751-765}$	CAESSTGNQFYF/CVVGTGTASKLTF	TRAV5/TRAV12-1	TRAJ49/TRAJ44	CASSTSGGGSYEQYF	TRBV6-5	TRBJ2-7
clone29	$S_{751-765}$						
clone30	$S_{751-765}$	CAMSPYGNNRLAF	TRAV12-3	TRAJ7	CASSEGMGRNTEAFF	TRBV6-1	TRBJ1-1
clone31	$S_{751-765}$	CAASRAGTASKLTF/CAPRGGGSGGSYIPTF	TRAV13-1/TRAV13-2	TRAJ44/TRAJ6	CASSLSGFVVDTQYF	TRBV7-2	TRBJ2-3
clone32	$S_{751-765}$						
clone33	$S_{751-765}$						

clone34	$S_{751-765}$						
clone35	$S_{751-765}$	CVVNRGYSTLTF/CVVNPPPHGGKLIF	TRAV12-1	TRAJ11/TRAJ23	CASSQSQVDTQYF	TRBV23-1	TRBJ2-3
clone36	$S_{751-765}$	CAYRGGDSNYQLIW	TRAV38-2DV8	TRAJ33	CSARSISIGPQPQHF	TRBV20-1	TRBJ1-5
clone37	$S_{751-765}$	CKGFRGGADGLTF/CVVNAISSNTGKLIF	TRAV26-1/TRAV12-1	TRAJ45/TRAJ37	CATSAPDRGDNQPQHF	TRBV24-1	TRBJ1-5
clone38	$S_{751-765}$	CVGGTGFQKLVF	TRAV12-1	TRAJ8	CASSALGQAPVGREKLFF	TRBV6-1	TRBJ1-4
clone39	$S_{751-765}$	CVVGSGGYQKVTF	TRAV8-2	TRAJ13	CASSLPSGRGNEQFF	TRBV7-3	TRBJ2-1
clone40	$S_{751-765}$	CVVNALSSNTGKLIF	TRAV12-1	TRAJ37	CATSDITGGDNQPQHF	TRBV24-1	TRBJ1-5
clone41	$S_{751-765}$	CVVNDRSSNTGKLIF	TRAV12-1	TRAJ37	CATSDPDRGDNQPQHF	TRBV24-1	TRBJ1-5
clone42	$S_{751-765}$	CVVNKGSAGNKLTF	TRAV12-1	TRAJ17	CAIQEGASNQPQHF	TRBV6-1	TRBJ1-5
clone43	$S_{751-765}$	CVVNPPPHGGKLIF	TRAV12-1	TRAJ23	CASSEGASNQPQHF	TRBV6-1	TRBJ1-5
clone44	$S_{751-765}$						
clone45	$S_{751-765}$						
clone46	$S_{751-765}$						
clone47	$S_{751-765}$						
clone48	$S_{751-765}$						
clone49	$S_{751-765}$	CVVNMRSSNTGKLIF/CVVGSGGYQKVTF	TRAV12-1/TRAV8-2	TRAJ37/TRAJ13	CATSAVNRGDYNEQFF	TRBV24-1	TRBJ2-1
clone50	$S_{751-765}$	CVVNSGYSTLTF	TRAV12-1	TRAJ11	CASSFLGGQGAAEQYV	TRBV11-3	TRBJ2-7
clone51	$S_{751-765}$	CVVNSGYSTLTF/CVVNTIGKSAGNMLTF	TRAV12-1	TRAJ11/TRAJ39	CASSFLGGQGAAEQYV	TRBV11-3	TRBJ2-7
clone52	$S_{751-765}$	CVVNTGSSASKIIF	TRAV12-1	TRAJ3	CASVQGAANQPQHF	TRBV6-1	TRBJ1-5
clone53	$S_{751-765}$	CVVNTLSSNTGKLIF	TRAV12-1	TRAJ37	CATSDPSRGNNQPQHF	TRBV24-1	TRBJ1-5
clone54	$S_{751-765}$	CVVSEGSSNTGKLIF	TRAV12-1	TRAJ37	CASSIRGRGGNQPQHF	TRBV19	TRBJ1-5

References

Abd Hamid, M., Wang, R. Z., Yao, X., Fan, P., Li, X., Chang, X. M., . . . Dong, T. (2019). Enriched HLA-E and CD94/NKG2A Interaction Limits Antitumor CD8(+) Tumor-Infiltrating T Lymphocyte Responses. *Cancer Immunol Res, 7*(8), 1293-1306. doi:10.1158/2326-6066.Cir-18-0885

Abel, A. M., Yang, C., Thakar, M. S., & Malarkannan, S. (2018). Natural Killer Cells: Development, Maturation, and Clinical Utilization. *Front Immunol, 9*, 1869. doi:10.3389/fimmu.2018.01869

Ahmed, S. F., Quadeer, A. A., & McKay, M. R. (2020). Preliminary Identification of Potential Vaccine Targets for the COVID-19 Coronavirus (SARS-CoV-2) Based on SARS-CoV Immunological Studies. *Viruses, 12*(3). doi:10.3390/v12030254

Arstila, T. P., Casrouge, A., Baron, V., Even, J., Kanellopoulos, J., & Kourilsky, P. (1999). A Direct Estimate of the Human αβ T Cell Receptor Diversity. *286*(5441), 958-961. doi:doi:10.1126/science.286.5441.958

Arunachalam, P. S., Wimmers, F., Mok, C. K. P., Perera, R., Scott, M., Hagan, T., . . . Pulendran, B. (2020). Systems biological assessment of immunity to mild versus severe COVID-19 infection in humans. *Science, 369*(6508), 1210-1220. doi:10.1126/science.abc6261

Aslan, N., Yurdaydin, C., Wiegand, J., Greten, T., Ciner, A., Meyer, M. F., . . . Wedemeyer, H. (2006). Cytotoxic CD4 T cells in viral hepatitis. *J Viral Hepat, 13*(8), 505-514. doi:10.1111/j.1365-2893.2006.00723.x

Barry, M., & Bleackley, R. C. (2002). Cytotoxic T lymphocytes: all roads lead to death. *Nat Rev Immunol, 2*(6), 401-409. doi:10.1038/nri819

Bassing, C. H., Swat, W., & Alt, F. W. (2002). The mechanism and regulation of chromosomal V (D) J recombination. *Cell, 109*(2), S45-S55.

Belloni, L., Allweiss, L., Guerrieri, F., Pediconi, N., Volz, T., Pollicino, T., . . . Levrero, M. (2012). IFN-α inhibits HBV transcription and replication in cell culture and in humanized mice by targeting the epigenetic regulation of the nuclear cccDNA minichromosome. *Journal of Clinical Investigation, 122*(2), 529-537. doi:10.1172/jci58847

Benacerraf, B., & McDevitt, H. O. J. S. (1972). Histocompatibility-linked immune response genes. *175*(4019), 273-279.

Bergamaschi, L., Mescia, F., Turner, L., Hanson, A. L., Kotagiri, P., Dunmore, B. J., . . . Smith, K. G. C. (2021). Longitudinal analysis reveals that delayed bystander CD8+ T cell activation and early immune pathology distinguish severe COVID-19 from mild disease. *Immunity, 54*(6), 1257-1275 e1258. doi:10.1016/j.immuni.2021.05.010

Bertoletti, A., & Ferrari, C. (2016). Adaptive immunity in HBV infection. *Journal of hepatology, 64*(1, Supplement), S71-S83. doi:https://doi.org/10.1016/j.jhep.2016.01.026

Bertoletti, A., Le Bert, N., Qui, M., & Tan, A. T. (2021). SARS-CoV-2-specific T cells in infection and vaccination. *Cell Mol Immunol, 18*(10), 2307-2312. doi:10.1038/s41423-021-00743-3

Blum, J. S., Wearsch, P. A., & Cresswell, P. (2013). Pathways of antigen processing. *Annu Rev Immunol, 31*, 443-473. doi:10.1146/annurev-immunol-032712-095910

Boni, C., Fisicaro, P., Valdatta, C., Amadei, B., Di Vincenzo, P., Giuberti, T., . . . Missale, G. (2007). Characterization of hepatitis B virus (HBV)-specific T-cell dysfunction in chronic HBV infection. *J Virol, 81*(8), 4215-4225.

Boni, C., Laccabue, D., Lampertico, P., Giuberti, T., Viganò, M., Schivazappa, S., . . . Brancaccio, G. (2012a). Restored function of HBV-specific T cells after long-term effective therapy with nucleos (t) ide analogues. *Gastroenterology, 143*(4), 963-973. e969.

Boni, C., Laccabue, D., Lampertico, P., Giuberti, T., Viganò, M., Schivazappa, S., . . . Brancaccio, G. J. G. (2012b). Restored function of HBV-specific T cells after long-term effective therapy with nucleos (t) ide analogues. *143*(4), 963-973. e969.

Boppana, S., Qin, K., Files, J. K., Russell, R. M., Stoltz, R., Bibollet-Ruche, F., . . . Goepfert, P. A. (2021). SARS-CoV-2-specific circulating T follicular helper cells correlate with neutralizing antibodies and increase during early convalescence. *PLoS Pathog, 17*(7), e1009761. doi:10.1371/journal.ppat.1009761

Brinkmann, V., Geiger, T., Alkan, S., & Heusser, C. H. (1993). Interferon alpha increases the frequency of interferon gamma-producing human CD4+ T cells. *The Journal of experimental medicine, 178*(5), 1655-1663.

Burton, D. R. (2002). Antibodies, viruses and vaccines. *Nature Reviews Immunology, 2*(9), 706-713. doi:10.1038/nri891

Busse, D., de la Rosa, M., Hobiger, K., Thurley, K., Flossdorf, M., Scheffold, A., & Höfer, T. J. P. o. t. N. A. o. S. (2010). Competing feedback loops shape IL-2 signaling between helper and regulatory T lymphocytes in cellular microenvironments. *107*(7), 3058-3063.

Cao, Y., Wang, J., Jian, F., Xiao, T., Song, W., Yisimayi, A., . . . Xie, X. S. (2022). Omicron escapes the majority of existing SARS-CoV-2 neutralizing antibodies. *Nature, 602*(7898), 657-663. doi:10.1038/s41586-021-04385-3

Chen, C. H., Lu, S. N., Hung, C. H., Wang, J. H., Hu, T. H., Changchien, C. S., & Lee, C. M. (2014). The role of hepatitis B surface antigen quantification in predicting HBsAg loss and HBV relapse after discontinuation of lamivudine treatment. *J Hepatol, 61*(3), 515-522. doi:10.1016/j.jhep.2014.04.029

Cheng, Y., Gunasegaran, B., Singh, H. D., Dutertre, C. A., Loh, C. Y., Lim, J. Q., . . . Newell, E. W. (2021). Non-terminally exhausted tumor-resident memory HBV-specific T cell responses correlate with relapse-free survival in hepatocellular carcinoma. *Immunity, 54*(8), 1825-1840 e1827. doi:10.1016/j.immuni.2021.06.013

Chicz, R. M., Urban, R. G., Lane, W. S., Gorga, J. C., Stern, L. J., Vignali, D. A. A., & Strominger, J. L. (1992). Predominant naturally processed peptides bound to HLA-DR1 are derived from MHC-related molecules and are heterogeneous in size. *Nature, 358*(6389), 764-768. doi:10.1038/358764a0

Choo, S. Y. (2007). The HLA system: genetics, immunology, clinical testing, and clinical implications. *Yonsei Med J, 48*(1), 11-23. doi:10.3349/ymj.2007.48.1.11

Cohen, K. W., Linderman, S. L., Moodie, Z., Czartoski, J., Lai, L., Mantus, G., . . . McElrath, M. J. (2021). Longitudinal analysis shows durable and broad immune memory after SARS-CoV-2 infection with persisting antibody responses and memory B and T cells. *Cell Rep Med, 2*(7), 100354. doi:10.1016/j.xcrm.2021.100354

Decorsière, A., Mueller, H., van Breugel, P. C., Abdul, F., Gerossier, L., Beran, R. K., . . . Strubin, M. (2016). Hepatitis B virus X protein identifies the Smc5/6 complex as a host restriction factor. *Nature, 531*(7594), 386-389. doi:10.1038/nature17170

Dejnirattisai, W., Huo, J., Zhou, D., Zahradník, J., Supasa, P., Liu, C., . . . Screaton, G. R. (2022). SARS-CoV-2 Omicron-B.1.1.529 leads to widespread escape from neutralizing antibody responses. *Cell*. doi:10.1016/j.cell.2021.12.046

Doherty, P. C., & Zinkernagel, R. M. (1975). Enhanced immunological surveillance in mice heterozygous at the H-2 gene complex. *Nature, 256*(5512), 50-52. doi:10.1038/256050a0

Ernst, B., Surh, C. D., & Sprent, J. J. T. J. o. e. m. (1995). Thymic selection and cell division. *182*(4), 961-971.

Feighery, C., & Stastny, P. (1979). HLA-D region-associated determinants serve as targets for human cell-mediated lysis. *J Exp Med, 149*(2), 485-494. doi:10.1084/jem.149.2.485

Ferrari, C., Penna, A., Bertoletti, A., Valli, A., Antoni, A. D., Giuberti, T., . . . Fiaccadori, F. J. T. J. o. I. (1990). Cellular immune response to hepatitis B virus-encoded antigens in acute and chronic hepatitis B virus infection. *145*(10), 3442-3449.

Ferretti, A. P., Kula, T., Wang, Y., Nguyen, D. M. V., Weinheimer, A., Dunlap, G. S., . . . MacBeath, G. (2020). Unbiased Screens Show CD8(+) T Cells of COVID-19 Patients Recognize Shared Epitopes in SARS-CoV-2 that Largely Reside outside the Spike Protein. *Immunity, 53*(5), 1095-1107.e1093. doi:10.1016/j.immuni.2020.10.006

Friedmann, M. C., Migone, T.-S., Russell, S. M., & Leonard, W. J. J. P. o. t. N. A. o. S. (1996). Different interleukin 2 receptor beta-chain tyrosines couple to at least two signaling pathways and synergistically mediate interleukin 2-induced proliferation. *93*(5), 2077-2082.

Gehring, A. J., & Protzer, U. (2019). Targeting Innate and Adaptive Immune Responses to Cure Chronic HBV Infection. *Gastroenterology, 156*(2), 325-337. doi:https://doi.org/10.1053/j.gastro.2018.10.032

Gehring, A. J., Xue, S. A., Ho, Z. Z., Teoh, D., Ruedl, C., Chia, A., . . . Bertoletti, A. (2011). Engineering virus-specific T cells that target HBV infected hepatocytes and hepatocellular carcinoma cell lines. *J Hepatol, 55*(1), 103-110. doi:10.1016/j.jhep.2010.10.025

Giri, J. G., Ahdieh, M., Eisenman, J., Shanebeck, K., Grabstein, K., Kumaki, S., . . . Anderson, D. (1994). Utilization of the beta and gamma chains of the IL-2 receptor by the novel cytokine IL-15. *Embo j, 13*(12), 2822-2830. doi:10.1002/j.1460-2075.1994.tb06576.x

Gish, R. G., Given, B. D., Lai, C. L., Locarnini, S. A., Lau, J. Y., Lewis, D. L., & Schluep, T. (2015). Chronic hepatitis B: Virology, natural history, current management and a glimpse at future opportunities. *Antiviral Res, 121*, 47-58. doi:10.1016/j.antiviral.2015.06.008

Goonetilleke, N., Liu, M. K., Salazar-Gonzalez, J. F., Ferrari, G., Giorgi, E., Ganusov, V. V., . . . McMichael, A. J. (2009). The first T cell response to transmitted/founder virus contributes to the control of acute viremia in HIV-1 infection. *J Exp Med, 206*(6), 1253-1272. doi:10.1084/jem.20090365

Guidotti, L. G., & Chisari, F. V. (2001). Noncytolytic control of viral infections by the innate and adaptive immune response. *Annual review of immunology, 19*, 65.

Hadjadj, J., Yatim, N., Barnabei, L., Corneau, A., Boussier, J., Smith, N., . . . Terrier, B. (2020). Impaired type I interferon activity and inflammatory responses in severe COVID-19 patients. *Science, 369*(6504), 718-724. doi:10.1126/science.abc6027

Han, X., Liu, H., Huang, H., Liu, X., Jia, B., Gao, G. F., & Zhang, F. (2019). ID2 and ID3 are indispensable for Th1 cell differentiation during influenza virus infection in mice. *Eur J Immunol, 49*(3), 476-489. doi:10.1002/eji.201847822

Haniffa, M., Shin, A., Bigley, V., McGovern, N., Teo, P., See, P., . . . Ginhoux, F. (2012). Human tissues contain CD141hi cross-presenting dendritic cells with functional homology to mouse CD103+ nonlymphoid dendritic cells. *Immunity, 37*(1), 60-73. doi:10.1016/j.immuni.2012.04.012

Hayward, A. C., Wang, L., Goonetilleke, N., Fragaszy, E. B., Bermingham, A., Copas, A., . . . McMichael, A. J. (2015). Natural T Cell-mediated Protection against Seasonal and Pandemic Influenza. Results of the Flu Watch Cohort Study. *Am J Respir Crit Care Med, 191*(12), 1422-1431. doi:10.1164/rccm.201411-1988OC

He, J. S., Gong, D. E., & Ostergaard, H. L. (2010). Stored Fas ligand, a mediator of rapid CTL-mediated killing, has a lower threshold for response than degranulation or newly synthesized Fas ligand. *J Immunol, 184*(2), 555-563. doi:10.4049/jimmunol.0902465

Hildemann, S. K., Eberlein, J., Davenport, B., Nguyen, T. T., Victorino, F., & Homann, D. (2013). High efficiency of antiviral CD4(+) killer T cells. *PLoS One, 8*(4), e60420. doi:10.1371/journal.pone.0060420

Hoh, A., Heeg, M., Ni, Y., Schuch, A., Binder, B., Hennecke, N., . . . Thimme, R. (2015). Hepatitis B Virus-Infected HepG2hNTCP Cells Serve as a Novel Immunological Tool To Analyze the Antiviral Efficacy of CD8+ T Cells In Vitro. *J Virol, 89*(14), 7433-7438. doi:10.1128/JVI.00605-15

Hoogeveen, R. C., Dijkstra, S., Bartsch, L. M., Drescher, H., Aneja, J., Robidoux, M. P., . . . Lauer, G. M. (2022). Hepatitis B virus-specific CD4 T-cell responses differentiate functional cure from chronic surface antigen(+) infection. *J Hepatol*. doi:10.1016/j.jhep.2022.05.041

Hoogeveen, R. C., Robidoux, M. P., Schwarz, T., Heydmann, L., Cheney, J. A., Kvistad, D., . . . Lauer, G. M. (2019). Phenotype and function of HBV-specific T cells is determined by the targeted epitope in addition to the stage of infection. *Gut, 68*(5), 893-904. doi:10.1136/gutjnl-2018-316644

Hua, L., Yao, S., Pham, D., Jiang, L., Wright, J., Sawant, D., . . . Sun, J. (2013). Cytokine-dependent induction of CD4+ T cells with cytotoxic potential during influenza virus infection. *J Virol, 87*(21), 11884-11893. doi:10.1128/JVI.01461-13

Hull, P. (1970). Notes on DR Snell's observations concerning the H-2 Locus polymorphism. *Heredity, 25*(3), 461-465. doi:10.1038/hdy.1970.47

Iannacone, M., & Guidotti, L. G. (2022). Immunobiology and pathogenesis of hepatitis B virus infection. *Nat Rev Immunol, 22*(1), 19-32. doi:10.1038/s41577-021-00549-4

Ijzermans, J. N. M., & Marquet, R. L. (1989). Interferon-gamma: A Review. *Immunobiology, 179*(4), 456-473. doi:https://doi.org/10.1016/S0171-2985(89)80049-X

Ivashkiv, L. B., & Donlin, L. T. (2014). Regulation of type I interferon responses. *Nat Rev Immunol, 14*(1), 36-49. doi:10.1038/nri3581

Jackson, C. B., Farzan, M., Chen, B., & Choe, H. (2022). Mechanisms of SARS-CoV-2 entry into cells. *Nat Rev Mol Cell Biol, 23*(1), 3-20. doi:10.1038/s41580-021-00418-x

Jin, Y., Shih, W., & Berkower, I. (1988). Human T cell response to the surface antigen of hepatitis B virus (HBsAg). Endosomal and nonendosomal processing pathways are accessible to both endogenous and exogenous antigen. *J Exp Med, 168*(1), 293-306.

Jones, S. A., & Hu, J. (2013). Hepatitis B virus reverse transcriptase: diverse functions as classical and emerging targets for antiviral intervention. *Emerg Microbes Infect, 2*(9), e56. doi:10.1038/emi.2013.56

Jung, M.-C., & Pape, G. R. (2002). Immunology of hepatitis B infection. *The Lancet infectious diseases, 2*(1), 43-50.

Jung, M.-C., Spengler, U., Schraut, W., Hoffmann, R., Zachoval, R., Eisenburg, J., . . . Ziegler-Heitbrock, H. J. J. o. h. (1991). Hepatitis B virus antigen-specific T-cell activation in patients with acute and chronic hepatitis B. *13*(3), 310-317.

Juno, J. A., Tan, H. X., Lee, W. S., Reynaldi, A., Kelly, H. G., Wragg, K., . . . Wheatley, A. K. (2020). Humoral and circulating follicular helper T cell responses in recovered patients with COVID-19. *Nat Med, 26*(9), 1428-1434. doi:10.1038/s41591-020-0995-0

Juno, J. A., van Bockel, D., Kent, S. J., Kelleher, A. D., Zaunders, J. J., & Munier, C. M. (2017). Cytotoxic CD4 T Cells-Friend or Foe during Viral Infection? *Front Immunol, 8*, 19. doi:10.3389/fimmu.2017.00019

Kaech, S. M., Wherry, E. J., & Ahmed, R. (2002). Effector and memory T-cell differentiation: implications for vaccine development. *Nat Rev Immunol, 2*(4), 251-262. doi:10.1038/nri778

Kägi, D., Vignaux, F., Ledermann, B., Bürki, K., Depraetere, V., Nagata, S., . . . Golstein, P. (1994). Fas and Perforin Pathways as Major Mechanisms of T Cell-Mediated Cytotoxicity. *265*(5171), 528-530. doi:doi:10.1126/science.7518614

Kaneko, N., Boucau, J., Kuo, H. H., Perugino, C., Mahajan, V. S., Farmer, J. R., . . . Pillai, S. (2021). Expansion of Cytotoxic CD4+ T cells in the lungs in severe COVID-19. *medRxiv*. doi:10.1101/2021.03.23.21253885

Kared, H., Redd, A. D., Bloch, E. M., Bonny, T. S., Sumatoh, H., Kairi, F., . . . Bettinotti, M. P. J. T. J. o. c. i. (2021). SARS-CoV-2–specific CD8+ T cell responses in convalescent COVID-19 individuals. *131*(5).

Kataoka, T., Shinohara, N., Takayama, H., Takaku, K., Kondo, S., Yonehara, S., & Nagai, K. (1996). Concanamycin A, a powerful tool for characterization and estimation of contribution of perforin- and Fas-based lytic pathways in cell-mediated cytotoxicity. *The Journal of Immunology, 156*(10), 3678.

Kawai, T., & Akira, S. (2006). Innate immune recognition of viral infection. *Nature Immunology, 7*(2), 131-137. doi:10.1038/ni1303

Keeton, R., Tincho, M. B., Ngomti, A., Baguma, R., Benede, N., Suzuki, A., . . . Riou, C. (2022). T cell responses to SARS-CoV-2 spike cross-recognize Omicron. *Nature, 603*(7901), 488-492. doi:10.1038/s41586-022-04460-3

Kim, D., Lee, J. Y., Yang, J. S., Kim, J. W., Kim, V. N., & Chang, H. (2020). The Architecture of SARS-CoV-2 Transcriptome. *Cell, 181*(4), 914-921 e910. doi:10.1016/j.cell.2020.04.011

Kim, G. A., Lim, Y. S., An, J., Lee, D., Shim, J. H., Kim, K. M., . . . Suh, D. J. (2014). HBsAg seroclearance after nucleoside analogue therapy in patients with chronic hepatitis B: clinical outcomes and durability. *Gut, 63*(8), 1325-1332. doi:10.1136/gutjnl-2013-305517

Kisielow, P., Teh, H. S., Blüthmann, H., & von Boehmer, H. (1988). Positive selection of antigen-specific T cells in thymus by restricting MHC molecules. *Nature, 335*(6192), 730-733. doi:10.1038/335730a0

Koutsakos, M., Nguyen, T. H. O., & Kedzierska, K. (2019). With a Little Help from T Follicular Helper Friends: Humoral Immunity to Influenza Vaccination. *J Immunol, 202*(2), 360-367. doi:10.4049/jimmunol.1800986

Kuri-Cervantes, L., Pampena, M. B., Meng, W., Rosenfeld, A. M., Ittner, C. A. G., Weisman, A. R., . . . Betts, M. R. (2020). Comprehensive mapping of immune perturbations associated with severe COVID-19. *Sci Immunol, 5*(49), eabd7114. doi:10.1126/sciimmunol.abd7114

Ladner, S. K., Otto, M. J., Barker, C. S., Zaifert, K., Wang, G. H., Guo, J. T., . . . King, R. W. (1997). Inducible expression of human hepatitis B virus (HBV) in stably transfected hepatoblastoma cells: a novel system for screening potential inhibitors of HBV replication. *Antimicrob Agents Chemother, 41*(8), 1715-1720. doi:10.1128/aac.41.8.1715

Laidlaw, B. J., Craft, J. E., & Kaech, S. M. (2016). The multifaceted role of CD4(+) T cells in CD8(+) T cell memory. *Nat Rev Immunol, 16*(2), 102-111. doi:10.1038/nri.2015.10

Laing, A. G., Lorenc, A., Del Molino Del Barrio, I., Das, A., Fish, M., Monin, L., . . . Hayday, A. C. (2020). A dynamic COVID-19 immune signature includes associations with poor prognosis. *Nat Med, 26*(10), 1623-1635. doi:10.1038/s41591-020-1038-6

Lanier, L. L. (2005). NK cell recognition. *Annual review of immunology, 23*(1), 225-274.

Lanier, L. L. (2008). Evolutionary struggles between NK cells and viruses. *Nat Rev Immunol, 8*(4), 259-268. doi:10.1038/nri2276

Laydon, D. J., Bangham, C. R., & Asquith, B. (2015). Estimating T-cell repertoire diversity: limitations of classical estimators and a new approach. *Philos Trans R Soc Lond B Biol Sci, 370*(1675). doi:10.1098/rstb.2014.0291

Le Bon, A., Durand, V., Kamphuis, E., Thompson, C., Bulfone-Paus, S., Rossmann, C., . . . Tough, D. F. (2006). Direct stimulation of T cells by type I IFN enhances the CD8+ T cell response during cross-priming. *The Journal of Immunology, 176*(8), 4682-4689.

Lee, L. Y., Ha do, L. A., Simmons, C., de Jong, M. D., Chau, N. V., Schumacher, R., . . . Dong, T. (2008). Memory T cells established by seasonal human influenza A infection cross-react with avian influenza A (H5N1) in healthy individuals. *J Clin Invest, 118*(10), 3478-3490. doi:10.1172/JCI32460

Levitskaya, J., Coram, M., Levitsky, V., Imreh, S., Steigerwald-Mullen, P. M., Klein, G., . . . Masucci, M. G. (1995). Inhibition of antigen processing by the internal repeat region of the Epstein–Barr virus nuclear antigen-1. *Nature, 375*(6533), 685-688. doi:10.1038/375685a0

Levrero, M., & Zucman-Rossi, J. (2016). Mechanisms of HBV-induced hepatocellular carcinoma. *J Hepatol, 64*(1 Suppl), S84-S101. doi:10.1016/j.jhep.2016.02.021

Li, W., Moore, M. J., Vasilieva, N., Sui, J., Wong, S. K., Berne, M. A., . . . Farzan, M. (2003). Angiotensin-converting enzyme 2 is a functional receptor for the SARS coronavirus. *Nature, 426*(6965), 450-454. doi:10.1038/nature02145

Liang, T. J., Block, T. M., McMahon, B. J., Ghany, M. G., Urban, S., Guo, J. T., . . . Lok, A. S. (2015). Present and future therapies of hepatitis B: From discovery to cure. *Hepatology, 62*(6), 1893-1908. doi:10.1002/hep.28025

Lin, L., Couturier, J., Yu, X., Medina, M. A., Kozinetz, C. A., & Lewis, D. E. (2014). Granzyme B secretion by human memory CD4 T cells is less strictly regulated compared to memory CD8 T cells. *BMC Immunology, 15*(1), 36. doi:10.1186/s12865-014-0036-1

Lisci, M., Barton, P. R., Randzavola, L. O., Ma, C. Y., Marchingo, J. M., Cantrell, D. A., . . . Griffiths, G. M. (2021). Mitochondrial translation is required for sustained killing by cytotoxic T cells. *Science, 374*(6565), eabe9977. doi:10.1126/science.abe9977

Liver, E. A. F. T. S. O. T. (2017). EASL 2017 Clinical Practice Guidelines on the management of hepatitis B virus infection. *J Hepatol, 67*(2), 370-398. doi:10.1016/j.jhep.2017.03.021

Lok, A. S., Zoulim, F., Dusheiko, G., & Ghany, M. G. J. J. o. H. (2017). Hepatitis B cure: From discovery to regulatory approval. *J Hepatol, 67*(4), 847-861.

Lotfi, M., Hamblin, M. R., & Rezaei, N. (2020). COVID-19: Transmission, prevention, and potential therapeutic opportunities. *Clin Chim Acta, 508*, 254-266. doi:10.1016/j.cca.2020.05.044

Low, J. S., Vaqueirinho, D., Mele, F., Foglierini, M., Jerak, J., Perotti, M., . . . Cassotta, A. (2021). Clonal analysis of immunodominance and cross-reactivity of the CD4 T cell response to SARS-CoV-2. *Science, 372*(6548), 1336-1341. doi:10.1126/science.abg8985

Lu, R., Zhao, X., Li, J., Niu, P., Yang, B., Wu, H., . . . Tan, W. (2020). Genomic characterisation

and epidemiology of 2019 novel coronavirus: implications for virus origins and receptor binding. *The Lancet, 395*(10224), 565-574. doi:10.1016/s0140-6736(20)30251-8

Maimone, M. M., Morrison, L. A., Braciale, V. L., & Braciale, T. J. (1986). Features of target cell lysis by class I and class II MHC-restricted cytolytic T lymphocytes. *J Immunol, 137*(11), 3639-3643.

Maini, M. K., Boni, C., Ogg, G. S., King, A. S., Reignat, S., Lee, C. K., . . . Bertoletti, A. (1999). Direct ex vivo analysis of hepatitis B virus-specific CD8(+) T cells associated with the control of infection. *Gastroenterology, 117*(6), 1386-1396. doi:10.1016/s0016-5085(99)70289-1

Maini, M. K., & Pallett, L. J. (2018). Defective T-cell immunity in hepatitis B virus infection: why therapeutic vaccination needs a helping hand. *The Lancet Gastroenterology & Hepatology, 3*(3), 192-202. doi:10.1016/s2468-1253(18)30007-4

Malarkannan, S. (2020). NKG7 makes a better killer. *Nature Immunology, 21*(10), 1139-1140. doi:10.1038/s41590-020-0767-5

Mann, E. R., Menon, M., Knight, S. B., Konkel, J. E., Jagger, C., Shaw, T. N., . . . Hussell, T. (2020). Longitudinal immune profiling reveals key myeloid signatures associated with COVID-19. *Sci Immunol, 5*(51). doi:10.1126/sciimmunol.abd6197

Mathew, D., Giles, J. R., Baxter, A. E., Oldridge, D. A., Greenplate, A. R., Wu, J. E., . . . Wherry, E. J. (2020). Deep immune profiling of COVID-19 patients reveals distinct immunotypes with therapeutic implications. *Science, 369*(6508). doi:10.1126/science.abc8511

McNab, F., Mayer-Barber, K., Sher, A., Wack, A., & O'Garra, A. (2015). Type I interferons in infectious disease. *Nat Rev Immunol, 15*(2), 87-103. doi:10.1038/nri3787

Meckiff, B. J., Ramirez-Suastegui, C., Fajardo, V., Chee, S. J., Kusnadi, A., Simon, H., . . . Vijayanand, P. (2020). Imbalance of Regulatory and Cytotoxic SARS-CoV-2-Reactive CD4(+) T Cells in COVID-19. *Cell, 183*(5), 1340-1353 e1316. doi:10.1016/j.cell.2020.10.001

Mestan, J., Digel, W., Mittnacht, S., Hillen, H., Blohm, D., Möller, A., . . . Kirchner, H. (1986). Antiviral effects of recombinant tumour necrosis factor in vitro. *Nature, 323*(6091), 816-819.

Meuer, S. C., Fitzgerald, K. A., Hussey, R. E., Hodgdon, J. C., Schlossman, S. F., & Reinherz, E. L. J. T. J. o. e. m. (1983). Clonotypic structures involved in antigen-specific human T cell function. Relationship to the T3 molecular complex. *157*(2), 705-719.

Micco, L., Peppa, D., Loggi, E., Schurich, A., Jefferson, L., Cursaro, C., . . . Maini, M. K. (2013). Differential boosting of innate and adaptive antiviral responses during pegylated-interferon-alpha therapy of chronic hepatitis B. *Journal of hepatology, 58*(2), 225-233. doi:10.1016/j.jhep.2012.09.029

Miles, J. J., Douek, D. C., & Price, D. A. (2011). Bias in the alphabeta T-cell repertoire: implications for disease pathogenesis and vaccination. *Immunol Cell Biol, 89*(3), 375-387. doi:10.1038/icb.2010.139

Mosmann, T. R., Cherwinski, H., Bond, M. W., Giedlin, M. A., & Coffman, R. L. (1986). Two types of murine helper T cell clone. I. Definition according to profiles of lymphokine activities and secreted proteins. *J Immunol, 136*(7), 2348-2357.

Moss, P. (2022). The T cell immune response against SARS-CoV-2. *Nat Immunol, 23*(2), 186-193. doi:10.1038/s41590-021-01122-w

Mudd, P. A., Minervina, A. A., Pogorelyy, M. V., Turner, J. S., Kim, W., Kalaidina, E., . . . Ellebedy,

A. H. (2021). SARS-CoV-2 mRNA vaccination elicits a robust and persistent T follicular helper cell response in humans. *Cell*. doi:10.1016/j.cell.2021.12.026

Nelde, A., Bilich, T., Heitmann, J. S., Maringer, Y., Salih, H. R., Roerden, M., . . . Wacker, M. J. N. i. (2021). SARS-CoV-2-derived peptides define heterologous and COVID-19-induced T cell recognition. *22*(1), 74-85.

Notarbartolo, S., Ranzani, V., Bandera, A., Gruarin, P., Bevilacqua, V., Putignano, A. R., . . . Abrignani, S. (2021). Integrated longitudinal immunophenotypic, transcriptional and repertoire analyses delineate immune responses in COVID-19 patients. *Sci Immunol, 6*(62). doi:10.1126/sciimmunol.abg5021

Notarbartolo, S., Ranzani, V., Bandera, A., Gruarin, P., Bevilacqua, V., Putignano, A. R., . . . Bombaci, M. J. S. i. (2021). Integrated longitudinal immunophenotypic, transcriptional, and repertoire analyses delineate immune responses in patients with COVID-19. *6*(62), eabg5021.

Oh, D. Y., Kwek, S. S., Raju, S. S., Li, T., McCarthy, E., Chow, E., . . . Fong, L. (2020). Intratumoral CD4(+) T Cells Mediate Anti-tumor Cytotoxicity in Human Bladder Cancer. *Cell, 181*(7), 1612-1625 e1613. doi:10.1016/j.cell.2020.05.017

Painter, M. M., Mathew, D., Goel, R. R., Apostolidis, S. A., Pattekar, A., Kuthuru, O., . . . Wherry, E. J. (2021). Rapid induction of antigen-specific CD4(+) T cells is associated with coordinated humoral and cellular immunity to SARS-CoV-2 mRNA vaccination. *Immunity, 54*(9), 2133-2142 e2133. doi:10.1016/j.immuni.2021.08.001

Pan, G., O'Rourke, K., Chinnaiyan, A. M., Gentz, R., Ebner, R., Ni, J., & Dixit, V. M. (1997). The Receptor for the Cytotoxic Ligand TRAIL. *276*(5309), 111-113. doi:doi:10.1126/science.276.5309.111

Park, J.-J., Wong, D. K., Wahed, A. S., Lee, W. M., Feld, J. J., Terrault, N., . . . Kleiner, D. (2016). Hepatitis B Virus–Specific and Global T-Cell Dysfunction in Chronic Hepatitis B. *Gastroenterology, 150*(3), 684-695.e685. doi:https://doi.org/10.1053/j.gastro.2015.11.050

Peng, Y., Felce, S. L., Dong, D., Penkava, F., Mentzer, A. J., Yao, X., . . . Dong, T. (2022). An immunodominant NP105-113-B*07:02 cytotoxic T cell response controls viral replication and is associated with less severe COVID-19 disease. *Nat Immunol, 23*(1), 50-61. doi:10.1038/s41590-021-01084-z

Peng, Y., Mentzer, A. J., Liu, G., Yao, X., Yin, Z., Dong, D., . . . Dong, T. (2020). Broad and strong memory CD4(+) and CD8(+) T cells induced by SARS-CoV-2 in UK convalescent individuals following COVID-19. *Nat Immunol, 21*(11), 1336-1345. doi:10.1038/s41590-020-0782-6

Penna, A., Del Prete, G., Cavalli, A., Bertoletti, A., D'Elios, M. M., Sorrentino, R., . . . Fiaccadori, F. (1997). Predominant T-helper 1 cytokine profile of hepatitis B virus nucleocapsid-specific T cells in acute self-limited hepatitis B. *Hepatology, 25*(4), 1022-1027.

Penna, A., Fowler, P., Bertoletti, A., Guilhot, S., Moss, B., Margolskee, R. F., . . . Chisari, F. V. (1992). Hepatitis B virus (HBV)-specific cytotoxic T-cell (CTL) response in humans: characterization of HLA class II-restricted CTLs that recognize endogenously synthesized HBV envelope antigens. *Journal of Virology, 66*(2), 1193.

Phillips, S., Chokshi, S., Riva, A., Evans, A., Williams, R., & Naoumov, N. V. (2010). CD8(+) T cell control of hepatitis B virus replication: direct comparison between cytolytic and noncytolytic functions. *J Immunol, 184*(1), 287-295. doi:10.4049/jimmunol.0902761

Planas, D., Veyer, D., Baidaliuk, A., Staropoli, I., Guivel-Benhassine, F., Rajah, M. M., . . . Schwartz,

O. (2021). Reduced sensitivity of SARS-CoV-2 variant Delta to antibody neutralization. *Nature, 596*(7871), 276-280. doi:10.1038/s41586-021-03777-9

Platanias, L. C. (2005). Mechanisms of type-I- and type-II-interferon-mediated signalling. *Nat Rev Immunol, 5*(5), 375-386. doi:10.1038/nri1604

Qui, H. Z., Hagymasi, A. T., Bandyopadhyay, S., St Rose, M. C., Ramanarasimhaiah, R., Menoret, A., . . . Adler, A. J. (2011). CD134 plus CD137 dual costimulation induces Eomesodermin in CD4 T cells to program cytotoxic Th1 differentiation. *J Immunol, 187*(7), 3555-3564. doi:10.4049/jimmunol.1101244

Rabbitts, T., Lefranc, M., Stinson, M., Sims, J., Schroder, J., Steinmetz, M., . . . Goodfellow, P. J. T. E. j. (1985). The chromosomal location of T-cell receptor genes and a T cell rearranging gene: possible correlation with specific translocations in human T cell leukaemia. *4*(6), 1461-1465.

Raziorrouh, B., Schraut, W., Gerlach, T., Nowack, D., Grüner, N. H., Ulsenheimer, A., . . . Jung, M.-C. (2010). The immunoregulatory role of CD244 in chronic hepatitis B infection and its inhibitory potential on virus-specific CD8+ T-cell function. *Hepatology, 52*(6), 1934-1947. doi:10.1002/hep.23936

Rehermann, B. (2013). Pathogenesis of chronic viral hepatitis: differential roles of T cells and NK cells. *Nat Med, 19*(7), 859-868. doi:10.1038/nm.3251

Revill, P. A., Chisari, F. V., Block, J. M., Dandri, M., Gehring, A. J., Guo, H., . . . Schinazi, R. F. (2019). A global scientific strategy to cure hepatitis B. *The Lancet Gastroenterology & Hepatology, 4*(7), 545-558. doi:10.1016/s2468-1253(19)30119-0

Rivino, L., Le Bert, N., Gill, U. S., Kunasegaran, K., Cheng, Y., Tan, D. Z., . . . Bertoletti, A. (2018). Hepatitis B virus-specific T cells associate with viral control upon nucleos(t)ide-analogue therapy discontinuation. *J Clin Invest, 128*(2), 668-681. doi:10.1172/JCI92812

Roche, P. A., & Furuta, K. (2015). The ins and outs of MHC class II-mediated antigen processing and presentation. *Nat Rev Immunol, 15*(4), 203-216. doi:10.1038/nri3818

Rock, K. L., & Goldberg, A. L. (1999). DEGRADATION OF CELL PROTEINS AND THE GENERATION OF MHC CLASS I-PRESENTED PEPTIDES. *17*(1), 739-779. doi:10.1146/annurev.immunol.17.1.739

Ruby, J., Bluethmann, H., & Peschon, J. J. (1997). Antiviral activity of tumor necrosis factor (TNF) is mediated via p55 and p75 TNF receptors. *The Journal of experimental medicine, 186*(9), 1591-1596.

Russell, S. M., Keegan, A. D., Harada, N., Nakamura, Y., Noguchi, M., Leland, P., . . . Paul, W. E. J. S. (1993). Interleukin-2 receptor γ chain: a functional component of the interleukin-4 receptor. *262*(5141), 1880-1883.

Sarin, S. K., Kumar, M., Lau, G. K., Abbas, Z., Chan, H. L., Chen, C. J., . . . Kao, J. H. (2016). Asian-Pacific clinical practice guidelines on the management of hepatitis B: a 2015 update. *Hepatol Int, 10*(1), 1-98. doi:10.1007/s12072-015-9675-4

Schuch, A., Salimi Alizei, E., Heim, K., Wieland, D., Kiraithe, M. M., Kemming, J., . . . Thimme, R. (2019). Phenotypic and functional differences of HBV core-specific versus HBV polymerase-specific CD8+ T cells in chronically HBV-infected patients with low viral load. *Gut, 68*(5), 905-915. doi:10.1136/gutjnl-2018-316641

Schurich, A., Khanna, P., Lopes, A. R., Han, K. J., Peppa, D., Micco, L., . . . Dusheiko, G. (2011). Role of the coinhibitory receptor cytotoxic T lymphocyte antigen-4 on apoptosis-Prone CD8 T cells in persistent hepatitis B virus infection. *J Hepatol, 53*(5), 1494-1503.

Schurich, A., Khanna, P., Lopes, A. R., Han, K. J., Peppa, D., Micco, L., . . . Maini, M. K. (2011). Role of the coinhibitory receptor cytotoxic T lymphocyte antigen-4 on apoptosis-Prone CD8 T cells in persistent hepatitis B virus infection. *Hepatology, 53*(5), 1494-1503. doi:10.1002/hep.24249

Sedger, L. M., & McDermott, M. F. (2014). TNF and TNF-receptors: From mediators of cell death and inflammation to therapeutic giants - past, present and future. *Cytokine Growth Factor Rev, 25*(4), 453-472. doi:10.1016/j.cytogfr.2014.07.016

Seeger, C., & Mason, W. S. (2015). Molecular biology of hepatitis B virus infection. *Virology, 479-480*, 672-686. doi:10.1016/j.virol.2015.02.031

Shaan Lakshmanappa, Y., Elizaldi, S. R., Roh, J. W., Schmidt, B. A., Carroll, T. D., Weaver, K. D., . . . Iyer, S. S. (2021). SARS-CoV-2 induces robust germinal center CD4 T follicular helper cell responses in rhesus macaques. *Nat Commun, 12*(1), 541. doi:10.1038/s41467-020-20642-x

Soghoian, D. Z., Jessen, H., Flanders, M., Sierra-Davidson, K., Cutler, S., Pertel, T., . . . Streeck, H. (2012). HIV-specific cytolytic CD4 T cell responses during acute HIV infection predict disease outcome. *Sci Transl Med, 4*(123), 123ra125. doi:10.1126/scitranslmed.3003165

Stauber, D. J., Debler, E. W., Horton, P. A., Smith, K. A., & Wilson, I. A. J. P. o. t. N. A. o. S. (2006). Crystal structure of the IL-2 signaling complex: paradigm for a heterotrimeric cytokine receptor. *103*(8), 2788-2793.

Stinchcombe, J. C., Bossi, G., Booth, S., & Griffiths, G. M. J. I. (2001). The immunological synapse of CTL contains a secretory domain and membrane bridges. *15*(5), 751-761.

Su, Y., Chen, D., Yuan, D., Lausted, C., Choi, J., Dai, C. L., . . . Heath, J. R. (2020). Multi-Omics Resolves a Sharp Disease-State Shift between Mild and Moderate COVID-19. *Cell, 183*(6), 1479-1495 e1420. doi:10.1016/j.cell.2020.10.037

Takeuchi, O., & Akira, S. (2009). Innate immunity to virus infection. *Immunological reviews, 227*(1), 75-86.

Tan, A. T., Linster, M., Tan, C. W., Le Bert, N., Chia, W. N., Kunasegaran, K., . . . Bertoletti, A. (2021). Early induction of functional SARS-CoV-2-specific T cells associates with rapid viral clearance and mild disease in COVID-19 patients. *Cell Rep, 34*(6), 108728. doi:10.1016/j.celrep.2021.108728

Tarke, A., Coelho, C. H., Zhang, Z., Dan, J. M., Yu, E. D., Methot, N., . . . Sette, A. (2022). SARS-CoV-2 vaccination induces immunological T cell memory able to cross-recognize variants from Alpha to Omicron. *Cell, 185*(5), 847-859 e811. doi:10.1016/j.cell.2022.01.015

Tong, S., & Revill, P. (2016). Overview of hepatitis B viral replication and genetic variability. *J Hepatol, 64*(1 Suppl), S4-S16. doi:10.1016/j.jhep.2016.01.027

Trépo, C., Chan, H. L. Y., & Lok, A. (2014). Hepatitis B virus infection. *The Lancet, 384*(9959), 2053-2063. doi:https://doi.org/10.1016/S0140-6736(14)60220-8

van Montfoort, N., van der Aa, E., van den Bosch, A., Brouwers, H., Vanwolleghem, T., Janssen, H. L. A., . . . Woltman, A. M. (2016). Hepatitis B Virus Surface Antigen Activates Myeloid Dendritic Cells via a Soluble CD14-Dependent Mechanism. *J Virol, 90*(14), 6187-6199. doi:10.1128/JVI.02903-15

Venturi, V., Price, D. A., Douek, D. C., & Davenport, M. P. (2008). The molecular basis for public T-cell responses? *Nature Reviews Immunology, 8*(3), 231-238. doi:10.1038/nri2260

Virgin, H. W., Wherry, E. J., & Ahmed, R. (2009). Redefining chronic viral infection. *Cell, 138*(1), 30-50. doi:10.1016/j.cell.2009.06.036

Voeten, J. T., Bestebroer, T. M., Nieuwkoop, N. J., Fouchier, R. A., Osterhaus, A. D., & Rimmelzwaan, G. F. (2000). Antigenic drift in the influenza A virus (H3N2) nucleoprotein and escape from recognition by cytotoxic T lymphocytes. *J Virol, 74*(15), 6800-6807. doi:10.1128/jvi.74.15.6800-6807.2000

Voskoboinik, I., Smyth, M. J., & Trapani, J. A. (2006). Perforin-mediated target-cell death and immune homeostasis. *Nat Rev Immunol, 6*(12), 940-952. doi:10.1038/nri1983

Vyas, J. M., Van der Veen, A. G., & Ploegh, H. L. (2008). The known unknowns of antigen processing and presentation. *Nat Rev Immunol, 8*(8), 607-618. doi:10.1038/nri2368

Wajant, H., Pfizenmaier, K., & Scheurich, P. (2003). Tumor necrosis factor signaling. *Cell Death & Differentiation, 10*(1), 45-65. doi:10.1038/sj.cdd.4401189

Walter, E., Keist, R., Niederöst, B., Pult, I., & Blum, H. E. J. H. (1996). Hepatitis B virus infection of tupaia hepatocytes in vitro and in vivo. *24*(1), 1-5.

Wang, H., Luo, H., Wan, X., Fu, X., Mao, Q., Xiang, X., . . . Deng, G. (2020). TNF-alpha/IFN-gamma profile of HBV-specific CD4 T cells is associated with liver damage and viral clearance in chronic HBV infection. *J Hepatol, 72*(1), 45-56. doi:10.1016/j.jhep.2019.08.024

Wherry, E. J. (2011). T cell exhaustion. *Nat Immunol, 12*(6), 492-499. doi:10.1038/ni.2035

Wherry, E. J., & Ahmed, R. (2004). Memory CD8 T-cell differentiation during viral infection. *J Virol, 78*(11), 5535-5545. doi:10.1128/JVI.78.11.5535-5545.2004

WHO. (2017). *Global hepatitis report 2017*: World Health Organization.

WHO. (2022a). https://www.who.int/activities/tracking-SARS-CoV-2-variants.

WHO. (2022b). WHO Coronavirus (COVID-19) Dishboard. Retrieved Accessed on September 10, 2022

Wilkinson, T. M., Li, C. K., Chui, C. S., Huang, A. K., Perkins, M., Liebner, J. C., . . . Xu, X. N. (2012). Preexisting influenza-specific CD4+ T cells correlate with disease protection against influenza challenge in humans. *Nat Med, 18*(2), 274-280. doi:10.1038/nm.2612

Wisskirchen, K., Kah, J., Malo, A., Asen, T., Volz, T., Allweiss, L., . . . Protzer, U. (2019). T cell receptor grafting allows virological control of Hepatitis B virus infection. *J Clin Invest, 129*(7), 2932-2945. doi:10.1172/jci120228

Wong, G. H., & Goeddel, D. V. (1986). Tumour necrosis factors alpha and beta inhibit virus replication and synergize with interferons. *Nature, 323*(6091), 819-822. doi:10.1038/323819a0

Woolthuis, R. G., van Dorp, C. H., Keşmir, C., de Boer, R. J., & van Boven, M. (2016). Long-term adaptation of the influenza A virus by escaping cytotoxic T-cell recognition. *Scientific Reports, 6*(1), 33334. doi:10.1038/srep33334

Wragg, K. M., Lee, W. S., Koutsakos, M., Tan, H. X., Amarasena, T., Reynaldi, A., . . . Juno, J. A. (2022). Establishment and recall of SARS-CoV-2 spike epitope-specific CD4(+) T cell memory. *Nat Immunol*. doi:10.1038/s41590-022-01175-5

Xia, Y., Stadler, D., Lucifora, J., Reisinger, F., Webb, D., Hösel, M., . . . Protzer, U. (2016). Interferon-γ and Tumor Necrosis Factor-α Produced by T Cells Reduce the HBV Persistence Form, cccDNA, Without Cytolysis. *Gastroenterology, 150*(1), 194-205. doi:https://doi.org/10.1053/j.gastro.2015.09.026

Yan, H., Zhong, G., Xu, G., He, W., Jing, Z., Gao, Z., . . . Li, W. (2012). Sodium taurocholate cotransporting polypeptide is a functional receptor for human hepatitis B and D virus. *eLife, 1*. doi:10.7554/eLife.00049

Yan, R., Zhang, Y., Li, Y., Xia, L., Guo, Y., & Zhou, Q. (2020). Structural basis for the recognition of SARS-CoV-2 by full-length human ACE2. *367*(6485), 1444-1448. doi:doi:10.1126/science.abb2762

Ye, B., Liu, X., Li, X., Kong, H., Tian, L., & Chen, Y. (2015). T-cell exhaustion in chronic hepatitis B infection: current knowledge and clinical significance. *Cell Death Dis, 6*, e1694. doi:10.1038/cddis.2015.42

Yeo, Y. H., Ho, H. J., Yang, H.-I., Tseng, T.-C., Hosaka, T., Trinh, H. N., . . . Buti, M. J. G. (2019). Factors associated with rates of HBsAg seroclearance in adults with chronic HBV infection: a systematic review and meta-analysis. *Gastroenterology, 156*(3), 635-646. e639.

Yuen, M. F., Chen, D. S., Dusheiko, G. M., Janssen, H. L. A., Lau, D. T. Y., Locarnini, S. A., . . . Lai, C. L. (2018). Hepatitis B virus infection. *Nat Rev Dis Primers, 4*, 18035. doi:10.1038/nrdp.2018.35

Zhang, R., Li, Y., Zhang, A. L., Wang, Y., & Molina, M. J. (2020). Identifying airborne transmission as the dominant route for the spread of COVID-19. *Proc Natl Acad Sci U S A, 117*(26), 14857-14863. doi:10.1073/pnas.2009637117

Zheng, Y., Chaudhry, A., Kas, A., deRoos, P., Kim, J. M., Chu, T. T., . . . Rudensky, A. Y. (2009). Regulatory T-cell suppressor program co-opts transcription factor IRF4 to control T(H)2 responses. *Nature, 458*(7236), 351-356. doi:10.1038/nature07674

Zhou, D., Dejnirattisai, W., Supasa, P., Liu, C., Mentzer, A. J., Ginn, H. M., . . . Screaton, G. R. (2021). Evidence of escape of SARS-CoV-2 variant B.1.351 from natural and vaccine-induced sera. *Cell, 184*(9), 2348-2361 e2346. doi:10.1016/j.cell.2021.02.037

Zhou, P., Yang, X. L., Wang, X. G., Hu, B., Zhang, L., Zhang, W., . . . Shi, Z. L. (2020). A pneumonia outbreak associated with a new coronavirus of probable bat origin. *Nature, 579*(7798), 270-273. doi:10.1038/s41586-020-2012-7

Zhu, D., Liu, L., Yang, D., Fu, S., Bian, Y., Sun, Z., . . . Peng, H. (2016). Clearing persistent extracellular antigen of hepatitis B virus: an immunomodulatory strategy to reverse tolerance for an effective therapeutic vaccination. *J Immunol, 196*(7), 3079-3087.

Zhu, J., & Paul, W. E. (2008). CD4 T cells: fates, functions, and faults. *Blood, 112*(5), 1557-1569. doi:10.1182/blood-2008-05-078154

Zhu, J., Yamane, H., & Paul, W. E. (2010). Differentiation of effector CD4 T cell populations (*). *Annu Rev Immunol, 28*, 445-489. doi:10.1146/annurev-immunol-030409-101212

Zhu, N., Zhang, D., Wang, W., Li, X., Yang, B., Song, J., . . . Research, T. (2020). A Novel Coronavirus from Patients with Pneumonia in China, 2019. *N Engl J Med, 382*(8), 727-733. doi:10.1056/NEJMoa2001017

Zou, J., Shen, G., Qiang, W., Zhu, Y. Y., & Li, W. X. (2021). Study on the polymorphisms of HLA-ABCDQB1DRB1 alleles and haplotypes in Hubei Han population of China. *Int J Immunogenet, 48*(1), 8-15. doi:10.1111/iji.12516